



**Molecular, cellular and clinical impact of ALCAM
(CD166) and its molecular complex in the skeletal
metastasis of endocrine related cancers**

By

Yiming Yang

Cardiff China Medical Research Collaborative

School of Medicine, Cardiff University

August 2022

Thesis submitted to Cardiff University for the degree of

Doctor of Medicine

Acknowledgement

I would like to express my sincere gratitude to my main supervisor, Professor Wen G. Jiang for his continued support, patience and guidance throughout my MD study. I also wish to thank my co-supervisors, particularly Dr Andrew Sanders who taught me so much in the laboratory and worked patiently with me during the strict COVID-19 pandemic lockdown. The thesis could not be completed without constant help and support from all staff and students, past and present, from CCMRC. Special thanks are extended to Ms. Fiona Ruge for her help and support during the immunohistochemical studies, as well as Dr Tracey A Martin and Dr Jane Lane for the constant discussions in research and critical readings. My fellow PhD and MD students are thanked for their constant laughs, support, and help during my study and in particular during the most difficult of the COVID lockdown. I also wish to thank the host department, the School of Medicine and the University that has made every effort to accommodate my laboratory studies whilst keeping all of us safe.

Finally, I would like to thank my parents for their continued encouragement, their trust in me and all the support, financial and emotional to the very least, during my study. I am especially grateful to them for their love and care when the COVID-19 pandemic had been so much of concern throughout my study. Their unconditional love and continued faith in me are the sources of my strength and determination to move forward and complete the study.

Publications and presentation

Full publications

1. **Yang Y**, Sanders AJ, Dou QP, Jiang DG, Li AX, Jiang WG. The Clinical and Theranostic Values of Activated Leukocyte Cell Adhesion Molecule (ALCAM)/CD166 in Human Solid Cancers. *Cancers (Basel)*. 2021 Oct 15;13(20):5187. doi: 10.3390/cancers13205187. PMID: 34680335; PMCID: PMC8533996.
2. **Yang Y**, Sanders AJ, Ruge F, Dong X, Cui Y, Dou QP, Jia S, Hao C, Ji J, Jiang WG. Activated leukocyte cell adhesion molecule (ALCAM)/CD166 in pancreatic cancer, a pivotal link to clinical outcome and vascular embolism. *Am J Cancer Res*. 2021 Dec 15;11(12):5917-5932. PMID: 35018233; PMCID: PMC8727815.

Conference presentations and publications

1. **Yang Y**, A J Sanders, E Davies, R E Mansel, W G Jiang. Activated leukocyte cell adhesion molecule (ALCAM) and its intracellular linkers in assessing the outcome of patients with breast cancer. Presented to the Surgical Research Society (UK) annual conference 2021. *British Journal of Surgery*, Volume 108, Issue Supplement_5, July 2021, znab282.023. <https://doi.org/10.1093/bjs/znab282.023>
2. **Yang Y**, A J Sanders, X Dong, Y Cui, C Hao, J Ji, W G Jiang. O11 'Activated leukocyte cell adhesion molecule (ALCAM/CD166) is an important clinical and prognostic indicator in pancreatic cancer. Presented to the Surgical Research Society (UK) annual conference 2021. *British Journal of Surgery*, Volume 108, Issue Supplement_5, July 2021, znab282.016. <https://doi.org/10.1093/bjs/znab282.016>
3. **Yang Y**, Wang Jia, Tracey A Martin, Andrew J Sanders, Wen G. Jiang; Expression of Activated leukocyte cell adhesion molecule (ALCAM) and bone invasion in human pituitary adenomas. Presented to European Association for Cancer Research Virtual Congress 2021.
4. **Yang Y**, Sanders AJ, Hao C, *et al.* Expression, clinical and prognostic value of dual specific protein phosphatase-7 (DUSP-7) in pancreatic cancer. Presented to The British Society of Gastroenterology Annual Meeting 2021. *Gut* 2021;70:A13. DOI: [10.1136/gutjnl-2021-BSG.23](https://doi.org/10.1136/gutjnl-2021-BSG.23)
5. **Yang Y**, Sanders AJ, Ji J, *et al.*, ALCAM, activated leukocyte cell adhesion

molecule, in clinical gastric cancer. Presented to The British Society of Gastroenterology Annual Meeting 2021. Gut 2021;70:A141. DOI: [10.1136/gutjnl-2021-BSG.261](https://doi.org/10.1136/gutjnl-2021-BSG.261)

6. **Yang Y**, Andrew J. Sanders, Wen G. Jiang, ALCAM (Activated Leukocyte Cell Adhesion Molecule) is associated with MET/HGF signalling pathway in different subtypes of breast cancer. San Antonio Breast Cancer Symposium 2022, December 2022.
7. **Yang Y**, Xuefei Dong, Tracey A. Martin, *et al.*, Identification of subpopulation of breast cancer patients with poor clinical outcome using CUB domain containing protein-1 (CDCP1)/CD318 and its interactive proteins SRC and the HGF axis. San Antonio Breast Cancer Symposium 2022, December 2022.

Summary

Activated leukocyte cell adhesion molecule (ALCAM/CD166) belongs to the immunoglobulin superfamily of cell adhesion molecules. It has demonstrated that ALCAM regulates cell adhesion and migration in multiple cancer types and is strongly correlated with the clinical outcome of patients with cancers, especially breast cancer. The present study examined the clinical implication of ALCAM in endocrine-related cancers (breast cancer and pituitary tumour). We also explored the role of ALCAM in a non-endocrine related cancer, pancreatic cancer, to further establish the relationship between ALCAM and endocrine tumours. The results showed that ALCAM acted as an inhibitory factor to bone metastasis and was shown to be a positive prognostic factor of survival in breast cancer. The relationships between ALCAM and the clinical course of the patients were contrasted between endocrine related and non-endocrine related cancers. The study also explored the effect of ALCAM on different subtypes of breast cancer cell lines and the signalling events underlying ALCAM and their involvement in hormonal receptor related bone metastasis. The results showed that ALCAM exerted different biological effects on breast cancer cell lines with different ER statuses in both normal and mimicked bone microenvironments. MET was found to be a vital signalling molecule in the context of ALCAM actions in these cancer cells. In addition, ALCAM was found to be able to influence the sensitivity of chemotherapy drugs in certain breast cancer cell lines and this influence was hormone receptor dependent. The study concludes that ALCAM is a vital factor in cancer progression including bone metastasis of breast cancer and assessing the prognosis of the patients, a connection contrasted to non-endocrine pancreatic cancer. The biological actions of ALCAM on breast cancer cells are hormone receptor dependent with MET protooncogene playing a key role.

Table of Contents

Chapter-1 Introduction.....	1
1.1 Bone biology and histology.....	2
1.2 Malignancies of the skeleton	2
1.2.1 Primary bone tumours.....	3
1.2.2 Metastatic bone tumours	3
1.2.2.1 Prevalence.....	4
1.2.2.2 Aetiology	7
1.2.2.3 Metastatic bone tumours from breast cancer	8
1.2.2.4 Metastatic bone tumours from prostate cancer	8
1.2.2.5 Metastatic bone tumours from lung cancer	10
1.2.2.6 Molecular and cellular aspect of bone metastasis.....	10
1.2.2.6.1 RANK and RANKL.....	10
1.2.2.6.2 PTHrP and PTH1R (PTHR)	11
1.3. Breast cancer	12
1.3.1 Prevalence of breast cancer	13
1.3.2 Metastasis of breast cancer	15
1.3.3 Metastatic spread of breast cancer to bones	18
1.3.4 Hormone dependency of breast cancer	18
1.3.4.1 Oestrogen Receptor (ER).....	19
1.3.4.2 Androgen Receptor (AR).....	21
1.3.4.3 Progesterone Receptor (PR)	22
1.3.4.4 Human Epidermal growth factor Receptor (HER) family	22
1.3.5 Treatment of breast cancer	24
1.3.6 Intervention in bone metastasis.....	24
1.4 ALCAM/CD166	26
1.4.1 Discovery	27
1.4.2 Molecular and genetic structure	28
1.4.3 Protein interactions	30
1.4.4 Molecular signalling.....	33
1.4.5 ALCAM in cancer.....	34
1.4.5.1 Breast cancer	35
1.4.5.2 Prostate cancer	37
1.4.5.3 Thyroid cancer.....	37
1.4.5.4 Colorectal cancer.....	37
1.4.5.5 Other cancer types	38
1.4.6 ALCAM shedding mechanisms.....	45

1.4.7 Circulating ALCAM (truncated ALCAM)	45
1.4.8 ALCAM and metastatic diseases	46
1.4.9 HGF/MET complex	47
1.4.10 Pancreatic ductal adenocarcinoma: an exocrine related cancer	49
1.5 Hypothesis	52
1.6 Aims of the study	52
Chapter-2 Materials and Methods	54
2.1 Materials	55
2.1.1 General materials and reagents.....	55
2.1.2 Special reagents	56
2.1.3 Source of chemotherapy drugs.....	57
2.2 Cell lines	57
2.3 Cell culture.....	58
2.3.1 Cell maintenance, sub-culture and quantification.....	58
2.3.2 Cryopreservation and revival of frozen stocks	60
2.4 Generation of ALCAM knockdown/Overexpression systems	61
2.4.1 Plasmid design	61
2.4.2 Plasmid extraction and quantification	62
2.4.3 Plasmid transfection of breast cancer, endothelial cells and pancreatic cancer cells.....	64
2.5 RNA extraction, quantification and Reverse Transcription	65
2.6 Polymerase Chain Reaction (PCR)	66
2.7 Quantitative Polymerase Chain Reaction (qPCR)	69
2.8 Western blotting	71
2.8.1 Protein extraction	71
2.8.2 Protein quantification	72
2.8.3 Sodium dodecyl sulfate-polyacrylamide gel electrophoresis (SDS-PAGE)	72
2.8.4 Protein transfer from gel to membrane	74
2.8.5 Immunoblotting	76
2.8.6 Detection of blotting.....	76
2.9 Clinical cohorts.....	77
2.9.1 Cardiff Breast Cancer cohort	77
2.9.2 Cancer Bank breast cancer patient serum cohort	78
2.9.3 Online datasets analysis	78
2.9.4 Pituitary cohort.....	78
2.9.5 Pancreatic cancer cohort	79
2.10 Enzyme Linked Immunosorbent Assay (ELISA)	79

2.11 Immunohistochemical (IHC) staining analysis	80
2.12 Immunoprecipitation (IP) assay.....	81
2.13 Cell growth assay.....	81
2.14 Drug toxicity assay.....	82
2.15 Fluorescence based Tumour-endothelial interaction assay	83
2.16 Electric cell-substrate impedance sensing (ECIS)	84
2.17 Antibody Microarrays for signalling pathway analysis.....	86
2.17.1 Kinexus™ KAM-900P Antibody Microarrays.....	86
2.17.2 Key information from KAM-900P antibody microarray reports	89
2.18 Statistical analysis	91
Chapter-3 ALCAM expression in breast cancer and the relationship to skeletal metastasis and clinical outcome of the patients	92
3.1 Introduction	93
3.2 Methods	93
3.2.1 Clinical Cohorts	93
3.2.2 Immunohistochemical (IHC) staining analysis	94
3.2.3 Statistical methods	95
3.3 Results	95
3.3.1 Protein expression of ALCAM in breast cancers, analysis by immunohistochemistry (IHC).....	95
3.3.2 Expression levels of ALCAM in breast cancers with bone metastasis	100
3.3.3 ALCAM, hormonal status and Bone Metastasis.....	100
3.3.4 ALCAM and the survival of patients with breast cancer	104
3.3.5 ALCAM and the survival of the patients, a hormonal connection	106
3.3.6 Circulating ALCAM in patients with breast cancer.....	120
3.3.7 ALCAM and bone metastasis, validation using an alternative endocrine cohort, pituitary tumours	125
3.4 Discussion	128
Chapter-4 The impact of ALCAM on cellular functions of breast cancer and the relationship with bone metastasis	131
4.1 Introduction	132
4.2 Methods	132
4.2.1 Special reagents.....	132
4.2.2 Cell lines and culture conditions.....	132
4.2.3 Manipulation of ALCAM expression	133
4.2.4 RNA preparation and reverse transcription polymerase chain reaction (RT-PCR)	133

4.2.5 Western blotting.....	134
4.2.6 Cell Growth assay	134
4.2.7 Statistical methods	134
4.3 Results	134
4.3.1 Expression of ALCAM in breast cancer cell lines.....	135
4.3.2 Construction of ALCAM knockdown model.....	135
4.3.3 Impact of genetic manipulation on the growth of breast cancer cells.	137
4.4 Discussion	140
Chapter-5 Exploring signalling events underlying ALCAM and their involvement in hormonal receptor related bone metastasis of breast cancer	142
5.1 Introduction	143
5.2 Methods	143
5.2.1 Special reagents.....	143
5.2.2 Genetic preparation of breast cancer cells.....	144
5.2.3 Protein preparation and the Protein kinase array (Kinexus™) analysis	144
5.2.4 Immunoprecipitation (IP)	144
5.2.5 Western blotting.....	145
5.2.6 ECIS (Electric Cell-substrate Impedance Sensing).....	145
5.2.7 Statistical methods	146
5.3 Results	146
5.3.1 The changes of signalling events following ALCAM knockdown in ER positive and negative breast cancer cell lines.....	146
5.3.1.1 <i>Protein kinases showing the same trend of changes in ER positive and ER negative group after knocking down ALCAM.....</i>	<i>148</i>
5.3.1.2 <i>Protein kinases showing contrast changes in ER positive and ER negative group after knocking down ALCAM</i>	<i>154</i>
5.3.2 Immunoprecipitation of ALCAM interacting protein	165
5.3.3 The interaction of ALCAM and MET in different ER status and in bone microenvironment, an ECIS based analysis	167
5.3.3.1 <i>Alterations in cell adhesion ability following ALCAM knockdown in normal and bone microenvironment.....</i>	<i>168</i>
5.3.3.2 <i>The effect of HGF and MET inhibitor on cell adhesion following ALCAM knockdown.....</i>	<i>172</i>
5.3.3.3 <i>The effect of Neratinib on cell adhesion following ALCAM knockdown.....</i>	<i>180</i>
5.3.3.4 <i>The effect of ROCK inhibitor on cell adhesion following ALCAM knockdown.....</i>	<i>183</i>
5.4 Discussion	186
Chapter-6 ALCAM and drug response to chemotherapies.....	189
6.1 Introduction	190
6.2 Methods	191

6.2.1 Genetic preparation of breast cancer cells.....	191
6.2.2 Cell cytotoxicity assay.....	191
6.2.3 Online datasets analysis.....	192
6.2.4 Statistical methods.....	192
6.3 Results.....	192
6.3.1 The effect of knocking down ALCAM in breast cancer cell lines on chemotherapy drug sensitivity.....	192
6.3.2 The relation of ALCAM expression levels and drug responsiveness in different breast cancer subgroups.....	198
6.3.2.1 ALCAM expression and endocrine therapy.....	199
6.3.2.2 ALCAM expression and anti-HER2 therapy.....	200
6.3.2.3 ALCAM expression and chemotherapy.....	201
6.3.2.4 ALCAM and chemo-response in molecular subtypes of breast cancer.....	206
6.4 Discussion.....	208
CHAPTER-7 ALCAM in pancreatic cancer, a pivotal link to clinical outcome and tumour vascular embolism.....	211
7.1 Introduction.....	212
7.2 Methods.....	212
7.2.1 Cohorts.....	212
7.2.2 Cell lines and culture conditions.....	213
7.2.3 Key materials.....	213
7.2.4 Anti-ALCAM shRNA and ALCAM expression constructs.....	214
7.2.5 Establishing pancreatic cancer and endothelial cell models with differential expression of ALCAM.....	214
7.2.6 Tumour-endothelial interaction assay.....	215
7.2.7 Cell adhesion and migration assay by ECIS (Electric Cell-Substrate Impedance Sensing).....	215
7.2.8 Pancreatic cancer tissue arrays (TMA) and staining of ALCAM by immunohistochemical assay.....	216
7.2.9 Extraction of RNA from tissues and quantitative analysis of ALCAM gene transcript.....	217
7.2.10 Statistical methods.....	217
7.3 Results.....	218
7.3.1 Levels of ALCAM expression in pancreatic tissues and pancreatic cancer tissues determined by immunohistochemistry (IHC).....	218
7.3.2 Expression of ALCAM gene transcript in pancreatic cancer.....	222
7.3.3 Levels of ALCAM transcript and clinical outcomes.....	224
7.3.4 ALCAM expression and link to tumour vascular embolism.....	227
7.3.5 Creation of cell models from pancreatic cancer cells and vascular endothelial cells that differentially express ALCAM and the impact on pancreatic cancer cells.....	228

7.3.6 ALCAM expression in endothelial cells and in pancreatic cancer cells, the impact on tumour-endothelial interactions.....	230
7.4 Discussion	232
CHAPTER-8 General discussion	235
8.1 Aims of the study	236
8.2 Clinical implication of ALCAM in endocrine related cancer (breast and pituitary tumour)	237
8.3 Signalling events underlying ALCAM and their involvement in hormonal receptor related bone metastasis of breast cancer.....	238
8.4 Effect of ALCAM on chemotherapy drugs of breast cancer	242
8.5 ALCAM in non-endocrine related cancer (pancreatic cancer)	243
8.6 Conclusion and future work.....	246
Chapter-9 References.....	249

List of Figures and Tables

Chapter 1

Figure 1.1 Incidence rates (per 100,000) of bone metastasis from 2010 to 2015.....	6
Figure 1.2 Median survival of patients with identified bone metastases, stratified by primary cancer sites.....	7
Figure 1.3 Breast cancer in UK, average number of new cases per year and age-specific incidence rates per 100,000 females, 2016-2018.....	14
Figure 1.4 Breast Cancer in UK, age-standardised one-, five- and ten-year survival, 2013-2017.....	14
Figure 1.5 Overview of breast cancer haematological metastases.....	17
Figure 1.6 ALCAM protein and domain structure.....	29
Figure 1.7 Protein interactions between ALCAM and other prospective molecules in a cell-cell adhesion context.....	32
Figure 1.8 Pancreatic cancer in UK, average number of new cases per year and age-specific incidence rates per 100,000 population.....	51
Figure 1.9 Pancreatic Cancer, age-standardised one-, five- and ten-year net survival.....	52
Table 1.1 First signs of bone metastases.....	6
Table 1.2 Distribution of bone metastases in breast cancer by sites.....	8
Table 1.3 Distribution of bone metastases in prostate cancer by sites.....	9
Table 1.4 Sites of breast cancer metastasis.....	17
Table 1.5 The major findings in all cancer types relate to ALCAM.....	39

Chapter 2

Figure 2.1 Inverted microscope (Leica Microsystems (UK) Ltd, Milton Keynes, UK).....	59
Figure 2.2 Class II laminar flow tissue culture hood (Wolf Laboratories, York, UK).....	60
Figure 2.3 Schematic of stuffer control and ALCAM overexpression plasmid.....	61
Figure 2.4 Schematic of scramble control and ALCAM shRNA knockdown plasmids.....	62
Figure 2.5 IMPLEN Nanophotometer (Geneflow Ltd., Litchfield, UK).....	64
Figure 2.6 SimpliAmp thermocycler (Fisher Scientific UK, Leicestershire, UK).....	68
Figure 2.7 Syngene U: Genius 3 System (Geneflow Ltd., Litchfield, UK).....	69
Figure 2.8 StepOne Plus qPCR system (Fisher Scientific UK, Leicestershire, UK).....	71
Figure 2.9 OmniPAGE VS10 vertical electrophoresis system (Wolf Laboratories, York, UK) ..	74
Figure 2.10 SD10 SemiDry Maxi System blotting unit (Wolf Laboratories, York, UK).....	75
Figure 2.11 G:BOX Chemi XRQ protein detection system (Syngene, Cambridge, UK).....	77
Figure 2.12 ELx800 spectrophotometer (Bio-Tek, Wolf laboratories, York, UK).....	82

Figure 2.13 EVOS FL2 Auto Imaging System (Life technologies, CA, USA)	84
Figure 2.14 Electric cell-substrate impedance sensing system	86
Figure 2.15 Families of protein targets for the KAM-900P antibody microarray.....	87
Figure 2.16 Detection method used in KAM-900 Antibody Microarray	88
Figure 2.17 A representative scanned image of KAM antibody microarray chips.....	89
Table 2.1 Materials and reagents used in the study.	55
Table 2.2 Clinical features of breast cancer cell lines.....	58
Table 2.3 Primers used in the current study	67
Table 2.4 Acrylamide gel preparation	73

Chapter 3

Figure 3.1 ALCAM staining in normal and breast cancer tissues.	97
Figure 3.2 ROC curve of ALCAM transcript level and patients with bone metastasis without bone metastasis.	100
Figure 3.3 Survival analysis of ALCAM and breast cancer patients (TCGA database).	105
Figure 3.4 Overall survival of low ALCAM level and high ALCAM level group, stratified by ER status.	108
Figure 3.5 Disease-free survival of low ALCAM level and high ALCAM level group, stratified by ER status.	109
Figure 3.6 Overall survival of low ALCAM level and high ALCAM level group in breast cancer patients, stratified by HER-2 status.	110
Figure 3.7 Disease-free survival of low ALCAM level and high ALCAM level group in breast cancer patients, stratified by HER-2 status.	111
Figure 3.8 Overall survival of low ALCAM level and high ALCAM level group in breast cancer patients, stratified by triple negative and non-triple negative breast cancer subtypes.	112
Figure 3.9 Disease-free survival of low ALCAM level and high ALCAM level group in breast cancer patients, stratified by triple negative and non-triple negative breast cancer subtypes.	113
Figure 3.10 Survival analysis of ER-positive and ER-negative breast cancer patients with ALCAM transcript levels.	116
Figure 3.11 Survival analysis of HER2 positive and HER2 negative breast cancer patients with ALCAM transcript levels.	117
Figure 3.12 Survival analysis of triple-negative and triple-positive breast cancer patients with ALCAM transcript levels.	118
Figure 3.13 Survival analysis of basal, Luminal-A and Liminal-B breast cancer patients with ALCAM transcript levels.	119
Figure 3.14 Circulating ALCAM in patients with breast cancer, grouped by the nodal status.	121
Figure 3.15 Circulating ALCAM in patients with breast cancer, grouped by tumour grade.	121
Figure 3.16 Circulating ALCAM in patients with breast cancer, grouped by ER status.	122

Figure 3.17 Circulating ALCAM in patients with breast cancer, grouped by PGR status.	122
Figure 3.18 Circulating ALCAM in patients with breast cancer, grouped by HER2 status. ...	123
Figure 3.19 Circulating ALCAM in patients with breast cancer, grouped by HR status.	123
Figure 3.20 Circulating ALCAM in patients with breast cancer, grouped by clinical outcome.	124
Figure 3.21 Circulating ALCAM in patients with breast cancer, grouped by tumour staging.	124
Figure 3.22 ALCAM transcript level of different tumour sizes.	126
Figure 3.23 ALCAM transcript level in the no destruction of sella turcica group and the with destruction of sella turcica group.....	127
Figure 3.24 ALCAM transcript level in the no invasion cavernous sinus group and the invaded cavernous sinus group.....	127
Figure 3.25 ALCAM transcript levels in different types of pituitary tumour.....	128
Table 3.1 ALCAM staining of breast cancer TMA.	99
Table 3.2 Comparison of ALCAM expression in different HR status	102
Table 3.3 The correlation between HR status and the bone metastasis of breast cancer ...	103

Chapter 4

Figure 4.1 PCR results demonstrating ALCAM expression in different breast cancer cell lines.	135
Figure 4.2 PCR image of ALCAM transcription in transfected breast cancer cell lines.	136
Figure 4.3 Semiquantitative analyse of PCR results of ALCAM transcript level in transfected MCF-7, MDA-MB-361 and MDA-231 cells.....	136
Figure 4.4 Western blotting image of ALCAM expression in transfected breast cancer cell lines.	137
Figure 4.5 Semiquantitative analyse of Western blotting results of ALCAM expression level in transfected MCF-7, MDA-MB-361 and MDA-MB-231 cells.....	137
Figure 4.6 Cell growth assay of MCF-7 cells with and without BME.	138
Figure 4.7 Cell growth assay of MDA-MB-361 cells with and without BME.	139
Figure 4.8 Cell growth assay of MDA-MB-231 cells with and without BME.	139

Chapter 5

Figure 5.1 Microarray images of the KAM900P for the present study	147
Figure 5.2 Proteins activated in both MDA-MB-231 and MCF-7 cells following knocking down ALCAM	151
Figure 5.3 Proteins inhibited in both MDA-MB-231 and MCF-7 cells following knocking down ALCAM	153
Figure 5.4 Proteins activated in MDA-MB-231 cells but inhibited in MCF-7 cells following knocking down ALCAM.....	155

Figure 5.5 Proteins inhibited in MDA-MB-231 but activated in MCF-7 cells following knocking down ALCAM	155
Figure 5.6 Contrast regulated protein kinases in MDA-MB-231 cells following ALCAM knockdown.	159
Figure 5.7 Contrast regulated protein kinases in MCF-7 cells following ALCAM knockdown.	160
Figure 5.8 Events of contrast regulated kinases in cellular events	163
Figure 5.9 MET as an example of those changes after ALCAM knockdown in MDA-MB-231 and MCF7 cells.....	164
Figure 5.10 Western blotting results of ALCAM immunoprecipitation in MCF-7 (top), MDA-MB-361 and MDA-MB-231 cell lines.	166
Figure 5.11 Western blotting results of MET immunoprecipitation in MCF-7, MDA-MB-361 and MDA-MB-231 cell lines.....	167
Figure 5.12 The cell adhesion of control and ALCAM-KD group as detected by ECIS.....	170
Figure 5.13 The cell adhesion of control and ALCAM-KD group with HGF as detected by ECIS	174
Figure 5.14 The cell adhesion of control and ALCAM-KD group with MET inhibitor as detected by ECIS.....	176
Figure 5.15 The cell adhesion of control and ALCAM-KD group with HGF and MET inhibitor as detected by ECIS.....	178
Figure 5.16 The cell adhesion of control and ALCAM-KD group with Neratinib as detected by ECIS	181
Figure 5.17 The cell adhesion of control and ALCAM-KD group with ROCK inhibitor as detected by ECIS.....	184
Table 5.1 Protein/kinase upregulated in both MDA-MB-231 and MCF-7 cells following ALCAM knockdown.....	149
Table 5.2 Protein/kinase downregulated in both MDA-MB-231 and MCF-7 cells following ALCAM knockdown.....	151
Table 5.3 Protein/kinase pattern contrasted in MDA-MB-231 and MCF-7 cells following ALCAM knockdown.....	156
Table 5.4 Top twenty-five signalling pathways based on contrast regulated protein kinases in MDA-MB-231 and MCF-7 cells after ALCAM knockdown	162
Table 5.5 Concentrations of the reagents used in ECIS.....	168
Table 5.6 Comparison of electrical impedance between Control and ALCAM-KD groups in ECIS assays.....	171
Table 5.7 Comparison of electrical impedance between Control and ALCAM-KD groups with HGF in ECIS assays	175
Table 5.8 Comparison of electrical impedance between Control and ALCAM-KD groups with MET inhibitor in ECIS assays	177
Table 5.9 Comparison of electrical impedance between Control and ALCAM-KD groups with HGF and MET inhibitor in ECIS assays	179

Table 5.10 Comparison of electrical impedance between Control and ALCAM-KD group with Neratinib in ECIS assays.....	182
Table 5.11 Comparison of electrical impedance between Control and ALCAM-KD group with ROCK inhibitor in ECIS assays	185

Chapter 6

Figure 6.1 Effect of ALCAM knockdown on chemotherapy drug toxicity in MCF-7 cells without BME.....	195
Figure 6.2 Effect of ALCAM knockdown on chemotherapy drug toxicity in MCF-7 cells with BME.	195
Figure 6.3 Effect of ALCAM knockdown on chemotherapy drug toxicity in MDA-MB-361 cells without BME.....	196
Figure 6.4 Effect of ALCAM knockdown on chemotherapy drug toxicity in MDA-MB-361 cells with BME.	196
Figure 6.5 Effect of ALCAM knockdown on chemotherapy drug toxicity in MDA-MB-231 cells without BME.....	197
Figure 6.6 Effect of ALCAM knockdown on chemotherapy drug toxicity in MDA-MB-231 cells with BME.	197
Figure 6.7 Expression of ALCAM in different subgroups of breast cancer patients who received endocrine therapies.....	199
Figure 6.8 Expression of ALCAM in different subgroups of breast cancer patients who received anti-HER2 therapy.....	200
Figure 6.9 Expression of ALCAM in different subgroups of breast cancer patients who received any chemotherapy.....	203
Figure 6.10 Expression of ALCAM in different subgroups of breast cancer patients who received Taxane treatment.	204
Figure 6.11 Expression of ALCAM in different subgroups of breast cancer patients who received Anthracycline treatment.	205
Figure 6.12 ALCAM expression and patient’s response to chemotherapeutics in different molecular subtypes of breast cancer.	207
Table 6.1 IC50 of chemotherapy drugs in control and ALCAM knockdown groups of different breast cancer cell lines, without BME.	194
Table 6.2 IC50 of chemotherapy drugs in control and ALCAM knockdown group of different breast cancer cell lines, with BME.....	194

Chapter 7

Figure 7.1 ALCAM staining in normal and pancreatic cancer tissues.....	219
Figure 7.2 Levels of expression of ALCAM transcript in normal and pancreatic cancer tissues and expression of ALCAM in those who died and remain alive	222

Figure 7.3 ALCAM levels and overall survival of the patients by Kaplan-Meier survival analysis	225
Figure 7.4 TCGA dataset of ALCAM transcription expression in human pancreatic cancer detected by RNAseq for overall survival and relapse free survival.....	226
Figure 7.5 ALCAM protein expression in pancreatic adenocarcinoma from the protein atlas dataset.....	226
Figure 7.6 Levels of ALCAM in tumour without and with microvessel emboli and the relationship between the presence of microvessel embolism and survival of the patients	227
Figure 7.7 Creation of pancreatic and endothelial cell models.....	229
Figure 7.8 ALCAM differential expression, cell adhesiveness and migration as detected by ECIS	229
Figure 7.9 The interaction between pancreatic cancer cells and endothelial cells	231
Figure 7.10 ECIS based analyses of tumour-endothelial cell interaction.....	232
Table 7.1 ALCAM staining score in pancreatic tissues	221
Table 7.2 Expression of ALCAM transcript and the clinical and pathological groupings	223
Table 7.3 ALCAM expression, clinical and pathological factors in relationship with the survival of the patients.....	225

Chapter 8

Figure 8.1 Possible molecular mechanism between ALCAM and MET interaction	242
Figure 8.2 The correlation between DNA methylation and mRNA of ALCAM in breast cancer and pancreatic cancer from the TCGA pan-cancer cohort.....	246

List of Abbreviations

Abbreviation	Full name
ACTH	Adrenocorticotrophic hormone
ADAM17	A Disintegrin and Metalloprotease 17
AF-1	Activation function 1
AF-2	Activation function 2
ALCAM	Activated leukocyte cell adhesion molecule
AR	Androgen receptor
ATCC	American Type Culture Collection
AUC	Area under curve
BME	Bone matrix extract
BSA	Bovine serum albumin
BSS	Balanced Salt Solution
CAMs	Cell adhesion molecules
CDK2	Cyclin dependent kinase 2
CytD	Cytochalasin D
DBD	DNA-binding domain
DEPC	Diethylpyrocarbonate
Dil	1,1'-dioctadecyl-3,3,3',3'-tetramethylindocarbocyanine perchlorate
DMEM	Dubecco's Modified Eagle Medium
DMSF	Distant metastasis free survival
DMSO	Dimethyl Sulphoxide
ECIS	Electric cell-substrate impedance sensing
EGF	Epidermal Growth Factor
ELISA	Enzyme Linked Immunosorbent Assay
EMMPRIN	Extracellular matrix metalloproteinase inducer
ER	Oestrogen receptor
ERK	Extracellular signal-regulated kinase
ERM	Ezrin-Moesin-Radixin
ET-1	Endothelin 1
FCS	Foetal calf serum
FSH	Follicle-stimulating hormone
GH	Growth hormone
HER	Human Epidermal growth factor Receptor
HGF	Hepatocyte growth factor
HIF1A	Hypoxia-inducible factor 1-alpha
HR	Hormone receptor
ICAMs	Intercellular cell adhesion molecules
IgSF	Immunoglobulin superfamily
IHC	Immunohistochemistry
ILT3	Immunoglobulin-like transcript 3
IP	Immunoprecipitation
L1CAM	L1 cell adhesion molecule
LatA	Latrunculin A

LB	Lysogeny Broth
LBD	COOH-terminal ligand-binding domain
LH	Luteinizing hormone
MCAM	Melanoma Cell Adhesion Molecule
MEK	Mitogen-activated protein kinase kinase
MEN1	Multiple Endocrine Neoplasia I
MET	Mesenchymal-epithelial transition factor
MMP14	Matrix Metalloprotease 14
NCAM	Neural cell adhesion molecules
NCOR1	Nuclear receptor co-repressor 1
NPTN-β	Neuroplastin-β
NRs	Nuclear receptors
NTD	NH ₂ -terminal domain
OPG	Osteoprotegerin
OS	Overall survival
PBS	Phosphate buffered saline
PCR	Polymerase Chain Reaction
PDPL	Podoplanin
PNET	Pancreatic neuroendocrine tumours
PPS	Post progression survival
PR	Progesterone Receptor
PRA	Progesterone receptor isoform B
PRB	Progesterone receptor isoform B
PRKCB1	Protein-serine kinase C beta 1
PRKCH	Protein-serine kinase C eta
PRL	Prolactin
PSA	Prostate specific antigen
PTH	Parathyroid hormone
PTH1R	Parathyroid Hormone 1 Receptor
PTHrP	Parathyroid hormone-related protein
PTTG1	Pituitary Tumour-Transforming Gene 1 Protein
PVDF	polyvinylidene fluoride
qPCR	Quantitative Polymerase Chain Reaction
RANK	Receptor activator of nuclear factor kappa B
RANKL	Receptor activator of nuclear factor kappa B ligand
RFS	Relapse free survival
ROCK	Rho-associated, coiled-coil-containing protein kinase
sALCAM	Soluble ALCAM
SCC	Squamous Cell Carcinoma
scFv	Single chain antibody fragment
SDS	Sodium dodecyl sulfate
SDS-PAGE	Sodium dodecyl sulfate-polyacrylamide gel electrophoresis
SEM	Standard Error of Mean
SF	Scatter factor
shRNA	Short interfering RNA
SNPs	Single nucleotide polymorphisms
TCGA	Cancer Genome Atlas
TLR4	Toll-like receptor 4

TNBC	Triple negative breast cancer
TNF	Tumour necrosis factor
TNF α	Tumour necrosis factor α
TrkB	BDNF/NT3/4/5 receptor- tyrosine kinase
TSH	Thyroid stimulating hormone
UC	Universal Container
VCAMs	Vascular cell adhesion molecule 1
VEGFR3	Vascular endothelial growth factor receptor-protein-tyrosine kinase 3

Chapter-1

Introduction

1.1 Bone biology and histology

Bone consists of cortical bone and cancellous bone, and is relatively rich in blood vessels, lymphatic vessels and nerves. There are 206 bones in the human body, each of which has a certain form and function. Like other organs of the body, the growth and development of bone is regulated by a variety of factors in the internal and external environment of the body, such as neurological, endocrine, nutritional, disease, genetic factors and geographical conditions. These factors, regulated by the nervous system, influence the metabolism of bone, causing it to undergo constant morphological and structural changes (Florencio-Silva et al. 2015).

Osteoblasts, osteoclasts, and osteocytes are the three primary types of cells in our bones that work together to keep the shape, strength, and health of our bones. When bone lesions appear, osteoblasts heal them by producing new bone. The osteoclasts restructure the bone by breaking down any additional bone structure made by the osteoblasts. Osteoblasts are trapped in the bone as it forms and become a component of the structure. They are known as osteocytes and are responsible for maintaining bone structure (Tresguerres et al. 2020).

1.2 Malignancies of the skeleton

A bone tumour is a neoplastic growth of tissue in bone. Any tumour originating in the bone, whether primary, secondary or metastatic, is termed a bone tumour (Esposito et al. 2018). Abnormal growths in the bone can be either benign (non-cancerous) or malignant (cancerous), with malignant bone tumours being the majority. Malignant bone tumours, often leading to devastating clinical outcomes, are generally classified into two types: primary and metastatic bone tumours, both

of which can lead to constant pain, pathological fractures, and neurological disorders (when involving the spine and spinal cord).

1.2.1 Primary bone tumours

Primary bone tumours are a group of carcinomas originating from bone and cartilage. They account for approximately 0.5% to 1% of all malignant tumours in the body and are one of the rarest types of cancer. The common types of primary bone malignancies include osteosarcoma, Ewing's sarcoma, chondrosarcoma and chordoma (Simpson and Brown 2018). Osteosarcoma, originating mainly from bone forming osteoblasts, is the most common type and mainly seen in children. Ewing's sarcoma and chordoma are derived from the soft tissues of bones and are more common in adults. The treatment of primary malignant bone tumours consists of surgical resection, chemotherapy and radiotherapy, but even now the current clinical prognosis of patients with primary bone tumours is generally poor. A large retrospective cohort study of osteosarcoma based on autopsy (Smeland et al. 2019) showed that the 3-year and 5-year event free survival were at 59% and 54% respectively and the 3-year and 5-year overall survival were 79% and 71%.

1.2.2 Metastatic bone tumours

Tumours from other tissues or organs in the human body, that have migrated to the bone via the blood or lymphatic system, are known as metastatic bone tumours, which is the most common type of malignant bone disease (Esposito et al. 2018). Bone is one of the most frequent sites of metastasis. In the 'seed and soil' theory of metastasis (Paget 1889), bone and bone environment is one of the most suited 'soil' environment for cancer cells to spread. In certain types of cancer, such as advanced

breast cancer or advanced prostate cancer, up to 70% of patients develop bone metastases, which leads to a decrease in life quality and poor clinical outcomes (Selvaggi and Scagliotti 2005).

According to the principal mechanism of interference with normal bone remodelling, bone metastasis can be divided into three kinds: osteolytic, which are characterized by destruction of normal bone; osteoblastic, which are characterized by deposition of new bone, or mixed with both osteolytic and osteoblastic lesions coexisting. Osteolytic bone metastasis can be seen in breast cancer, renal clear cell carcinoma and non-small cell lung cancer and osteoblastic bone metastases mainly exist in prostate cancer and small cell lung cancer.

1.2.2.1 Prevalence

The main prevalent area of bone metastasis is the spine, especially the thoracolumbar segment, followed by the pelvis, femur and proximal humerus. There is an obvious trend that bone metastasis is more likely to involve the axial skeleton, which contains more red bone marrow. That means the axial skeleton has a rich source of blood supply and variety of extracellular matrix, providing a reliable structural basis for bone metastasis.

Bone metastasis is commonly derived from primary tumours of breast, prostate, lung, kidney, bladder and thyroid origin (Coleman 2006). In some cases, metastases appear at an early stage and in some special cases, metastatic bone tumours are diagnosed though the primary lesion is difficult or impossible to find. The first signs of bone metastases including bone pain (78.7%), neurological symptoms (12.7%) and pathological fracture (8.0%), etc. (Debois 2002) (Table 1.1).

The overall incidence and incidence rated by primary cancer sites were listed in Figure 1.1 (Ryan et al. 2022). In patients with advanced metastatic disease, the relative incidence of bone metastasis by types of tumour are: 65-75% in breast cancer; 65-75% in prostate cancer; 30-40% in lung cancer; 40% in bladder; 60% in thyroid; 20-25% in renal cell carcinoma and 14-45% in melanoma (Macedo *et al.* 2017). At autopsy, breast cancer (67% (47-85%)), prostate cancer (66% (33%-85%)), thyroid cancers (38% (28%-60%)), lung cancers (36% (30%-55%)) and kidney cancers (34% (33%-40%)) make up the top five primary cancers with most frequently occurring bone metastatic lesions. In the presence of bone metastasis, the median survival is described to range between 10 to 12 weeks depending on the nature of the cohorts, type of data collection, and the way that bone metastases were diagnosed and the origin of primary tumours (Migliorini *et al.* 2020). The median survival time from diagnosis of bone metastases from breast cancer and prostate cancer is longer and can be measured in years, while the median survival time from the diagnosis of advanced lung cancer is normally measured in a small number of months (Jiang et al. 2020) (Figure 1.2).

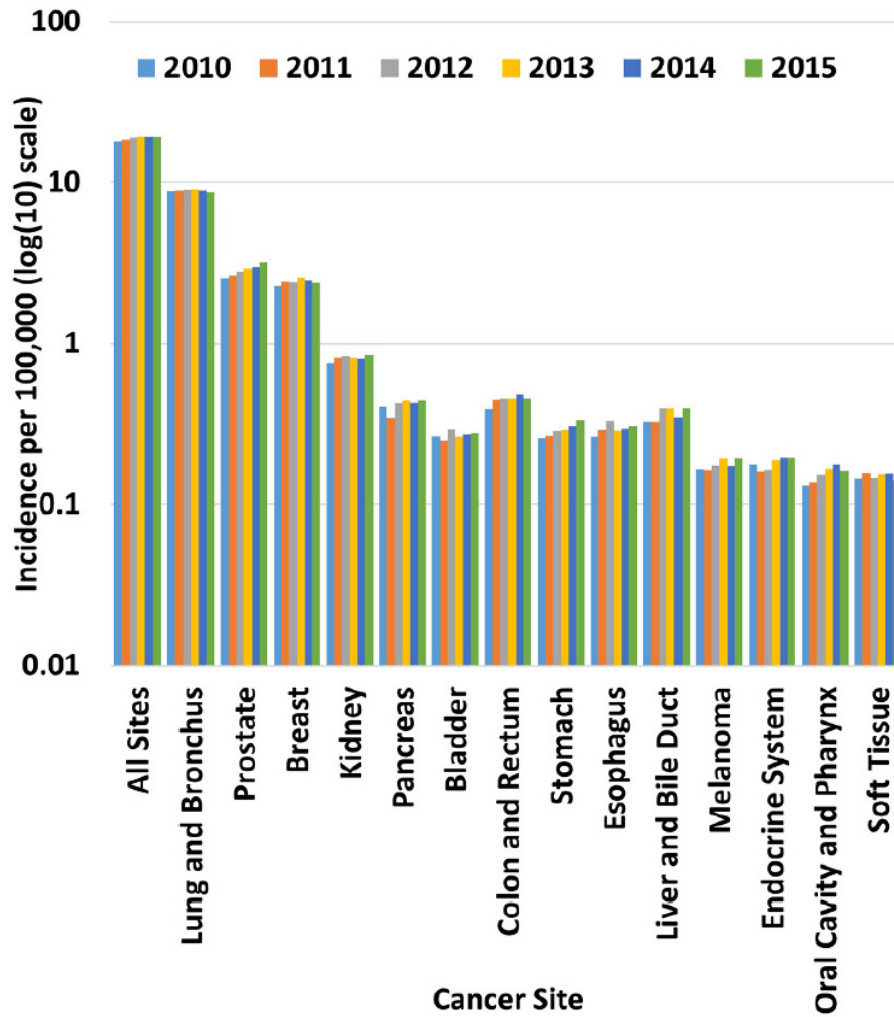


Figure 1.1 Incidence rates (per 100,000) of bone metastasis from 2010 to 2015 (Ryan et al. 2022). The x-axis represents the primary cancer site; The y-axis represents the incidence rate per 100,000 people on the log (10) scale. The bar colours depict year of diagnosis.

Table 1.1 First signs of bone metastases (Debois 2002).

Symptom	Percentage%
Bone pain	78.7
Neurological Symptoms (epidural compression and other)	12.7
Pathological Fracture	8.0
Tumour forming	3.3
Hypercalcemia	2.9
General condition (Anaemia)	0.5
No Symptoms	
Found during staging	8.0
At follow-up	3.7

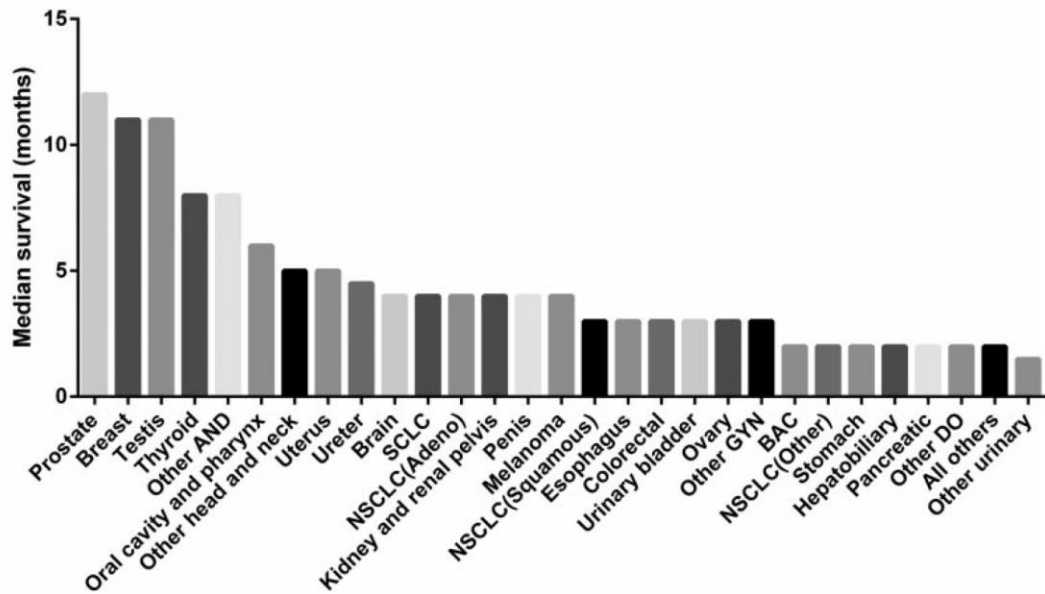


Figure 1.2 Median survival of patients with identified bone metastases, stratified by primary cancer sites (Jiang et al. 2020).

1.2.2.2 Aetiology

Although highly interesting and important from a clinical point of view, the underlying reasons for skeletal metastasis are, so far, largely unclear. It is particularly less clear why some tumours, namely breast and prostate cancers, more readily develop bone metastasis, whereas others are less active. However, the regulation of bone remodelling is important for the understanding of metastatic bone disease since cancers commonly utilize these pathways to facilitate tumour development while causing bone damage. In a healthy skeleton, remodelling occurs regularly to maintain calcium homeostasis, repair bone injury, replace ageing bone and adapt to new external stresses (Esposito et al. 2018).

To grow in such dense tissue like the skeleton, metastatic lesions must have the ability to promote bone resorption thereby creating room for tumour cell entry and expansion. Normal bone remodelling involves a well-coordinated activity of the interaction between osteoblasts and osteoclasts. In general, tumour cells exert their

effects on the balance between osteoblasts and osteoclasts to invade the skeleton system.

1.2.2.3 Metastatic bone tumours from breast cancer

Bone metastasis is a commonly seen clinical and pathological change in breast cancer patients. In nearly 70% of breast cancer patients, bone metastasis can be detected according to autopsy results (Coleman 2006). The lesions can be osteolytic (67.2%), osteoblastic (12.1%) or mixed (20.7%), although the majority of them are of osteolytic in nature. The distribution pattern of bone metastases in breast cancer was outlined in Table 1.2. Notably, recent study (Pareek et al. 2019) demonstrated that the bone metastasis in breast cancer strongly correlate with various breast cancer receptors, mainly designated by ER, PR, and HER2.

Table 1.2 Distribution of bone metastases in breast cancer by sites (Debois 2002).

Sites	Percentage (%)
Skull	8.8
Femur	10.0
Clavicula-Ribs	12.2
Cervical spine	9.5
Thoracal spine	24.4
Lumbar spine	13.7
Pelvis	14.2
Others	7.2

1.2.2.4 Metastatic bone tumours from prostate cancer

Prostate cancer is the most prevalent cancer in males. Approximately 10% of prostate cancer patients have bone metastases, and the incidence of bone metastases at post mortem examination in prostate cancer patients is 68% (Coleman 2006). The distribution Pattern of bone metastases in prostate cancer was outlined

in Table 1.3 (Debois 2002). The clinical course of patients with metastatic prostate cancer can be relatively long, and several prognostic factors have been identified, including tumour grade, performance status, haemoglobin, prostate-specific antigen, serum lactate dehydrogenase and alkaline phosphatase. The bone metastasis of prostate cancer is predominantly osteoblastic (84%), with mixed (12%) and osteolytic (4%) accounting for only a small proportion. Only a small percentage of these lesions develop pathological fractures, however, if fractures do occur the prognosis of patients is generally poor (Coleman 2006).

Table 1.3 Distribution of bone metastases in prostate cancer by sites. Bone metastases occurred at autopsy in 70 to 80% of the cases (Debois 2002).

Sites	Percentage in the entire cohort (%)
Skull	2.0
Cervical Spine	0.4
Thoracic Spine	5
Lumbar Spine	14.7
Spine, unspecified	13.9
Sternum	9.2
Ribs	11.4
Scapula	0.4
Ilium	5.1
Pubis	2.6
Ischium	0.4
Sacrum	1.5
Pelvis	2.9
Femur	5
Arm	0.9

1.2.2.5 Metastatic bone tumours from lung cancer

The incidence of bone metastases at post mortem examination in lung cancer is 36% (Coleman 2006). Lesions have a 3:1 osteolytic to osteoblastic distribution and, unusually, lesions more often occur in the peripheries. The overall prognosis for patients suffering from lung cancers is poor and so therapeutic approaches to lesions are more geared towards palliation.

1.2.2.6 Molecular and cellular aspect of bone metastasis

1.2.2.6.1 RANK and RANKL

RANKL (Receptor activator of nuclear factor kappa B ligand) is a member of the tumour necrosis factor (TNF) family. To promote osteoclast differentiation, RANKL interacts with its receptor RANK (Receptor activator of nuclear factor kappa B) which is expressed on osteoclast precursor cells. Excess RANKL signal leads to abnormal osteoclast activation in bone metastasis (Okamoto 2021). Bone remodelling occurs when osteoclast precursors are attracted to the site of bone damage or ageing in response to chemokine signals. After differentiation and fusion, the osteoclast precursors convert to multinucleated osteoclasts which exert osteolytic functions. The combination of RANK and RANKL can promote the fusion, differentiation and maturation of osteoclast precursors. RANK is expressed on the surface of osteoblast precursors and osteoclasts, and RANKL is mainly produced by osteoblasts, osteoclasts, bone marrow stromal cells and activated T cells. RANKL has two existing forms: transmembrane protein type (expressed on the cell surface) and free polypeptide type (formed by the shedding of extracellular regions of transmembrane

type at amino acid 140 or 145), both of which can be functional, while the transmembrane protein is biologically more active. Osteoprotegerin (OPG) functions as a receptor for RANKL, balancing osteoclastogenesis and osteolysis by binding to RANKL, blocking RANKL signalling and preventing RANKL from binding to RANK (Nakashima *et al.* 2011). In breast cancer, RANK has been shown to correlate with mammary progenitor populations and promote breast tumour formation (Pellegrini *et al.* 2013). The overexpression of RANK in breast cancer cells led to greater bone colonisation and growth (Blake *et al.* 2014). Study by Owen and colleagues (Owen *et al.* 2016) showed that low levels of RANK expression in breast cancer cell lines was related to reduced ability of cell adhesion, migration and invasion. In conclusion, RANKL, its receptor RANK and its naturally secreted decoy OPG play vital roles in the progression of cancer progression as well as bone metastasis.

1.2.2.6.2 PTHrP and PTH1R (PTHR)

PTHrP (Parathyroid hormone-related protein) is an active molecule secreted by a variety of tissue cells and shows a wide range of biological effects. Its gene structure is similar to parathyroid hormone (PTH), thus can also activate parathyroid hormone receptors. PTHrP binds to its receptor PTH1R (Parathyroid Hormone 1 Receptor, or PTHR) and exerts its biological effects by activating various intracellular signalling pathways. The known biological effects of PTHrP and PTH1R are diverse: involved in the growth and development of the skeletal system; regulating differentiation, proliferation and apoptosis of osteoblasts; balancing bone repair and bone remodelling. In terms of its role in cancer progression, PTHrP has been shown to be released from tumour cells outside the parathyroid gland. PTHrP is able to upregulate the expression of RANKL in the precursors of osteoblast, whilst suppress the expression of OPG, resulting in the activation of osteoclast. Previous study has

indicated that PTHrP acts as an oncogenic factor, participates in the progression and metastasis of different types of tumours, particularly breast cancer (Henderson *et al.* 2006). Although PTHrP has been shown to have osteolytic effect, its expression in prostate cancer, which usually develops osteoblastic bone metastasis, is also relatively high. One possible explanation is that PTHrP is able to produce osteoblastic fragments by its interaction with prostate-specific antigen (PSA). The strong sequence homology of N-terminal fragments of PTHrP and Endothelin 1 (ET-1) has also shown to be responsible for the osteoblastic pathological changes in prostate cancer with high PTHrP expression (Ye et al. 2011).

1.3. Breast cancer

Breast cancer is the most common type of malignant breast disease, accounting for approximately 98% of the total. Glandular epithelial cells in the breast are mutated under a variety of oncogenic factors, resulting in uncontrolled cell proliferation, which in turn leads to the development of breast cancer. As a result of the altered biological behaviour of cancer cells, breast cancer cells present a disorderly and unrestricted malignant proliferation, destroying the surrounding normal tissues and damaging the normal cells (Winters et al. 2017).

Breast cells lose their normal cellular characteristics after mutation. The tissue structures and cell connections are disturbed so that the cancer cells can easily detach and spread throughout the body via blood or lymphatic systems, resulting in early systemic metastasis. Metastases to vital organs throughout the body such as lung, brain and bone are direct threats to life, making breast cancer a serious life-threatening malignant tumour.

1.3.1 Prevalence of breast cancer

Breast cancer is one of the major diseases affecting women's health worldwide. In females, breast cancer is the most frequently diagnosed cancer and the most frequent cause of death from cancer in most regions of the world. It accounts for 24.5% of newly diagnosed cancer cases and 15.5% of cancer-related deaths according to recent global research (Ferlay *et al.* 2021). There were approximately 2.26 million newly diagnosed breast cancer cases in 2020. Approximately 1 in 8 women will be diagnosed with invasive breast cancer in their lifetime and 1 in 39 women would have died from breast cancer in 2020 and, for the first time, breast cancer has overtaken lung cancer as the worldwide highest occurring cancer in men and women combined. Thus, research on breast cancer is essential and vital worldwide.

Breast cancer strikes mostly postmenopausal females (Figure 1.3), with only 20% of incidences occurring in female patients under the age of 50. Tumours in younger patients, on the other hand, usually have a worse prognosis due to their aggressive malignant character. Females under the age of 40 were found to have had a worse 5-year cancer-specific survival rate, while females over the age of 40 have higher overall recurrence rates. When compared to female patients aged 60 years or older, younger patients often present with more aggressive cancers and more commonly with lymph node involvement (Wang *et al.* 2018). The one-, five- and ten-year survival of breast cancer in UK were shown in Figure 1.4

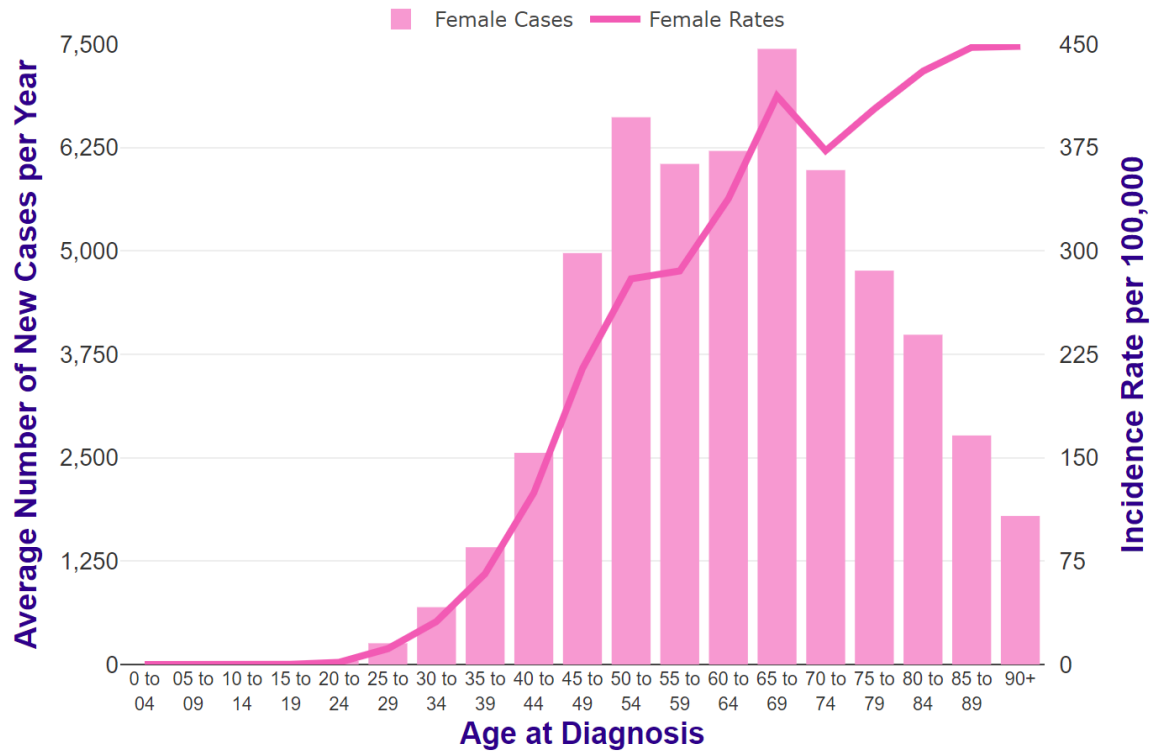


Figure 1.3 Breast cancer in UK, average number of new cases per year and age-specific incidence rates per 100,000 females, 2016-2018. Source: <https://www.cancerresearchuk.org>.

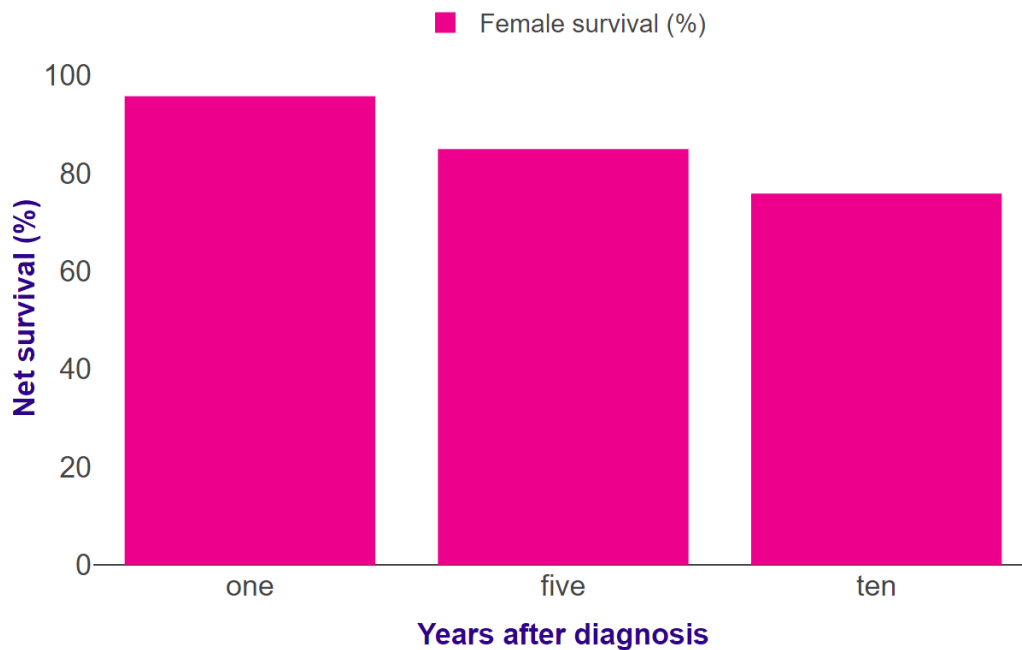


Figure 1.4 Breast Cancer in UK, age-standardised one-, five- and ten-year survival, 2013-2017. Source: www.cancerresearchuk.org.

1.3.2 Metastasis of breast cancer

Nearly 6% of patients have metastatic disease at the time of diagnosis, and 20% to 50% of patients diagnosed with primary breast cancer will have metastatic disease later, according to the estimate of researchers (Weigelt et al. 2005). The most common sites of breast cancer metastasis are bone, lung and liver (Table 1.4). Despite significant advancements in research and clinical management, current treatment strategies for breast cancer metastasis still rely heavily on the use of systemic cytotoxic agents, which worsen the patient's quality of life due to severe side effects and have limited long-term efficacy in many cases.

There are three key routes of breast cancer metastasis: local invasion, lymphatic metastasis and hematogenous metastasis (Tahara et al. 2019). Localised lesions in breast cancer, although not usually life-threatening, can influence the choice of clinical treatment and prognosis. Normally local invasion is the earliest process of tumour dissemination to occur and can affect lymphatic and hematogenous metastasis. This is because as the tumour progresses locally, the chance of lymphatic and haematological metastases increases. The abundant supply of blood and good lymphatic circulation of the breast tissue makes lymphatic and hematogenous metastasis very easy to occur, when abnormal proliferation of breast cancer cells disturbs adjacent normal tissue structures and growth (Figure 1.5). When lymphatic and hematogenous metastasis occurs, it means that breast cancer changes from a localized disease, which can be treated with surgery and other localized treatment, to a systemic disease, which needs comprehensive treatment.

The poor prognosis of breast cancer metastasis is not only due to the size of tumours and the number of cancer cells. In fact, some patients do not develop cancer metastasis even though their localised lesions were quite large, while some patients

developed distant metastasis with a smaller localized lesion. Even when the former had more cancer cells than the latter, the prognosis was far better. It is obvious that the change of malignant degree of breast cancer cells is the main reason for poorer prognosis when the metastasis of breast cancer occurs. The invasion and progression of cancer cells require a variety of aberrant cellular pathways. The cancer cells which do not contain these specific aberrations cannot metastasise and colonise distant organs, even though they possess a certain degree of malignant features. Hence, cancer cells that transfer to distant organs tend to have less differentiation and a higher grade of malignancy, making treatment of such metastatic breast cancers extremely hard to control and eradicate (Fornetti et al. 2018).

Table 1.4 Sites of breast cancer metastasis (Debois 2002).

Sites	Percentage (%)
Bone	16.9
Lung	10.9
Liver	4.2
Distant Lymph node	2.3
Brain	0.8
Other sites	0.2
Multiple sites	5.8

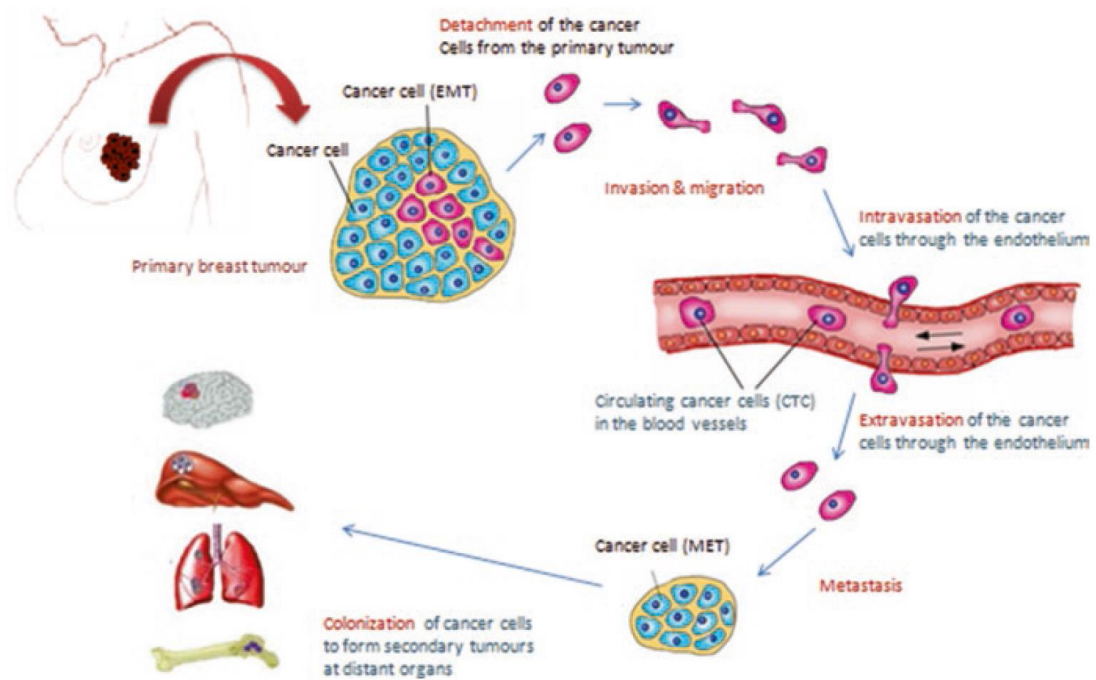


Figure 1.5 Overview of breast cancer haematological metastases (Tahara et al. 2019). EMT: Epithelial - Mesenchymal Transition; MET: Mesenchymal - Epithelial Transition.

1.3.3 Metastatic spread of breast cancer to bones

Bone metastasis is a commonly seen clinical and pathological change in breast cancer patients. According to research, the supraclavicular lymph nodes and bones are the most common sites of breast cancer metastasis, followed by lung and liver. In post mortem examination, 73% of breast cancer patients have evidence of metastatic bone disease (Coleman 2006). Cancers with a long natural history, such as breast cancer, present a high prevalence of bone metastasis, thus constituting one of the major causes of morbidity. The prognosis after the development of bone metastases in breast cancer is considerably better than that after a recurrence in visceral sites (Tahara et al. 2019).

1.3.4 Hormone dependency of breast cancer

Breast cancer has a strong link to the human endocrine system. As previously described, there is a clear difference in the incidence and prognosis of breast cancer between postmenopausal females and younger females, which has a critical correlation with their different hormone levels.

Breast tumours are categorized into four subtypes (Luminal A, Luminal B, HER-2 overexpression type and triple-negative type) based on the expression of specific protein markers: oestrogen receptor α (ER α), progesterone receptor (PR) and HER2 (Gradishar et al. 2020). The classification has been shown to be of high prognostic and predictive significance for breast cancer. Approximately 75% of all patients with invasive breast cancer present with hormone receptor-positive (HR-positive) disease and almost all of these female patients should be offered adjuvant endocrine therapy.

1.3.4.1 Oestrogen Receptor (ER)

The Oestrogen Receptor (ER) is a member of the steroid hormone superfamily of nuclear receptors (NRs). In 1986, Greene *et al.*, (Greene et al. 1986) cloned the oestrogen receptor, the first protein receptor binding with oestrogen, now known as ER α . In 1996, Kuiper *et al.*, (Kuiper et al. 1996) discovered and cloned a new kind of ER, which was subsequently named as ER β . ER α and ER β genes are located on different chromosomes, at 6q25.1 and 14q23.2 respectively. ER α and ER β share the same protein structure, and both consist of three separated but interacting functional domains: the NH₂-terminal domain (NTD), the DNA-binding domain (DBD) and the COOH-terminal ligand-binding domain (LBD). Structurally, the receptor core consists of a central DNA-binding domain (DBD) flanked by transactivation function domains AF-1 and AF-2. Except for the NTD region, these two receptors share a high level of amino acid sequence identity. The NTD contains an activation function (AF-1) domain associated with ligand-independent transcriptional activation of target genes. The NTD has only 16% similarity between ER α and ER β , whereas the DBD has very high similarity between ER α and ER β , with 97% amino acid identity. The LBD region of ER α and ER β share 59% amino acid sequence identity, but the two subtypes differ only slightly in their molecular structure, and this minor structural difference allows them to bind different ligands. LBD contains the ligand-dependent activation function 2 (AF-2), which is critical to ligand binding and dimerisation of the receptor. Co-repressors nuclear receptor co-repressor 1 (NCOR1) and other coactivators have the ability to interact with ligand-bound ER α or ER β to affect ER activation or activate ER repressor genes (Stashi et al. 2014).

ER signalling is a complex biological pathway driven by oestrogen that is exploited by breast cancer cells and enables cell proliferation, survival, apoptosis, invasion, and angiogenesis. AF-1 can be activated by oestrogen-independent mechanisms (often termed ligand-independent), while AF-2 responses have a stricter dependence on the presence of ER ligands (ligand-dependent) (Huang *et al.* 2014).

The varied and complex pathways of ER regulation have significant clinical implications in the prognosis and treatment of breast cancer. Oestrogen can regulate c-Myc and cyclinD1 function and expression, activating the cell cycle protein cyclin dependent kinase 2 (CDK2) complex and accelerating the cell cycle from G1 to S phase in mammary epithelial cells (Frasor *et al.* 2003). It is therefore demonstrated that ER can promote the expression of oestrogen target genes, leading to the development of oestrogen-stimulated breast cancer.

ER α and ER β have different correlations toward breast cancer progression. ER α is expressed in no more than 10% of normal breast epithelium but accounts for approximately 50% to 80% expression in breast tumours (Huang *et al.* 2014). Transcription of the human ER α gene occurs at least 2 different promoters; the distal promoter (promoter B) located 2 kb upstream of the proximal promoter (promoter A). Transcription resulting from the 2 promoters differs only in the non-coding region at the 5' end, and both types of ER α mRNA encode the same protein. The total expression level of ER α mRNA and the transcript level of promoter B are closely related to the amount of ER α protein in human primary breast cancer. Among them, promoter B leads to overexpression of ER α protein, indicating that promoter B plays a facilitating role in regulating ER α gene expression in breast cancer (Tanimoto *et al.* 1999). However, the expression levels of ER β are higher in normal breast tissue than in tumour tissue. In tumour tissues, the levels decrease as tumour progresses. Interestingly, normal mammary tissues with increased levels of ER β are suggested to

have a decreased risk of developing into breast cancer (Huang et al. 2014). In recent studies, ER β was described as a dominant negative regulator of ER signalling, as ER β was demonstrated to suppress ER α transcription by forming heterodimers with ER α (Matthews and Gustafsson 2003). These studies collectively suggest that ER β may play a tumour suppression role and the loss of ER β may promote the development of breast cancer.

1.3.4.2 Androgen Receptor (AR)

The Androgen Receptor (AR), similar to the ER and PR, belongs to the family of steroid receptors and has high levels of expression in breast cancer. AR is a ligand-activated transcription factor. When ligands are lacking, AR is found mainly in the cytoplasm and in the inactivated state in combination with heat shock proteins. When ligands are abundant, AR dissociates with heat shock proteins, combining with its ligand and entering into the cell nucleus to play a regulatory role in cell proliferation and migration.

Many studies have demonstrated that AR and ER have a strong correlation with breast cancer. Grober *et al.*, (Grober et al. 2011) have shown that AR suppressed breast cancer cell progression and proliferation by up-regulated expression levels of ER β . Gene-chip analysis (Need et al. 2012) showed that the binding sites of the transcription factors of AR and ER α were located within 10 kb of the other receptor, and enrichment of androgen response elements in ER α -binding sites was observed and vice versa, indicating a clear association between the two. Hence, researchers generally believe that the expression levels of AR have clear implications in breast cancer patients. A meta-analysis of 17000 cases demonstrated that AR expression was a positive indicator of disease-free survival and overall survival and AR

expression enhanced prognosis in the ER (+) subtype in breast cancer patients (Bozovic-Spasojevic *et al.* 2017).

1.3.4.3 Progesterone Receptor (PR)

Progesterone Receptor (PR) is also a member of the steroid hormone superfamily of nuclear receptors, composed of a C-terminal ligand-binding domain (LBD), a central DNA-binding domain and an amino-terminal domain (NTD) (Cenciarini and Proietti 2019). A large number of studies have demonstrated that multiple PR subtypes exist in the human body. Two of the most important subtypes are isoform B (PRB), of higher molecular weight and isoform A (PRA), which is a truncated protein that lacks the first 161 amino acids (Elizalde and Proietti 2012). PR functions not only as a critical regulator of transcription but also activates rapid signal transduction pathways, many of which are involved in pro-proliferative signalling in the breast.

PR is induced by the interaction between ER and E2 (oestrogen) and the synthesis of PR must be initiated by oestrogen. Thus, the expression of PR, together with ER, is a significant prognosis factor and are parameters for predicting the effect of hormone therapy in breast cancer patients (Yip and Rhodes 2014).

1.3.4.4 Human Epidermal growth factor Receptor (HER) family

The Human Epidermal growth factor Receptor (HER) family is a group of transmembrane proteins that have roles in regulating cell differentiation, apoptosis, metastasis, proliferation and angiogenesis (Krishnamurti and Silverman 2014). It contains four members, namely EGFR (HER1, c-erbB1), HER2 (erbB2, HER2/neu), HER3 (erbB3) and HER4 (erbB4). All HER family members consist of an extracellular

ligand binding domain, a transmembrane region and a tyrosine kinase intracellular catalytic domain. Among all the family members, HER3 has impaired kinase activity and HER2 has no direct ligand. Hence compared with homodimerization, heterodimerization is a more significant molecular mechanism in the activation of all ErbB receptors in response to ligands (Wang 2017). To date, there are two main downstream pathways related to the regulation of the HER family, phosphatidylinositol 3-kinase/protein kinase B (PI3K/AKT) pathway, which is associated with cell survival and proliferation, and the RAS/RAF/MAPK pathway, which is associated with cell growth and differentiation. Therefore, the abnormal expression of the HER family can affect tumour survival, proliferation, local invasion and remote metastasis.

HER2 positive breast cancer refers to a breast cancer subtype that has erbB2 proto-oncogene amplification or HER2 transmembrane receptor protein over-expression. The over-expression of HER2 occurs in 13–15% of breast cancers and is associated with aggressive tumour behaviour and poor prognosis (Harbeck et al. 2019). Substantial evidence indicates that HER2 positive breast cancer generally has the following characteristics: faster growth; enhanced metastatic potential; lower responsiveness to conventional treatment; increased potential to relapse after conventional treatment; poorer patient prognosis and shorter median survival compared to HER2 negative breast cancer patients.

Currently, there are three main categories of targeted therapies for HER2-positive breast cancer that are commonly used in clinical practice: Tyrosine kinase inhibitor (Lapatinib, Neratinib), Monoclonal antibody (Trastuzumab) and Antibody-drug conjugate (Trastuzumab emtansine) (Loibl and Gianni 2017). Lapatinib and Neratinib are representative drugs of Tyrosine kinase inhibitor, which exert a therapeutic role by inhibiting the intracellular tyrosine kinase role of HER2 or multiple HER family

members. The monoclonal antibody drug, Trastuzumab, can inhibit ligand-independent HER2 and HER3 signalling and might trigger antibody-dependent cellular cytotoxicity. Trastuzumab emtansine is an antibody-drug conjugate that links trastuzumab to a potent microtubule inhibitor. The advent of anti-HER2 therapy has greatly improved the prognosis of HER2 positive breast cancer patients and has increasingly made HER2 the focus of breast cancer research.

1.3.5 Treatment of breast cancer

Breast cancer is one of the major malignant diseases threatening the health of the female population worldwide. Thus, clinicians and researchers are continually researching new methods, agents and biological targets to develop better and novel treatments for breast cancer. Normally, breast cancer can be treated with surgery, radiation, or drugs (chemotherapy, hormonal therapy and anti-HER2 therapy). The choice of treatment options should depend on the individual circumstances of patients.

1.3.6 Intervention in bone metastasis

As discussed previously, Bone metastasis is a commonly seen clinical and pathological change in breast cancer patients. Nearly 70% of breast cancer patients can be found to have detectable bone metastasis according to autopsy results (Coleman 2006). Due to its high prevalence, it is important to develop therapies that can reduce patient morbidity and arrest disease progression. Currently, there are several types of non-surgical therapies available to treat metastatic lesions of breast cancer including:

- A. Endocrine therapy: In premenopausal patients, endocrine therapy is frequently combined with ovarian ablation. Unless the clinician considers that a more radical medication response is required, this is usually the first-line treatment of choice for patients with hormone-sensitive diseases.
- B. Chemotherapy: Used in patients with ER negative and hormone-resistant tumours. Various medications (anthracyclines, taxanes, vinorelbine, capecitabine, etc.) may be beneficial, but the choice of treatment is influenced by various circumstances. The argument about sequential versus combination therapy is still going on.
- C. Radiotherapy: Radiotherapy has an essential role in pain management, particularly in the treatment of severe painful bone metastases, as well as in the treatment of spinal cord compression, stridor, and superior vena caval obstruction in emergencies.
- D. Trastuzumab: Trastuzumab may benefit patients with HER2 positive breast cancer, even if they have received it in the adjuvant setting. However, it is still unclear how to proceed with further treatment for the patients who have failed in trastuzumab treatment.
- E. Bisphosphonates: Bisphosphonates are used in patients with lytic bone metastases to reduce the risk of pathological fracture, future skeletal events and improving pain control (O'Carrigan et al. 2017).
- F. RANKL inhibitors: Denosumab is a humanised monoclonal antibody of RANKL. It has been shown to significantly reduce the skeleton-related events in various cancer types, especially breast cancer (Simatou et al. 2020).

Apart from non-surgical treatment, surgical treatment is also an important method when breast cancer patients develop bone metastasis. Most patients with bone metastases have a short-term prognosis, so intervention should be limited to cases in which the patient is expected to recover rapidly following surgery or when

fractures could possibly cause substantial morbidity. In addition, long bone fractures, vital joint damage (hip or knee) and spinal cord occupancy, which may lead to spinal cord or peripheral nerve compression, all require surgery in a limited duration (Cleazardin et al. 2021).

1.4 ALCAM/CD166

The formation, organisation, and maintenance of multicellular tissues is mediated in large part through cell adhesion molecules (CAMs), which consist of 4 main families: the cadherin family (including type-I, Type-II cadherins and desmosomal cadherins); the integrin family (a large family with each member made up of an alpha- and a beta-subunit); selectins and the immunoglobulin superfamily (IgSF) (von Lersner *et al.* 2019).

IgSF proteins utilise Ig-like domains to mediate calcium-independent cell-cell adhesion, identifying both homophilic and heterophilic ligands. Members of the IgSF superfamily are more diverse in their functions and their cell/tissue distributions. They are transmembrane proteins that act not only as cell adhesion receptors but also as mediators in intracellular signalling pathways. Well documented members include VCAMs (vascular cell adhesion molecule-1, or CD106), ICAMs (intercellular cell adhesion molecules, ICAM1 (CD54), ICAM2 (CD102), ICAM3 (CD50), ICAM4 (CD242), ICAM5 (TLCN), L1CAM (L1 cell adhesion molecule, or CD171), the Nectin family (Nectin-1 (CD111 or PVRL1), Nectin-2 (CD112 or PVRL2), Nectin-3 (CD113 or PVRL3) and Nectin-4 (PVRL4), NCAM (neural cell adhesion molecules, NCAM1 (CD56) and NCAM2) and ALCAM (CD166). Compared with cadherin-mediated or integrin-mediated adhesion, the interaction of IgSF in cell adhesion seems weaker and is independent of the presence of extracellular calcium, but it appears to contribute

more to the regulation of tissue formation and maintenance and to some more specific function of the cells, namely the Nectin family in the formation of tight junctions.

Activated leukocyte cell adhesion molecule (ALCAM), also known as CD166, belongs to the immunoglobulin superfamily of cell adhesion molecules and is widely expressed in various human tissues, including central and peripheral nervous systems, haematopoiesis, sensory organs and endothelial and epithelial linings. Numerous studies have demonstrated that ALCAM plays an important role in the progression of malignant diseases and tumour metastasis (Yang et al. 2021b). Hence, Studies on ALCAM and its related molecules have great importance to cancer research.

1.4.1 Discovery

The orthologs of ALCAM in fish and chicken were reported primarily in the early 90s (Tanaka *et al.* 1991; Paschke *et al.* 1992). After that ALCAM was discovered in 1995 as a ligand for CD6 (Bowen *et al.* 1995; Patel *et al.* 1995). By transfecting CHO cells (Chinese hamster ovary cells) to overexpress CD6, it was found that a protein, subsequently named ALCAM, supported the thymocyte-thymic epithelial interactions (Bowen *et al.* 1995). Uchida *et al.* (Uchida *et al.* 1997) identified a haematopoietic cell antigen, which is identical to ALCAM, on haemopoietic stem cells and myeloid progenitors two years later. The protein subsequently purified was found to be a protein of 65kDa or 100-105kDa, as the result of glycosylation, and is a type I membrane protein. An interacting partner for CD6 and highly expressed in activated leukocytes, the protein has since been found to be expressed ubiquitously in the majority of cell and tissue types.

1.4.2 Molecular and genetic structure

The single-copy gene encoding human ALCAM is located on chromosome 3q13.1-q13, is over 200 kb in length and produces a mature transcript of 4.5 kb, containing 16 exons (average length 110 bp; range 39–220 bp), of which the first and last possess extended untranslated 5'- and 3'-region respectively (Swart *et al.* 2005). From recent research, we understand that the promoter elements NF- κ B, Ets, Sp1, and a GC-box upstream of the translation start site, regulate ALCAM gene expression (von Lersner *et al.* 2019). However, the complete mechanism through which ALCAM is regulated still needs to be fully elucidated.

ALCAM is a type I transmembrane glycoprotein that belongs to the immunoglobulin superfamily (IgSF) and has a molecular mass of 100-105 kDa. It contains one short cytoplasmic tail (34 amino acids), one transmembrane region (22 amino acids) and an extracellular domain (500 amino acids) which is composed of five Ig-like domains: two amino-terminal membrane distal variable-(V)-domains and three membrane-proximal constant-(C)-domains (V1V2C1C2C3) (Figure 1.6). The consecutive Ig domains V1V2C1C2C3, which mediate homophilic ALCAM–ALCAM interactions and heterophilic interactions, is the characteristic sequence of this subgroup of cell adhesion molecules and may constitute key information for molecular targeting (van Kempen *et al.* 2001).

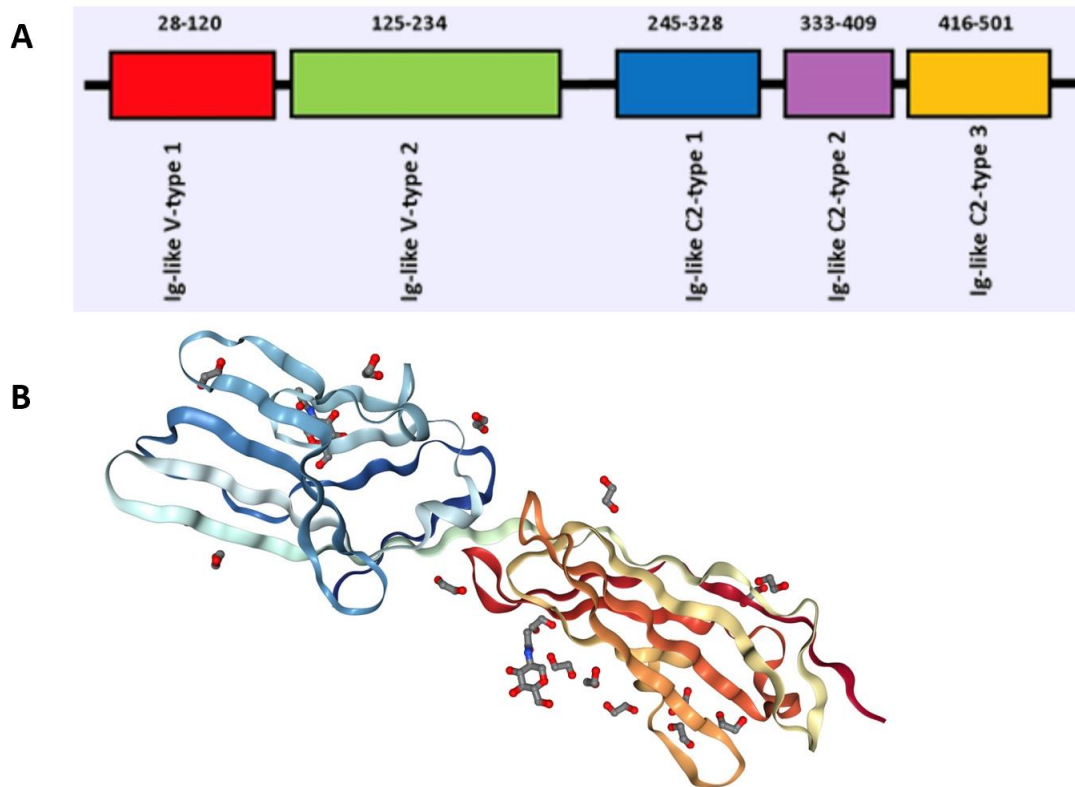


Figure 1.6 ALCAM protein and domain structure. A: ALCAM domain structure (<http://atlasgeneticsoncology.org>). B: Two membrane distal IgSF domains

1.4.3 Protein interactions

ALCAM regulates cell adhesion through heterotypic and homotypic interactions. Heterotypic ALCAM-mediated cell adhesion refers to the extracellular interplay between ALCAM and its protein partners. CD6 is a major binding partner of ALCAM. It belongs to a type of lymphocyte antigen, which are mostly expressed by T cells and a subset of B cells. Starling *et al.*, (Starling *et al.* 1996) demonstrated that the ALCAM binding site was located in the membrane-proximal scavenger receptor cysteine-rich (SRCR) domain of CD6. Additionally, work conducted by Bowen *et al.*, (Bowen *et al.* 1997) demonstrated that the N-terminal Ig-like domain D1 was necessary and sufficient to achieve specific binding to mouse CD6, using a series of amino-terminally truncated human ALCAM constructs. The addition of other domains to the D1 domain had an augmenting effect on the binding for the extracellular part of ALCAM and CD6. Other work by this group (Bowen *et al.* 1996) also reported that the N-terminal Ig-like domain of ALCAM bound to the membrane-proximal SRCR domain of CD6 with a 1:1 stoichiometry. In addition, a study showed that L1CAM is another binding partner of ALCAM, in that L1CAM interacts with ALCAM on endothelial cells as part of tumour-endothelial interactions in breast cancer (Dippel *et al.* 2013). Certain integrin family members were also able to interact with ALCAM as detected by *in vitro* assays in colorectal cancer (Bartolome *et al.* 2020).

Homotypic interaction in ALCAM-mediated cell adhesion refers to the extracellular interplay between ALCAM itself. Work by van Kempen *et al.*, (van Kempen *et al.* 2001), using a series of amino-terminally truncated ALCAM mutants, showed that the presence of the NH₂-terminal V-type Ig domain D1 was required for both these cell-cell interactions, which was later defined as a major ligand-binding domain. The membrane-proximal C-type domains C2C3, however, did not engage in homotypic ligand-binding. Thus, extracellular ALCAM-ALCAM ligand-binding itself was

exclusively mediated by the binding of opposing amino-terminal D1 domains. However, these results did not imply that the membrane-proximal domains C2C3 were not associated with ALCAM-mediated cell adhesion completely. These C-type Ig domains were postulated to be involved in the formation of cis-homo-oligomers at the cell surface, via lateral oligomerization in analogy with other IgSF molecules.

Both heterotypic and homotypic interactions are essential to ALCAM-mediated cell adhesion, though the heterotypic interaction appears to be stronger and more stable than homotypic interaction. Hassan *et al.*, (Hassan *et al.* 2004) reported that the homotypic interaction of ALCAM has around 100-fold lower affinity than the heterotypic interaction between ALCAM and CD6. Te Riet *et al.*, (Te Riet *et al.* 2007) showed that the ALCAM-CD6 bond is significantly more stable under mechanical stress compared to the ALCAM-ALCAM bond. Specifically, the interactions between ALCAM-CD6 showed higher tensile strengths and significantly smaller reactive compliance under single-cell force spectroscopy, indicating that this heterotypical bond was more resistant to applied force, therefore more stable under mechanical stress than the homotypical bond. The amino acids and domains, that are required for the CD6-ALCAM heterotypic interaction, have been fully identified by Chappell in 2015 (Chappell *et al.* 2015), in that it has been shown that the heterotypic CD6-ALCAM interaction and the homotypic ALCAM-ALCAM interaction share a region of the N-terminal domain of the ALCAM protein, also that the CD6-ALCAM interaction appears to be stronger than the ALCAM-ALCAM interaction. Thus, the CD6-ALCAM interaction is in competition with the ALCAM-ALCAM interaction of the two opposing cells and that formation of CD6-ALCAM binding is likely to be at the cost of the ALCAM-ALCAM bindings.

The interactions between ALCAM and other protein partners are summarised in Figure 1.7.

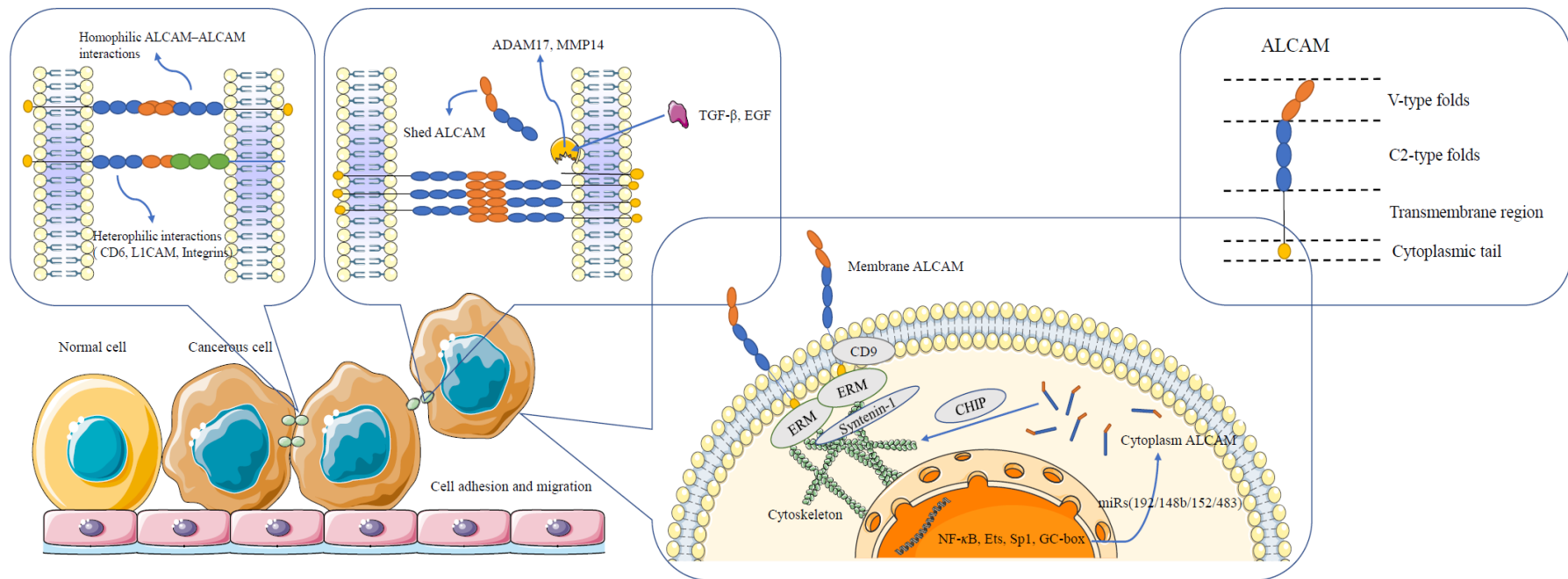


Figure 1.7 Protein interactions between ALCAM and other prospective molecules in a cell-cell adhesion context (Yang et al. 2021b). ALCAM regulates cell adhesion through both heterotypic and homotypic interactions (left); ALCAM contains one short cytoplasmic, one transmembrane region and an extracellular domain (right); ALCAM is anchored to the actin cytoskeleton via the ERM protein family and Syntenin-1 (middle).

1.4.4 Molecular signalling

The mechanisms involved in the molecular signalling of ALCAM are still not completely elucidated. However, there is a consensus that the actin cytoskeleton plays a significant role in ALCAM intracellular regulation. Nelissen *et al.*, (Nelissen *et al.* 2000) discovered that the actin cytoskeleton inhibitors, cytochalasin D (CytD) and latrunculin A (LatA), significantly enhanced ALCAM-specific cell adhesion. Actin cytoskeleton inhibitors CytD could increase the lateral mobility of ALCAM molecules and cluster them at the cell surface, which resulted in the enhancement of ALCAM-mediated cell adhesion. Another group (Tudor *et al.* 2014) have shown that ALCAM lacked a direct actin-binding site. The group demonstrated that ALCAM's cytoplasmic tail could be connected to the cytoskeleton via the scaffolding proteins syntenin-1 and ezrin, with the heterotypic interaction between ALCAM and CD6 further strengthening and augmenting this connection.

Ruma *et al.*, (Ruma *et al.* 2016) have shown that ALCAM acts as the 'soil' sensor receptor for S100A8/A9/S100P, which in turn serve as 'Soil Signals'. Other 'Soil Sensor Receptors' include MCAM (Melanoma cell adhesion molecule), NPTN- β (Neuroplastin- β), EMMPRIN (Extracellular matrix metalloproteinase inducer) and TLR4 (Toll-like receptor 4). Cell surface ALCAM is endocytosed for recycling by the expressing cell, and this requires endophilin, particularly the A3 isoform (Renard *et al.* 2020). The endocytosis process of ALCAM appears to be driven by galactin-8 of extracellular origin. The authors have further demonstrated that blocking endophilin-A3 markedly increased the amount of cell surface ALCAM and ALCAM mediated cell adhesiveness (Renard *et al.* 2020).

King and colleagues (King *et al.* 2010) have reported that the change of ALCAM in cancer may be a methylation regulated mechanism, which involved NK κ B (p65) and

other cis active elements, in the promoter region of the ALCAM gene. The study has also shown that the methylation could be partly reverted by 5-aza-2-deoxycytidine.

1.4.5 ALCAM in cancer

Cell adhesion is an integral part of the formation, proliferation and progression of cancer tissue. There is considerable evidence to implicate ALCAM in the regulation of tumour cell growth and the impact of ALCAM expression on prognosis seems to vary among different tumour types.

The importance of ALCAM/CD166 in leukaemia has been well demonstrated, in that blocking CD166-ILT3 (Immunoglobulin-like transcript 3) interactions with an ILT3-Fc dramatically reduced the proliferation and growth of leukaemia cells and increased the survival of tumour bearing mice (in both H9 and JURKAT models) (Xu *et al.* 2018). ALCAM's well-established binding partner CD6 has been proposed to be a useful therapeutic target in conditions such as autoimmune diseases (Pinto and Carmo 2013). It was recently established that CD318 is also a binding partner for CD6 (Enyindah-Asonye *et al.* 2017). This is very interesting in that ALCAM/CD166 is widely expressed in haematopoietic cells and also widely existed in almost all other cell types, whereas CD318 is only expressed in non-haematopoietic cells, indicating a way for cell-specific targeting. L1CAM on breast cancer cells has been shown to interact with ALCAM on endothelial cells as part of tumour-endothelial interactions (Dippel *et al.* 2013). 14-3-3 ζ and 14-3-3 σ have also been also shown to be interacting partner proteins for ALCAM in oral Squamous Cell Carcinoma (SCC) cells (Sawhney *et al.* 2009).

The role of ALCAM in cancer cells has been an interesting matter of debate. For example, in Benzo[a]pyrene transformed human bronchial epithelial cells, 16HBE,

knockdown of ALCAM rendered the cells with lower growth and colony formation but, in contrast with an increase in cellular migration and lung metastasis *in vivo* (Li *et al.* 2020). Similarly in lung cancer cells, knocking down ALCAM resulted in a reduction in adhesion to a matrix in both quiescent and stress conditions (Munsterberg *et al.* 2020).

It is clear from the literature that ALCAM plays a significant through complex role in cancer development and progression. This role is often seen as differential between and within different cancer types and may partially arise from its cellular localisation. Significant research has focused on ALCAM's role in cancer over the past several decades, with the goal of realising the potential of this molecule in therapeutic design or as a novel predictive factor.

1.4.5.1 Breast cancer

Ihnen *et al.*, (Ihnen *et al.* 2010b), utilising clinical materials from 481 breast tumours, discovered that a subset of the patients with low-ALCAM/high-Osteopontin/ER-negative/HER2-negative tumours had markedly shorter disease-free and overall survival and that the combination is a strong independent prognostic indicator. In a different study by Hein *et al.*, (Hein *et al.* 2011), it was shown that ALCAM staining in primary breast tumours was associated with nodal involvement and the presence of cancer cells in bone marrow, and indeed with both shorter overall and recurrence-free survival of the patients. In a comprehensive and classical immunohistochemical analysis (Tissue microarray (TMA)) of 2197 breast tumour cases, Burandt and colleagues (Burandt *et al.* 2014) analysed the ALCAM staining pattern and found that almost all the histological types of breast cancer cases had strong ALCAM staining, except the medullary subtype with over 40% showing

negative staining. High grade, ER-positive and PR-positive tumours tended to be more intensive in staining and the loss of ALCAM staining was significantly associated with shorter overall and disease-free survival of the patients.

Polymorphisms have been reported as a frequent feature in breast cancer. In a cohort of 1,033 breast cancer samples (compared with 1,116 controls) from a Chinese study, two single nucleotide polymorphisms (SNPs) were identified, rs6437585 (C/T) and rs11559013 (A/G) (Zhou *et al.* 2011). The presence of rs6437585 in the patients had a significantly raised risk of developing breast cancer, a phenomenon that was not seen with rs11559013.

Breast tumour tissues with high levels of ALCAM gene methylation showed low levels of ALCAM transcript expression (Jeong *et al.* 2018). Levels of ALCAM transcripts in tumours were found to be positively correlated with some of the inflammatory markers, including TNF α , IL4 and NF- κ B. HER2 positive high-grade tumours had high ALCAM proteins and Luminal-A tumours had the strongest ALCAM staining.

Tan *et al.*, (Tan *et al.* 2014) compared the pattern of ALCAM staining in two different ethnic populations of US patients, namely tumours from African Americans (n=78) and Caucasian Americans (n=95). Although relatively small in the study cohorts, it did reveal a rather different staining pattern between the two groups, namely tumours from African American patients were four-times as likely to have reduced or loss of membranous ALCAM staining compared to the Caucasian patients, yet the cytoplasmic staining of ALCAM did not differ between the two groups. The relationship between ALCAM with other clinical and pathological factors otherwise similarly impacted both ethnic groups.

1.4.5.2 Prostate cancer

In a large TMA cohort (n=2,390) (Minner *et al.* 2011), ALCAM was found to be largely membranous stained in prostate cancers (69.9%). Cytoplasmic staining was seen as a unique pattern in a small proportion of the samples. However, the authors noted that it was the membrane staining in prostate tumours that were associated with favourable clinical, pathological and outcomes of the patients. Instead, cytoplasmic staining did not appear to have significant meaning. Prostate cancer cells in prostate tumour tissues displayed both membrane and cytoplasm staining. Hansen *et al.*, (Hansen *et al.* 2014) used a TCGA database and reported a significant link between high levels of ALCAM transcript with shorter survival of the patients and that the high levels are particularly seen in metastatic prostate cancers.

1.4.5.3 Thyroid cancer

Miccichè *et al.*, (Micciche *et al.* 2011) has reported in early findings that in thyroid cancer ALCAM is expressed at both membrane and cytoplasmic regions and is able to be shed from the cell membrane. The study conducted by Chaker *et al.*, (Chaker *et al.* 2013) showed that total ALCAM in poorly differential thyroid tumours was markedly lower than in those with well or moderately differentiated tumours and the reduction was associated with distant metastasis and shortened survival (6 years vs 13.7 years, low vs high cytoplasmic ALCAM respectively).

1.4.5.4 Colorectal cancer

There have been some extensive studies on the role of ALCAM in colorectal cancer. This was reflected in a subsequent meta-analysis (Zhang *et al.* 2017), revealing that high levels of ALCAM in colorectal cancer are associated with poor overall survival, nodal status, tumour grade and distant metastasis.

1.4.5.5 Other cancer types

The regulatory role of ALCAM in cancer progression and metastasis has caught the attention of numerous studies. The research results over the years have shown that the effect of ALCAM seems to be strikingly different among different cancer types. Hence, major findings in all cancer types are summarised in Table 1.5 to gain a more comprehensive understanding of correlation between ALCAM and cancer progression (Yang *et al.* 2021b).

Table 1.5 The major findings in all cancer types relate to ALCAM.

Tumour Type	Study methods	Findings	References
Colorectal cancer	IHC (n=111)	Both membranous and cytoplasmic staining of ALCAM is seen in colon cancer tissues. However, membranous ALCAM is linked with shortened survival of the patients.	(Weichert <i>et al.</i> 2004)
	IHC (n=9)	Tumour tissues showed highly stained ALCAM compared with normal tissues.	(Bartolome <i>et al.</i> 2020)
	IHC and PCR (n=58)	ALCAM positive staining is seen in 43%. ALCAM negative tumours had greater incidence of lymph node metastasis, a link greatly increased when there is concurrent KRAS mutation.	(Ribeiro <i>et al.</i> 2016)
	IHC (n=112)	High levels of ALCAM were associated with longer recurrence free survival	(Sim <i>et al.</i> 2014)
	Gene expression (n=250), IHC (n=105) and ELISA (n=91)	ALCAM is highly expression in tumour tissues and is linked to shorter survival of the patients	(Hansen <i>et al.</i> 2014)
	IHC (n=299)	More than 70% and 60% of primary and secondary tumours stained positive for ALCAM respectively. Positive ALCAM staining is a positive prognostic factor for the patients.	(Tachezy <i>et al.</i> 2012b)
	Gene array (n=64)	ALCAM transcripts were significantly raised in colorectal tissues compared with normal tissues	(Badic <i>et al.</i> 2019)
	Germline polymorphism of peripheral blood of patients who resisted to 5FU therapies (n=234)	Polymorphisms of ALCAM, along with LGR5, CD44 and ALDH1, form an independent signature in predicting the time to recurrence of patients with colon cancer who received 5-FU based chemotherapies	(Gerger <i>et al.</i> 2011)
	IHC (n=458)	ALCAM alone had no significant correlations with clinical and pathological factors but a combined expression pattern with EpCAM had clinical significance.	(Kalantari <i>et al.</i> 2022)
Metastatic liver tumours from colorectal cancer	Paired primary and secondary (n=9 pairs), IHC	Stepwise increase of ALCAM protein from normal colorectal tissues, primary colorectal cancer tissues to metastatic liver tumours.	(Bartolome <i>et al.</i> 2020)
Oesophageal SCC	IHC (n=299)	High levels of ALCAM in primary tumours associated with recurrence free and overall survival of the patients.	(Tachezy <i>et al.</i> 2012a)
	IHC (n=65)	ALCAM staining seen in 87.69% of tumours, compared with negative in control normal tissues. ALCAM linked to tumour grade, TNM staining and survival	(Zhang <i>et al.</i> 2020)

Laryngeal, Head and Neck SCC	IHC and RNAseq (n=44) and gene array.	High levels of staining associated with shorter survival of the patients	(Nicolau-Neto <i>et al.</i> 2020)
	IHC (n=400)	Seventy per cent of HNSCC tumours stained positive for ALCAM, including 12.4% membranous, 40.1% cytoplasmic and mixed membranous/cytoplasmic in 17.9%	(Clauditz <i>et al.</i> 2014)
	HNSCC IHC (n=96)	Patients with high levels of ALCAM staining in HNSCC (n=96) had shorter survival. Primary HNSCC (n=68) had significantly lower ALCAM staining than the recurrent HNSCC (n=36) tumours.	(Yan <i>et al.</i> 2013)
Oral dysplasia and cancer	Oral SCC, IHC (n=105)	ALCAM total and cytoplasmic staining was correlated with loss of membranous E-cadherin and beta-catenin in oral squamous cell carcinoma. ALCAM expression, together with cytoplasmic/nucleus beta-catenin, is an indicator of nodal metastasis and late stage of tumours.	(Kaur <i>et al.</i> 2013)
Oral melanoma	IHC (n=35)	ALCAM positive staining in oral melanoma is associated with vascular invasion.	(Bologna <i>et al.</i> 2013)
Non-small cell lung cancer and brain metastasis	IHC (n=143 comprised of 51 primary NSCLC, 15 metastatic nodes and 76 metastatic brain tumours)	Metastatic brain tumours and metastatic lymph nodes stained higher ALCAM, compared with primary NSCLC. High staining in NSCLC and in metastatic brain lesions associated with poor survival.	(Munsterberg <i>et al.</i> 2020)
Breast cancer	IHC and QPCR (n=120, tumour and 32 normal)	ALCAM transcript expression was lower in tumours with lymph node metastasis compared to those without. ALCAM levels were also lower in high grade/TNM stage compared to lower stage/grade samples. ALCAM levels were lower in those with poorer outcomes.	(King <i>et al.</i> 2004)
	IHC (n=162)	Cytoplasmic staining of ALCAM is associated with shorten survival, nodal status and early recurrence.	(Burkhardt <i>et al.</i> 2006)
	Protein blotting (n=160) and gene microarray	Neither protein nor mRNA expressions are linked to pathological factor. Protein ALCAM is seen more in ER positive tumours. Patients with high levels of ALCAM when receiving chemotherapy, has a better clinical survival, but those who did not receive chemotherapy had a worse survival.	(Ihnen <i>et al.</i> 2008)
	Gene microarray (n=481)	Low ALCAM expression, together with the status of ER, Her2 and osteopontin, identified a set of patients with markedly shorter survival from three separate cohorts with combined number of 481 patients.	(Ihnen <i>et al.</i> 2010b)
	GWS (6,669)	A SNP on <i>ALCAM</i> (rs9862599 on chromosome 3q13.11) associated with breast cancer (Japan) and together with <i>CLIC6-RUNX1</i> , it makes susceptibility SNPs of breast cancer	(Low <i>et al.</i> 2019)

	IHC (n=153)	ALCAM is largely membranous when present. Seventy out of 153 stained positive for ALCAM and the remaining 83 negative; the staining has intimate relationship with the levels of Wnt5a.	(Kobayashi <i>et al.</i> 2018)
	IHC and microarray (n=110)	Patients with high levels of ALCAM transcript had a longer disease free survival. The correlation is more significant in patients with high levels of membranous ALCAM and high levels of mannonidase (MAN1A).	(Legler <i>et al.</i> 2018)
	Transcript analysis and IHC (n=47)	Breast tumour tissues had higher levels of ALCAM gene methylation than normal tissues and the raised ALCAM gene methylation was seen with lower levels of ALCAM transcript.	(Jeong <i>et al.</i> 2018)
	IHC (n=161)	Patients had highly raised circulating levels of soluble ALCAM and had potential diagnostic value in breast cancer amongst the particular ethnic population (Saudi patients).	(Al-Shehri and Abd El Azeem 2015)
	IHC (n=2,197)	Reduced/loss of ALCAM staining was seen in most tumour types and was linked to high tumour grade and poor OS and RFS	(Burandt <i>et al.</i> 2014)
Pancreatic cancer	Circulating cancer cells (CTC) (n=20)	Patients with circulating cancer cells showing high levels of ALCAM had shorter survival	(Amantini <i>et al.</i> 2019)
	IHC (n=264) and ELISA (n=116)	At tissue level, there was no significant correlation with tumour grade and staging. However, the circulating levels of ALCAM were significantly higher than the control and those with pancreatitis.	(Tachezy <i>et al.</i> 2012c)
	IHC (n=97)	Patients who died of pancreatic cancer had high levels of ALCAM staining in pancreatic cancer cells.	(Kahlert <i>et al.</i> 2009)
	IHC (n=98)	Twelve percent of pancreatic cancers were positive for ALCAM staining, compared with none in normal pancreatic tissues.	(Fujiwara <i>et al.</i> 2014)
Ampulla of Vater	IHC	In a rather large series of this uncommon cancer, there was a progressive increase in ALCAM staining from normal mucosa (n=152) to adenoma (n=111) to carcinoma of ampulla of Vater (n=175).	(Piscuoglio <i>et al.</i> 2012)
Lung cancer	IHC (n=147 NSCLC)	Membrane ALCAM staining is seen in 44.9% of NSCLC tumours and is an independent prognostic factor for shorter overall survival of the patients.	(Ishiguro <i>et al.</i> 2013)
Small intestinal adenocarcinoma	IHC (n=191)	Forty two percent of the tumours stained positive.	(Eom <i>et al.</i> 2015)
Ovarian cancer	IHC (n=204)	Concurrent High levels of ALCAM and mannosidase MAN1A1 linked to shorter relapse free survival of the patients, yet low levels of MAN1A1 and high levels of ALCAM linked to better survival of the patients	(Hamester <i>et al.</i> 2019)

	IHC (n=109)	Cytoplasmic staining or loss of membrane staining of ALCAM is a prognostic factor for patients with ovarian cancer.	(Mezzanzanica <i>et al.</i> 2008)
Endometrial cancer	IHC	For early endometrioid endometrial cancer (n=174), positive ALCAM (76.2%) is seen in patients with short recurrence free survival. Of all the tumours (n=116), 67.4% stained positive for ALCAM with remaining negative. Weak or negative staining was seen at the invading front of cancer tissues.	(Devis <i>et al.</i> 2017; Devis <i>et al.</i> 2018)
Oral Squamous cell carcinoma	IHC (n=41)	Staining of ALCAM on the membrane of the leading front of the SCC cells was seen in tumours with node involvement, high tumour grade	(van den Brand <i>et al.</i> 2010)
	IHC (n=101)	Less than half (47.5%) of the oral SCC tumours stained positive for ALCAM.	(Chen <i>et al.</i> 2018)
	IHC (n=107)	Membranous and cytoplasmic staining were seen in OSCC, but it was the cytoplasmic staining which was associated with clinical outcome and survival of the patients.	(Sawhney <i>et al.</i> 2009)
Giant cell bone tumours	IHC (n=64)	Patients with high levels of ALCAM staining in the giant cell tumour had shorter disease free survival.	(Zhou <i>et al.</i> 2018)
Bladder cancer	TCGA analysis and cell work	Bladder cancer cells and bladder tumour tissues expressed high levels of an ALCAM variant (ALCAM-iso2), which is subject to easy shedding in response to MMP14.	(Hebron <i>et al.</i> 2018)
	IHC (n=198) and ELISA (n=120)	Bladder tumours had reduced ALCAM staining with increased staging. Both circulating and urinary soluble ALCAM seen to markedly increase in patients with bladder cancer.	(Arnold Egloff <i>et al.</i> 2017)
Thyroid cancer	IHC (n=158)	Total ALCAM in poorly differential thyroid tumours was markedly lower than in well/moderately differentiated tumours and the reduction is associated with distant metastasis and shortened survival.	(Chaker <i>et al.</i> 2013)
Prostate cancer	IHC (n=54 pairs)	Over eighty percent of tumours have raised ALCAM staining, which is largely seen in low grade and low Gleason scores.	(Kristiansen <i>et al.</i> 2003)
	IHC (n=2,390)	Approximate 70% had membrane ALCAM staining.	(Minner <i>et al.</i> 2011)
	Gene microarray and IHC (n=42 pairs)	86% of prostate tumours are positive for ALCAM and it is a prognostic marker for prostate cancer.	(Kristiansen <i>et al.</i> 2005)
	IHC (n=48) and ELISA (n=229)	Patients with metastatic disease, nodal positive tumours and died from prostate cancer had high ALCAM staining. Circulating ALCAM has a prognostic value for the survival of the patients.	(Sanders <i>et al.</i> 2019)
Hepatocellular carcinoma	IHC (n=129)	In Recurrent hepatocellular carcinoma (RHCC), positive ALCAM was associated with time to recurrence and microvascular invasion.	(Lu <i>et al.</i> 2017)

Nasopharyngeal carcinoma	ELISA (n=60)	Patients with radioresistant response had high levels of circulating ALCAM. High staining of ALCAM is linked to favourable clinical and pathological features and with low risk of biochemical recurrence for the patients.	(Lin <i>et al.</i> 2017)
Mesothelioma of the pleural cavity	IHC (n=175)	Patients with ALCAM positive mesotheliomas had a significantly shorter survival for the patients.	(Inaguma <i>et al.</i> 2018)
Intracranial meningioma	IHC (n=20)	Meningioma tissues had significantly higher levels of ALCAM compared with normal tissues.	(Atukeren <i>et al.</i> 2017)
Neuroblastoma	IHC (n=66)	Weak ALCAM staining is linked to a short RFS and OS.	(Wachowiak <i>et al.</i> 2016)
Glioblastoma	IHC (n=39)	Tumours rich in ALCAM had shorter overall and disease free survival.	(Kijima <i>et al.</i> 2012)
Medulloblastoma	IHC (n=45)	Majority of the tumours (67%) were negative for ALCAM staining. The positive stained tumours (18) were seen in WNT group and SHH group. The presence of ALCAM is associated with CTNNB1 and Nuclear β -catenin expression	(Achiha <i>et al.</i> 2020)
Melanoma	IHC	There is a progressively increased staining of ALCAM from nevi (15%, n=71), primary melanoma (53%, n=71) to metastatic melanoma (69%, n=84).	(Klein <i>et al.</i> 2007)
	IHC (n=104)	High levels of ALCAM staining seen in patients with shorter overall and disease-free survival. In addition, low ALCAM staining in metastatic lymph nodes is also seen with shorter overall survival of the patients.	(Donizy <i>et al.</i> 2015)
	IHC (n=110)	65% melanoma were positive for ALCAM compared with 74% nevi.	(Shanesmith <i>et al.</i> 2011)
Hepatocellular Carcinoma	IHC and ELISA	HCC tumours stained more strongly for ALCAM than normal liver tissues and HCC patients had markedly high levels of circulating HCC.	(Ma <i>et al.</i> 2015)
Salivary gland tumours	IHC (n=45)	Adenoid cystic carcinoma and mucoepidermoid carcinoma ALCAM staining was markedly higher than in benign pleomorphic adenomas and normal tissues. High grade and late stage malignant tumours had higher staining than early stages.	(Andisheh-Tadbir <i>et al.</i> 2015)
Gastric cancer	IHC (n=142)	Both membrane and cytoplasmic staining are present and linked to nodal metastasis and vascular invasion.	(Ishigami <i>et al.</i> 2011)
	IHC and PCR (n=66), ELISA (n=72)	Both protein (IHC staining) and transcript levels of ALCAM were highly raised in gastric cancer compared with control tissues. The patients also had significant higher levels of circulating ALCAM than controls and those with non-cancerous conditions.	(Ye <i>et al.</i> 2015)
Ewing's Sarcoma	(N=98)	Most sarcomas stained positively for membranous ALCAM and high levels of staining was seen in patients with good MFS survival. Furthermore, high levels of HDGF (an ALCAM	(Yang <i>et al.</i> 2021a)

		transcription suppressor) and low levels of ALCAM collectively presented patients with the worse prognosis	
Osteosarcoma	IHC (n=10)	Membrane and cytoplasmic staining are seen in both primary and metastatic tumours	(Federman <i>et al.</i> 2012)
Malignant mesothelioma	IHC (n=55)	55% of the 47 malignant mesothelioma stained positive for ALCAM. Over-expression is linked to shorter survival.	(Ishiguro <i>et al.</i> 2012)
Cervical cancer	IHC (n=233)	Over half (58.4%) of tumours were strongly positive for ALCAM.	(Ihnen <i>et al.</i> 2012)
Oesophageal squamous cell carcinoma	IHC and PCR (n=65)	ALCAM expression is increased in SCC compared with control tissues, and the increase is seen with nodal metastasis and late clinical stages	(Verma <i>et al.</i> 2005)

1.4.6 ALCAM shedding mechanisms

Soluble ALCAM, also known as sALCAM, is an exfoliated product of the extracellular region of ALCAM. Studies have shown that the shedding of ALCAM exists widely in various tissue types and is regulated by a series of metalloproteases including A Disintegrin and Metalloprotease 17 (ADAM17) and Matrix Metalloprotease 14 (MMP14). Rosso *et al.*, (Rosso *et al.* 2007) demonstrated that metalloprotease activators such as pervanadate, Epidermal Growth Factor (EGF) and phorbol esters were able to enhance the spontaneous release of soluble ALCAM, whereas, adding inhibitors of MMPs and ADAMs could inhibit ALCAM shedding in epithelial ovarian cancer cells. The metalloproteases ADAM17 and MMP14 cleave ALCAM molecules on the extracellular membrane-proximal part of the molecule, releasing the soluble ALCAM into the extracellular matrix.

1.4.7 Circulating ALCAM (truncated ALCAM)

Many studies have speculated that the detection of sALCAM could function as a biomarker of cancer progression considering that in cancer tissue ALCAM shedding, to a certain extent, can regulate the strength of ALCAM-mediated cell adhesion, which is critical to the formation and migration of cancer cells. Sanders *et al.*, (Sanders *et al.* 2019) found that, in patients with prostate cancer, those with metastasis, with nodal positive tumours and, in particular, those who died of prostate cancer, had significantly higher levels of circulating ALCAM and circulating ALCAM, similar to prostate specific antigen (PSA), is a prognostic indicator for the patients. Carbotti *et al.*, (Carbotti *et al.* 2013) showed that in patients with ovarian cancer (n=61), serum levels of ALCAM were higher than controls and significantly

correlated with protein marker CA125/MUC16. This high level was seen in aggressive and high stage tumours.

In patients with pancreatic cancer (n=115), the levels of circulating ALCAM were significantly higher than those with chronic pancreatitis and the control individuals (Tachezy et al. 2012c). Interestingly, there appears to be a diagnostic value in pancreatic cancer (RUC=0.695).

In patients with breast cancer (n=157), the serum level of soluble ALCAM was significantly higher than control individuals and the levels correlated with shorter disease-free survival, although not with other clinical and pathological factors (Witzel *et al.* 2012). The study has reported that there was no correlation between serum ALCAM and tissue ALCAM protein or mRNA levels, indicating non-transcription and non-translational contribution to the raised serum levels, possibly due to protease cleavage of the protein, as later demonstrated in many other studies.

1.4.8 ALCAM and metastatic diseases

The change in cell adhesion is an important mechanism for the migration of cancer cells, so it is tempting to speculate the impact of ALCAM regulation on cancer metastasis. Kulasingam et al., (Kulasingam et al. 2009) has measured the serum levels of ALCAM and another two tumour markers, CEA and CA15-3, in 150 patients with breast cancer and compared the results with control groups (including 100 healthy women and 50 men). They highlight that circulating ALCAM appeared to be a better diagnostic marker than the others for the patients.

Ihnen (Ihnen *et al.* 2010a) has examined 29 samples that came from patients who died of breast cancer and the tissues collected from autopsies (n=84 in total),

including primary tumours and multiple metastasis tumours. The results have shown that the levels of ALCAM in primary tumours and metastatic tumours correlated exceptionally well ($p < 0.001$), and that metastatic tumours in different sites (liver, lung, bone, brain and lymph nodes) stained reasonably similar to primary tumours.

In summary, ALCAM is an important cell adhesion molecule and has important roles to play, both in physiological conditions and, in particular, in pathological conditions such as cancer. At the cellular level, the role of ALCAM in mediating cell adhesion and the methods of ALCAM mediated cell adhesion are becoming clear. One of the most important advancements over the past two decades is establishing its impact in clinical cancer and that, depending on tumour type and cell type, ALCAM is indeed an important factor that is linked to the disease progression, spreading and ultimately the clinical outcome of the patients as Table 1.5 well documented. There are, however, some highly interesting findings yet to fully investigated. One of them is the finding that ALCAM is linked to bone metastasis in breast cancer and to a degree prostate cancer, two cancer types making up over 70% of all bone metastatic legions. There are also wider and mechanistic questions to be asked and explored, including if the role of ALCAM in bone metastases is hormone and hormone receptor dependent; if ALCAM plays a wider role in endocrine related malignancies; to what extent does hormone receptor(s) contribute to ALCAM mediated cell adhesion and intracellular signalling; how does the bone microenvironment (including bone stroma and stromal cells) orchestrate ALCAM mediated bone metastasis; if a possible endocrine link between ALCAM and bone metastasis poses new opportunities for therapeutic targeting. The current study aims to answer some of the fundamental questions.

1.4.9 HGF/MET complex

A key part of this present study involves investigation of the role played by the HGF/MET receptor complex, identified in the study (presented in Chapter 5). HGF (hepatocyte growth factor) was initially identified as a most powerful liver regeneration protein (Nakamura et al. 1989) which was subsequently found to be the same factor as Scatter Factor (SF) produced by fibroblasts and able to drive cell migration of epithelial cells (Stoker et al. 1987). HGF is also the same protein as another factor known as hepatopoietin which appeared rapidly after liver resection (Thaler and Michalopoulos 1985). The receptor for HGF was subsequently identified to be the same as the transmembrane kinase cMET protein (Thaler and Michalopoulos 1985), a molecule initially discovered as a proto-oncogene (Trent and Witkowski 1987; Giordano et al. 1989).

The receptor tyrosine kinase (cMET, Mesenchymal-epithelial transition factor) and its ligand, hepatocyte growth factor (HGF), are an important receptor-ligand pair in the tumour-associated signalling network. They are involved in the regulation of tumour progression and migration (Jiang et al. 2005; Duplaquet et al. 2018). cMET pathways have emerged as important actionable targets in many solid tumours. Therefore, biomarker discovery has become essential to guide clinical assessment of the disease progression, evaluate therapy response and importantly drug targeting. The HGF/c-MET pathway is active in tumour development, suggesting that inhibition of HGF/c-MET signalling may have therapeutic potential.

HGF is a multifunctional cytokine whose gene is located on the long arm (7q21.1) of human chromosome 7 and consists of 18 exons and 17 introns (Moosavi et al. 2019). All biological activities of HGF are mediated through the cell surface receptor c-MET (encoded by the c-MET proto-oncogene). The binding of HGF to c-MET induces the catalytic activity of receptor kinases, which triggers the transphosphorylation of Tyr (tyrosine) 1234 and Tyr 1235. The binding reaction participates in various signal

transduction processes, which in turn activate a variety of intracellular signalling pathways, including intracellular phosphatidylinositol kinase/protein kinase B (PI3K/Akt), JAK kinase/signalling and activator of transcription (JAK/STAT3), mitogen-activated protein kinase/extracellular regulated protein kinase (MAPK/ ERK) and other signalling pathways. Its downstream signalling pathways are involved in a variety of cellular responses, such as proliferation, survival, motility, invasion, and stimulation of angiogenesis.

The HGF/c-MET signalling pathway is relatively active in tumour progression, suggesting that it may become a diagnosis or prognostic indicator and inhibition of this signalling pathway may have therapeutic potential. So, the HGF/c-MET signalling pathway has become a hot spot in cancer research.

1.4.10 Pancreatic ductal adenocarcinoma: an exocrine related cancer

Pancreatic cancer is currently the fourth leading cause of cancer death worldwide, and its incidence is increasing every year in many developed and developing countries. Ninety percent of newly diagnosed pancreatic cancer patients are aged over 55 and the worldwide incidence of pancreatic cancer in females is lower than males (McGuigan et al. 2018) (Figure 1.8). The overall 5-year survival rate of pancreatic cancer patients is approximately 6.5% to 10% according to previous research (McGuigan et al. 2018; Park et al. 2021) (Figure 1.9). Among all pathological types of pancreatic cancer, Pancreatic ductal adenocarcinoma (PDAC) is the most common type (90%). Despite years of research, pancreatic cancer is still a highly lethal cancer type, with a high rate of mortality. This high mortality rate is attributed to the lack of early symptoms, rapid disease progression, lack of effective diagnostic methods, susceptibility to early lymph node metastases and distant metastases, the difficulty of surgical treatment and the insensitivity to chemotherapy.

In the present study, we chose pancreatic ductal adenocarcinoma as a representative exocrine related cancer to compare with breast cancer. The reasoning for this is that a small number of previous studies, together with our preliminary results, indicate that ALCAM has an opposite effect on patients' clinical outcomes between endocrine related cancer and non-endocrine related cancer (also referring to Table 1.5). As we mentioned above, the ALCAM expression of breast cancer tends to be lower compared to normal tissue and breast cancer patients with higher levels of ALCAM had longer survival. The similar results can be found in other endocrine related cancers, such as prostate cancer (Minner et al. 2011) and thyroid cancer (Chaker et al. 2013), in which ALCAM acts as a tumour suppressor. While in non-endocrine related cancer, high levels of ALCAM often lead to poor survival. An early study by Kahlert *et al.*, (Kahlert et al. 2009), using immunohistochemistry on 97 pancreatic tumours patients, showed that strong ALCAM staining, as well as the cellular location of the staining, had significant links to recurrence free survival and overall survival. In another cohort of 20 patients, with metastatic or locally advanced pancreatic adenocarcinoma, it was reported that circulating cancer cells had higher levels of ALCAM message and, when circulating cancer cells had high levels of ALCAM, patients tended to have significantly shorter survival (Amantini et al. 2019). In contrast to that, ALCAM levels in endocrine tumours from the pancreas, namely pancreatic neuroendocrine tumours (PNET), was found to be a favourable prognostic factor for both recurrence free survival and disease specific survival (n=38) (Hong et al. 2010; Tachezy et al. 2011). The impact of ALCAM on the adhesion and migration of pancreatic cancer cells has also been reported (Hong et al. 2010; Fujiwara et al. 2014). In conclusion, high levels of ALCAM in pancreatic cancer cells and tissues often lead to poorer clinical outcomes of the patients and an increased tendency for distant metastases. This connection seems to exist in other exocrine tumour types, including cancers derived from squamous cell lineages (namely squamous cell

carcinoma) in skin and oesophagus (Verma et al. 2005; Tachezy et al. 2012a), as well as in malignant melanoma (Donizy et al. 2015), gastrointestinal cancers (Tachezy et al. 2012b; Hansen et al. 2013; Ye et al. 2015) and neurological malignancies (Kijima et al. 2012).

As part of the larger study, conducted throughout this thesis, we investigate an available pancreatic cancer cohort and *in vitro* assays to explore the effect of ALCAM on an exocrine cancer, namely pancreatic cancer, and the role of the endocrine system in ALCAM-related oncogenic pathways.

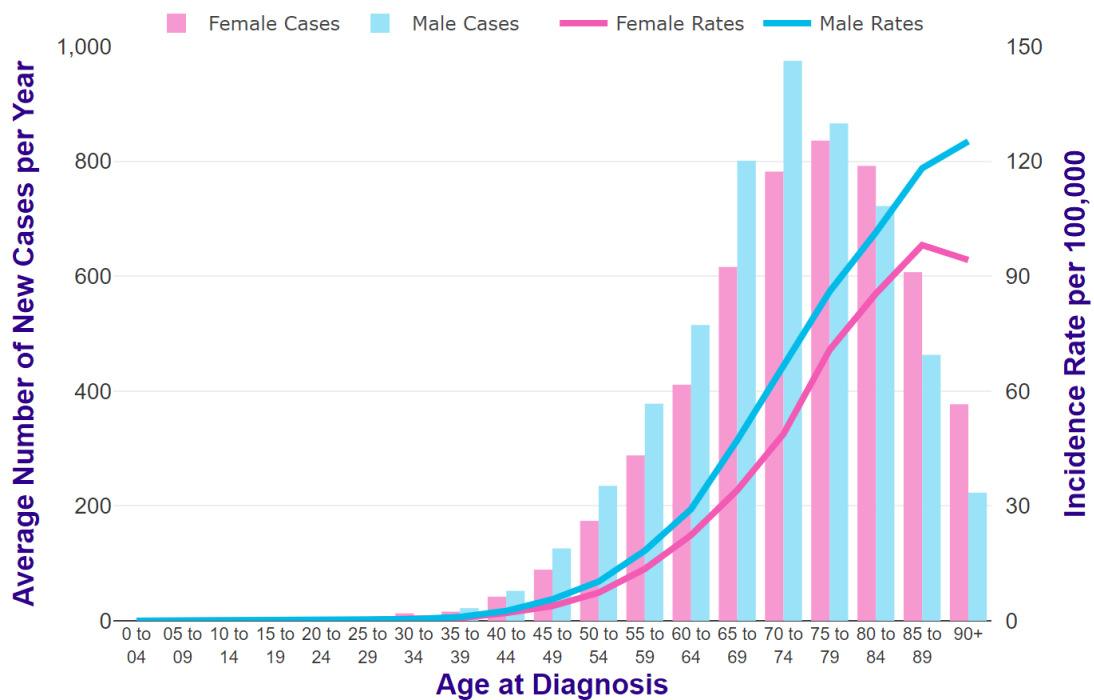


Figure 1.8 Pancreatic cancer in UK, average number of new cases per year and age-specific incidence rates per 100,000 population, 2016-2018. Source: <https://www.cancerresearchuk.org>

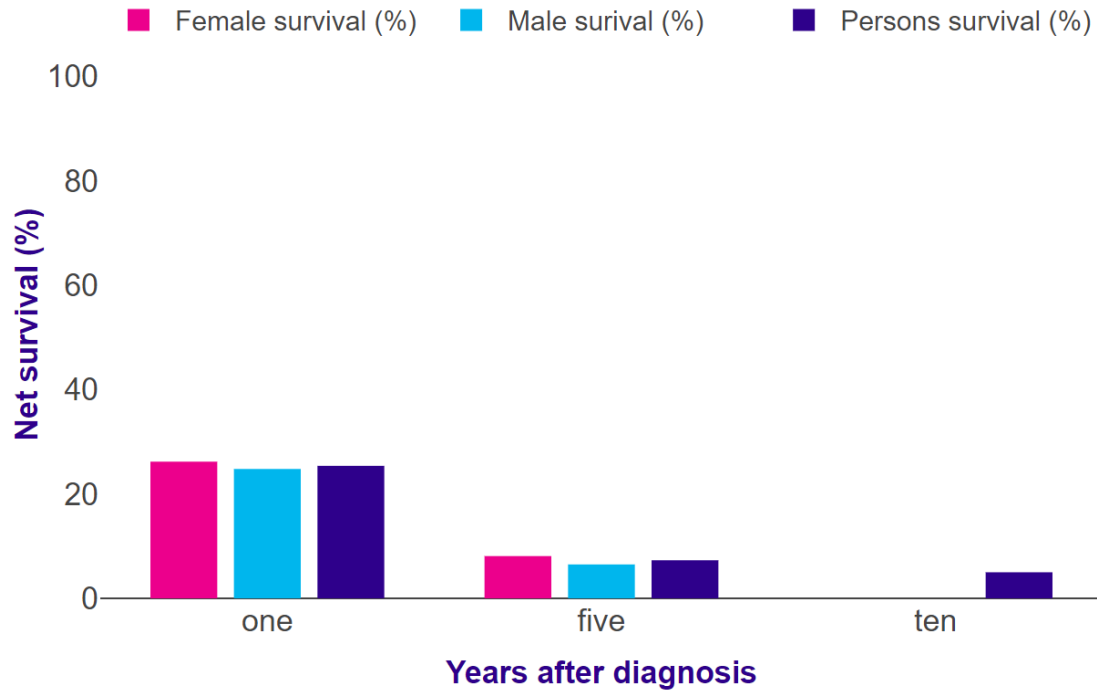


Figure 1.9 Pancreatic Cancer, age-standardised one-, five- and ten-year net survival, adults (aged 15-99), England, 2013-2017. Source: <https://www.cancerresearchuk.org>

1.5 Hypothesis

ALCAM plays a key role in regulating bone metastasis in endocrine-related cancers, particularly in breast cancer. This regulation has correlated with hormone receptor status and can influence the patient’s prognosis. The intracellular signalling interaction between the ALCAM complex and hormonal receptors is key to this interplay.

1.6 Aims of the study

The aims of this research were:

1. To fully explore the molecular correlation between ALCAM and the hormone receptors, along with other partners in the context of survival benefits and bone metastasis in breast cancer. The study also aimed to investigate

additional cohorts (pituitary tumour and pancreatic cancer) beyond breast cancer and further establish a role between ALCAM and bone metastasis and clinical outcomes.

2. To establish cellular mechanisms, including cellular signalling events, of ER interaction with ALCAM and how this influences the establishment of breast cancer cells in bone microenvironment.
3. To explore the effect of ALCAM on chemotherapy drug effectiveness in both normal and bone microenvironment.

Chapter-2

Materials and Methods

2.1 Materials

2.1.1 General materials and reagents

Materials and reagents used in the study are outlined in Table 2.1.

Table 2.1 Materials and reagents used in the study.

Material/Reagent	Supplier
1-Bromo-3-chloropropane	Sigma-Aldrich, Dorset, UK
6 well plates	Griener Bio-One, Gloucestershire, UK)
Agarose	Melford Laboratories, Suffolk, UK
Ampicillin	Sigma-Aldrich, Dorset, UK
100X antimicrobial solution	Sigma-Aldrich, Dorset, UK
Cryotubes	Griener Bio-One, Gloucestershire, UK)
Diethylpyrocarbonate (DEPC)	Sigma-Aldrich, Dorset, UK
Dimethyl Sulphoxide (DMSO)	Sigma-Aldrich, Dorset, UK
DMEM/Ham's F12 with L-glutamine	Sigma-Aldrich, Dorset, UK
DPX	Sigma-Aldrich, Dorset, UK
Eppendorf tubes	Griener Bio-One, Gloucestershire, UK)
Foetal Calf Serum (FCS)	Sigma-Aldrich, Dorset, UK
Fugene HD Transfection reagent	Promega, Southampton, UK
Gill's hematoxylin	Vector Laboratories Ltd., Peterborough, UK
GoScript Oligo dT mix reverse transcription kit	Promega, Southampton, UK
GoTaq Green Mastermix PCR kit	Promega, Southampton, UK
Miracloth	Sigma-Aldrich, Dorset, UK
MicroAmp Fast Optical 96 well reaction plate	Fisher Scientific, Leicestershire, UK
Mycoplasma kit	Promega, Southampton, UK
OptiMEM medium	Fisher Scientific, Leicestershire, UK
Optical seals for qPCR	PrimerDesign, Southampton, UK
Phosphate Buffered Saline (10X)	Sigma-Aldrich, Dorset, UK
PrecisionFAST (2X) qPCR master mix	PrimerDesign, Southampton, UK
PureYield Maxi Prep plasmid extraction kit	Promega, Southampton, UK
Puromycin	Fisher Scientific, Leicestershire, UK
RPMI 1640 medium	Sigma-Aldrich, Dorset, UK
SYBRsafe DNA stain	Fisher Scientific, Leicestershire, UK
T25 and T75 tissue culture flasks	Griener Bio-One, Gloucestershire, UK
Tri reagent	Sigma-Aldrich, Dorset, UK
Tris, Boric Acid, EDTA (TBE; 10X)	Sigma-Aldrich, Dorset, UK
Trypsin-EDTA (10X)	Sigma-Aldrich, Dorset, UK
Uniprimer probe	Intergen company, New York, USA
Universal Container	Griener Bio-One, Gloucestershire, UK
Vectastain Elite Universal ABC kit	Vector Laboratories Ltd., Peterborough, UK

2.1.2 Special reagents

Recombinant human hepatocyte growth factor (rhHGF) was a gift from Professor Toshikazu Nakamura of Osaka University (Osaka, Japan). A stock was prepared at 10µg/ml in sterile BSS (Balanced Salt Solution which is made up in the following: 137mM NaCl, 2.6mM KCl, 1.7mM Na₂HPO₄ and 8mM KH₂PO₄) with 0.1% BSA and stored at -80°C. A HGF receptor MET small compound inhibitor, PF02341066 (also known as Crizotinib) was a gift from Pfizer, Inc. The inhibitor was dissolved in DMSO and diluted in sterile BSS to a concentration 10mM and stored at -80°C until use. A ROCK (Rho-associated, coiled-coil-containing protein kinase) small compound inhibitor, Y27632 was purchased from Tocris (Tocris Biologicals, Bristol, England) and stocks were prepared with DMSO. A fluorescence dye used to label cell membrane, Dil (1,1'-Dioctadecyl-3,3,3',3'-Tetramethylindocarbocyanine Perchlorate) was purchased from Sigma-Aldrich (Dorset, UK). Dil stocks were prepared in DMSO at 1mM, stored in aluminium foil at -80°C until use. Recombinant human ALCAM-Fc chimera (soluble ALCAM), containing ALCAM Trp28 – Ala526 and the human IgG Fc region, was purchased from R&D systems (Abingdon, UK).

Bone matrix extract (BME) was a central resource of the host laboratory and the preparation was described in full in previous studies (Davies and Jiang 2010; Owen et al. 2016). Briefly, bone proteins were extracted from fresh human bone tissues collected immediately after hip replacement under the local health board ethics committee guidelines. Bones were crushed at ice-cold temperatures and subsequently processed in a Bioraptor sonicator (Wolf Laboratories, York, UK) to extract matrix proteins. The matrix proteins were then quantified and stored at -80°C until use.

2.1.3 Source of chemotherapy drugs

Purified drug compounds used in the present study were purchased from Sigma-Aldrich (Dorset, UK) including Paclitaxel, Docetaxel, Cisplatin, Neratinib and Gemcitabine, which were dissolved in DMSO and diluted in sterile BSS to a concentration 10mM and stored at -80°C until use.

2.2 Cell lines

An immortalised human vascular endothelial cell line HECV, was purchased from Interlab, Naples, Italy. Other cell lines were obtained from the ATCC (American Type Culture Collection), provided by the LGC Standards (LGCstandards.com), ATCC's European supplier (Teddington, Middlesex, UK). A panel of human breast cancer cell lines were utilised in the current study with a range of receptor status (shown in Table 2.2). Upon arrival, low passage stocks were generated within the department and were confirmed as mycoplasma free.

ZR-751, MDA-MB-231, MDA-MB-361, MCF-7, BT-20, MDA-MB-436, SK-BR-3, PANC1, Mia PaCa-2, HECV cells were routinely cultured in Dubecco's Modified Eagle Medium (DMEM)/Ham's F12 with L-glutamine. BT-549 and MDA-MB-468 cells were grown in RPMI 1640 medium (Sigma-Aldrich, Dorset, UK). All growth medium was supplemented with 10% foetal calf serum (FCS) (Sigma-Aldrich, Dorset, UK) and 1X antimicrobial solutions (Sigma-Aldrich, Dorset, UK). Cells were cultured in an incubator at 95% humidity, 5% CO₂ and 37°C.

Table 2.2 Cell lines used in the study.

Cell line name	Origin	Morphology	Tissue type	Receptors
BT-20	74/F/Caucasian	Epithelial	Human, Breast Adenocarcinoma	ER(-)/PR(-)/HER2(-)
BT-549	72/F/Caucasian	Epithelial	Human, Breast Adenocarcinoma	ER(-)/PR(-)/HER2(-)
ZR-75-1	63/F/Caucasian	Epithelial	Human, Breast Adenocarcinoma	ER(+)/PR(+)/HER2(-)
MDA-MB-361	40/F/Caucasian	Epithelial	Human, Breast Adenocarcinoma	ER(+)/PR(+)/HER2(+)
MDA-MB-436	43/F/Caucasian	Epithelial	Human, Breast Adenocarcinoma	ER(-)/PR(-)/HER2(-)
MDA-MB-468	51/F/Black	Epithelial	Human, Breast Adenocarcinoma	ER(-)/PR(-)/HER2(-)
MDA-MB-231	51/F/Caucasian	Epithelial	Human, Breast Adenocarcinoma	ER(-)/PR(-)/HER2(-)
SK-BR-3	43/F/Caucasian	Epithelial	Human, Breast Adenocarcinoma	ER(-)/PR(-)/HER2(+)
MCF-7	69/F/Caucasian	Epithelial	Human, Breast Adenocarcinoma	ER(+)/PR(+)/HER2(-)
PANC-1	56/M/White	Epithelial	Human, Pancreas Carcinoma	-
MIA PaCa-2	65/M/White	Epithelial	Human, Pancreas Carcinoma	-
HECV	F/Caucasian	Endothelial	Human, Umbilical cord cells	-

2.3 Cell culture

2.3.1 Cell maintenance, sub-culture and quantification

Growing cultures were routinely maintained to ensure cell health and prevent over confluence. Cells were routinely grown and maintained in T25 and T75 tissue culture flasks (Griener Bio-One, Gloucestershire, UK). Cells were inspected visually using an inverted microscope as shown in Figure 2.1 (Leica Microsystems (UK) Ltd, Milton Keynes, UK) and when approaching confluence, or required for experimental work, were trypsinised.

All cell culture was performed under sterile conditions in a class II laminar flow tissue culture hood (Figure 2.2, Wolf Laboratories, York, UK) using aseptic technique. Cell medium was aspirated using a glass pipette and vacuum pump before adding 1 to 5

ml (depending on the size of flasks) of phosphate buffered saline (PBS; Sigma-Aldrich, Dorset, UK) to wash the monolayer and remove remnant medium. The PBS was subsequently removed before adding 1 to 5 ml of trypsin-EDTA (Sigma-Aldrich, Dorset, UK) and incubating briefly in the incubator, until cells were visibly detached when viewed under the microscope. Once fully detached, the cells were collected in a Universal Container (UC; Greiner Bio-one Gloucestershire, UK) and centrifuged at 1600rpm for 5 minutes to pellet the cells. Following centrifugation, supernatant was aspirated, and the cell pellet was resuspended in fresh growth medium. This suspension was subsequently used to quantify cells using a haemocytometer counting chamber (Fisher Scientific UK, Leicestershire, UK) to allow seeding of required cell numbers. Alternatively, for routine subculture, a small amount of the cell suspension was seeded back into a flask and cells placed back in the incubator.



Figure 2.1 Inverted microscope (Leica Microsystems (UK) Ltd, Milton Keynes, UK).



Figure 2.2 Class II laminar flow tissue culture hood (Wolf Laboratories, York, UK)

2.3.2 Cryopreservation and revival of frozen stocks

Cell lines used in this study were obtained from the departmental bank of breast cancer cell lines, stored in liquid nitrogen. For revival, frozen cell stocks were quickly thawed and immediately placed into 10ml of pre-warmed growth medium.

Subsequently, cells were centrifuged at 1600rpm for 5 minutes to pellet cells, before resuspending cells in fresh growth medium and seeding into a T25 tissue culture flask. Revived cells were incubated overnight and visualised the following day to assess cell health. Cell medium was changed the day following revival, to remove cell debris or dead cells.

Cell stocks were also prepared for wild type cells and also manipulated cells as part of this study. Cells were trypsinised and quantified as outlined in section 2.3.1.

Subsequently, solutions were prepared containing 1 million cells in 1ml of growth

medium containing 10% Dimethyl Sulphoxide (DMSO; Sigma-Aldrich, Dorset, UK). Required numbers of 1ml aliquots were added to cryotubes (Griener Bio-On, Gloucestershire, UK) before placing in the -80°C freezer. Cells were subsequently transferred to liquid nitrogen for longer term storage (only low-passaged cells were used in the study).

2.4 Generation of ALCAM knockdown/Overexpression systems

2.4.1 Plasmid design

Plasmids containing either the full coding sequence of ALCAM or shRNA sequences targeting ALCAM, together with stuffer control or scramble sequences respectively, were designed and ordered from Vector Builder (Chicago, USA). Plasmids were designed to contain the ampicillin and puromycin resistance genes to allow selection in both *E. coli* and mammalian cells respectively. Plasmid maps for the overexpression plasmids and shRNA knockdown plasmids and are outlined in Figure 2.3 and 2.4 respectively.

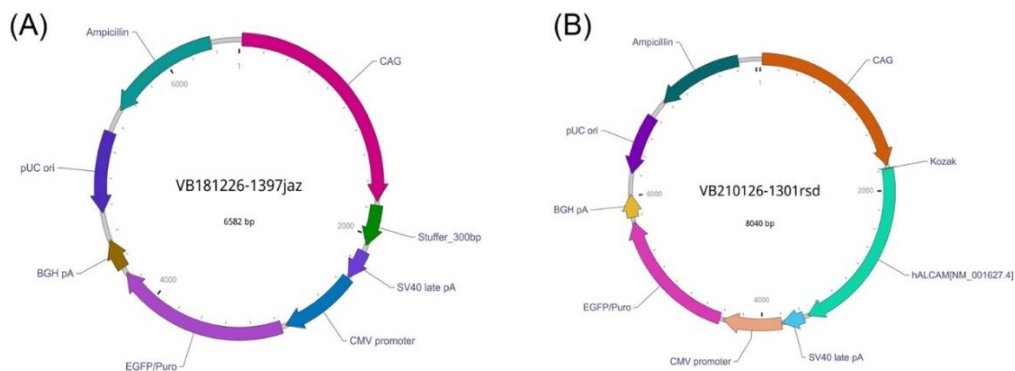


Figure 2.3 Schematic of (A) stuffer control and (B) ALCAM overexpression plasmid. Images obtained from Vector Builder.

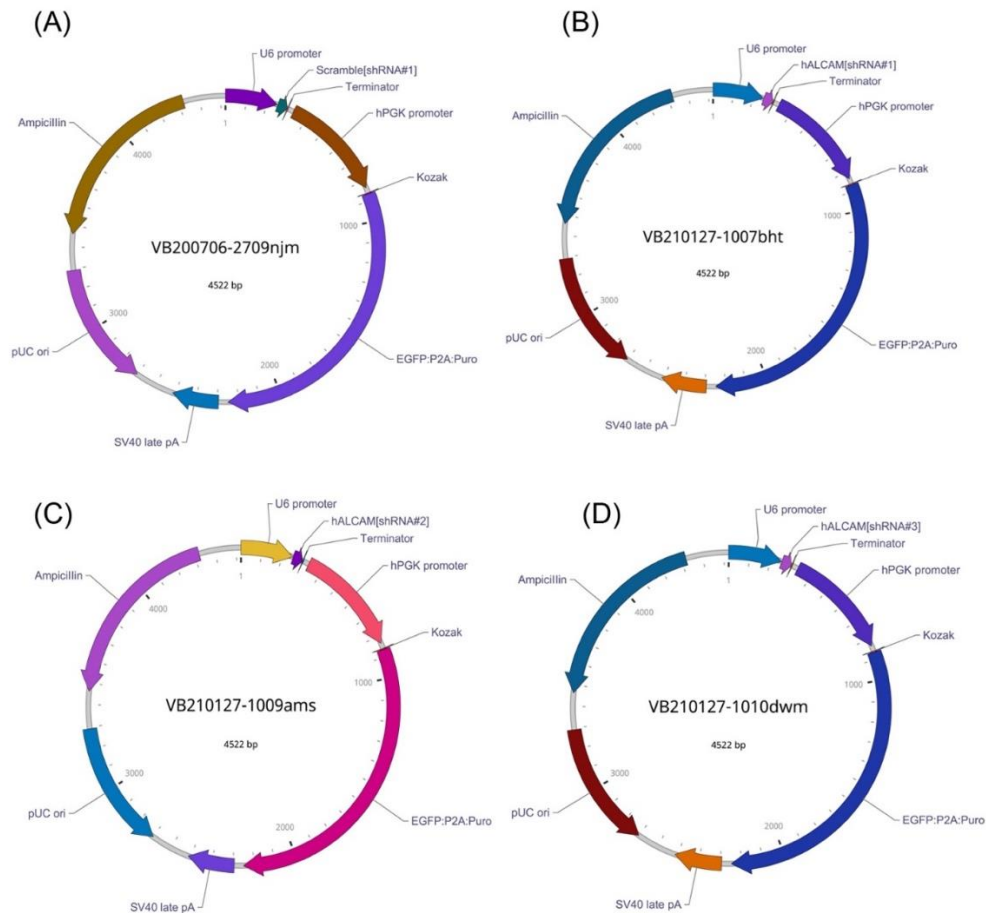


Figure 2.4 Schematic of (A) scramble control and ALCAM (B) shRNA 1, (C) shRNA 2 and (D) shRNA 3 knockdown plasmids. Images obtained from Vector Builder.

2.4.2 Plasmid extraction and quantification

Plasmids were ordered as an *E. coli* stock which was subsequently amplified and subject to plasmid extraction using a PureYield Maxi Prep plasmid extraction kit (Promega, Southampton, UK), in accordance with the manufacturer's instructions. In brief, 150ml of LB (Lysogeny Broth) medium containing 100µg/ml Ampicillin (Sigma-Aldrich, Dorset, UK) was inoculated with the *E. coli* purchased stock and cultured overnight. Following this, bacteria were pelleted at 3,000rpm for 10 minutes, supernatant discarded, and the pellet resuspended in 12ml of resuspension solution. Following this, 12ml of lysis buffer was added and the tube inverted gently 5 times before incubating for 3 minutes. Subsequently, 12ml of Neutralisation solution was added and mixed through 15 inversions of the tube, before centrifuging at 3000rpm

for 30 minutes and then filtering the supernatant through a Miracloth (Sigma-Aldrich, Dorset, UK). DNA was subsequently purified using the vacuum method and a stack consisting of a clearing column, placed on top of a binding column, was prepared and attached to the vacuum manifold (Promega, Southampton, UK). The lysate was then passed through these columns by action of the vacuum before removing and discarding the top clearing column. Following this, 5ml of Endotoxin Removal wash (prepared, through addition of 57ml 2-propanol, in accordance with manufacturer instructions) was added to the binding column and drawn through under vacuum. The binding column was then washed with 20ml Column wash (prepared, through addition of 350ml 95% ethanol, in accordance with manufacturer instructions), drawn through under vacuum. Next DNA was eluted by constructing the Vacuum Elution Device to capture DNA from the column in a 1.5ml microfuge tube, adding 1ml of nuclease free water to the binding column and drawing through on vacuum. The plasmid was then subsequently quantified using an IMPLEN nanophotometer (Figure 2.5, Geneflow Ltd., Litchfield, UK) and stored at -20°C until required.



Figure 2.5 IMPLen NanoPhotometer (Geneflow Ltd., Litchfield, UK)

2.4.3 Plasmid transfection of breast cancer, endothelial cells and pancreatic cancer cells

These plasmids were used to transfect cell lines originated from breast cancer, endothelium and pancreatic cancer using the Fugene HD (Promega, Southampton, UK) transfection reagent, in accordance with manufacturer's instructions. It is a novel, nonliposomal transfection reagent designed to transfect DNA into a wide variety of cell lines with high efficiency and low toxicity. In brief, cells were plated the day before transfection so as to reach approximately 80% confluence at the time of transfection. Transfections were undertaken using 6 well plates (Greiner BioOne, Gloucestershire, UK) and reagent volumes amplified as recommended in the manufacturer's instructions. Cells were prepared in medium containing no antibiotics. Appropriate volume mixes of reagents and DNA were prepared

depending on the number of transfections undertaken. For each transfection, 3µg of plasmid was diluted, mixed by vortex and prepared to a final volume of 150µl in OptiMEM medium (Fisher Scientific UK, Leicestershire, UK). Subsequently, 9µl FuGENE HD transfection reagent was added directly to the medium (3:1 ratio with DNA), mixed and incubated for 10 minutes before adding 150µl of the solution to the cell culture plate. Following this, the plate was agitated by gentle rotation and cells placed in the incubator for 24 hours. Following this time, cells were subject to 2µg/ml puromycin (Fisher Scientific UK, Leicestershire, UK) selection, prepared in growth medium. Once sufficient cell death had occurred, cells were taken out of selection and grown routinely in maintenance medium containing 0.2µg/ml puromycin.

2.5 RNA extraction, quantification and Reverse Transcription

RNA was extracted using Tri reagent (Sigma-Aldrich, Dorset, UK) in accordance with the manufacturer's instructions. In brief, cells were cultured in either T25 flasks or 6 well plates and subject to extraction when approximately 80% confluent by addition of 1ml Tri reagent. The Tri reagent suspension was then collected in a 1.5ml microfuge tube and left to stand at room temperature for 5 minutes. Subsequently, 100µl of 1-Bromo-3-chloropropane (Sigma-Aldrich, Dorset, UK) was added, samples were shaken vigorously for 15 seconds and left to stand for 5 minutes before centrifuging at 12,000rpm for 15 minutes at 4°C. Following centrifugation, phase separation was observed and the top, clear, aqueous phase collected and added to 0.5ml 2-propanol (Fisher Scientific UK, Leicestershire, UK) before mixing by inversion, leaving to stand at room temperature for 5 minutes and centrifuging at 12,000rpm for 10 minutes at 4°C. The supernatant was removed from the resulting RNA pellet and discarded. The pellet was then washed with 1ml of 75% ethanol in Diethylpyrocarbonate water (DEPC, Sigma-Aldrich, Dorset, UK) and centrifuged at

7,500rpm for 5 minutes at 4°C. Following this, the solution was removed and the RNA pellet air dried briefly before being dissolved in 20-50µl of DEPC water (depending on pellet size) and quantified in comparison to a DEPC water blank on a nanophotometer (Figure 2.5).

Following quantification, samples were standardised to 500ng/µl RNA and subject to Reverse Transcription using a GoScript Oligo dT mix reverse transcription kit (Promega, Southampton, UK), under the following conditions: 25°C for 5 minutes; 42°C for 60 minutes; 70°C for 15 minutes; 4°C hold. Following completion of the reaction, samples were diluted 1:4 with molecular biology grade water and stored at -20°C until needed for PCR analysis.

2.6 Polymerase Chain Reaction (PCR)

PCR was undertaken using the GoTaq Green Mastermix PCR kit (Promega, Southampton, UK). The mix contained all reagents and buffers required for the PCR reaction as well as a loading dye. A 16µl reaction was prepared as followed:

8µl – 2X GoTaq Green master mix

1µl – Forward primer (10µM)

1µl – Reverse primer (10µM)

5µl – Molecular biology grade water

1µl – Sample cDNA

Primers were designed using the Beacon Designer (Biosoft International, Palo Alto, California, USA) or Primer BLAST software and were ordered from Sigma-Aldrich (Dorset, UK). All stock primers were diluted to 100µM for storage within the

department and further diluted to 10 μ M before use. Primers used in the study are outlined in Table 2.3.

Table 2.3 Primers used in the current study, *actgaacctgaccgtaca* represents the z sequence

Target	Forward	Reverse
ALCAM (PCR)	ttatcacaccttgccgatt	gggtggaagtcatggtatag
GAPDH (PCR)	ggctgctttaactctgga	gactgtggtcatgagtcctt
ALCAM (qPCR)	caggaggttgaaggactaaa	<i>actgaacctgaccgtaca</i> gggatcagtttctttgtca
GAPDH (qPCR)	aaggtcatccatgacaactt	<i>actgaacctgaccgtaca</i> gcatccacagtcttctg
PDPL (qPCR)	gaatcatcggttggttatg	<i>actgaacctgaccgtaca</i> ctttcattgcctatcacat

Once prepared, samples were run in a SimpliAmp thermocycler as shown in Figure 2.6 (Fisher Scientific UK, Leicestershire, UK) under the following conditions: Initial denaturing 94°C for 5 minutes; 30 – 36 cycles of 94°C for 30 seconds; 55°C for 30 seconds; 72°C for 40 seconds; Final extension 72°C for 10 minutes; 4°C hold.

Samples were subsequently loaded on a 1% agarose gel, prepared in Tris, Boric Acid, EDTA (TBE; Sigma-Aldrich, Dorset, UK) gel containing SYBRsafe DNA stain (Fisher Scientific UK, Leicestershire, UK) and run at 95V, 50mA, 50W until sufficiently separated. Following this, samples were visualised in a Syngene U: Genius 3 System (Figure 2.7, Geneflow Ltd., Litchfield, UK) and images captured.



Figure 2.6 SimpliAmp thermocycler (Fisher Scientific UK, Leicestershire, UK).



Figure 2.7 Syngene U: Genius 3 System (Geneflow Ltd., Litchfield, UK).

2.7 Quantitative Polymerase Chain Reaction (qPCR)

The Amplifluor Molecular Beacon system was used to conduct qPCR. This system has been well established and reported by the host laboratories. Reactions (10 μ l) were prepared as outlined below:

5 μ l – 2X precisionFAST qPCR master mix (PrimerDesign, Southampton, UK)

0.3 μ l – Forward Primer (10 μ M)

0.3 μ l – Reverse primer (1 μ M) containing the Z-sequence

0.3 μ l – Uniprimer probe (Intergen company, New York, USA)

4.1 μ l – cDNA/water mixture

Reactions were prepared in a MicroAmp fast Optical 96-well plate (Fisher Scientific UK, Leicestershire, UK) using primers specific to the molecule of interest (see Table 2.3). In addition to unknown samples, reactions were prepared for a known standard that was run alongside the unknown samples. The standard was based on the detections of podoplanin (PDPL) in pre generated standard samples, serially diluted from 10^8 – 10^1 copy numbers. Once all samples and unknowns were added to the plate, the plate was sealed with Optical seals (PrimerDesign, Southampton, UK) and the samples ran on a StepOne Plus qPCR system (Figure 2.8, Fisher Scientific UK, Leicestershire, UK) under the following conditions:

Initial 95°C for 10 minutes

100 cycles: 95°C for 10 seconds; 55°C for 35 seconds; 72°C for 10 seconds

Following the run, relative copy numbers of unknown samples were calculated as part of the system analysis, in accordance with the standard curve and were subsequently exported to excel for further analysis.



Figure 2.8 StepOne Plus qPCR system (Fisher Scientific UK, Leicestershire, UK)

2.8 Western blotting

2.8.1 Protein extraction

Cells were grown in T25 flasks until confluent and lysed using 150 to 200 μ l lysis buffer and the resultant lysates were then transferred to 1ml microfuge tubes. These tubes were placed on a rotator for 60 minutes at 4°C to allow the cells to be fully

lysed. The mixture was then centrifuged at 13,000rpm for 15 minutes. The supernatant was retained and stored at -20°C for protein quantification. Lysis buffer used in the present study was prepared as follows: NaCl 150mM (8.76g), Tris 50mM (6.05g), sodium azide 0.02% (200mg), sodium deoxycholate 0.5% (5g), Triton X-100 1.5% (15ml), Aprotinin 1µg/ml (1mg), Na₃VO₄ 5mM (919.5mg) and Leupeptin 1µg/ml (1mg) in 1 litre of distilled water.

2.8.2 Protein quantification

Protein quantification was performed using Bio-Rad DC Protein Assay kit (Bio-Rad Laboratories, Hemel-Hempstead, UK) in accordance with the manufacturer's instructions. In brief, bovine serum albumin (BSA, 50mg/ml) was serially diluted 8 times to be used as standards. Firstly, 5µl of standard and protein samples were added to a 96-well plate separately. Then working reagent A' was made by adding 20µl of reagent S to each millilitre of reagent A, and 25µl of reagent A' was added to each well followed by 200µl of reagent B. The plate was then rested in the dark for 15 minutes. Once developed, the plate was read in an ELx800 spectrophotometer (Bio-Tek, Wolf laboratories, York, UK) at 595nm. The absorbance values of standards were used to generate a standard curve and the absorbance values of samples were used to calculate protein concentration according to the standard curve.

2.8.3 Sodium dodecyl sulfate-polyacrylamide gel electrophoresis (SDS-PAGE)

SDS-PAGE was performed using the OmniPAGE VS10 vertical electrophoresis system (Figure 2.9, Wolf Laboratories, York, UK). Specifically, two gel cassettes containing four cleaned and assembled glass plates were placed on a casting stand. Following assembly, ethanol was used to test for leaks by filling the area between the glass panels.

The concentration of Acrylamide gels used in the study was between 8% to 10% depending on the molecular weight of the target protein. In general, low molecular weight proteins are best resolved on high percentage gels, whereas large proteins require lower percentage gels for sufficient resolution. Initially, 15ml resolving gel and 5ml stacking gel were prepared according to Table 2.4

Table 2.4 Acrylamide gel preparation

	10% Resolving gel (ml)	8% Resolving gel (ml)	5% Stacking gel (ml)
H ₂ O	5.9	6.9	3.4
30% acrylamide mix	5.0	4.0	0.83
Tris	3.8 (pH 8.8)	3.8 (pH 8.8)	0.63 (pH 6.8)
10% SDS	0.15	0.15	0.05
10% Ammonia Persulphate	0.15	0.15	0.05
TEMED	0.006	0.006	0.005

Once all the components of the resolving gel were added and mixed in a universal container, the gel mixture was then quickly poured into the slot of the two glass plates, using a plastic pipette until 1cm below the bottom edge of the comb. The top edge of the resolving gel was then covered with 75% ethanol and the gel left to set for 30 to 45 minutes (depending on room temperature). Following that, ethanol was removed and the stacking gel was added on top of the resolving gel. Plastic combs were gently inserted between the glasses before the stacking gel set to form wells for protein loading. Once both resolving and stacking gels had set, the cassette was placed in an electrophoresis tank which was filled with running buffer (Tris-Glycine-SDS Buffer; Sigma-Aldrich, Dorset, UK). The comb was then carefully removed from the gel and a broad range protein marker (Santa Cruz Biotechnology, England, UK) and protein samples were loaded into the wells (10µl to 15µl, depending on the size of combs). Finally, the electrophoresis began under the conditions of 90-120V, 40mA, and 50W until the protein maker was fully separated.

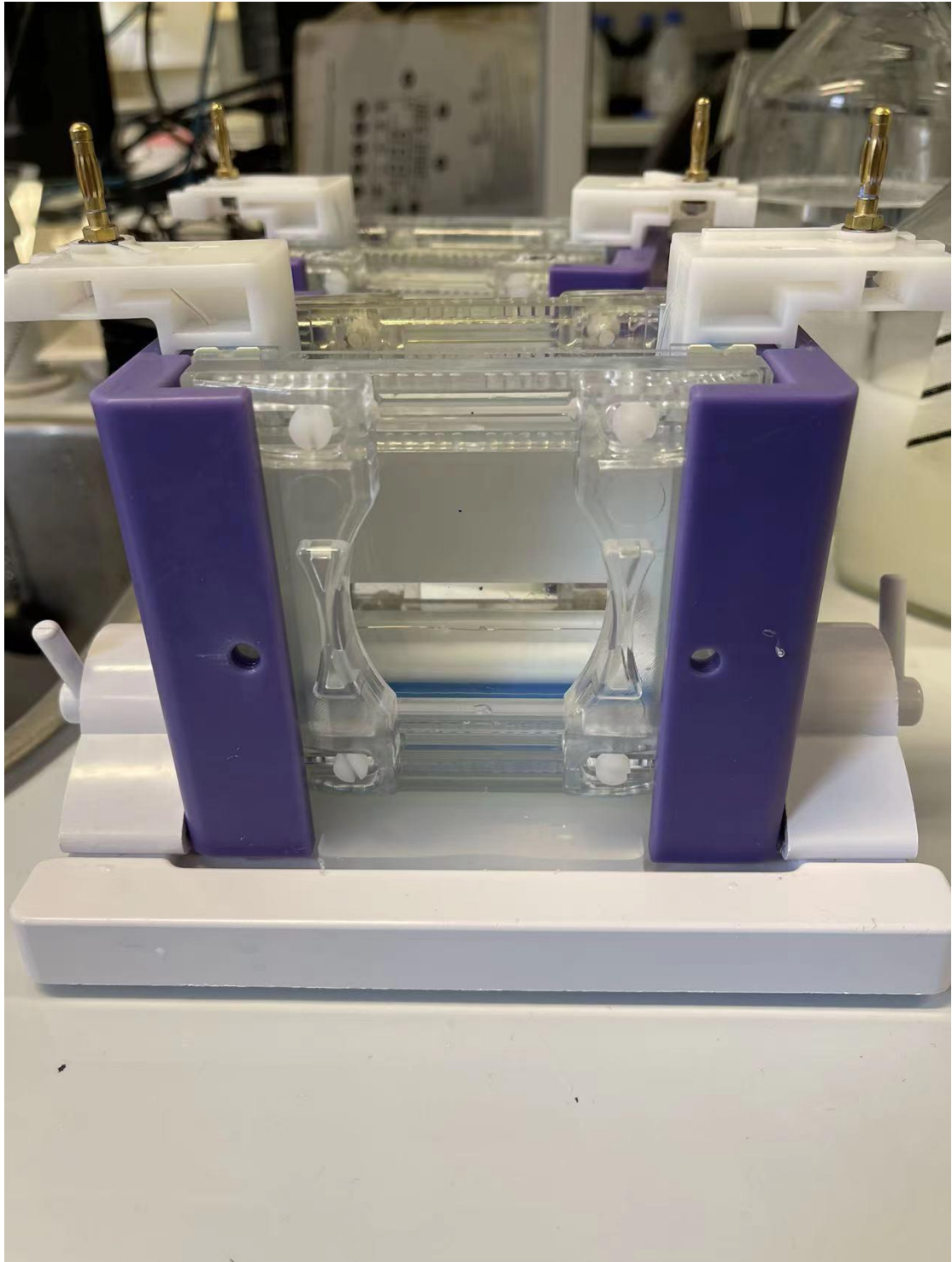


Figure 2.9 OmniPAGE VS10 vertical electrophoresis system (Wolf Laboratories, York, UK)

2.8.4 Protein transfer from gel to membrane

After electrophoresis was complete, proteins needed to be transferred from the gel onto polyvinylidene fluoride (PVDF) membrane (Millipore UK, United Kingdom). First, the PVDF membrane was prepared by wetting it in 99% methanol for 5 minutes and then soaking it briefly in distilled water followed by transfer buffer. Filter papers were also soaked in the transfer buffer for 10 minutes in advance. Then the resolving gel was taken out from the tank and assembled together with filter papers and PVDF membrane (Transfer sandwich). Any air bubbles were gently removed with a roller after placing the gel in an SD10 SemiDry Maxi System blotting unit (Figure 2.10, Wolf Laboratories, York, UK) for semi-dry transfer. Electroblotting was then performed under the conditions of 15V, 500mA, and 8W for 50 to 90 minutes (depending on the size of target proteins).



Figure 2.10 SD10 SemiDry Maxi System blotting unit (Wolf Laboratories, York, UK)

2.8.5 Immunoblotting

The first step of immunoblotting was to wash and block the membrane with non-specific protein. After semi-dry transfer, the membrane was placed in a UC and rinsed with blocking buffer (TBS-T with 5% milk) for 1 hour on a rotator. Following blocking, primary antibody diluted (1:500) in washing buffer (TBS-T with 2.5% milk) was added and incubated overnight at 4°C. The primary antibody solution was then removed and the membrane was washed with washing buffer three times.

After washing to remove unbound primary antibody, corresponding secondary antibody was added (1:1000 dilution in washing buffer) and incubated for 1 hour at room temperature. The membrane was then ready for chemiluminescence detection after washed three times with TBS-T.

2.8.6 Detection of blotting

The detection of blotting was conducted by a chemiluminescence imaging system. First, the membrane was developed using an EZ-ECL detection kit (Geneflow, Litchfield, UK). An equal amount of solution A and B was mixed and rested in the dark for 20 minutes before use. The membrane was covered with the mixture and developed for approximately 3 minutes and placed in G:BOX Chemi XRQ protein detection system (Figure 2.11, Syngene, Cambridge, UK) to generate the image.



Figure 2.11 G:BOX Chemi XRQ protein detection system (Syngene, Cambridge, UK)

2.9 Clinical cohorts

2.9.1 Cardiff Breast Cancer cohort

A clinical cohort of breast cancer was available within the host laboratory. The cohort consists of both tumour tissue samples and background normal tissue samples, collected in the University Hospital of Wales. The samples were collected under ethical approval (Bro Taf Health Authority; ethics approval number 01/4303 and 01/4046). Tissue samples were homogenised using a handheld homogeniser before being subject to Tri Reagent RNA extraction, as outlined in section 2.5, standardised and used to generate cDNA. This cohort has been previously described (Davies et al. 2008).

2.9.2 Cancer Bank breast cancer patient serum cohort

A cohort and database of breast cancer serum samples were available in the host laboratory. These samples had previously been obtained as part of an application to the Wales Cancer Bank (application reference 15/009). In total 150 serum samples from patients with breast cancer were obtained from Wales Cancer Bank together with follow up information (median patient follow up time 7.5 years). These samples were used for Enzyme Linked Immunosorbent Assay (ELISA) analysis of serum ALCAM levels.

2.9.3 Online datasets analysis

The clinical cohorts available within the host laboratory were supplemented with information available through online datasets. The KMplot (www.kmplot.com) website and resource (Gyorffy 2021) was accessed to further explore the clinical significance of ALCAM in breast cancer and its implication in the context of the hormone receptor status.

2.9.4 Pituitary cohort

As a secondary endocrine cohort, we were able to access a pituitary clinical cancer cohort to supplement our breast cancer analysis within the host department. This cohort derived from the collaboration between Cardiff University and Capital Medical University and has been previously described in full (Jia et al. 2013). Pituitary adenoma samples were freshly collected within the Department of Neurosurgery of Beijing TianTan Hospital immediately following microsurgical resection. Ethical approval for this cohort was obtained from Local Research Ethics Committee and samples collected with patient's consent. A total of 95 patients were involved in the study and tissues were immediately frozen and stored in liquid nitrogen following

collection. The clinical and pathological information was obtained and recorded for analysis. The presence of bone invasion and metastasis was confirmed by medical imaging, namely MRI scanner. The endocrine nature of the tumours was based on clinical serological tests and pathological examination.

2.9.5 Pancreatic cancer cohort

Two hundred and twenty-three cases were included in the study cohort. Pancreatic cancer tissues and adjacent normal tissues from patients who underwent surgical treatment were obtained immediately after surgery, stored in liquid nitrogen until further use. Clinical and pathological information, as well as follow-up data (median follow-up time: 12 month), was collected by specially assigned personnel. This study follows the Helsinki Declaration and was approved by the Ethics Committee of Peking University Cancer Hospital (Ethics approval number 2006021).

2.10 Enzyme Linked Immunosorbent Assay (ELISA)

ELISA was used to detect serum ALCAM within breast cancer patient samples using a Human ALCAM (CD166) ELISA kit (Fisher Scientific UK, Leicestershire, UK), in accordance with the manufacturer's instructions. In brief, samples, standards and all other reagent provided by the kit were diluted or prepared as instructed.

Either 100µl of standard or unknown sample was added to the ELISA plates, covered and incubated for 2.5 hours at room temperature with gentle shaking. Following this, the solution was discarded, and the plate washed four times with 300µl wash buffer, with complete removal of the wash buffer at each step and a final inverted blotting against tissue paper to ensure complete removal. Subsequently, 100µl of the biotinylated antibody (prepared in Diluent B) was added to each well and the plate incubated for 1 hour on a rotating platform. Following this, the plate was

washed four times as previously described before adding 100µl of Streptavidin-HRP solution (in Diluent B) to each well and incubating for 45 minutes at room temperature on a rotating platform. The plate was then subject to a further four washes as previously described before adding 100µl of the TMB substrate to each well and incubating for 30 minutes in the dark (covered in foil) on a rotating platform. Following this 50µl of Stop solution was added to each well and the plate read on a plate reader (450nm) within 30 minutes and results recorded and analysed in conjunction with patient pathological information.

2.11 Immunohistochemical (IHC) staining analysis

IHC analysis was used to assess ALCAM tissue expression in clinical samples, using tissue microarrays (TMA). A breast cancer tissue array (No. BR1503f) and a pancreatic tissue array (No. PA2081c) (US Biomax, Inc., Derwood, MD, USA) were used in the study. The TMA was processed for antigen retrieval in 0.1M EDTA buffer, heated in a microwave for 20 minutes. Subsequently this was cooled under running tap water before being blocked for 2 hours in 5–10% horse serum and, following this, incubated overnight with an anti-ALCAM primary antibody (2 µg/ml; Novacastra, Milton Keynes, UK). Following this, the TMA was incubated with secondary and tertiary reagents from a Vectastain Elite Universal ABC kit (Vector Laboratories Ltd., Peterborough, UK), in accordance with the manufacturer's guidelines. The TMA was then developed with diaminobenzidine (5mg/ml; Sigma-Aldrich, Dorset, UK) for 10 minutes, counterstained with Gill's hematoxylin (Vector Laboratories Ltd., Peterborough, UK), dehydrated, cleared in xylene and mounted in DPX (Sigma-Aldrich, Dorset, UK). Once dried, sections were viewed under the microscope and digital images captured and scored.

2.12 Immunoprecipitation (IP) assay

Protein samples were prepared using lysis buffer without SDS and quantified as mentioned in section 2.8. After protein quantification, samples were adjusted to be the same concentration (4mg/ml) in 1.5ml microfuge tubes. Next, primary antibodies were added to the samples. The tubes were then placed on a rotating wheel (Wolf laboratories, York, UK) at 35rpm and at 4°C overnight. Following that, A/G agarose (Insight Biotechnologies, Middlesex, UK) was added to the samples and again placed on a rotating wheel for 2 to 4 hours. After the protein/antibody had fully interacted with A/G agarose, the mixture was then transfer into tubes and centrifuged at 4°C, 7500 rpm for 5 minutes. After removing supernatants, the samples were washed three times with lysis buffer.

Following this, the extra lysis buffer was removed, 1× samples buffer was mixed with the precipitate and the samples were then boiled at 98°C for 10 to 15 minutes. The supernatant, which contains the proteins precipitated by the antibody, was then stored at -20°C for further study.

2.13 Cell growth assay

Equal numbers of cells were seeded in 96-well plates and incubated at 37°C, with 5% CO₂ for 72 hours. The incubation time was decided based on the doubling time of the cells and previous studies in the host laboratory using the same cell lines.

Following incubation, the cells were fixed with 4% formalin, stained with 0.5% crystal violet and extracted with 10% acetic acid after washing. Measuring the absorbance at 595nm was carried out using an ELx800 spectrophotometer (Bio-Tek, Wolf laboratories, York, UK) as shown in Figure 2.12 to detect their respective cell density.



Figure 2.12 ELx800 spectrophotometer (Bio-Tek, Wolf laboratories, York, UK)

2.14 Drug toxicity assay

Cells were seeded into 96 well plates and treated with serial-diluted drugs, then incubated in suitable conditions. The concentrations of the drugs were respectively chosen based on their known IC₅₀ and previous studies. After 72 hours, the cells were fixed with 4% formalin, stained with 0.5% crystal violet and extracted with 10% acetic acid after washing. The absorbance was measured at 595 nm using a spectrophotometer to detect their respective cell densities. The percentage drug toxicity was calculated as follow:

$$\text{Percentage drug toxicity} = (\text{Absorbance in untreated well} - \text{Absorbance in drug treated well}) / \text{Absorbance in untreated well}$$

The scatter plots of percentage toxicity and drug concentration were plotted, and fitting curves were used to calculate IC₅₀ value.

2.15 Fluorescence based Tumour-endothelial interaction assay

Tumour-endothelial interaction was assessed using a method previously described (Hiscox and Jiang 1997). Briefly, cancer cells were cultured to sub confluence. On collection of the cell suspension with EDTA/Trypsin buffer, they were subjected to staining for 30 minutes with 5 μ M Dil (1,1'-Dioctadecyl-3,3,3',3'Tetramethylindocarbocyanine Perchlorate), a red fluorophore that only stains the cellular membrane without affecting other cell fractions. After extensive washing to remove the free dyes, a fixed number of cells was added to an endothelial cell confluent monolayer, established on the 96-well plates prior to the preparation of cancer cells. After 20 minutes, the culture wells were carefully washed with PBS to remove the non-adherent cancer cells. The remaining cells, that adhered to the endothelial cell monolayer, were fixed with 4% formalin. Representative bright field and fluorescence images were captured on an EVOS automated cell analyser (Figure 2.13). The merged images were generated and attached cancer cells were quantified using the cell counting function provided by the EVOS system.

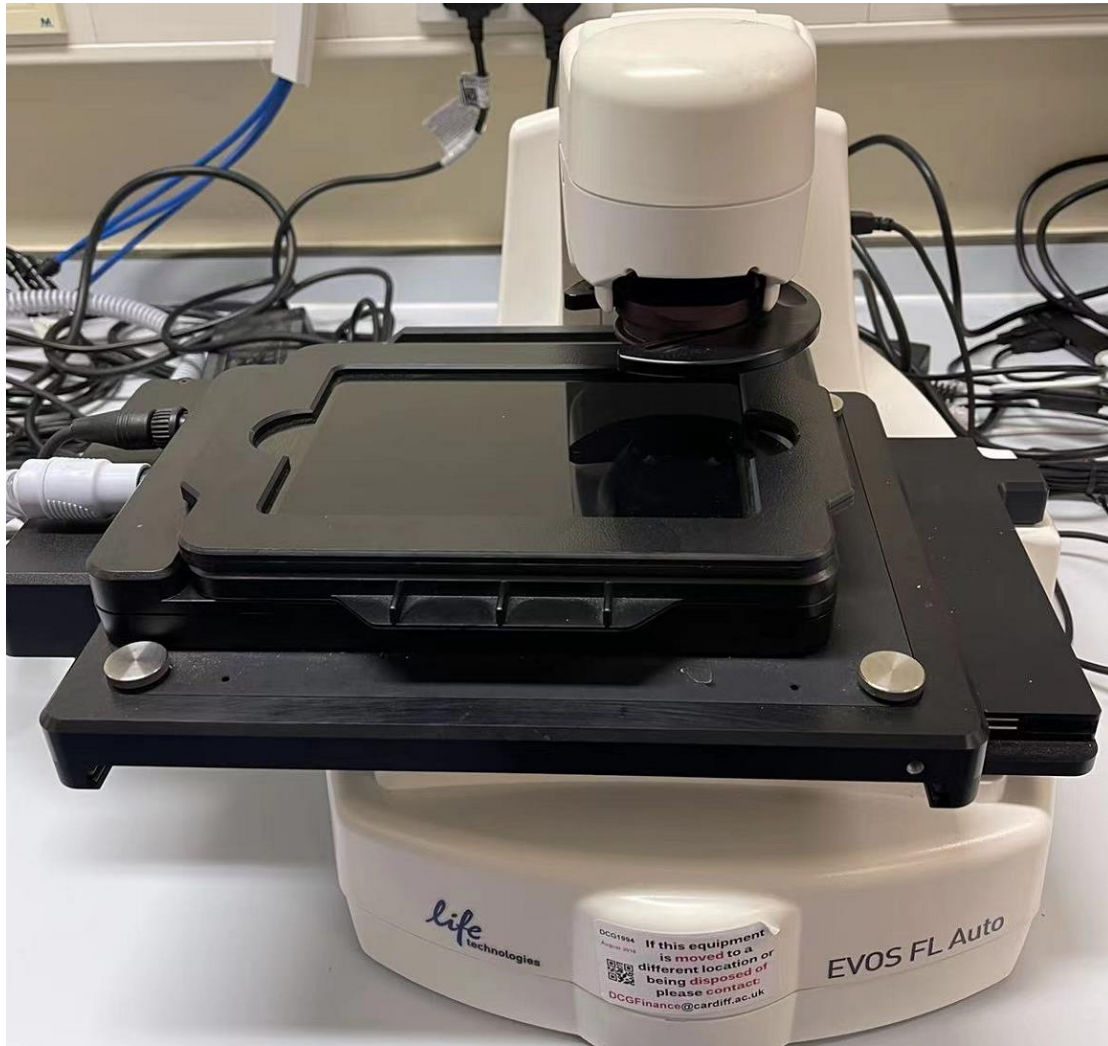


Figure 2.13 EVOS FL2 Auto Imaging System (Life technologies, CA, USA)

2.16 Electric cell-substrate impedance sensing (ECIS)

ECIS (Electric cell-substrate impedance sensing) assay was applied to investigate cellular behaviour based on the impedance parameter detected from gold electrodes coated on the bottom of a 96 well array (Figure 2.14, Applied Biophysics Inc., NJ, USA). The basic principle of ECIS based on the dynamic change of electrical resistance in the process of cell adherence to gold electrodes in each well. From the electrical resistance and impedance changes, effects on cell attachment and motility can be examined. This offers a real-time, human interface free, multiple replicate and

automated *in vitro* approach to monitoring and quantifying the functional behaviour of cells including cell adhesion and migration and indeed a wider range of cell functions including barrier function and paracellular permeability of the cells (Keese et al. 2002; Jiang et al. 2009).

In my study, I have selected the ECIS-Z0 (Figure 2.14A) which offers the most diverse range of measurement of cell functions including the automated cell wounding and transfection functions. I have also selected 96W1E as the key array for my study. 96W1E is the array with 96 well and 1 gold plated electrode. The size and area of the electrode offers a versatile tool for cell adhesion assays. In brief, prior to cell seeding, 96W1E ECIS arrays containing growth medium were stabilised to clean the oxidised surface. This was done by using the stabilisation function within the system and washed. Cells were seeded at an appropriate density (20,000 to 30,000 per well) before the 96 well array was equipped in the incubated array station and changes in resistance/impedance measured over the course of the experiment. In my study, I automatically traced the cells over multiple frequencies, namely from 1,000Hz, 2,000Hz, 4,000Hz, 8,000Hz, 16,000Hz, 32,000Hz, and 64,000Hz. The first 4 hours of data was analysed for initial attachment and spreading.

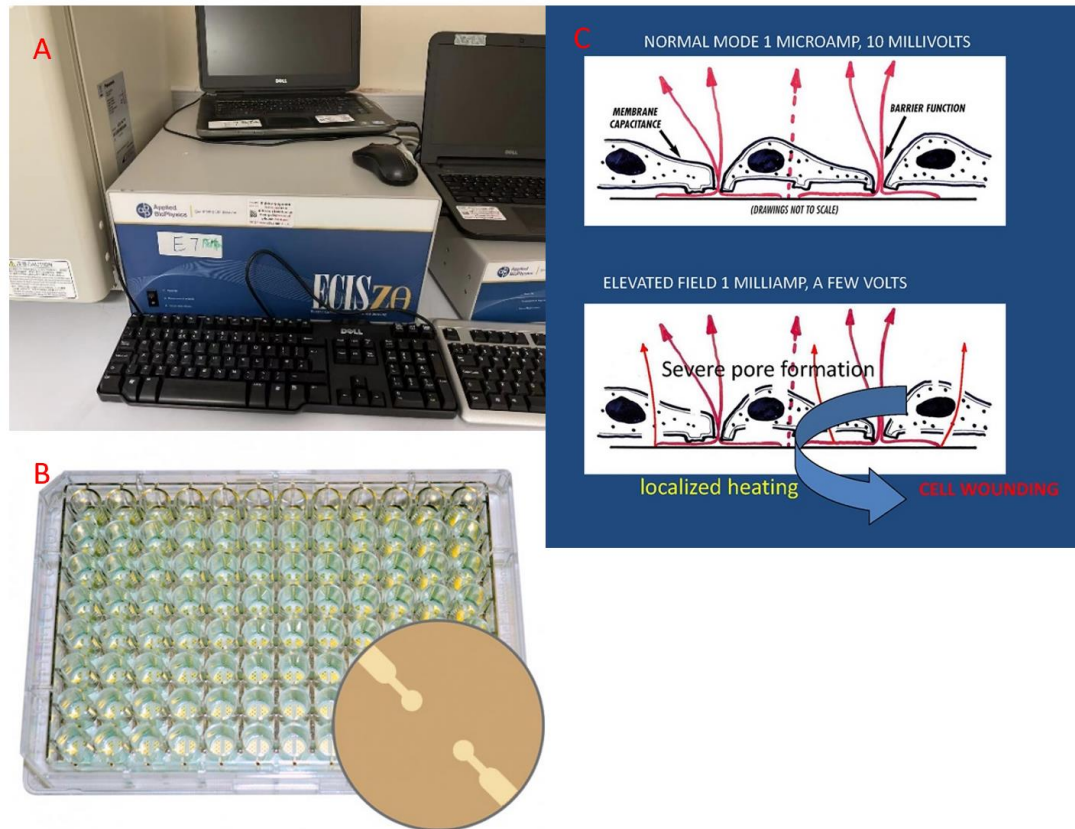


Figure 2.14 Electric cell-substrate impedance sensing system. A: The ECISZ0 unit used in the present study. B: The 96W1E electrode array used in the present study. (Applied Biophysics Inc., NJ, USA) C: Method to measure cell-substrate impedance (www.biophysics.com)

2.17 Antibody Microarrays for signalling pathway analysis

2.17.1 Kinexus™ KAM-900P Antibody Microarrays

To perform a comprehensive analysis of protein interaction and molecular signalling pathway, an antibody protein microarray KAM900P was used in the study. The KAM-900P antibody microarray featured 613 phosphosite-specific antibodies (for phosphorylation) and 265 pan-specific antibodies (for expression levels of these phosphoproteins). These antibodies, which have been selected from more than 6000 different commercial antibodies from over 26 companies, have been independently tested by Kinexus to identify many of the best immunological reagents available to

track important signal transduction proteins. Specific descriptions of the antibodies are listed in Figure 2.15.

KAM-900P Content	Total %	Total Number
Total number of pan-specific antibodies:	30%	265
Total number of phospho-specific antibodies:	70%	613
Total Number of Antibodies	100%	878
Total number of protein kinase pan-specific antibodies:	25%	219
Total number of protein kinase phosphosite-specific antibodies:	50%	443
Total number of protein phosphatase pan-specific antibodies:	0.2%	2
Total number of protein phosphatase phosphosite-specific antibodies:	0.7%	6
Total number of transcription factor pan-specific antibodies:	1.7%	15
Total number of transcription factor phosphosite-specific antibodies:	4%	37

Figure 2.15 Families of protein targets for the KAM-900P antibody microarray (www.kinexus.ca).

Several different methodologies were used with KAM-900 antibody microarrays, and these are outlined in Figure 2.16. A representative image for the microarray is shown in Figure 2.17.

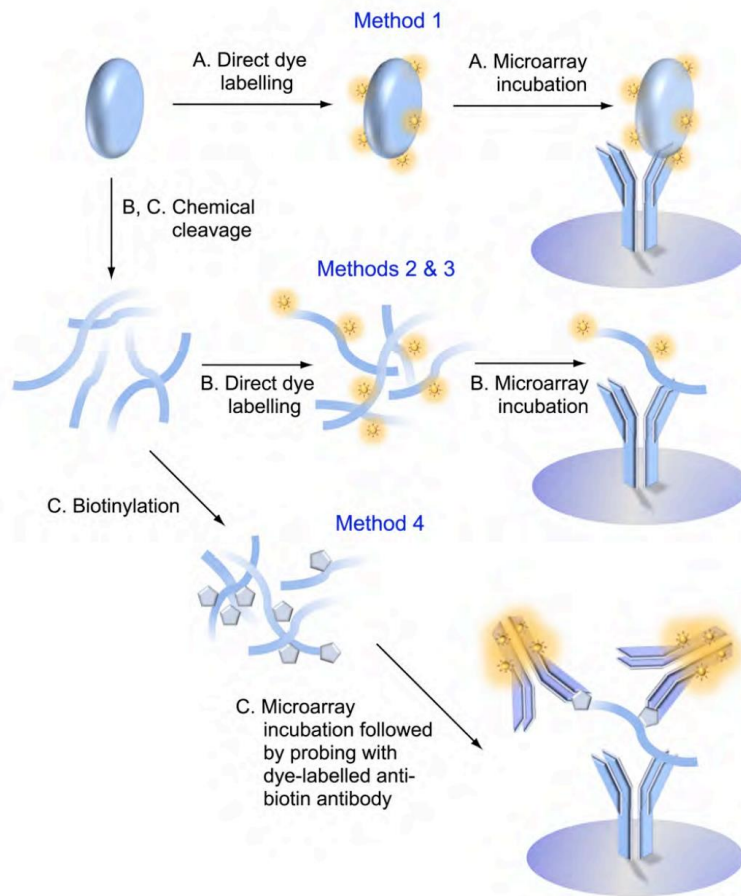


Figure 2.16 Detection method used in KAM-900 Antibody Microarray (www.kinexus.ca). Four different methods were used in the microarray analysis based on the biological feature of the respective kinases.

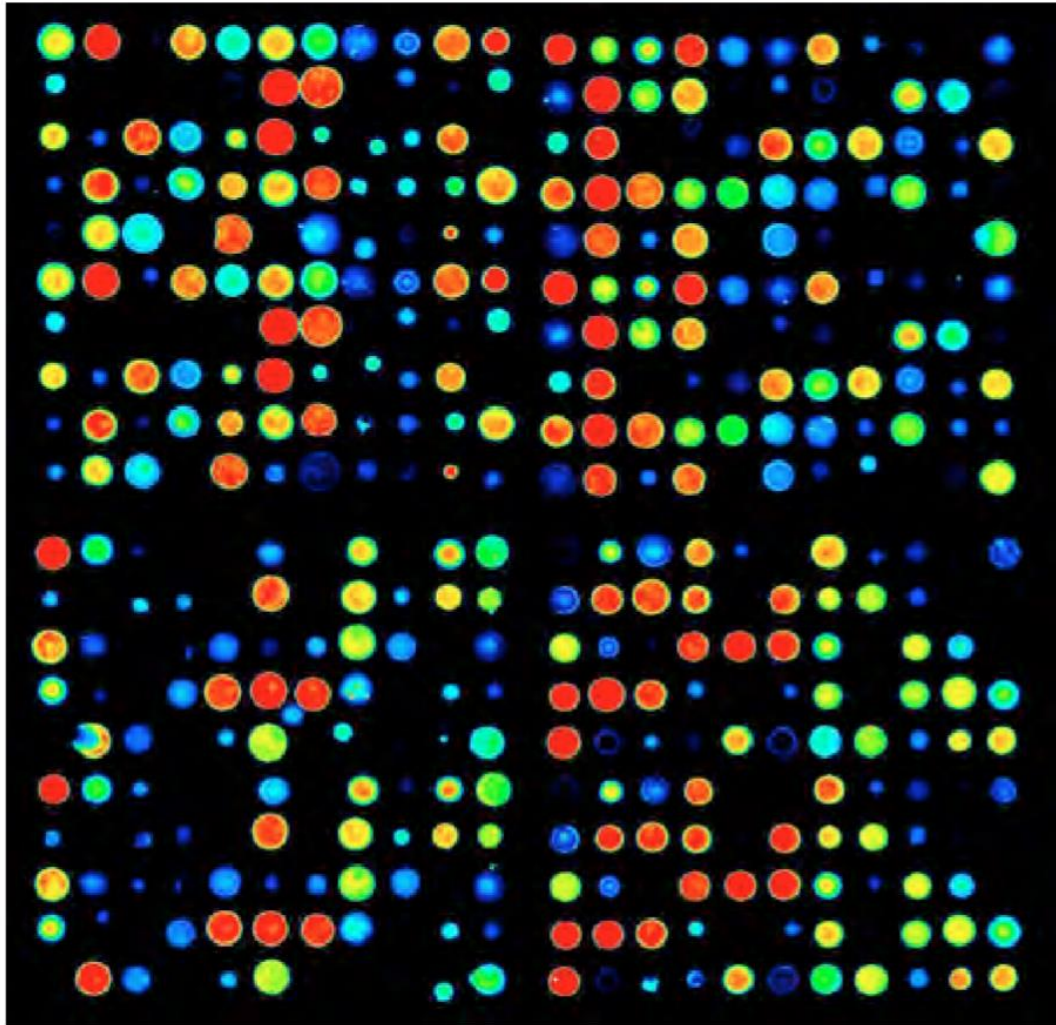


Figure 2.17 A representative close up scanned image which is divided into two fields on a KAM antibody microarray chip, incubated with dye-labelled lysate proteins. Decreasing signal intensity corresponds with a red to orange to yellow to green to blue transition

2.17.2 Key information from KAM-900P antibody microarray reports

The following are the key parameters collected and used for the data analyses (www.kinexus.ca):

Globally Normalized Signal Intensity: Background corrected intensity values are globally normalized. The Globally Normalized Signal Intensity is calculated by summing the intensities of all the net signal median values for a sample.

Flag: An indication of the quality of the spot, based on its morphology and background. The flagging codes used in the reports are as follows:

0: acceptable spots.

1: spots manually flagged for reasons and may not be very reliable.

3: poor spots defined by various parameters.

%CFC: The percent change of the treated sample in Normalized Intensity from the specified control.

Calculation = $((\text{Globally Normalized Treated} - \text{Globally Normalized Control}) / \text{Globally Normalized Control}) * 100\%$

% Error Range: A parameter to show how tightly the “Globally Normalized Net Signal Intensity” for adjacent duplicate spots of the same protein in the sample compared to each other.

Calculation = $(\text{ABS}(\text{Globally Normalized Spot 1} - \text{Globally Normalized Spot 2}) / \text{Globally Normalized Spot 2}) * 100\%$

Log2 (Intensity Corrected): Spot intensity corrected for background is log transformed with the base of 2.

Calculation = $\text{LOG}(\text{Average Net Signal Median}, 2)$

Z Scores: Z score transformation corrects data internally within a single sample.

Z Score Difference: The difference between the observed protein Z scores in samples in comparison.

Z Ratios: Divide the Z Score Differences by the SD of all the differences for the comparison.

2.18 Statistical analysis

Data was analysed using the Sigmaplot 11, Minitab and SPSS 26 statistical software packages. A combination of T-Test, Mann-Whitney, ANOVA, Kruskal Wallis, Fisher Exact Test, Kaplan-Meier survival analysis, Cox regression and ROC analysis was undertaken. Specific methods used are given in the respective result section. Values of $p < 0.05$ were regarded as significant.

Chapter-3

ALCAM expression in breast cancer and the relationship to skeletal metastasis and clinical outcome of the patients

3.1 Introduction

As previously discussed, there have been studies, including the first study from the host laboratory, that have reported that ALCAM has a clear relationship with disease progression and bone metastasis of breast cancer (King et al. 2004; Davies et al. 2008) and that breast cancer cells appear to have responded to a microenvironment mimicking bone (Davies and Jiang 2010). Here, we analysed available clinical cohorts to further explore, in detail, the link between ALCAM and clinical outcomes and whether the endocrine system, including hormone receptor status of breast cancer, acts as a potential regulator in cancer progression and bone metastases in the context of hormone receptors status (including oestrogen receptors and HER family receptors). From the initial findings that ALCAM mediated bone metastasis appears to be endocrine receptor related, we explored a second cohort of human endocrine tumours, namely pituitary tumours, and tried to establish if the relationship between ALCAM and bone metastases of the endocrine tumour type also existed.

3.2 Methods

3.2.1 Clinical Cohorts

Breast tumour/serum cohort: The breast tumour cohort was based on a collection by the host laboratory, as has been previously reported (Davies *et al.* 2008), supported by Ethics Approval from the Bro Taf Research Ethics Committee (Ethics approval numbers 01/4303 and 01/4046). This cohort was used for gene transcript analysis. A cohort of serum samples from patients with breast cancer were obtained from the Wales Cancer Bank, a central collection of tumour samples in Wales, supported by the Wales Government and Cancer Research Wales. The present study

was under ethical approval by the WCB ethics panel (application, 15/009, WCB). The serum cohort was used for detection of circulating ALCAM.

Breast tissue array: The breast tissue array, BR1503f, was purchased from Biomax (Insight Biotechnologies, Sussex, England). It has 150 tissue cores from 75 patients, supported by tumour grade, staging, hormone receptor status (details in Supplement-1). The tissue array was used for immunohistochemical staining of ALCAM.

Pituitary tumour cohort: The Pituitary tumour cohort was based on a resource available at the host research laboratory and in collaboration with the Cardiff University collaborative partner, TianTan Hospital of Capital Medical University. The present study benefited from this existing collection and was described in full detail previously (Jia et al. 2013). Again, this cohort was used for gene transcript analysis.

TCGA datasets. This present study has taken advantage of the available TCGA database of breast cancer and has analysed the relationship between ALCAM and clinical outcome OS (overall survival), RFS (relapse free survival), DMSF (distant metastasis free survival) and PPS (post progression survival), and again in the context of hormone receptor status. Here, the web resource Kaplan-Meier Plotter (www.kmplot.com) was used.

3.2.2 Immunohistochemical (IHC) staining analysis

IHC analysis was used to assess ALCAM tissue expression in clinical samples, using tissue microarrays (TMA). A breast cancer tissue array (No. BR1503f) was used in the study as described in section 2.11.

3.2.3 Statistical methods

Statistical analysis of the data was performed using SPSS 26 software. Mann-Whitney U-test and Kruskal-Wallis test were used for continuous data and Fisher Exact test for categorical data. Survival was analysed using Kaplan-Meier survival analysis. ROC curve was used to test the diagnostic value. The statistical significance was defined as $p < 0.05$.

3.3 Results

3.3.1 Protein expression of ALCAM in breast cancers, analysis by immunohistochemistry (IHC)

I first investigated the presence and the pattern of ALCAM protein in a cohort of breast cancer tissues by way of IHC. Figure 3.1 shows the typical staining of ALCAM in normal breast tissue and cancer tissue. The intensity of ALCAM staining was assessed and scored based on the established method (Xin et al. 2021) and was shown here as follows: 0, negative staining; 1, weak staining; 2, moderate staining; 3, strong staining (Figure 3.1a). Table 3.1 summarises the ALCAM staining and statistical analysis results of the breast cancer tissue microarray. Although the case number of some subgroups was too small to compare, there are meaningful information that can be concluded from here. All the tissues with positive ALCAM staining had both cytoplasm and membrane staining (Figure 3.1b). Patients with T2 stage breast cancer had significantly higher levels of ALCAM staining compared with T3 ($p=0.001$) and T4 ($p=0.006$) stages. Although there appear to be some difference in ALCAM staining between the ER positive and negative groups, the p-value is marginally in short of reaching significance ($p=0.083$). It is interesting to note that in

HER2 positive group, the ALCAM staining was significantly lower than in HER2 negative group ($p < 0.001$) (Figure 3.1c).

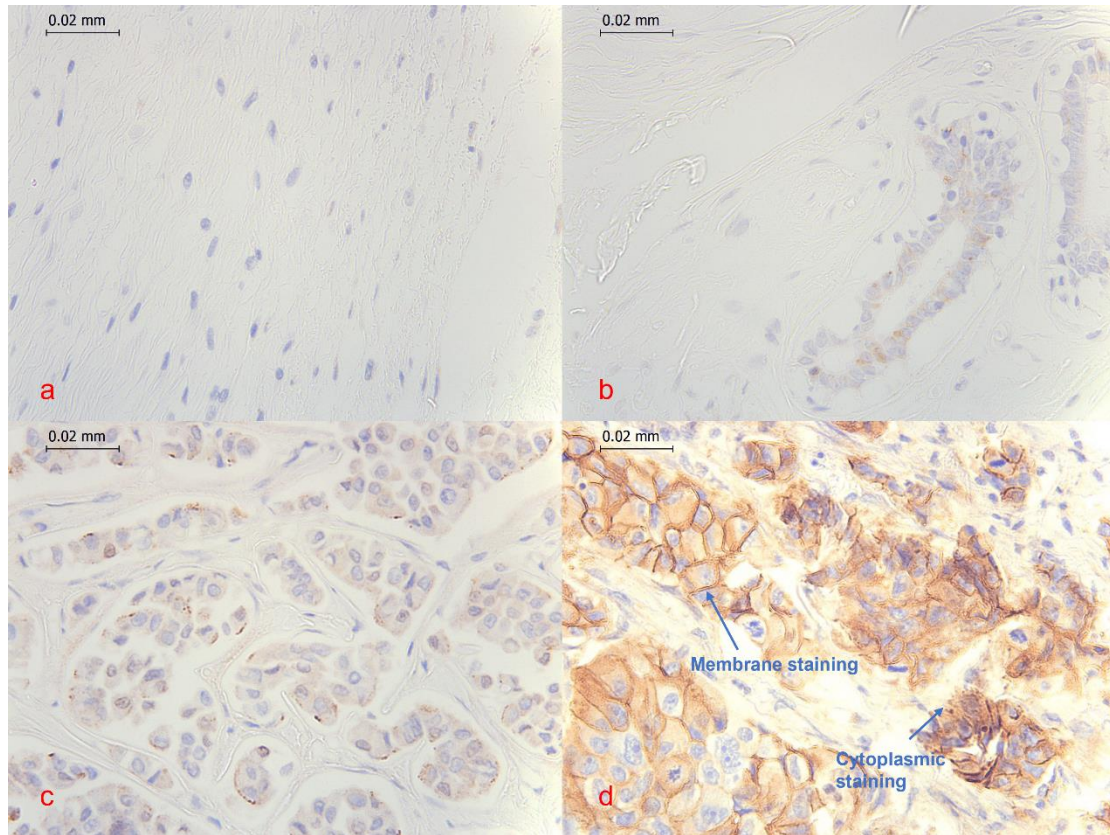


Figure 3.1a Representative images of ALCAM staining in breast cancer TMA. Image a: negative staining (0); Image b: weak staining (1); Image c: moderate staining (2); Image d: strong staining (3).

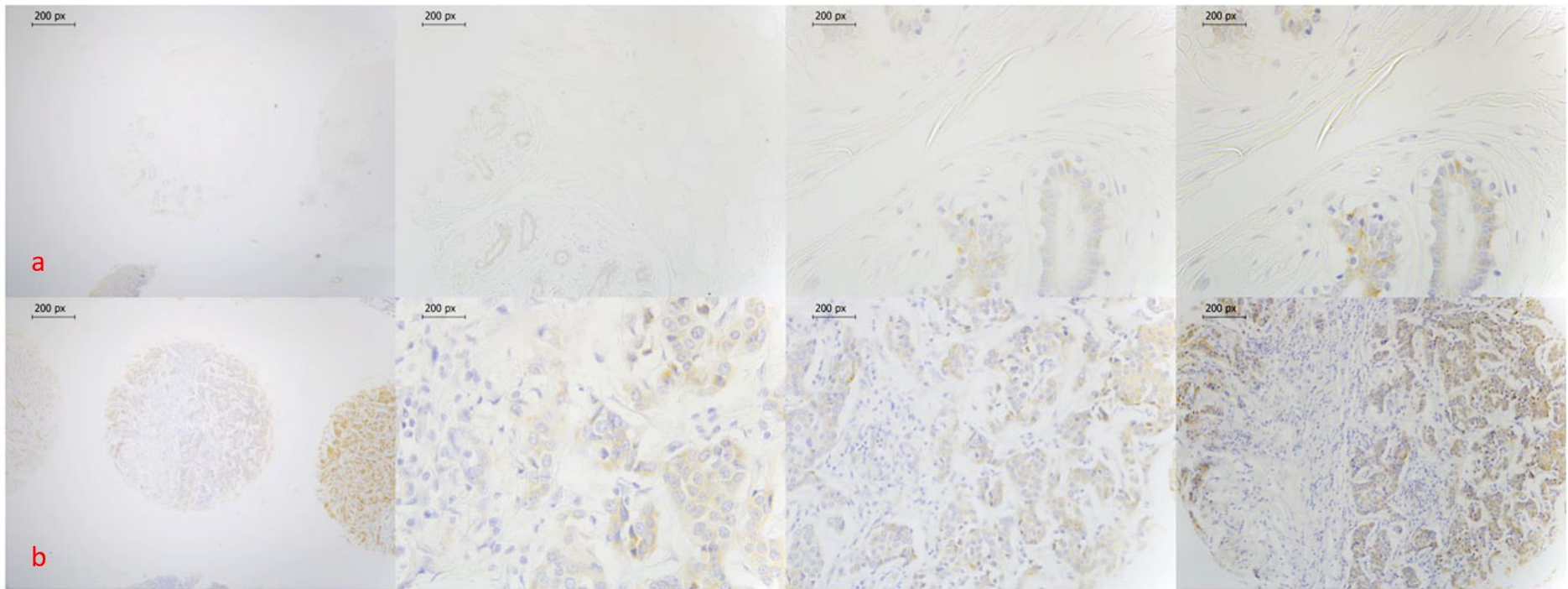


Figure 3.1b ALCAM staining in normal and breast cancer tissues. Line a: Normal breast tissues; Line b: Invasive ductal carcinoma. Representative images shown.

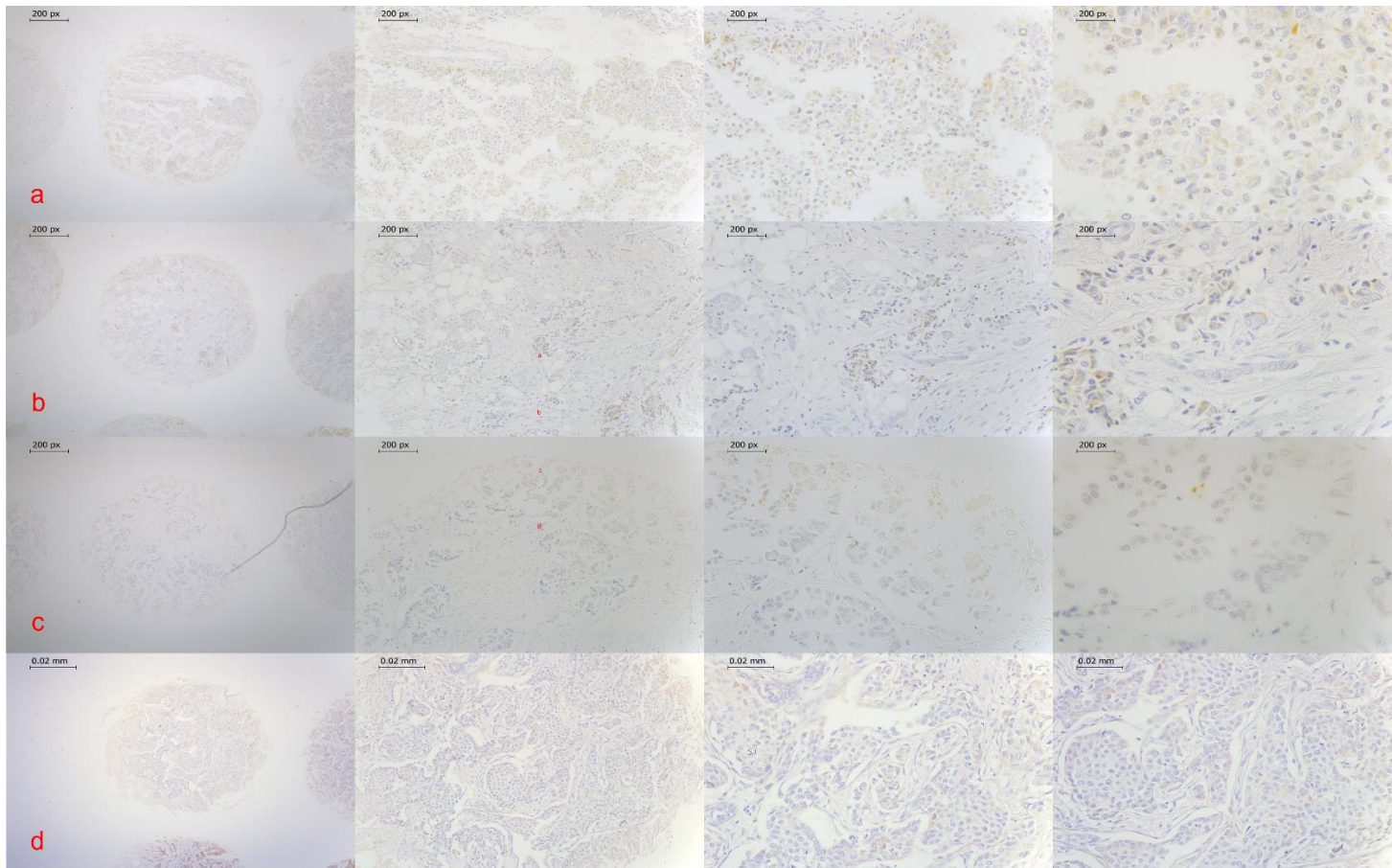


Figure 3.1c ALCAM staining in breast cancer tissues. Line a: ER(+)/HER2(+) breast cancer tissue; Line b: ER(+)/HER2(-) breast cancer tissue; Line c: ER(-)/HER2(+) breast cancer tissue; ER(-)/HER2(-) breast cancer tissue. Representative images shown.

Table 3.1 ALCAM staining of breast cancer TMA.

	Total number	Intensity				Statistical significance	
		0	1	2	3	Chi value	p
Pathology							
Invasive ductal carcinoma	120	21	42	35	22		
Intraductal carcinoma	14	3	8	3	0		
Fibroadenoma	6	2	3	1	0		
Adjacent normal breast tissue	6	2	3	1	0		
Tumour stage							
T1	6	1	4	1	0		
T2	72	5	34	23	10	19.284	0.004 ^a
T3	26	10	6	6	4	15.663	0.001 ^b
T4	16	6	3	5	2	12.322	0.006 ^b
Differentiation Grade							
1	4	1	2	1	0		
2	60	8	27	18	7	2.607	0.456 ^c
3	30	1	17	9	3		
ER							
Positive	73	19	22	18	14	6.672	0.083
Negative	68	9	31	20	8		
HER2							
Positive	42	12	8	11	11	19.957	<0.001
Negative	99	10	48	30	8		

^a Overall chi-square test among T2, T3 and T4; ^b Compared with T2 group; ^c Compared with Grade 3 group;

3.3.2 Expression levels of ALCAM in breast cancers with bone metastasis

Our previous study (Davies *et al.* 2008) has shown that the ALCAM expression level of breast cancer patients with bone metastasis was significantly lower than those without bone metastasis. To further validate the previous results, we carried out a ROC analysis to explore the relationship between ALCAM and bone metastasis in the Cardiff cohort of breast cancer. As shown in Figure 3.2, there was a significant predictive value of bone metastasis by tumour ALCAM levels (AUC=0.662, $p=0.033$).

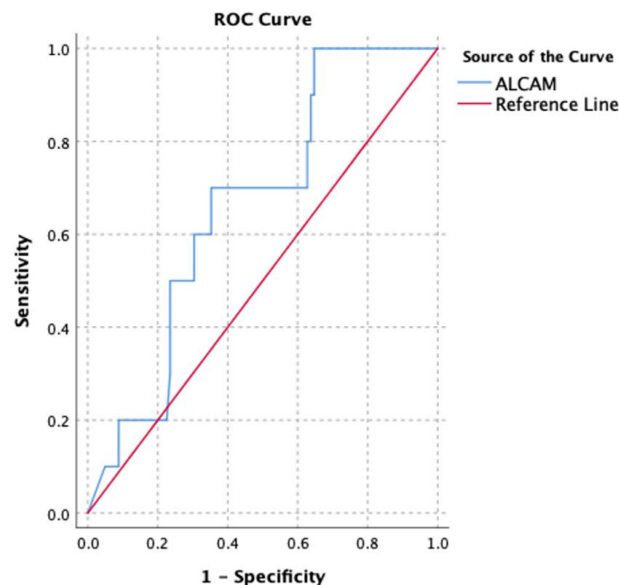


Figure 3.2 ROC curve of ALCAM transcript level and patients with bone metastasis (n=10)/without bone metastasis (n=102). The levels of ALCAM from breast tumours were analysed against the presence of bone metastasis by the ROC model on SPSS (version 26). The levels of ALCAM in tumour exhibited a good predictive value for the development of bone metastases (AUC=0.662, $p=0.033$, Overall model quality=0.51).

3.3.3 ALCAM, hormonal status and Bone Metastasis

We further used available information to explore the effect of hormone receptors on the regulation of ALCAM-mediated bone metastasis in breast cancer patients. The Cardiff cohort has the following hormone receptors (HR) tested by qPCR: ER, ER β , HER family (HER1 (EGFR), HER2, HER3, HER4) and AR (Androgen receptor). The

cohort has the datasets on the following hormones related to bone development and metastasis: PTHrP and PTHrPR, Multiple Endocrine Neoplasia I (MEN1) and Pituitary Tumour-Transforming Gene 1 Protein (PTTG1). The cohort was divided into those with high receptor expression (marked as “+” in Table 3.2) and low receptor expression (marked as “-“ in Table 3.2), dichotomised based on the best cut-off from ROC analysis. As illustrated in Table 3.2, ALCAM expression levels were significantly different between AR ($p=0.013$) and Aromatase ($p=0.002$) high expression and low expression groups. In the rest of the study groups, the differences were not found to be statistically significant.

To further explore if grouping may assist the analysis, breast tumours were divided into those with bone metastasis (marked as +) or without bone metastasis (marked as -) levels. The results (Table 3.3) showed no statistically significant differences in the subgroups, indicating that HR status may have no direct effect on bone metastasis of breast cancer patients.

Table 3.2 Comparison of ALCAM expression in different HR status.

	HR status	N	ALCAM expression (median)	p value*
ER	ER-	81	11.40	0.586
	ER+	19	19.30	
ER β	Er β -	82	13.70	0.314
	Er β +	21	8.34	
Her1	Her1-	56	19.35	0.195
	Her1+	56	8.72	
Her2	Her2-	56	18.60	0.503
	Her2+	56	10.90	
Her3	Her3-	56	11.05	0.981
	Her3+	56	20.30	
Her4	Her4-	56	23.85	0.121
	Her4+	56	8.79	
AR	AR-	53	6.32	0.013
	AR+	52	30.15	
Aromatase	Aromatase-	56	5.86	0.002
	Aromatase+	56	34.90	
PTHrPR	PTHrPR-	50	25.80	0.339
	PTHrPR+	62	11.20	
PTHrP	PTHrP-	50	9.67	0.363
	PTHrP+	49	19.30	
MEN1	MEN1-	56	13.70	0.478
	MEN1+	56	11.45	
PTTG1	PTTG1-	56	19.35	0.247
	PTTG1+	56	10.20	

* By Mann-Whitney U test

Table 3.3 Analyses of the correlation between HR status and the metastasis of breast cancer were conducted by Fisher Exact test. P < 0.05 indicated statistical significance.

	Bone (-)	Bone (+)	
ER(-)	76	5	
ER(+)	15	4	p=0.0637

	Bone (-)	Bone (+)	
ERβ(-)	75	7	
ERβ(+)	19	2	p=1

	Bone (-)	Bone (+)	
AR(-)	50	3	
AR(+)	47	5	P=0.4882

	Bone (-)	Bone (+)	
Her1(-)	51	5	
Her1(+)	51	5	p=1

	Bone (-)	Bone (+)	
Her2(-)	53	3	
Her2(+)	49	7	P=1

	Bone (-)	Bone (+)	
Her3(-)	51	5	
Her3(+)	51	5	P=1

	Bone (-)	Bone (+)	
Her4(-)	53	3	
Her4(+)	49	7	P=0.327

	Bone (-)	Bone (+)	
Aromatase(-)	52	4	
Aromatase(+)	50	6	0.7442

	Bone (-)	Bone (+)	
PTHrPR(-)	47	3	
PTHrPR(+)	55	7	0.5076

	Bone (-)	Bone (+)	
PTHrP(-)	47	3	
PTHrP(+)	44	5	0.487

	Bone (-)	Bone (+)	
MEN1(-)	49	7	
MEN1(+)	53	3	0.3207

	Bone (-)	Bone (+)	
PTTG1(-)	51	5	
PTTG1(+)	51	5	1

3.3.4 ALCAM and the survival of patients with breast cancer

The early study from the host laboratory had reported a relationship between ALCAM and the survival of the patients, based on the same breast cancer cohort as our present study (King *et al.* 2004). The results showed that patients with high levels of ALCAM had significant longer survival compared with those who had low levels of ALCAM (100.5 months vs 79.6 months, $p=0.009$).

Here, we further analysed the TCGA cohort regarding this relationship, which has demonstrated the same survival benefits observed in the Cardiff cohort. As shown in Figure 3.3 in which the ROC value was used as the cut-off point of the cohorts, patients with a higher level of ALCAM had a significantly longer relapse-free survival (RFS) (HR=0.77, $p<0.001$), distant metastasis-free survival (DMFS), (HR=0.77, $p=0.003$) and post-progression survival (PPS), (HR=0.74, $p=0.016$). The overall survival (OS) of the ALCAM high-expression group and low-expression group, although demonstrating the trend as others, did not reach statistical significance (HR=0.85, $p=0.110$).

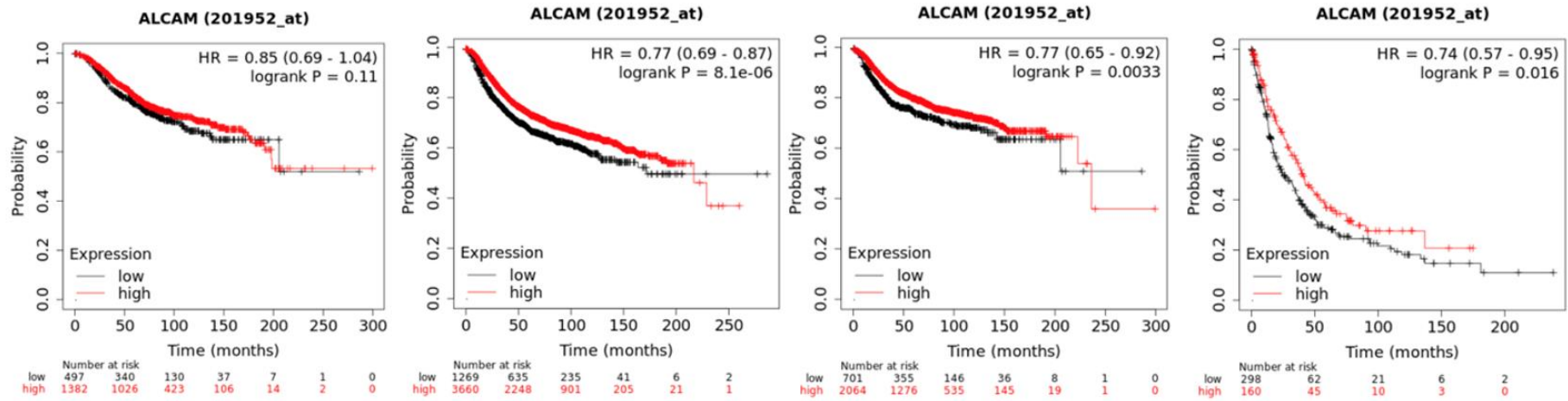


Figure 3.3 Survival analysis of ALCAM and breast cancer patients (TCGA database). OS, RFS, DMFS and PPS (from left to right). Data analysis was conducted and images obtained from the KMplot website. ROC value was used as the cut-off point of the cohorts.

3.3.5 ALCAM and the survival of the patients, a hormonal connection

To investigate the prognostic impact of ALCAM on breast cancer patients in relation to hormone receptors, we separated the cohort into different subgroups based on their receptor (ER and HER2) status and conducted survival analysis respectively. ROC value was used as the cut-off point of the cohorts. As shown in Figure 3.4, patients with higher levels of ALCAM had significantly longer overall survival compared to low ALCAM level patients in ER negative breast cancer (138.1 months vs 114.9 months, $p=0.017$). While in patients with ER positive breast cancer, no statistical significance was observed between the OS of high ALCAM group and low ALCAM group (132.0 months vs 65.2 months, $p=0.271$). In terms of disease-free survival, the cohort showed similar results with overall survival (Figure 3.5). DFS of the high ALCAM group was significantly higher than low ALCAM group (133.9 months vs 114.9 months, $p=0.048$) in patients with ER negative breast cancer. In ER positive breast cancer, no statistical significance was seen between the DFS of the high ALCAM group and low ALCAM group (124.5 months vs 59.5 months, $p=0.094$).

Figure 3.6 shows the overall survival of low ALCAM level and high ALCAM level groups in breast cancer patients with different HER2 status. Kaplan-Meier survival analysis showed no statistical significance between the OS of the high ALCAM group and low ALCAM group (150.2 months vs 130.7 months, $p=0.264$) in HER2 negative patients. However, the OS of the high ALCAM group was longer compared to the low ALCAM group in HER2 positive breast cancer patients (132.0 months vs 83.1 months, $p=0.010$). Similar results were also seen in disease-free survival. As shown in Figure 3.7, there was no difference between the DFS of the two groups with HER2 negative breast cancer ($p=0.084$) and statistical significance was found between high and low ALCAM groups with HER2 positive breast cancer ($p=0.019$).

Additionally, we also analysed the survival of triple negative and non-triple negative breast cancer cases in the cohort. Kaplan-Meier survival analysis (Figure 3.8) showed no statistical significance between the OS of the high ALCAM group and low ALCAM group in patients with triple negative breast cancer (140.2 months vs 133.8 months, $p=0.650$). However, in non-triple negative breast cancer, the OS of the high ALCAM group was longer compared to low ALCAM group (146.5 months vs 85.0 months, $p=0.001$). The results of disease-free survival were similar to overall survival. As shown in Figure 3.9, patients with non-triple negative breast cancer and higher levels of ALCAM had significantly longer DFS compared to those with lower levels of ALCAM (136.4 vs 79.3 months, $p=0.002$), while in patients with triple negative breast cancer, no difference was observed between the high and low ALCAM groups (141.5 vs 133.8 months, $p=0.516$).

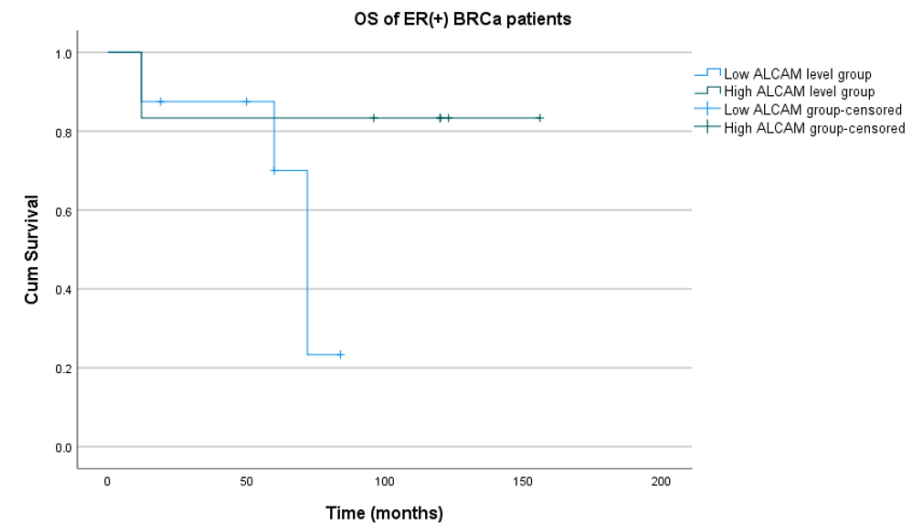
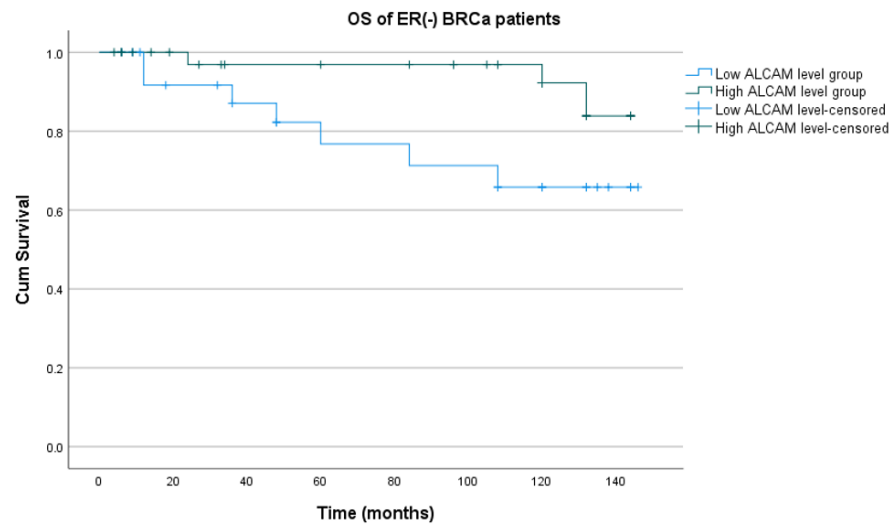


Figure 3.4 Overall survival of low ALCAM level and high ALCAM level group, stratified by ER status. Left: ER negative breast cancer, OS of high ALCAM group was significantly longer than low ALCAM group (138.1 months vs 114.9 months, $p=0.017$). Right: ER positive breast cancer, no statistical significance was observed between the OS of high ALCAM group and low ALCAM group (132.0 months vs 65.2 months, $p=0.271$).

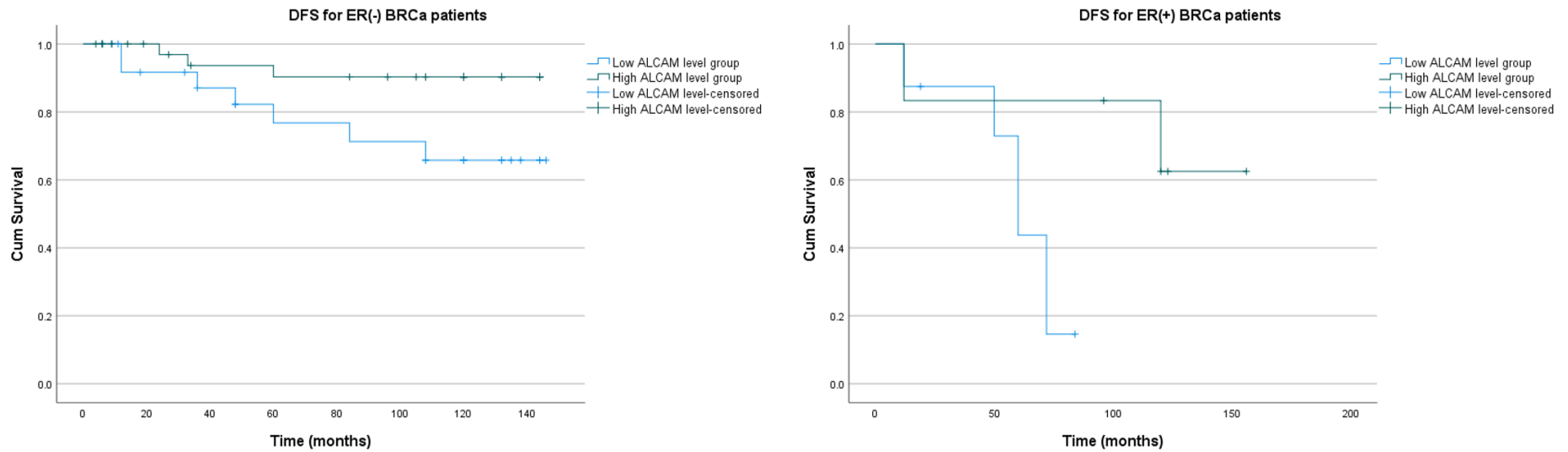


Figure 3.5 Disease-free survival of low ALCAM level and high ALCAM level group, stratified by ER status. Left: ER negative breast cancer, DFS of high ALCAM group was significantly longer than low ALCAM group (133.9 months vs 114.9 months, $p=0.048$). Right: ER positive breast cancer, no statistical significance was observed between the DFS of high ALCAM group and low ALCAM group (124.5 months vs 59.5 months, $p=0.094$).

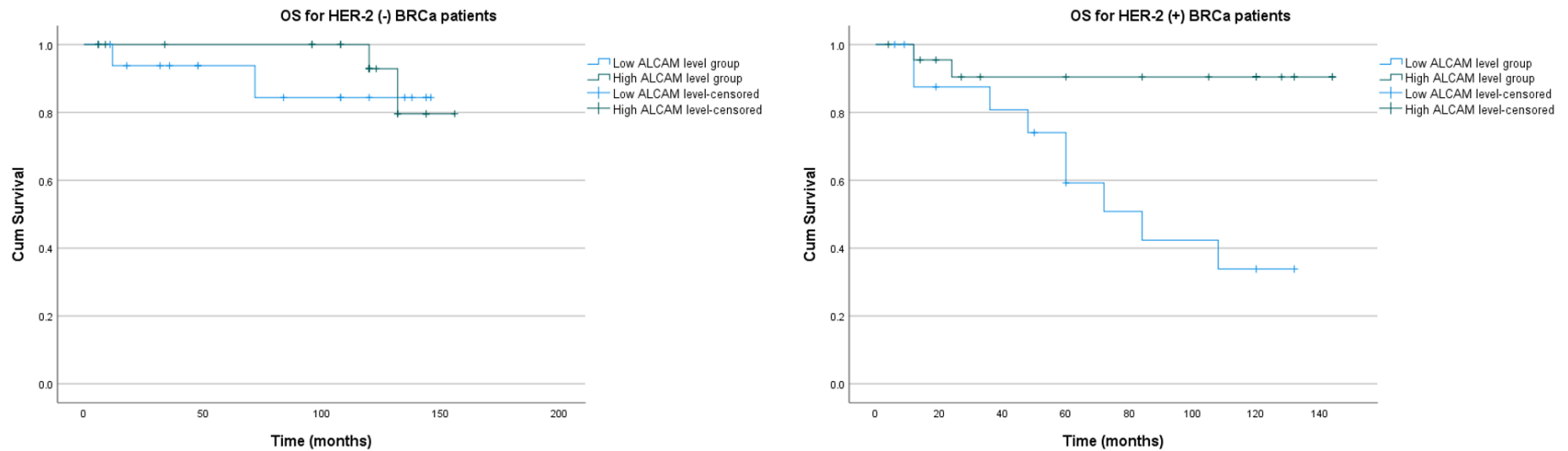


Figure 3.6 Overall survival of low ALCAM level and high ALCAM level group in breast cancer patients, stratified by HER-2 status. Left: HER-2 negative breast cancer, Kaplan-Meier survival analysis showed no statistical significance between the OS of high ALCAM group and low ALCAM group (150.2 months vs 130.7 months, $p=0.264$). Right: HER-2 positive breast cancer, the OS of high ALCAM group was longer compared to low ALCAM group (132.0 months vs 83.1 months, $p=0.010$).

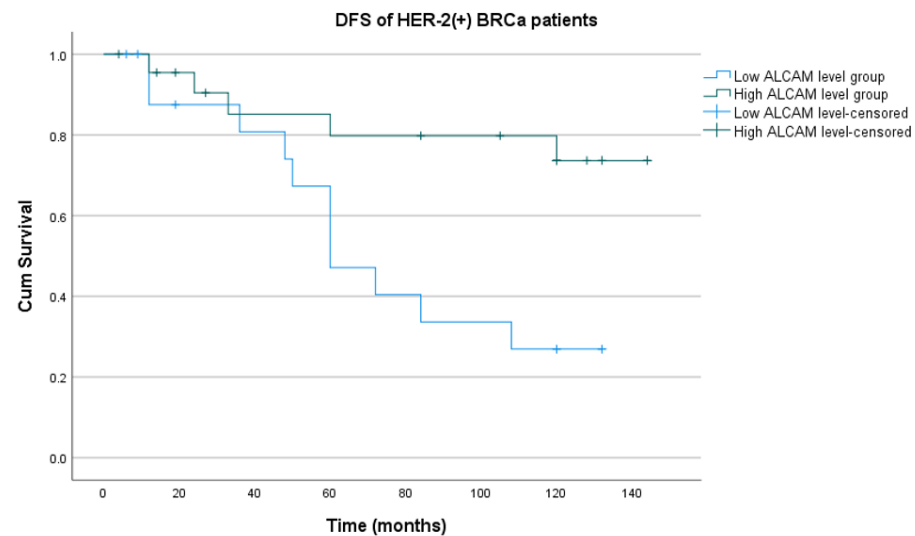
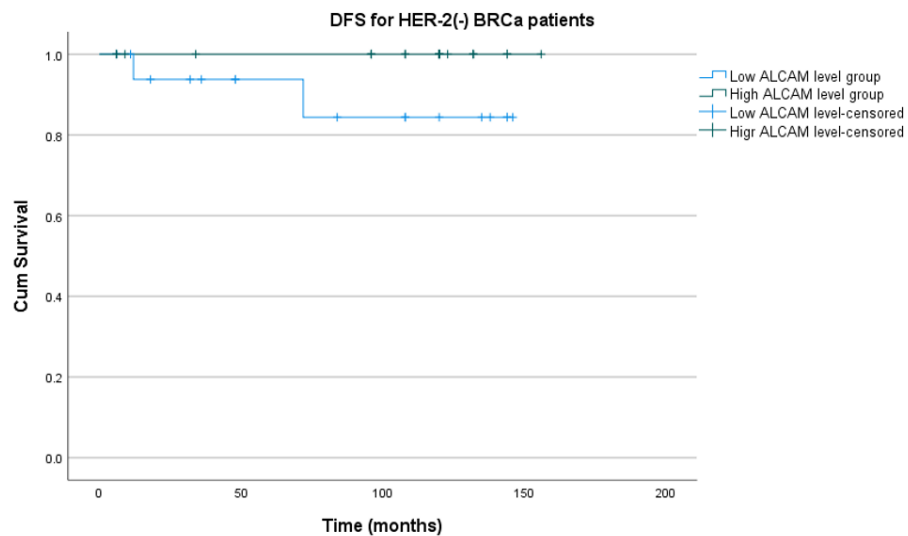


Figure 3.7 Disease-free survival of low ALCAM level and high ALCAM level group in breast cancer patients, stratified by HER-2 status. Left: HER-2 negative breast cancer, Kaplan-Meier survival analysis showed no statistical significance between the DFS of low ALCAM group and high ALCAM group ($p=0.084$). Right: HER-2 positive breast cancer, the DFS of high ALCAM group was longer compared to low ALCAM group ($p=0.019$).

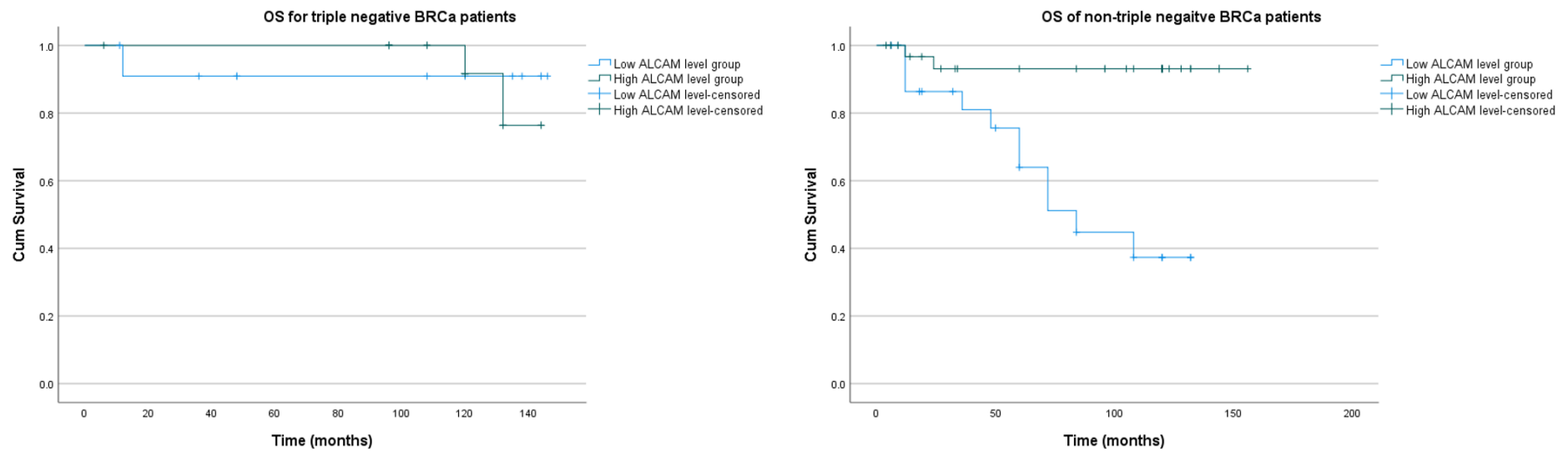


Figure 3.8 Overall survival of low ALCAM level and high ALCAM level group in breast cancer patients, stratified by triple negative and non-triple negative breast cancer subtypes. Left: Triple negative breast cancer, Kaplan-Meier survival analysis showed no statistical significance between the OS of high ALCAM group and low ALCAM group (140.2 months vs 133.8 months, $p=0.650$). Right: Non-triple negative breast cancer, the OS of high ALCAM group was longer compared to low ALCAM group (146.5 months vs 85.0 months, $p=0.001$).

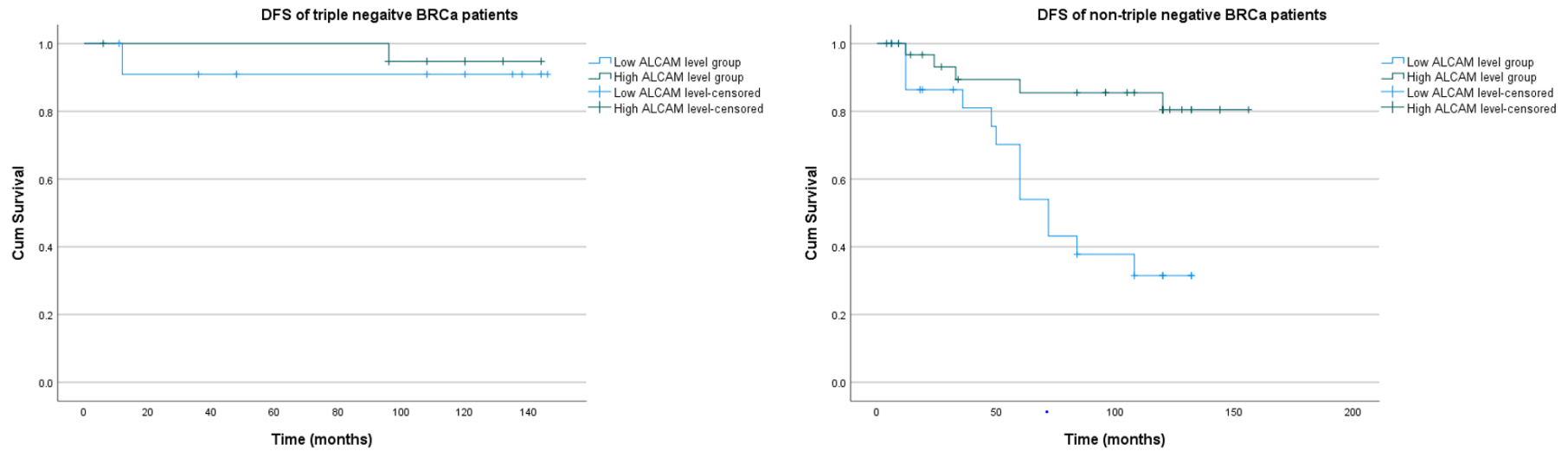


Figure 3.9 Disease-free survival of low ALCAM level and high ALCAM level group in breast cancer patients, stratified by triple negative and non-triple negative breast cancer subtypes. Left: Triple negative breast cancer, no statistical significance was found between the DFS of low ALCAM group and high ALCAM group (141.5 vs 133.8 months, $p=0.516$). Right: Non-triple negative breast cancer, the DFS of high ALCAM group was longer compared to low ALCAM group (136.4 vs 79.3 months, $p=0.002$).

Due to the relatively small number of the cases in the cohort, we additionally made use of TCGA database to analyse the relationship of ALCAM and the survival of the patients, by stratifying the patients based on their hormone receptor status. As shown in Figure 3.10, patients with a higher level of ALCAM had a significantly higher level of PPS (HR=0.75, P=0.047) in the ER positive group. The OS, RFS and DMFS of breast cancer patients showed no statistically significant difference between the ALCAM high-expression group and low-expression group (p=0.110, 0.052 and 0.085 respectively). In ER negative patients, the OS (HR=1.49, p= 0.042) and DMFS (HR=1.39, p=0.014) was shorter in the high ALCAM expression group compared with low expression group, while the PPS showed an opposite result, namely, patients with higher levels of ALCAM tended to have longer survival. The RFS of ER negative patients showed no statistical significance in survival analysis (p=0.093). Notably, in this cohort, the effects of ALCAM on survival were roughly opposite in patients with different ER statuses. This result may indicate that ER plays an important role in the ALCAM-mediated regulation of cancer progression.

As shown in Figure 3.11, patients with higher levels of ALCAM had longer RFS (p=0.028), and DMFS (p=0.017) but shorter PPS (p=0.001) in the HER2 positive group. While in the HER2 negative group, the results were in contrast with the HER2 positive group. Patients with higher levels of ALCAM had shorter OS (p=0.045), RFS (p<0.001) and DMFS (p<0.001). In the triple-negative breast cancer group, significantly higher levels of ALCAM were observed in patients with shorter OS (p=0.006) and longer RFS (p=0.028) (Figure 3.12). Patients in the triple-positive group (ER, PR and HER2 positive) with higher levels of ALCAM also had shorter OS (p=0.028) according to our statistical analysis (Figure 3.12). In the survival analysis of luminal-A and luminal-B patients, there was no significant difference between the ALCAM high-expression group and low-expression group, except for PPS of the

luminal-B group ($p=0.029$) (Figure 3.13). Patients with lower levels of ALCAM had longer OS in the basal breast cancer group (Figure 3.13).

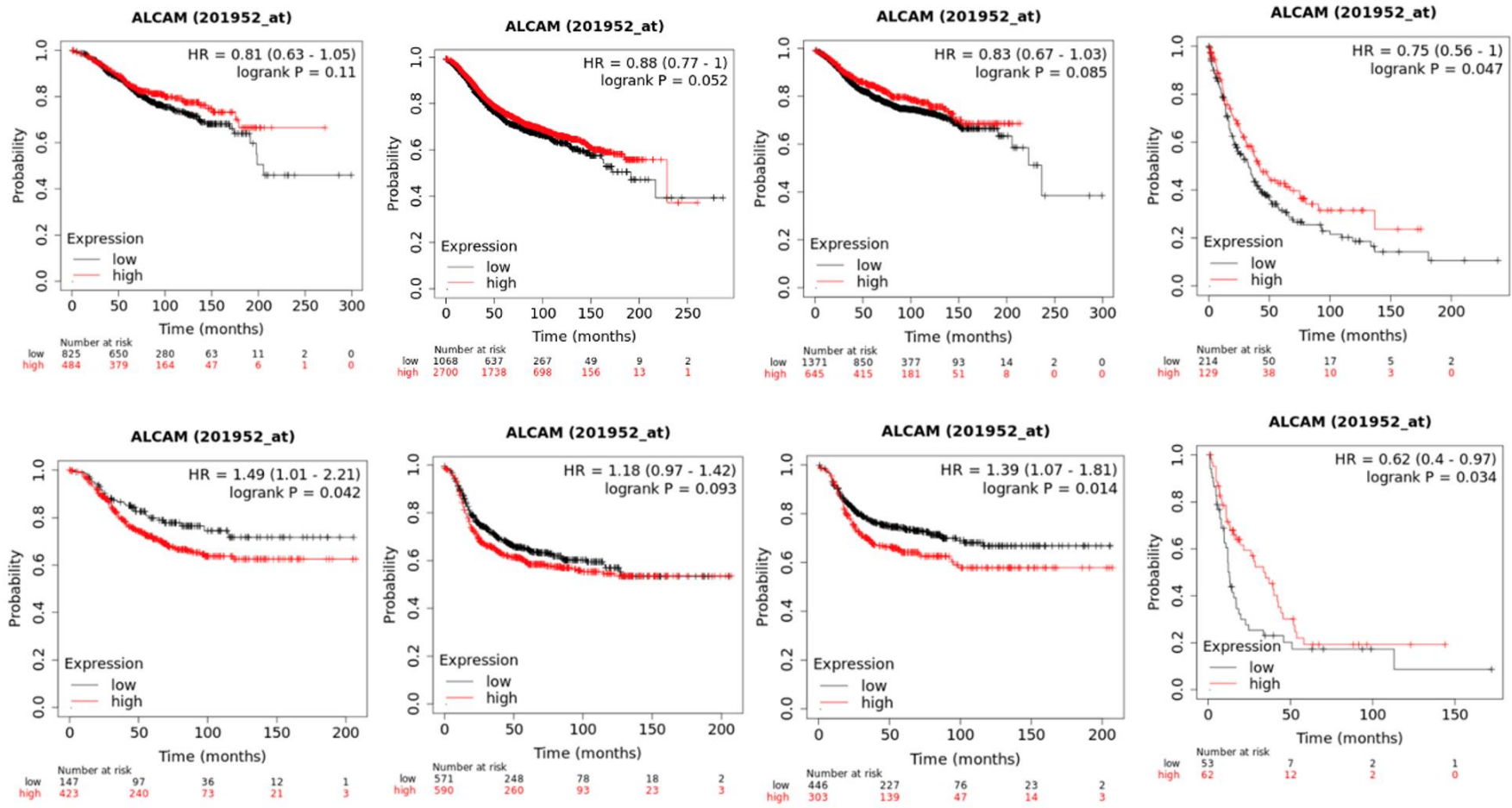


Figure 3.10 Survival analysis of ER-positive (top) and ER-negative (bottom) breast cancer patients with ALCAM transcript levels. OS, RFS, DMFS and PPS (from left to right). Data analysis was conducted and images obtained from the KMplot website.

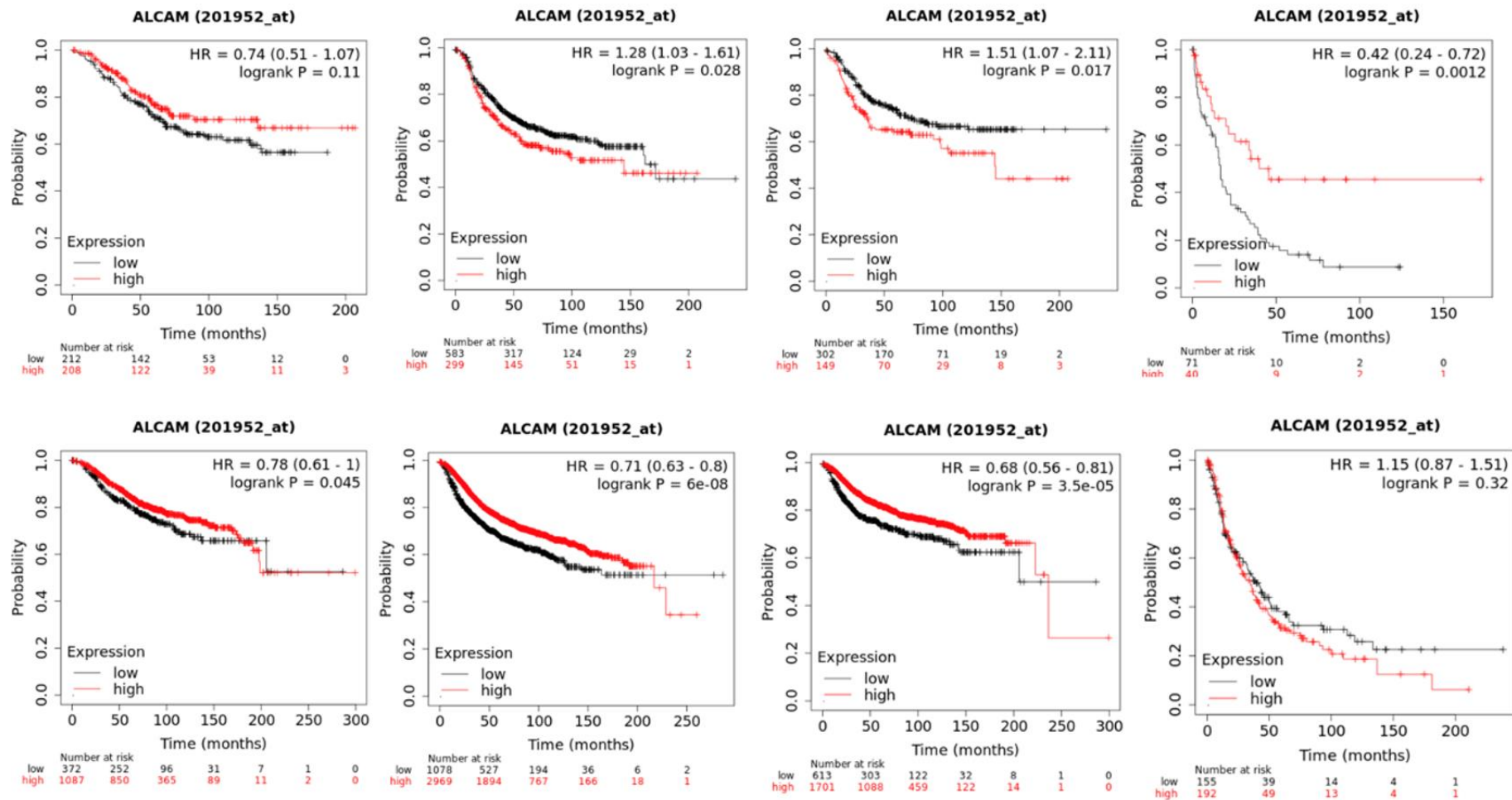


Figure 3.11 Survival analysis of HER2 positive (top) and HER2 negative (bottom) breast cancer patients with ALCAM transcript levels. OS, RFS, DMFS and PPS (from left to right). Data analysis was conducted and images obtained from the KMplot website.

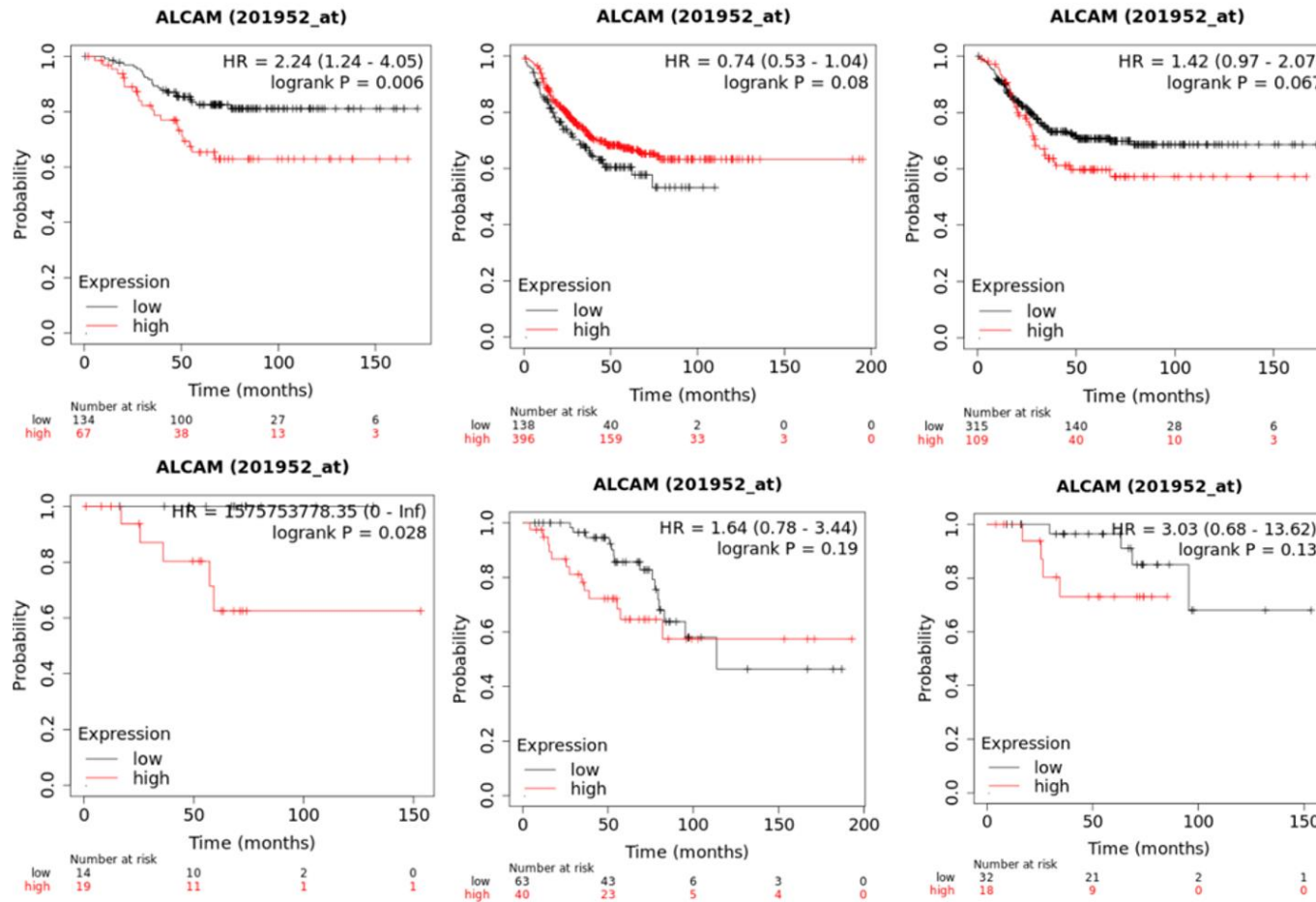


Figure 3.12 Survival analysis of triple-negative (top) and triple-positive (bottom) breast cancer patients with ALCAM transcript levels. OS, RFS and DMFS (from left to right). Data analysis was conducted and images obtained from the KMplot website.

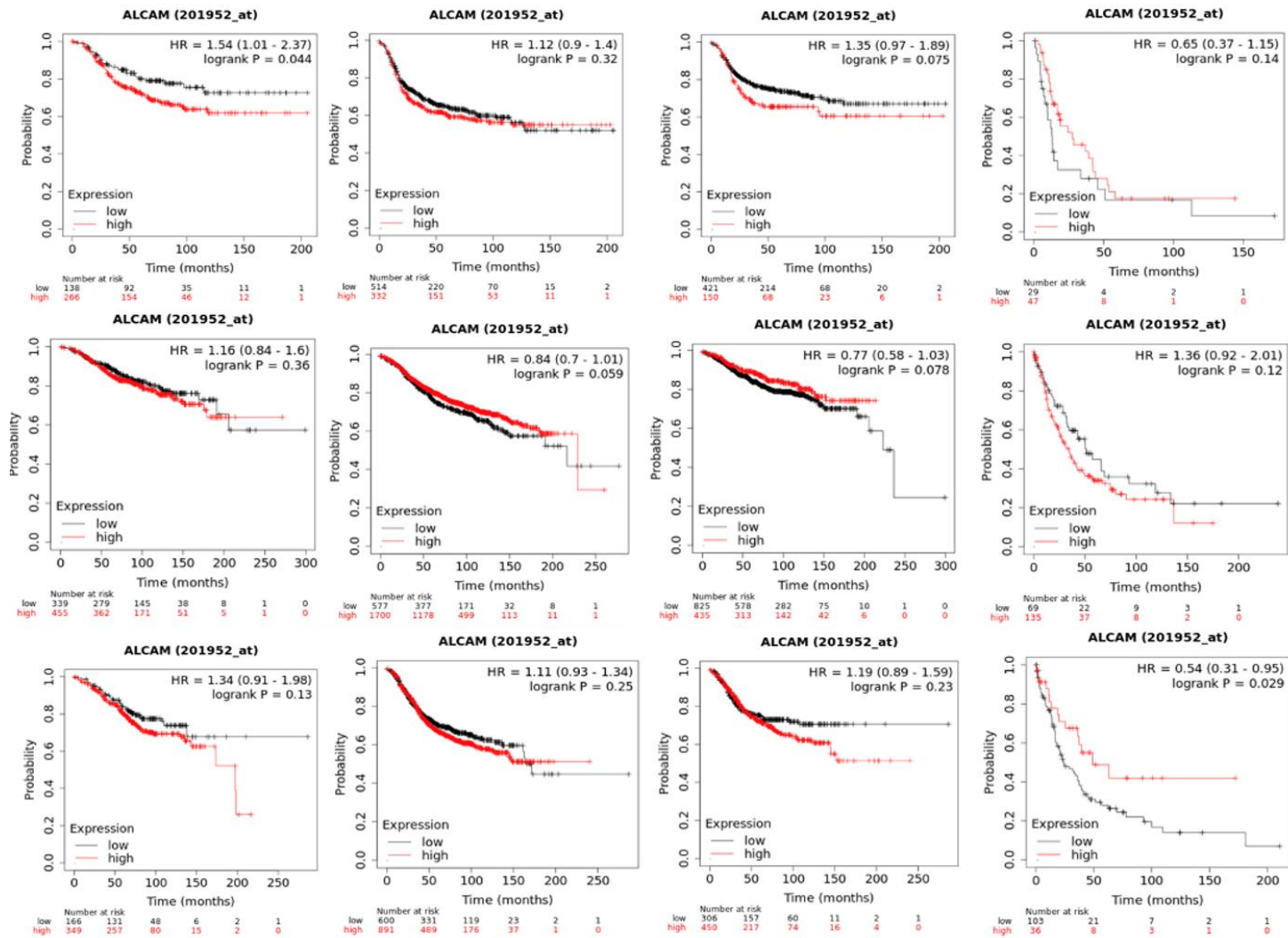
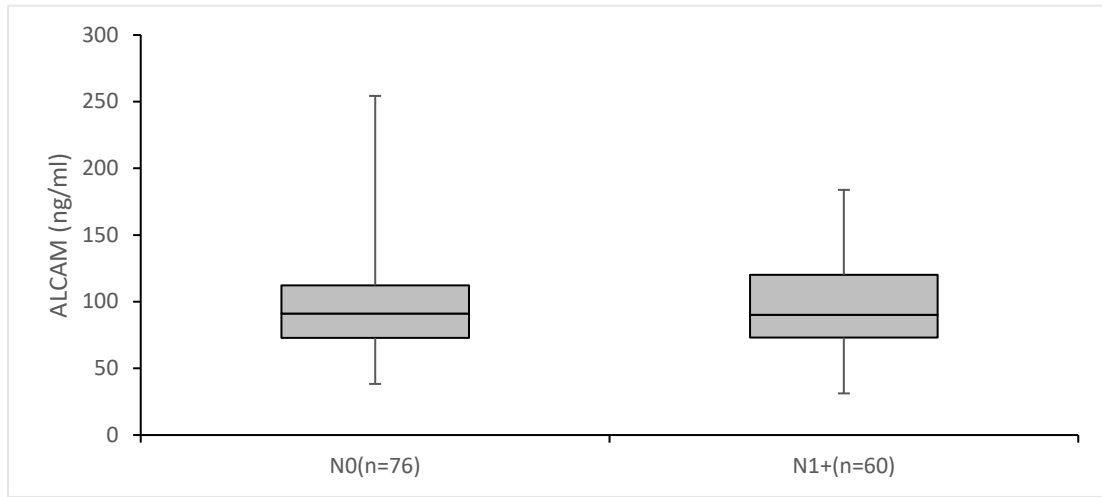


Figure 3.13 Survival analysis of basal (top), Luminal-A (middle) and Liminal-B (bottom) breast cancer patients with ALCAM transcript levels. OS, RFS, DMFS and PPS (from left to right). Data analysis was conducted and images obtained from the KMplot website.

3.3.6 Circulating ALCAM in patients with breast cancer

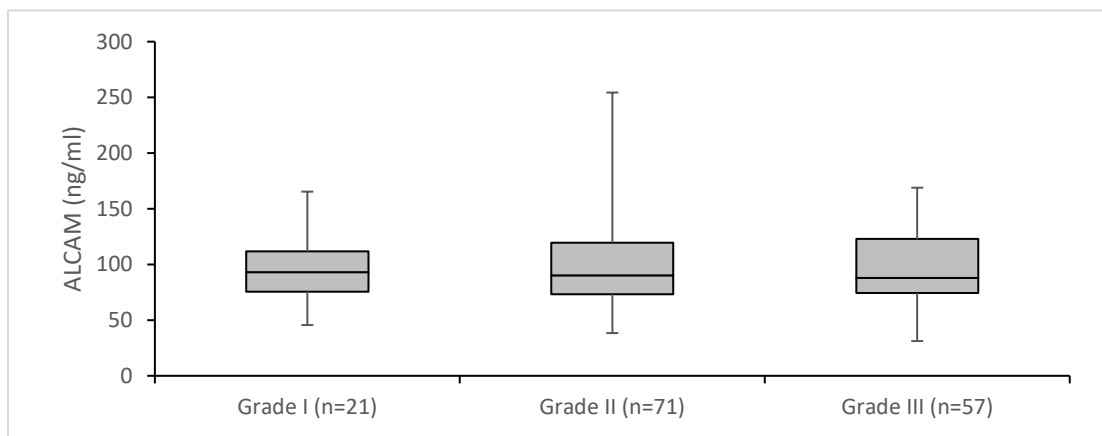
To explore the effect of circulating ALCAM (also referred to as soluble ALCAM or truncated ALCAM) in patients with breast cancer, the serum ALCAM level was assessed in our study (n=149).

As shown below, there was no statistical difference of serum ALCAM level in relation to patient nodal status ($p=0.096$) (Figure 3.14), tumour grade ($p=0.958$) (Figure 3.15), ER status ($p=0.199$) (Figure 3.16), progesterone receptor (PGR) status ($p=0.112$) (Figure 3.17), HER2 status ($p=0.439$) (Figure 3.18) or in triple negative breast cancers (TNBC) and non-triple negative breast cancer ($p=0.257$) (Figure 3.19). Furthermore, no significant differences in levels of serum ALCAM levels were seen in relation to clinical outcomes (patients who died of cancer or who were alive at the time of last follow-up) ($p=0.277$) (Figure 3.20). Significant differences were observed among tumour stages ($p=0.023$) (Figure 3.21), with the multiple comparison indicating that patients in T1 stage had higher levels of serum ALCAM compared to T4 stage breast cancer patients ($p<0.05$).



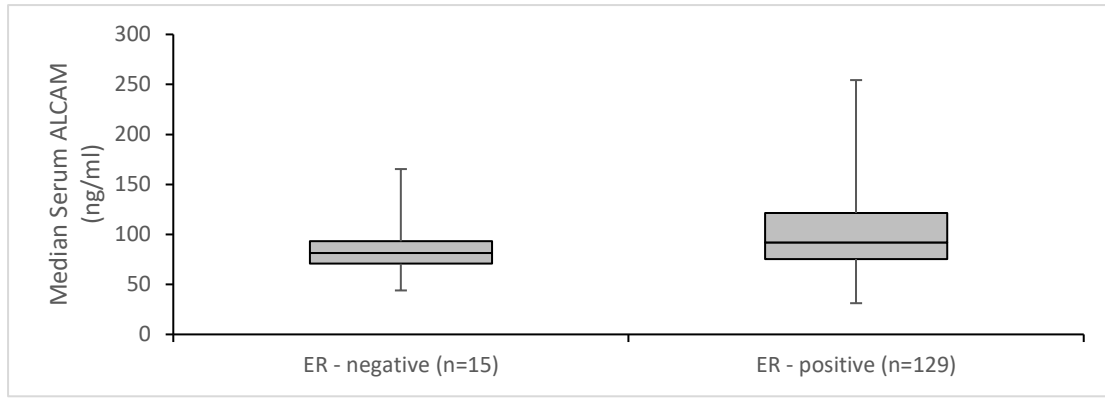
ALCAM (ng/ml)	Median	91.19	90.04
	IQR	72.77-112.23	73.07-120.16

Figure 3.14 Circulating ALCAM in patients with breast cancer, grouped by the nodal status. N0: node-negative; N1+: node-positive. Shown in the figure are median level of circulating ALCAM and interquartile range of the data, whiskers represent min and max values. There was no statistical significance between groups by Mann-Whitney U test ($p=0.096$).



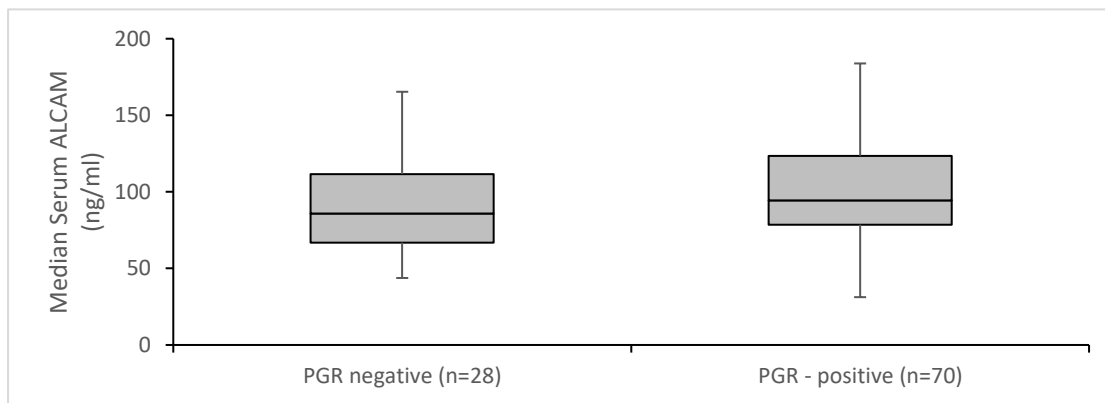
	Grade-1	Grade-2	Grade3	
ALCAM (ng/ml)	Median	92.97	90.24	87.99
	IQR	75.59-111.68	73.12-119.59	74.34-122.82

Figure 3.15 Circulating ALCAM in patients with breast cancer, grouped by tumour grade. Shown in the figure are median level of circulating ALCAM and Interquartile range of the data, whiskers represent min and max values. There was no statistical significance among groups by Kruskal-Wallis H test ($p=0.958$).



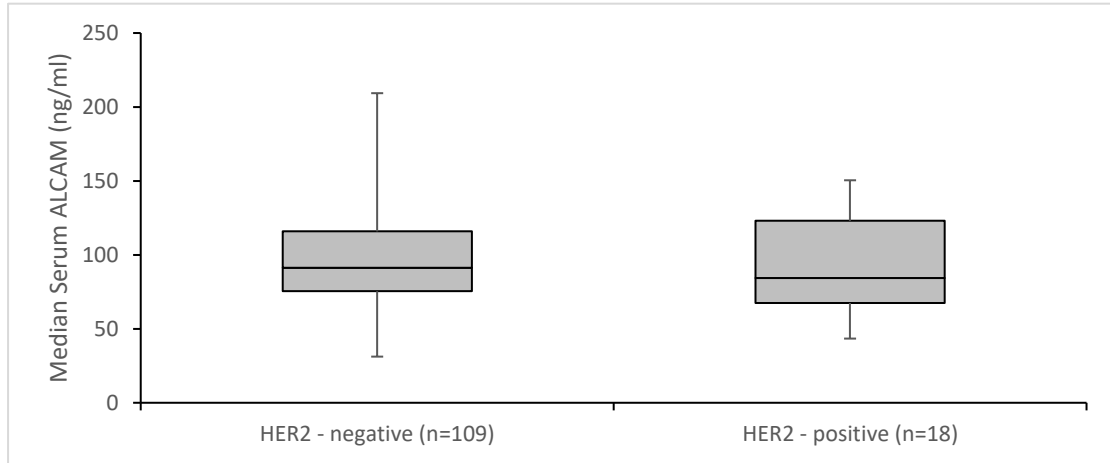
		ER-negative	ER-positive
ALCAM (ng/ml)	Median	81.31	91.91
	IQR	70.70-93.12	75.41-121.52

Figure 3.16 Circulating ALCAM in patients with breast cancer, grouped by ER status. Shown in the figure are median level of circulating ALCAM and Interquartile range of the data, whiskers represent min and max values. There was no statistical significance between groups by Mann-Whitney U test ($p=0.199$)



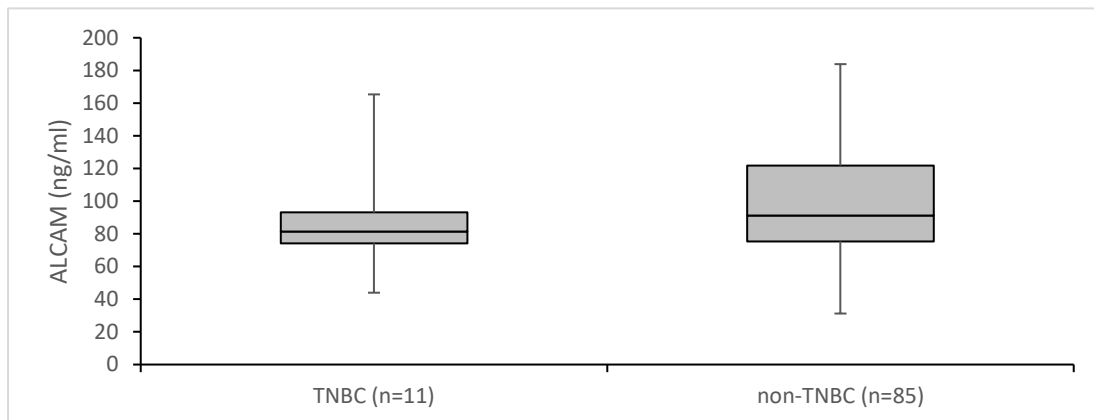
		PGR negative	PGR positive
ALCAM (ng/ml)	Median	85.88	94.46
	IQR	66.88-111.62	78.59-123.55

Figure 3.17 Circulating ALCAM in patients with breast cancer, grouped by PGR status. Shown in the figure are median level of circulating ALCAM and Interquartile range of the data, whiskers represent min and max values. There was no statistical significance between groups by Mann-Whitney U test ($p=0.112$)



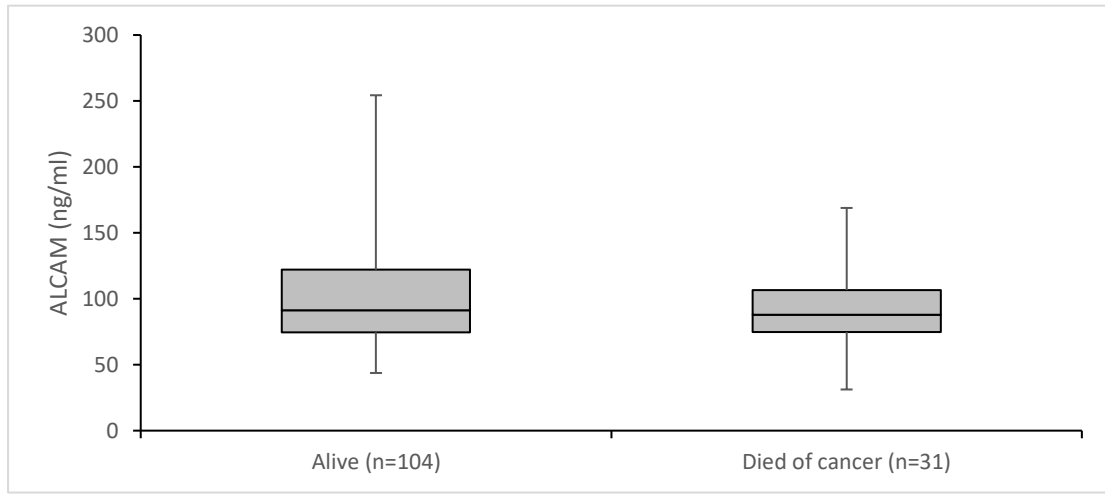
		HER2 - negative	HER2 - positive
ALCAM (ng/ml)	Median	91.28	84.33
	IQR	75.41-115.89	67.48-123.02

Figure 3.18 Circulating ALCAM in patients with breast cancer, grouped by HER2 status. Shown in the figure are median level of circulating ALCAM and Interquartile range of the data, whiskers represent min and max values. There was no statistical significance between groups by Mann-Whitney U test ($p=0.439$).



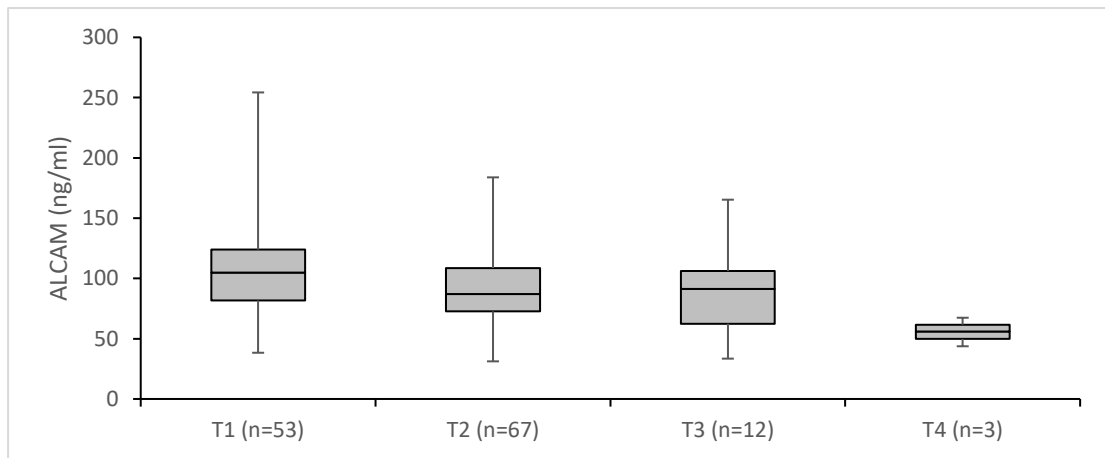
		TNBC	non-TNBC
ALCAM (ng/ml)	Median	81.31	91.28
	IQR	74.167-93.12	75.41-121.78

Figure 3.19 Circulating ALCAM in patients with breast cancer, grouped by HR status. TNBC: triple-negative breast cancer. Shown in the figure are median level of circulating ALCAM and Interquartile range of the data, whiskers represent min and max values. There was no statistical significance between groups by Mann-Whitney U test ($p=0.257$).



		Alive	Died of cancer
ALCAM (ng/ml)	Median	91.39	87.99
	IQR	74.601-122.04	74.70-106.65

Figure 3.20 Circulating ALCAM in patients with breast cancer, grouped by clinical outcome. Shown in the figure are median level of circulating ALCAM and Interquartile range of the data, whiskers represent min and max values. There was no statistical significance between groups by Mann-Whitney U test ($p=0.277$)



		T1	T2	T3	T4
ALCAM (ng/ml)	Median	104.76	87.18	91.33	55.86
	IQR	81.689-123.87	72.68-108.65	62.44-106.10	49.79-61.63

Figure 3.21 Circulating ALCAM in patients with breast cancer, grouped by tumour staging. Shown in the figure are median level of circulating ALCAM and Interquartile range of the data, whiskers represent min and max values. The results were analysed using Kruskal-Wallis H test ($p=0.023$). In multiple comparisons among groups, the T1 group had significantly higher levels of ALCAM than T4 group ($p<0.05$). No statistical differences between groups were found for the remaining comparisons.

3.3.7 ALCAM and bone metastasis, validation using an alternative endocrine cohort, pituitary tumours

Limited by the current cohort size and availability of additional resources of breast cancer bone metastasis cohort samples during the course of the study, and indeed in consideration of the connection between ALCAM and hormone related cancer (Chapter 1), we tested another cohort that was available at the host laboratory, a pituitary tumour cohort which was comprised of hormone related pituitary tumours as reported previously from the host laboratory (Jia et al. 2013). This also allows the possibility of answering an additional question raised at the beginning of the study, is ALCAM related bone metastasis confined to a specific tumour type, namely breast cancer or has the link a wider endocrine context? Pituitary tumours (often referred to as pituitary adenomas) are an endocrine related tumour type. Owing to their unique anatomical location, these tumours, although most of them are benign, have an aggressive growth phenotype and often invade and destroy the surrounding bone tissues. Our cohort analysis is based on gene transcript quantitation and the ALCAM expression levels are compared with the clinical, pathological, endocrine parameters and most importantly the involvement of bones.

As shown in Figure 3.22, larger pituitary adenomas tended to have higher levels of ALCAM compared with smaller tumours ($p < 0.05$). Levels of ALCAM did not differ significantly between gender and age. However, adenomas that invaded sphenoid bone had significantly lower levels of ALCAM than those non-invasive tumours (23.9 ± 15.6 versus 56.8 ± 18.4 , with and without sphenoid bone invasion respectively, $p = 0.038$) (Figure 3.23). Likewise, tumours that invaded cavernous sinus also had low levels of ALCAM, compared with those without ($p < 0.05$) (Figure 3.24). Non-functional adenomas had higher levels of ALCAM than endocrine active tumours ($p < 0.001$), which is comprised of PRL (Prolactin), GH (Growth hormone), TSH (Thyroid stimulating hormone), ACTH (Adrenocorticotrophic hormone), FSH (Follicle-

stimulating hormone) and LH (Luteinizing hormone) functioning tumours (Figure 3.25).

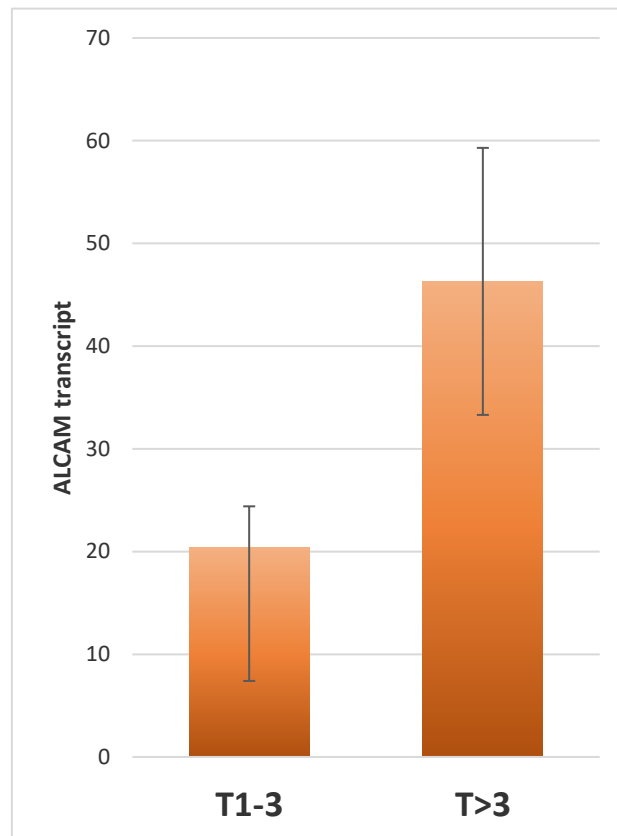


Figure 3.22 ALCAM transcript level of different tumour sizes. The comparison showed that larger tumours (T>3cm, n=93) tended to have higher levels of ALCAM compared with smaller tumours (T1-3cm, n=19) ($p<0.05$).

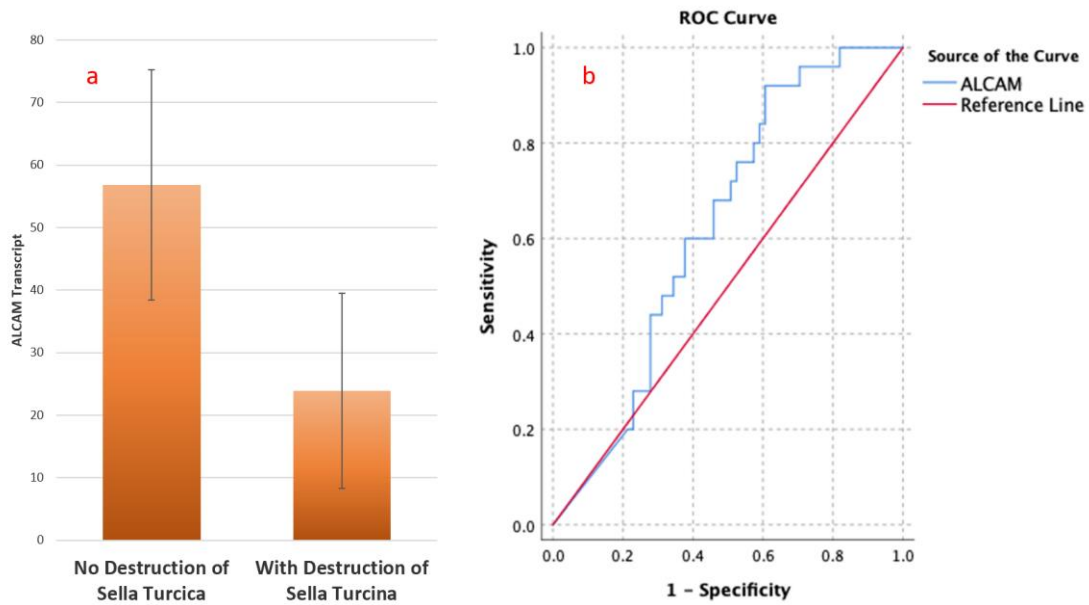


Figure 3.23 ALCAM transcript level in the no destruction of sella turcica group (n=60) and the with destruction of sella turcica group (n=29). a. the comparison between the groups showed that tumours which invaded sphenoid bone had significantly lower levels of ALCAM than those non-invasive tumours ($p < 0.05$). b: ROC analysis showed that ALCAM had diagnostic value in diagnosing destruction of sella turcica ($p = 0.038$).

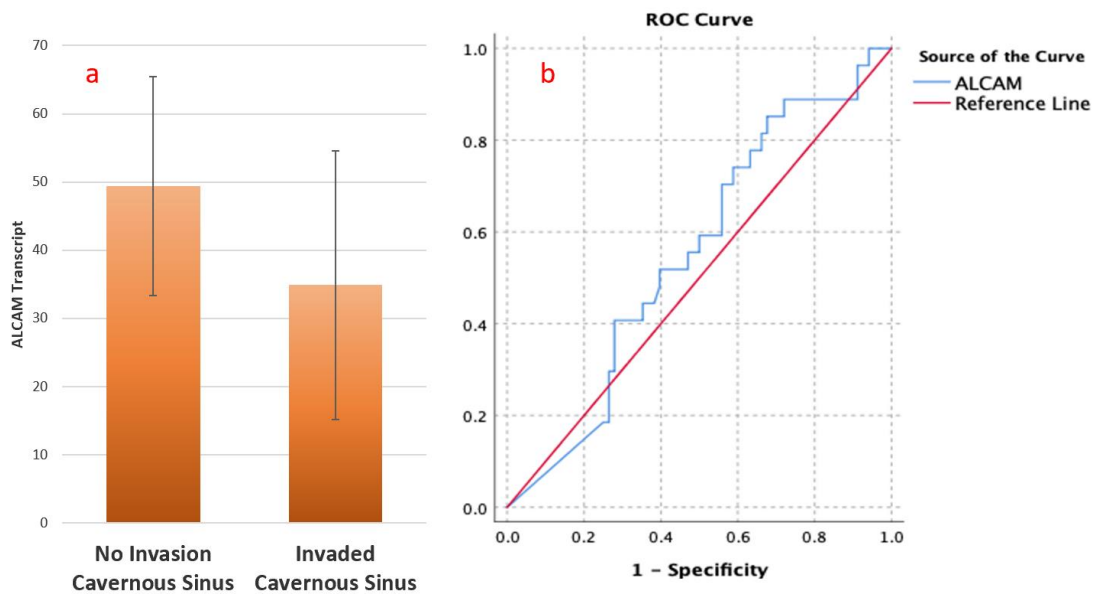


Figure 3.24 ALCAM transcript level in the no invasion cavernous sinus group (n=68) and the invaded cavernous sinus group (n=27). a: the comparison between the groups showed that tumours which invaded cavernous sinus had low levels of ALCAM compared with those without ($p < 0.05$). b: ROC analysis showed that ALCAM had no diagnostic value in diagnosing cavernous sinus invasion ($p = 0.403$).

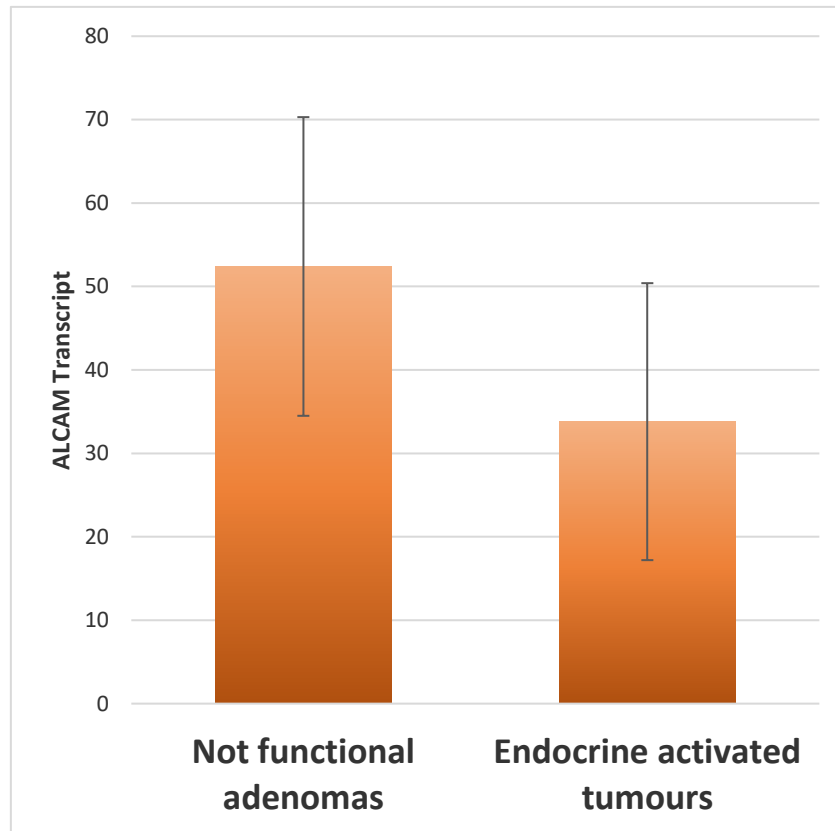


Figure 3.25 ALCAM transcript levels in different types of pituitary tumour. The comparison among these groups showed that non-functional adenomas (n=59) had higher levels of ALCAM expression than endocrine active tumours (n=36) ($p < 0.001$).

3.4 Discussion

In this chapter, we mainly focussed on ALCAM expression in breast cancer and the relationship to skeletal metastasis and clinical outcome of the patients. ALCAM represents an interesting molecule for investigation in cancer research. Intense research has focused on the study of ALCAM and its use as a prognostic factor throughout many different human cancers (summarised in Table 1.5). Whilst this demonstrates the great potential of ALCAM as a predictive factor, it also highlights its complexity. Contrasting findings have been reported regarding ALCAM's use as a biomarker for patient risk and this may, in part, be due to the capacity for ALCAM to occupy several cellular locations. For example, work by Burkhardt *et al.*, (Burkhardt *et al.* 2006) reported that high levels of cytoplasmic ALCAM expression were associated

with poorer survival in breast cancer patients. Study (Piao et al. 2012) have demonstrated that high ALCAM expression at the membrane was associated with lymph node involvement and metastasis, whilst higher levels of cytoplasmic ALCAM were associated with local recurrence and patient survival. In addition to membranous and cytoplasmic locations, ALCAM has also been shown to be cleaved at the membrane by proteases such as ADAM17 (Micciche et al. 2011), further raising the prognostic potential of ALCAM and fuelling scientific interest. Indeed, serum ALCAM has been shown to be elevated in high grade breast cancers and may be comparable to other serum markers such as CEA and CA15-3 in a Saudi Arabian cohort (Al-Shehri and Abd El Azeem 2015). Interestingly, our current work exploring serum ALCAM in breast cancer patient samples obtained from the Wales cancer bank appears in some contrast to this, demonstrating few significant observations and a decrease in levels in higher stage tumours. This may be due to the cohort size or nature of the collections and requires further analysis in a larger number of samples.

Early work with the host laboratory demonstrated enhanced staining in background tissues compared to tumour tissues, at both cytoplasmic and membranous locations and found lower ALCAM transcript expression was associated with poorer patient outlooks and survival (King et al. 2004). Subsequently, reduced ALCAM levels were seen in patients who developed skeletal metastasis, highlighting the important link between ALCAM and bone metastasis (Davies et al. 2008)

From the Cardiff breast cancer cohort, we can see that the ALCAM expression level of breast cancer patients with bone metastasis was significantly lower than those without bone metastasis and patients with higher levels of ALCAM had longer survival. Notably, the effects of ALCAM on survival were roughly opposite in patients with different ER statuses. This result may indicate that ER plays an important role in the ALCAM-mediated regulation of cancer progression and metastasis. Previous work has also shown a possible correlation between ALCAM and ER status (Ihnen et

al. 2008) and the effect of the endocrine system on ALCAM and cancer progression was also supported by our findings from the pituitary tumour cohort. To be more specific, lower levels of ALCAM in pituitary tumours could lead to adjacent bone invasion, and the non-functional pituitary adenomas had higher levels of ALCAM expression than endocrine active tumours. Collectively, this provides further insights into the complexities surrounding ALCAM and its use as a novel biomarker of disease progression. Subsequent Chapters will focus on further exploring the implications of this relationship in cellular and mechanistic settings. The results presented in this chapter, which is mainly based on gene transcript analyses, have indicated that ALCAM has a strong link to endocrine cancer-related bone metastases, namely breast cancer and pituitary cancers. Together with those reported in prostate cancer, it is argued that this link is wider than breast cancer. This forms a strong basis of the next stage of the research, namely to establish the connection between ALCAM, hormone receptors and bone microenvironment in the context of bone metastasis.

Chapter-4

The impact of ALCAM on cellular functions of breast cancer and the relationship with bone metastasis

4.1 Introduction

From the previous literature and the first part of the present study, it was clear that ALCAM has an important connection to bone metastasis, and indeed disease progression, and this connection has an endocrine and hormone receptor dimension. To further advance this knowledge and explore the molecular and signalling events underlying this connection, the present study aimed to create cell models with differential expression of ALCAM from cell lines with differing receptor status, namely ER and HER2 negative and positive cell lines. This would allow extensive studies to be carried out with regard to the role of ALCAM in bone related cell functions.

4.2 Methods

4.2.1 Special reagents

Bone matrix extract (BME) was a central resource of the host laboratory and the preparation was described in full in previous studies use (Davies and Jiang 2010; Owen et al. 2016). Briefly, bone proteins were extracted from fresh human bone tissues collected immediately after hip replacement under the local health board ethics committee guidelines. Bones were crushed at ice-cold temperatures and subsequently processed in a Bioraptor sonicator (Wolf Laboratories, York, UK) to extract matrix proteins. The matrix proteins were then quantified as mentioned in section 2.8.2 and stored at -80°C until use.

4.2.2 Cell lines and culture conditions

ZR-751, MDA- 231, MDA-361, MCF-7, BT-20, BT-549, MDA-468, MDA-436 and SK-BR-3 were obtained from the ATCC (American Type Culture Collection), provided by the

LGC Standards (LGCstandards.com), ATCC's European supplier (Teddington, Middlesex, UK). ZR-751, MDA-231, MDA-361, MCF-7, BT-20, MDA-436 and SK-BR-3 cells were cultured in Dubecco's Modified Eagle Medium (DMEM)/Ham's F12 with L-glutamine (Sigma-Aldrich, Dorset, UK). BT-549 and MDA-468 cells were grown in RPMI 1640 medium (Sigma-Aldrich, Dorset, UK). All the mediums were supplemented with 10% foetal calf serum (FCS) (Sigma-Aldrich, Dorset, UK) and antimicrobial solutions (Sigma-Aldrich, Dorset, UK). Cells were cultured at 95% humidity, 5% CO₂ and 37° C.

4.2.3 Manipulation of ALCAM expression

Plasmids were designed and purchased from Vector Builder (Chicago, USA). Both overexpression and shRNA mediated knockdown plasmids were designed and purchased. Plasmid stocks were amplified from *E. coli* using a PureYield Maxi Prep plasmid extraction kit (Promega, Southampton, UK). Cells were subsequently transfected using FuGene HD (Promega, Southampton, UK) in accordance with the manufacturer's instructions. Following transfection, cells were subject to puromycin selection (2µg/ml) before being placed and routinely grown in maintenance medium (0.2µg/ml).

4.2.4 RNA preparation and reverse transcription polymerase chain reaction (RT-PCR)

RNA was extracted from cells using TRI-reagent (Sigma-Aldrich, Dorset, UK) in accordance with the manufacturer's instructions and the concentration was quantified using a nanophotometer (Geneflow Ltd., Litchfield, UK). cDNA was synthesized using a GoScript oligo dT reverse transcription kit (Promega, Southampton, UK) in accordance with the manufacturer's instructions. PCR was performed using GoTaq Green Mastermix (Promega, Southampton, UK) with the following conditions: 5 min at 94°C, then 40 sec at 94°C, 40 sec at 55°C, 50 sec at

72°C for 28-32 cycles, and finally 72°C for 10 min before holding at 4 °C. Samples were then separated electrophoretically on an agarose gel stained with SYBRsafe (Fisher Scientific UK, Leicestershire, UK) and visualised in a Syngene U: Genius 3 System (Geneflow Ltd., Litchfield, UK)

4.2.5 Western blotting

Protein samples of MCF-7, MDA-MB-361 and MDA-MB-231 ALCAM knockdown cell models were extracted and performed Western blotting to detect the ALCAM expression as outlined in section 2.8.

4.2.6 Cell Growth assay

Equal number of cells (3000 cells per well) were seeded in 96-well plates and incubated at 37°C, with 5% CO₂ for 72 hours. Following incubation, the cells were fixed with 4% formalin, stained with 0.5% crystal violet and extracted with 10% acetic acid after washing. the absorbance was measured at 595 nm using a spectrophotometer to detect their respective cell density. Each experiment was repeated at least three times.

4.2.7 Statistical methods

The comparison between group was performed by two sample T-Test. All the analyses were carried out using SPSS version 26. The statistical significance was defined as $p < 0.05$.

4.3 Results

4.3.1 Expression of ALCAM in breast cancer cell lines

As shown in Figure 4.1, the ALCAM expression in BT-20, SK-BR-3, MCF-7, MDA-MB-436, MDA-MB-231, MDA-MB-468, BT-549, ZR-751, MDA-MB-361 cell lines was all positive.

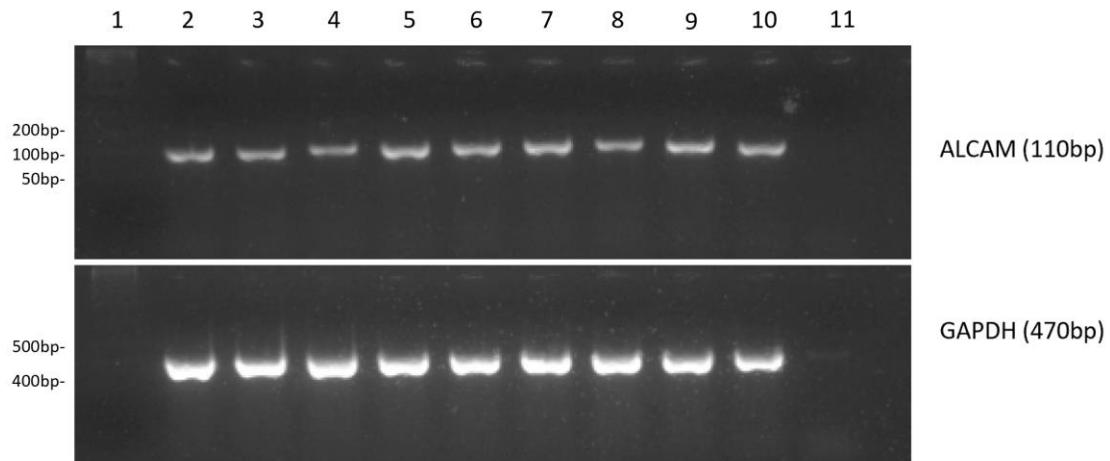


Figure 4.1 PCR results demonstrating ALCAM expression in different breast cancer cell lines. From left to right: 1. DNA ladder; 2. MDA-MB-436; 3. BT-20; 4. SK-Br-3; 5. MDA-MB-231; 6. MDA-MB-468; 7. MDA-MB-361; 8. MCF- 7; 9. BT-549; 10. ZR-751; 11. negative control. Shown are representative image from three independent experiments.

4.3.2 Construction of ALCAM knockdown model

Based on our ALCAM expression data, a number of cell lines with differing hormone receptor status were chosen to develop manipulated models. MCF-7 was selected as an ER positive/HER2 negative cell line, MDA-MB-361 was selected as an ER positive/HER2 positive cell line and MDA-MB-231 was selected as an ER negative/HER2 negative cell line, to create ALCAM knockdown models. Cells were transfected with either scramble control or shRNA plasmids as described in Chapter 2. Following successful selection, samples were tested to establish the efficiency of the knockdown. Figures 4.2 to 4.5 demonstrate the transfection of the three cell models. ALCAM suppression was seen in all of the ALCAM shRNA transfected cells with PCR (Figure 4.2). This knockdown was further demonstrated following semi-

quantitative band analysis and normalisation against GAPDH (Figure 4.3), where a clear reduction in ALCAM transcript levels was seen in comparison to the scramble shRNA control. Similarly, the Western blotting results (Figure 4.4 and Figure 4.5) also demonstrated knockdowns of ALCAM in all the three cell lines.

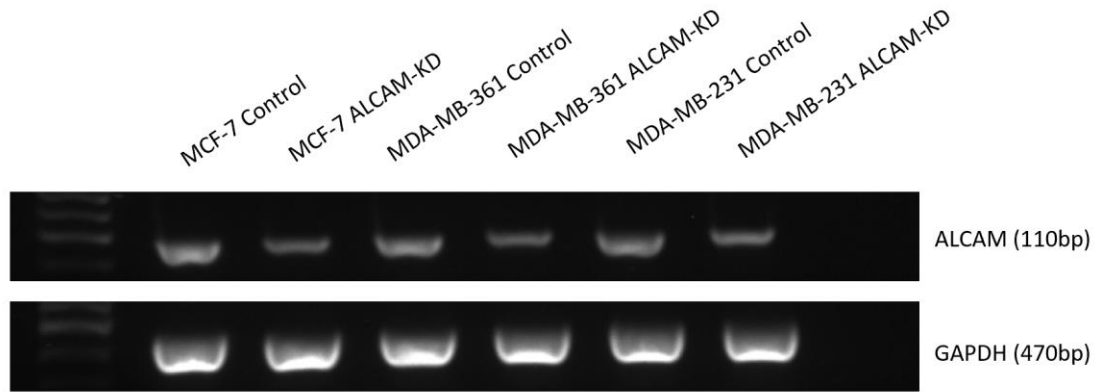


Figure 4.2 PCR image of ALCAM transcription in transfected breast cancer cell lines. From left to right: MCF-7 scramble control cells; MCF-7 ALCAM-KD cells; MDA-MB-361 scramble control cells; MDA-MB-361 ALCAM-KD cells; MDA-MB-231 scramble control cells; MDA-MB-231 ALCAM-KD cells. Shown are representative image from three independent experiments.

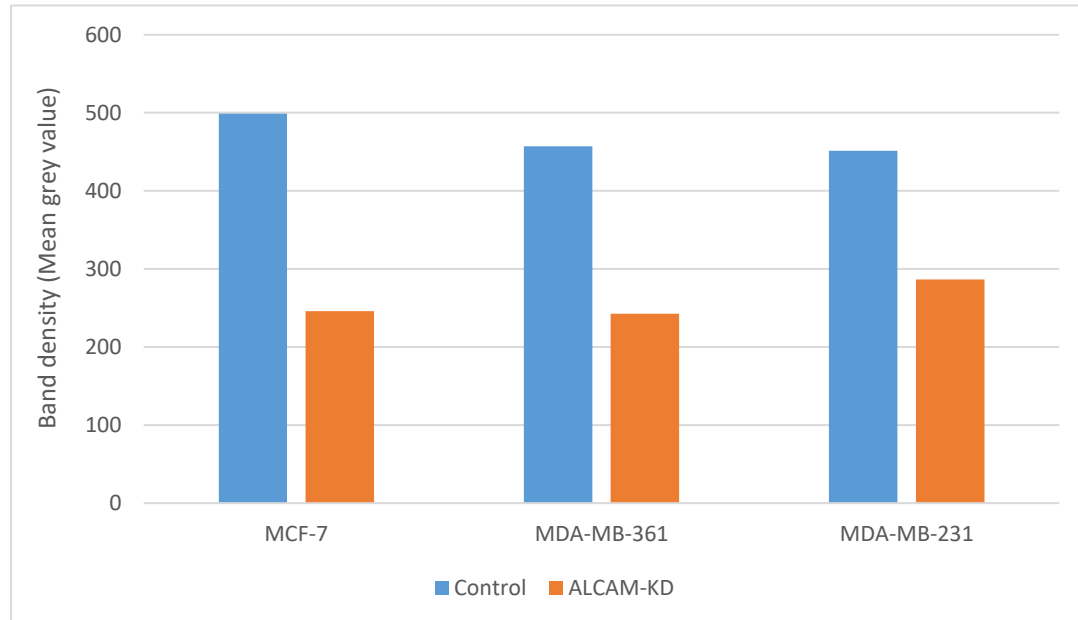


Figure 4.3 Semiquantitative analysis of PCR results of ALCAM transcript level in transfected MCF-7, MDA-MB-361 and MDA-231 cells. Expression values are normalised to the GAPDH housekeeping gene expression in the samples. The percentage reduction of ALCAM transcription for each cell line was: MCF-7 (50.7%), MDA-MB-361 (46.9%) and MDA-MB-231 (36.6%).



Figure 4.4 Western blotting image of ALCAM expression in transfected breast cancer cell lines. From left to right: MCF-7 scramble control cells; MCF-7 ALCAM-KD cells; MDA-MB-361 scramble control cells; MDA-MB-361 ALCAM-KD cells; MDA-MB-231 scramble control cells; MDA-MB-231 ALCAM-KD cells. Shown are representative image from three independent experiments.

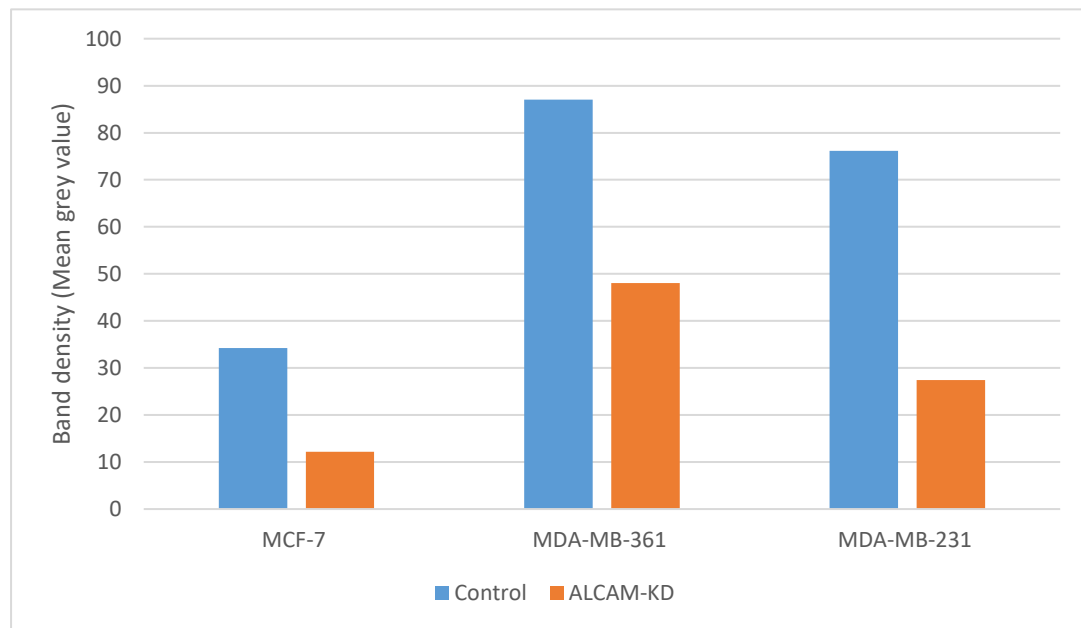


Figure 4.5 Semiquantitative analysis of Western blotting results of ALCAM expression level in transfected MCF-7, MDA-MB-361 and MDA-MB-231 cells. Expression values are normalised to the GAPDH housekeeping protein expression in the samples. The percentage reduction of ALCAM transcription for each cell line was: MCF-7 (64.4%), MDA-MB-361 (44.8%) and MDA-MB-231 (63.9%).

4.3.3 Impact of genetic manipulation on the growth of breast cancer cells.

In order to evaluate the effect of knocking down ALCAM on cell growth in breast cancer, we performed cell growth assays using the ALCAM knockdown cell model in

both normal conditions and bone microenvironment. As shown in Figure 4.6, the cell growth rate of MCF-7 control group was lower compared to MCF-7 ALCAM-KD group in the absence ($p < 0.001$) and presence ($p < 0.001$) of bone matrix extract (BME). Similar results could be observed between MDA-MB-361 control group and ALCAM-KD group (without/with BME: $p = 0.011/p = 0.040$), as well as in the MDA-MB-231 control and ALCAM-KD groups (without/with BME: $p < 0.001/p < 0.001$) (Figure 4.7 and 4.8). No statistical difference was seen between control groups with/without BME, as well as ALCAM-KD groups with/without BME, in all three cell models ($p > 0.05$).

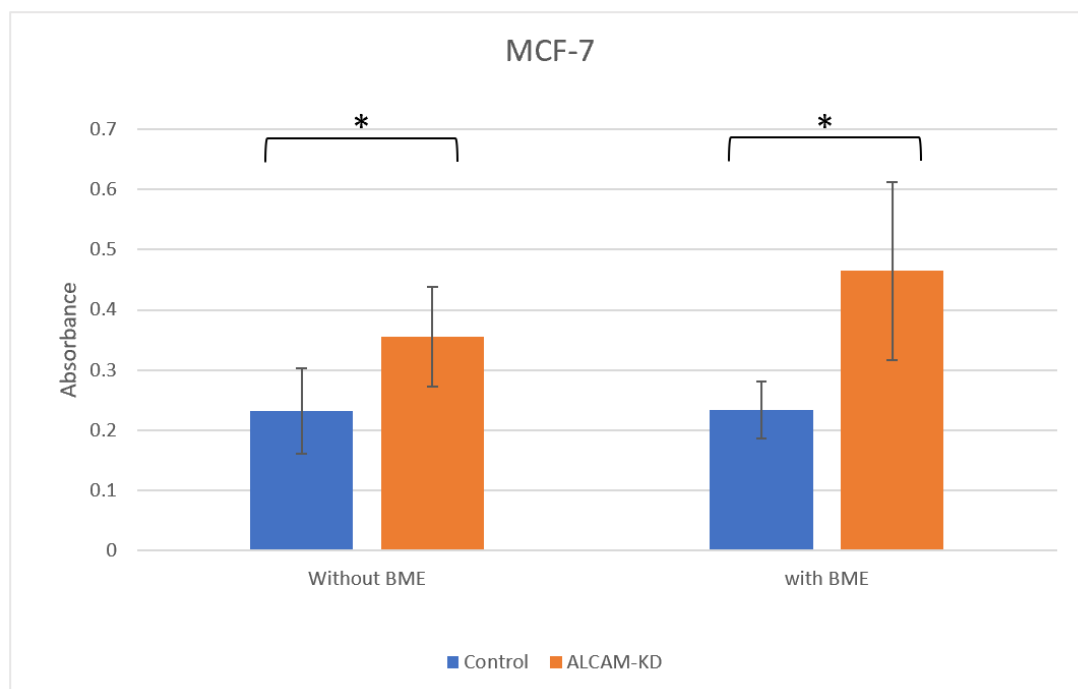


Figure 4.6 Cell growth assay of MCF-7 cells with (right) and without (left) BME (50 μ g/ml). Shown are mean absorbance of cell staining of MCF-7 control and ALCAM-KD group in cell growth assay (Mean data shown, error bars represent SEM, * represents statistical significance).

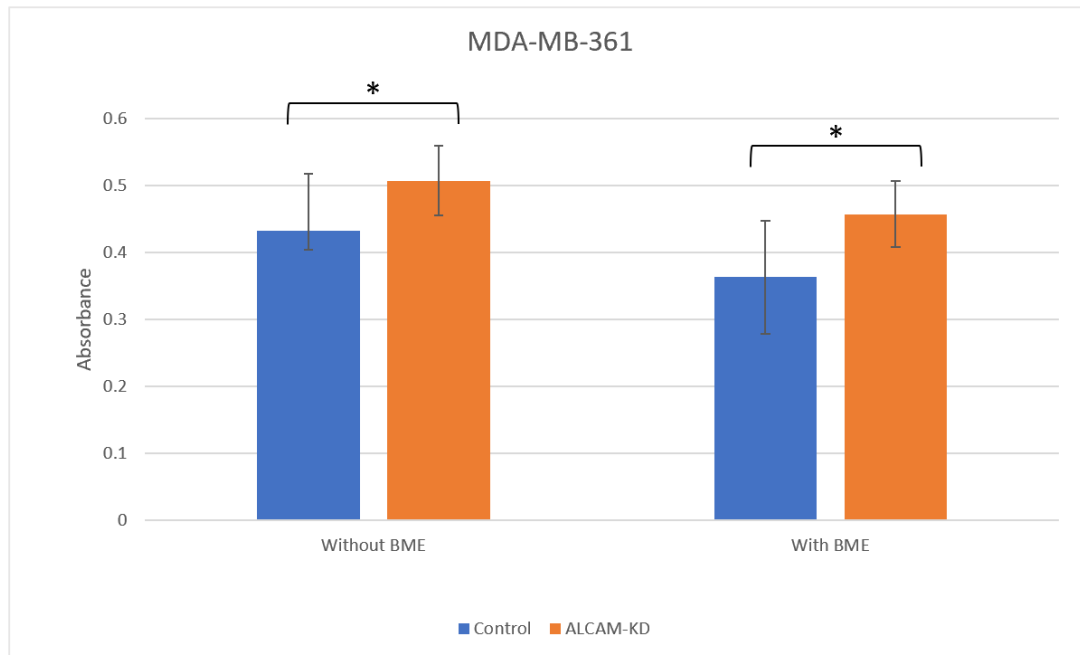


Figure 4.7 Cell growth assay of MDA-MB-361 cells with (right) and without (left) BME (50µg/ml). Shown are mean absorbance of cell staining of MDA-MB-361 control and ALCAM-KD group in cell growth assay (Mean data shown, error bars represent SEM, * represents statistical significance).

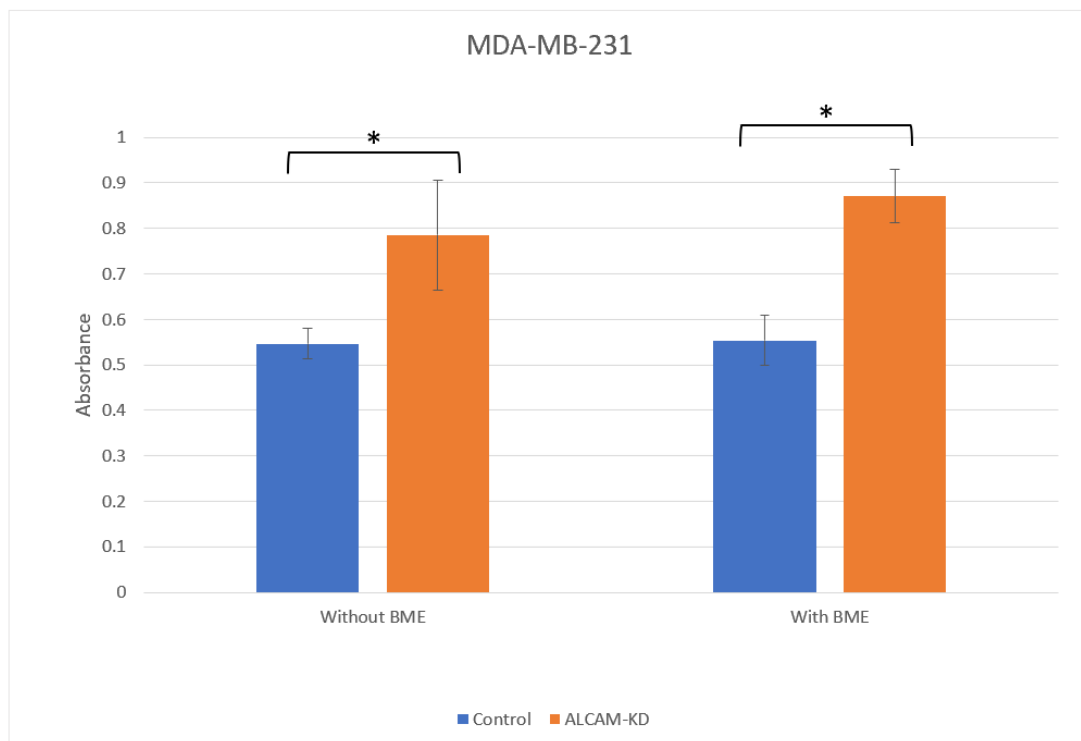


Figure 4.8 Cell growth assay of MDA-MB-231 cells with (right) and without (left) BME (50µg/ml). Shown are mean absorbance of cell staining of MDA-MB-231 control and ALCAM-

KD group in cell growth assay (Mean data shown, error bars represent SEM, * represents statistical significance).

4.4 Discussion

This Chapter has described the work in establishing ALCAM knockdown cell models in breast cancer cell lines of varying ER and HER2 statuses. It was clear that shRNA transgene has been highly successful in that three cell lines, namely MCF-7, MDA-MB-361 and MDA-MB-231 displayed a clear reduction of ALCAM transcript. This successfully established model has been a vital tool in the following work, establishing the cellular relationship of ALCAM and hormone receptors.

Manipulation of ALCAM expression has been previously demonstrated to impact the cellular functions of many different human cancer cell lines, including breast (Davies and Jiang 2010; Hein et al. 2011), prostate (Hansen et al. 2014; Sanders et al. 2019), gastric (Jin et al. 2011) and malignant mesothelioma (Ishiguro et al. 2012). Davies and Jiang (Davies and Jiang 2010) using a series of ALCAM gene transfected cell lines demonstrated that loss of ALCAM in breast cancer increased the growth rate of cancer cells. In addition, their study results showed that breast cancer cells which had lower levels of ALCAM grow faster in the presence of bone matrix proteins (BMP), which indicated a possibility that low levels of ALCAM may facilitate the worsening of bone metastasis in breast cancer. In our study, the cell growth rates of ALCAM knockdown in breast cancer cells, including both ER positive and negative, were higher than cells in the control group. These results were therefore in line with the previous study, although no difference was seen in the groups in which BME was added.

In conclusion, breast cancer ALCAM knockdown cell models with different hormonal receptor statuses were established, and the effect of ALCAM on cell growth in both normal conditions and bone microenvironment was explored in this Chapter. We

hope to use such models, in conjunction with our clinical data, to investigate both the clinical and cellular implications of ALCAM and hormone/receptor status in breast cancer progression and to fully explore this important relationship *in vitro*. Future work will concentrate on this relationship in the context of bone model and interaction assays in combination with potential mechanistic drivers to aid in the further elucidation of ALCAM's role in breast cancer progression and bone metastasis.

Chapter-5

Exploring signalling events underlying ALCAM and their involvement in hormonal receptor related bone metastasis of breast cancer

5.1 Introduction

In the last Chapter, I explored the expression pattern of ALCAM in different breast cancer cell lines and created ALCAM knockdown cell models using three representative cell lines. The transfection efficacy of the cell models was verified at both gene and protein level. We also performed cell growth assays, which demonstrated that loss of ALCAM would increase cell growth rate of breast cancer in normal conditions as well as bone microenvironment.

To further probe the regulatory role of ALCAM, in both ER positive and ER negative breast cancer cells, we conducted a protein microarray analysis to identify potential regulatory pathways and verified the results with *in vitro* assays, including immunoprecipitation and ECIS (Electric Cell-Substrate Impedance Sensing). The aims of this chapter were to identify some key intermediate molecules in ALCAM signalling pathways and preliminarily explain the mechanisms of ALCAM in different subgroups of breast cancer.

5.2 Methods

5.2.1 Special reagents

Recombinant human hepatocyte growth factor (rhHGF) was prepared at 10 μ g/ml in sterile BSS with 0.1% BSA and stored at -80°C. A HGF receptor MET small compound inhibitor, PF02341066 was also dissolved in DMSO and diluted in sterile BSS to a concentration 10mM and stored at -80°C until use. A ROCK kinase small compound inhibitor, Y27632 was used, and stocks were prepared with DMSO. Bone matrix extract (BME) was a central resource of the host laboratory and was prepared from fresh frozen femur as previously reported (Davies and Jiang 2010; Owen et al. 2016).

5.2.2 Genetic preparation of breast cancer cells

The transcription level of ALCAM in different breast cancer cell lines was tested by PCR as mentioned previously. Among them, MCF-7 (ER+/HER2-), MDA-MB-361(ER+/HER2+) and MDA-MB-231 (ER-/HER2-) cell lines were selected to create ALCAM knockdown models. Plasmids, which contained both scramble control and shRNA targeting ALCAM, were used for gene transfection. The transfection was performed using Fugene HD (Promega, Southampton, UK) transfection reagent in accordance with manufacturer's instructions.

5.2.3 Protein preparation and the Protein kinase array (Kinexus™) analysis

Protein samples from MCF-7 and MDA-MB-231 ALCAM knockdown cell models were prepared and quantified as mentioned previously. After protein quantification, samples were adjusted to the same concentration (2mg/ml) in 1.5ml microfuge tubes. The protein samples were tested on the Kinex-900p protein array (Kinexus Bioinformatics, Vancouver, Canada). Detailed methods are given in Chapter 2. Bioinformatics analyses were carried out by comparing the proteins that were impacted by knocking down ALCAM and the wider implications of the affected proteins in the context of protein networking were examined. The results are shown here as the normalised fluorescence unit representing protein kinase levels of each sample, the degree of change of a given protein kinase by way of percentage CFC and Z ratio.

5.2.4 Immunoprecipitation (IP)

The protein samples from MCF-7, MDA-MB-361 and MDA-MB-231 wild type cells were prepared using lysis buffer without SDS and quantified as mentioned previously. A portion of protein was removed from respective samples as the control group and used for immunoprecipitation with antibodies of interested, in this case

with antibodies against MET, a key protein identified from the Kinexus assay as being markedly influenced following ALCAM knockdown. Primary antibodies (ALCAM and MET antibodies) were added to the samples. The tubes which contained the mixture of sample and antibody were then placed on a rotating wheel (35rpm, 4 °C) for 24 hours. Following that, A/G agarose was added to the samples and again placed on a rotating wheel for 2 to 4 hours. The protein-antibody-agarose mixture was dispensed into microfuge tubes which were centrifuged at 4°C, 7500 rpm for 5 minutes. After removing supernatants, the samples were washed three times with lysis buffer.

After removing the washing solutions, 1× sample buffer was added to the immunoprecipitants, and the samples were then boiled at 98°C for 5 to 7 minutes. The supernatant, which contains the proteins precipitated by the antibody was then carefully collected and stored at -20°C, ready for Western blotting assays.

5.2.5 Western blotting

After immunoprecipitation samples were ready to use, Western blotting was performed as mentioned in Section 2.8. The protein samples, precipitated with the ALCAM antibody, were probed with MET antibody and samples, precipitated with MET antibody, were probed with the ALCAM antibody.

5.2.6 ECIS (Electric Cell-substrate Impedance Sensing)

ECIS assay was applied to investigate cellular behaviour based on the impedance parameter detected from gold electrodes coated on the bottom of a 96-well array (96W1E) (Applied Biophysics Inc., NJ, USA). In brief, MCF-7 control/ALCAM knockdown cells, MDA-MB-361 control/ALCAM knockdown cells and MDA-MB-231 control/ALCAM knockdown cells were seeded at an appropriate density (20,000 to 30,000 cells per well). The reagents used in the study (BME, HGF, MET inhibitor, Neratinib and ROCK inhibitor) were added before the 96-well array was placed into

the incubated array station and changes in resistance/impedance measured over the course of the experiment. The first 4 hours of data was analysed for attachment of the cells.

5.2.7 Statistical methods

The comparison between group was performed by two sample T-Test. All the analyses were carried out using SPSS version 26. The statistical significance was defined as $p < 0.05$.

5.3 Results

5.3.1 The changes of signalling events following ALCAM knockdown in ER positive and negative breast cancer cell lines.

To explore the potential role of ER in ALCAM signalling pathway, one ER positive (MCF-7) and one ER negative (MDA-MB-231) were selected to create ALCAM knockdown cell models. Protein samples, including MCF-7 Control/ALCAM-KD and MDA-MB-231 Control/ALCAM-KD cells, were collected and Kinexus™ protein kinase microarray analysis was performed. Microarray KAM900 contained 900 antibody spots which could either recognise phosphorylated specific kinases or total kinase proteins. Figure 5.1 shows the fluorescence staining images of the protein microarray in different experimental groups.

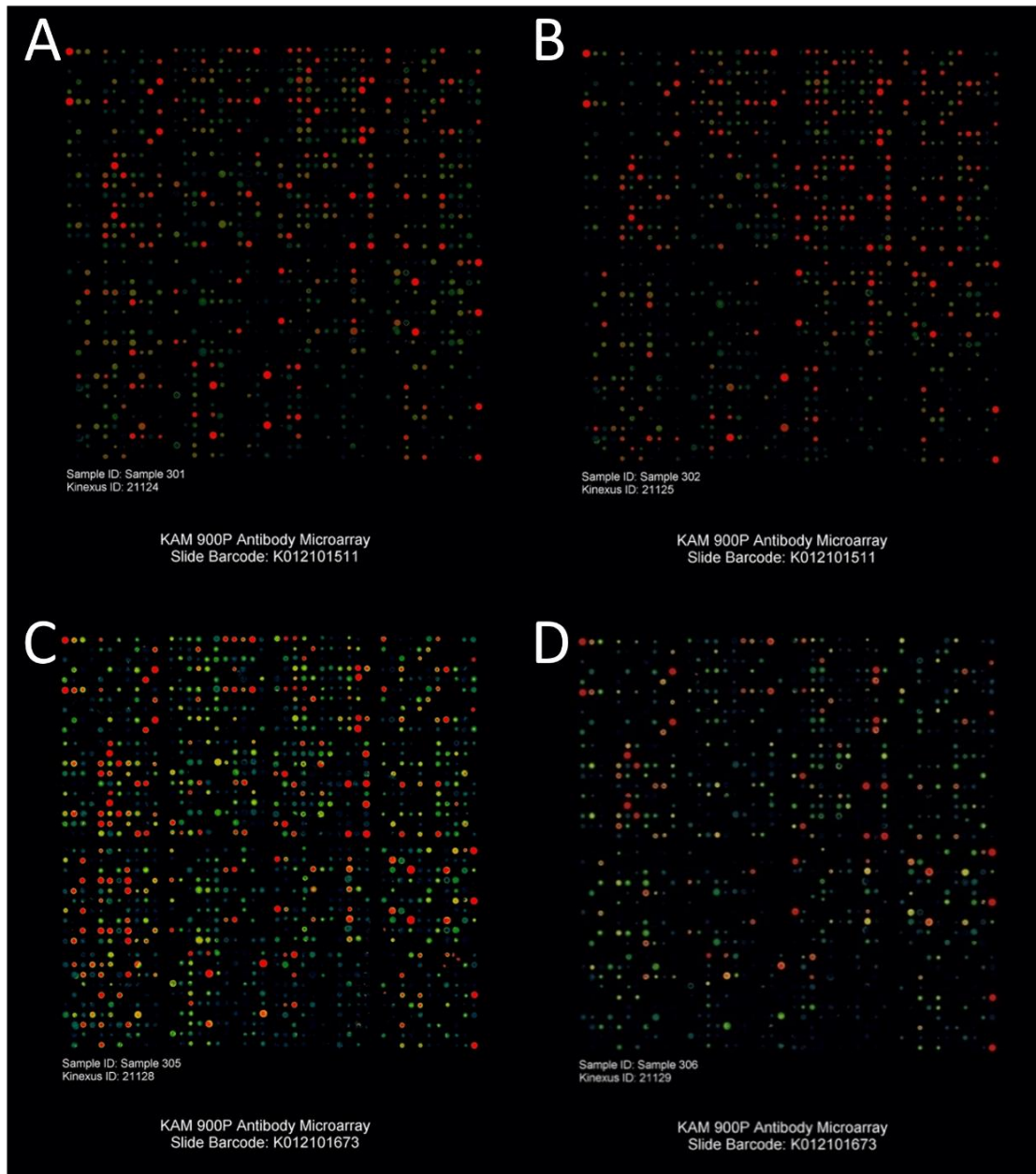


Figure 5.1 Microarray images of the KAM900P for the present study. A: Detecting the protein sample from MDA-MB-231 control cells; B: Detecting the protein sample from MDA-MB-231 ALCAM knockdown cells; C: Detecting the protein sample from MCF-7 control cells; D: Detecting the protein sample from MCF-7 ALCAM knockdown cells.

The kinase reactions in breast cancer ALCAM knockdown models were then compared and analysed, based on the fluorescence quantification of the protein microarrays mentioned above. The analyses identified three patterns of changes, when taken into consideration of the direction of the change and the hormone receptor status. They include those protein kinases upregulated both in the ER (+) MCF-7 and ER (-) MDA-MB-231 cells following ALCAM knockdown, those downregulated in both cells and, most interestingly, those showing contrasting changes between ER (+) and ER (-) cells. These groups proteins are separately shown in the following sections.

5.3.1.1 Protein kinases showing the same trend of changes in ER positive and ER negative group after knocking down ALCAM

Table 5.1 and Figure 5.2 show proteins activated in both MDA-MB-231 and MCF7 cells and proteins inhibited in both MDA-MB-231 and MCF-7 cells are listed in Table 5.2 and Figure 5.3.

Table 5.1 Protein/kinase upregulated in both MDA-MB-231 and MCF-7 cells following ALCAM knockdown.

Protein Target Name	Phospho Site (Human)	MDA-MB-231 Control (Globally Normalized Signal Intensity) *	MDA-MB-231 ALCAM-KD (Globally Normalized Signal Intensity) *	Z-Score Ratio [#]	MCF-7 Control (Globally Normalized Signal Intensity) *	MCF7 ALCAM-KD (Globally Normalized Signal Intensity) *	Z-Score Ratio [#]
A-Raf (RafA)	Y302	20	61	1.65	47	54	1.26
CDK6	Pan-specific	70	178	1.43	42	59	1.67
Cyclin B1 (CCNB1)	Pan-specific	2624	6527	1.78	3332	6940	1.63
ERK1 (MAPK3)	T202+Y204	25	57	1.09	25	25	1.17
GATA1	S142	4914	16687	2.44	5269	9389	1.28
GSK3b	Y279	228	741	2.03	317	561	1.73
GSK3a	Y284+Y285	104	319	1.82	37	42	1.32
HDAC5	S498	7749	12143	1.01	4802	8918	1.37
Histone H2B	S14	8834	32053	2.64	7590	12372	1.06
Histone H3	S28	8329	16193	1.43	5223	9500	1.32
Histone H3	T3	13264	21673	1.15	9080	16634	1.24
Hsp27	S78	6595	14238	1.61	4650	9148	1.47
Hsp90a/b	Pan-specific	14928	34353	1.82	10142	17278	1.09
HSP90AB1 (HSP90; HSP84; HSP90B; HSPC2; HSPCB)	Pan-specific	15075	44710	2.31	11355	22245	1.32
IKKa (IkbKA)	Pan-specific	269	548	1.15	170	214	1.23
ILK1	Pan-specific	836	2463	1.98	1210	2069	1.45
Integrin a4 (ITGA4)	S1021	8214	16133	1.45	5643	9575	1.18
IRS1	S312	5227	9785	1.31	4373	6531	1.00
IRS1	S639	3086	5264	1.07	2145	5147	1.95
JAK2	Y1007+Y1008	1455	3007	1.36	1138	2541	1.93
JAK3	Pan-specific	675	1598	1.53	740	1010	1.13
Met	T1355+Y1356	34	114	1.87	31	47	1.81
p53	S392	2840	5409	1.27	1558	2416	1.23
p53	S6	5104	9019	1.19	4098	6741	1.18
PRKACA	T198	504	1093	1.33	1490	2489	1.37
PKCe (PRKCE)	Pan-specific	3202	5847	1.21	5729	10922	1.38
PTP1D (PTPN11; SHP2)	S580	1430	2735	1.21	891	1751	1.75
PIK1 (PLK)	T210	71	297	2.38	50	77	1.80
Rb	S807	104	312	1.79	356	426	1.02

ROCK2 (ROKa)	Pan-specific	77	330	2.45	37	40	1.24
RSK1 (RPS6KA1, p90RSK)	Y220+S221	88	643	3.48	41	52	1.46
RSK1 (RPS6KA1, p90RSK)	S363/S369	1240	2164	1.02	1697	3134	1.53
RSK1 (RPS6KA1, p90RSK)	S363/S369	724	1642	1.46	948	1975	1.84
RSK3 (RPS6KA2)	T573/T577/T570	97	294	1.8	77	130	1.89
S6Ka (RPS6KB1)	T252	3491	8189	1.7	3101	5039	1.20
SHIP2 (INPPL1)	Pan-specific	59	201	1.97	26	33	1.57
SIK2 (QIK)	Pan-specific	47	143	1.73	47	56	1.33
SIT	Y95	29	119	2.25	35	86	2.66
SRPK2	Y319	82	229	1.63	22	46	2.41
Syk	Y525+Y526	141	328	1.33	128	195	1.61
Tau	S713	2301	4456	1.28	1777	2608	1.12
WASP	Y291	53	157	1.69	91	284	2.94

Note: * Fluorescence signal reading for the particular protein kinase normalised to housekeeping protein control; # Z ratio: a parameter showing the difference between the two samples. It was obtained by dividing the Z score difference between the two samples by the standard deviation (SD).

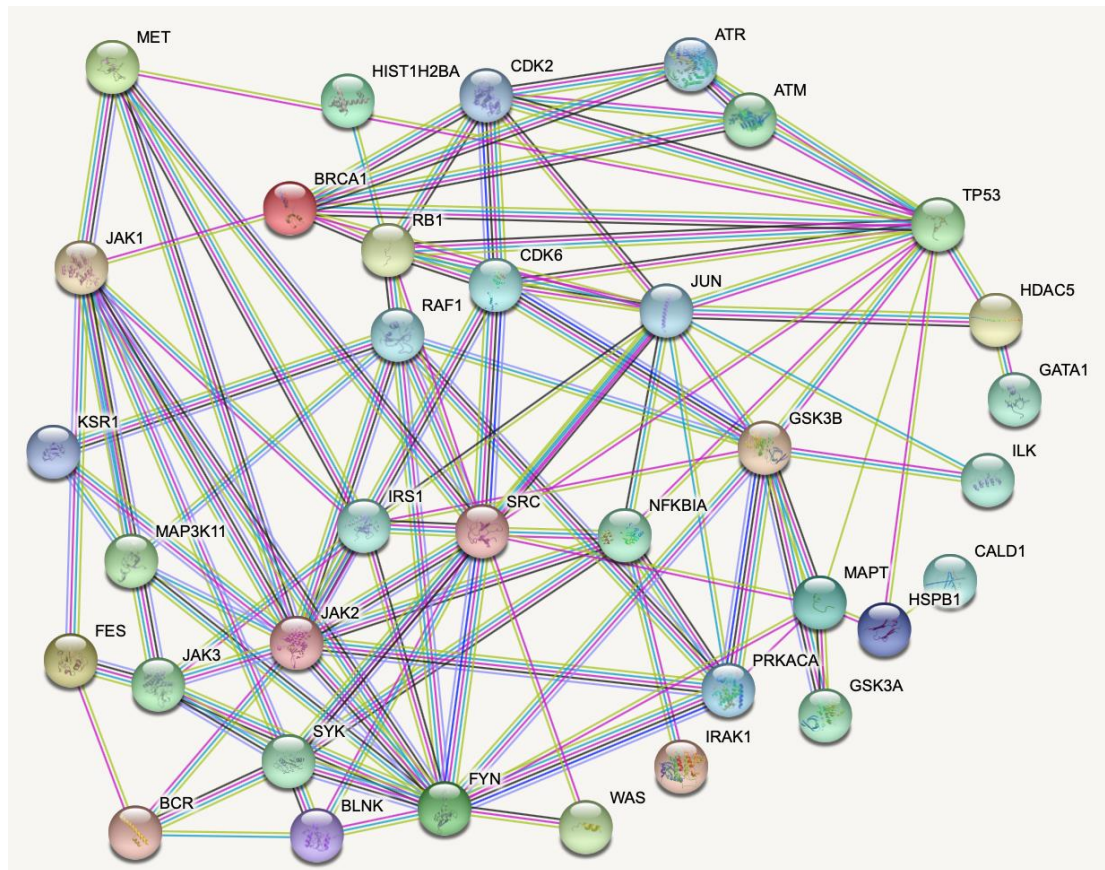


Figure 5.2 Proteins activated in both MDA-MB-231 and MCF-7 cells following knocking down ALCAM (<https://string-db.org>)

Table 5.2 Protein/kinase downregulated in both MDA-MB-231 and MCF-7 cells following ALCAM knockdown.

Protein Target Name	Phospho Site (Human)	MDA-MB-231 control*	MDA-MB-231 ALCAM-KD*	Z-Score Ratio [#]	MCF7 control*	MCF7 ALCAM-kd*	Z-Score Ratio [#]
ASK1 (MAP3K5)	Pan-specific	4445	1423	-2.1	3938	1876	-1.01
CDC7	T376	2530	1215	-1.39	2291	654	-1.83
CDK1 (CDC2)	Y19	2242	1309	-1.02	2004	732	-1.37
EGFR (ErbB1)	Y1172	1971	1147	-1.05	2275	829	-1.39
ErbB2 (HER2, Neu)	Y877	451	134	-2.49	888	284	-1.46
EphB2	Y780	406	219	-1.36	965	332	-1.35
ERK1 (MAPK3)	T207	746	306	-1.82	1692	696	-1.13
ERK1 (MAPK3)	Y204+T207	309	184	-1.21	663	267	-1.02
ERK4 (MAPK4)	Pan-specific	989	339	-2.14	943	393	-1.01
ERK5 (MAPK7)	T219+Y221	5508	2573	-1.36	6101	2948	-1.06
ERK5 (MAPK7)	Y221	1015	414	-1.8	1631	500	-1.64
FAK (PTK2)	Y397	3228	1354	-1.62	2702	1213	-1.05
FGFR2 (BEK)	Y656+Y657	460	228	-1.51	953	191	-2.31
FGFR2 (BEK)	Pan-specific	1435	789	-1.19	2058	644	-1.64

FRK	Y387	20679	9984	-1.15	19340	10585	-1.03
GCK	S170	4006	1661	-1.62	8193	3105	-1.53
GSK3a	S278+Y279	33766	12352	-1.63	21862	11648	-1.09
GSK3a	T19+S21	10836	4005	-1.73	12576	5208	-1.45
IRS1	Y612	1164	118	-4.46	973	47	-4.85
MAK	T157	1496	870	-1.08	3666	1552	-1.21
MAPKAPK5 (PRAK)	T186	2591	1414	-1.14	3450	1574	-1.06
MARK1	T215	5359	2796	-1.15	7400	3187	-1.29
MEK2 (MKK2, MAP2K2)	Pan-specific	131	49	-2.2	251	33	-2.82
MEK2 (MKK2, MAP2K2)	Pan-specific	610	255	-1.81	1000	389	-1.14
MEKK2 (MAP3K2)	S239	1009	492	-1.46	1804	699	-1.24
MKK4 (MAP2K4, MEK4)	S257	2001	1015	-1.31	3243	1363	-1.20
MKK4 (MEK4, MAP2K4)	Pan-specific	8258	2990	-1.8	8277	3641	-1.27
MKK6 (MEK6, MAP2K6)	Pan-specific	2079	992	-1.42	3494	1226	-1.53
MKK7 (MEK7, MAP2K7)	Pan-specific	4561	2273	-1.25	7825	3071	-1.47
MLTK (ZAK)	T161+T162	1387	737	-1.26	3073	933	-1.77
MOK (RAGE)	T159+Y161	3815	1369	-1.9	4409	1673	-1.43
MEK1 (MKK1, MAP2K1)	Pan-specific	197	118	-1.24	468	170	-1.14
MERTK (MER)	Y749	235	127	-1.42	617	218	-1.23
Met	T1241	3204	1359	-1.6	4663	2155	-1.09
Met	Y1234+Y1235	13906	5842	-1.46	15363	8249	-1.02
MST3 (STK24)	T190	2404	1087	-1.51	5119	2012	-1.39
mTOR (FRAP)	S2448	2636	1324	-1.3	5248	2273	-1.22
NFkappaB p65 (Rel A)	S276	8525	2950	-1.89	11956	4831	-1.48
NDR1 (NDR, STK38)	S281+T282	2184	1085	-1.34	5126	1892	-1.50
NuaK1 (ARK5)/Nuak2	T211	2731	1452	-1.18	4662	1930	-1.29
OSR1 (OXSR1)	T185	4446	2079	-1.38	6535	3016	-1.15
TYK2	Pan-specific	39	22	-1.54	102	29	-1.32

Note: * Fluorescence signal reading for the particular protein kinase normalised to housekeeping protein control; # Z ratio: a parameter showing the difference between the two comparing samples. It was obtained by dividing the Z score difference between the two samples by the standard deviation (SD).

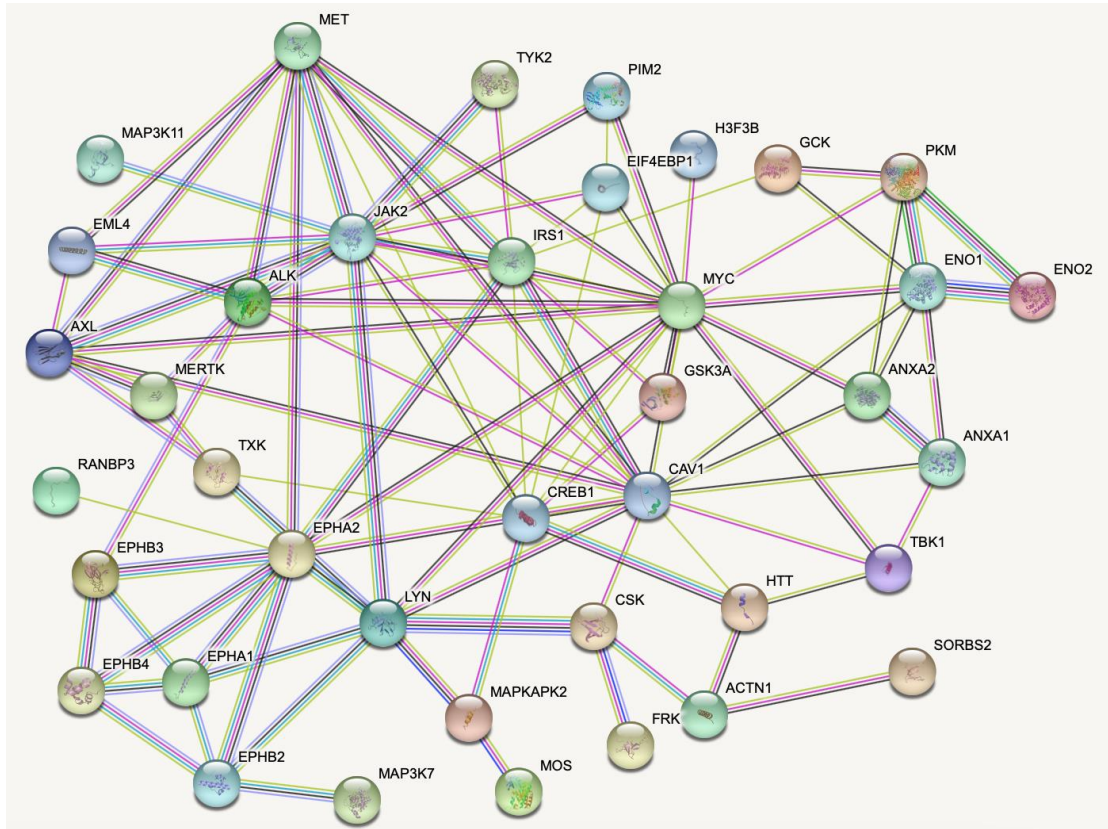


Figure 5.3 Proteins inhibited in both MDA-MB-231 and MCF-7 cells following knocking down ALCAM (<https://string-db.org>).

5.3.1.2 Protein kinases showing contrast changes in ER positive and ER negative group after knocking down ALCAM

The analysis identified a particular group of protein kinases in which the changes between the ER positive and ER negative breast cancer cells were contrasted, following ALCAM knockdown. The list of these candidates can be seen in Table 5.3, Figure 5.4 through to Figure 5.7.

Of particular interest are two of the protein kinase C, PRKCH and PRKCB1, and two of the angiogenic and neurogenic factor receptors, VEGFR3 and TrkB. These kinases were seen to rise in the ER positive MCF-7 cells and were markedly reduced in the ER negative MDA-MB-231 cells after ALCAM knockdown (Figure 5.6 and 5.7). When looking at the protein kinases that were downregulated in ER positive yet upregulated in ER negative cells, the list (Table 5.3) is a lot longer and more diverse in terms of the portrayed function of these kinases. The largest proportion of the list are MEK (Mitogen-activated protein kinase kinase) and MKK family members. In this case, of particular interest is MET which is amongst few cytokine receptor kinases showing the interesting change.

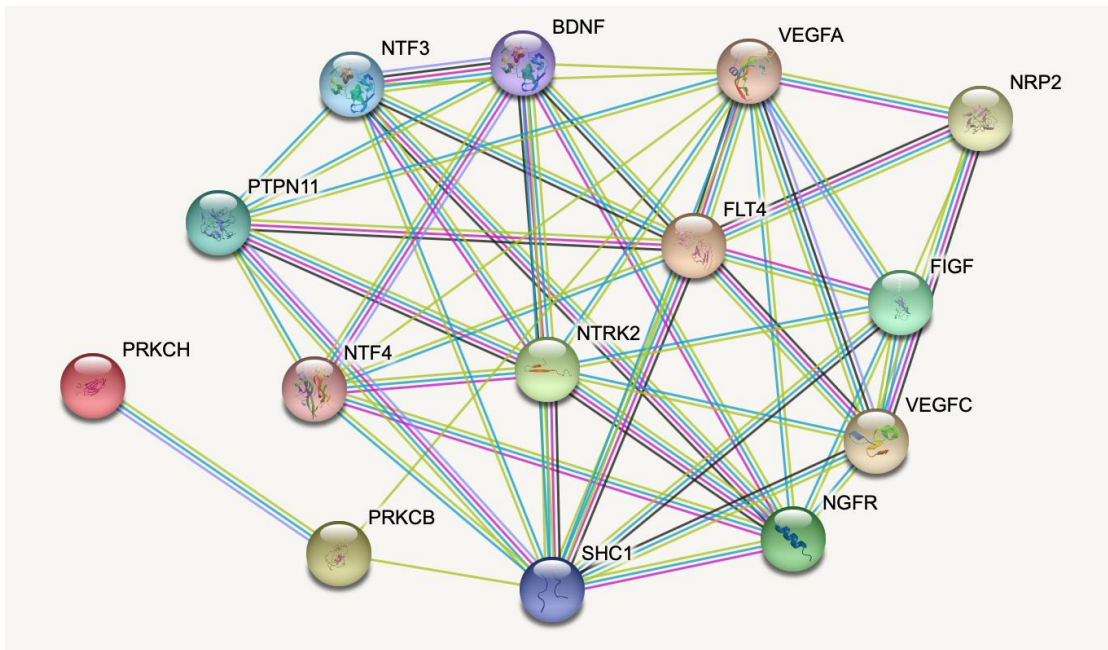


Figure 5.4 Proteins activated in MDA-MB-231 cells but inhibited in MCF-7 cells following knocking down ALCAM (<https://string-db.org>).

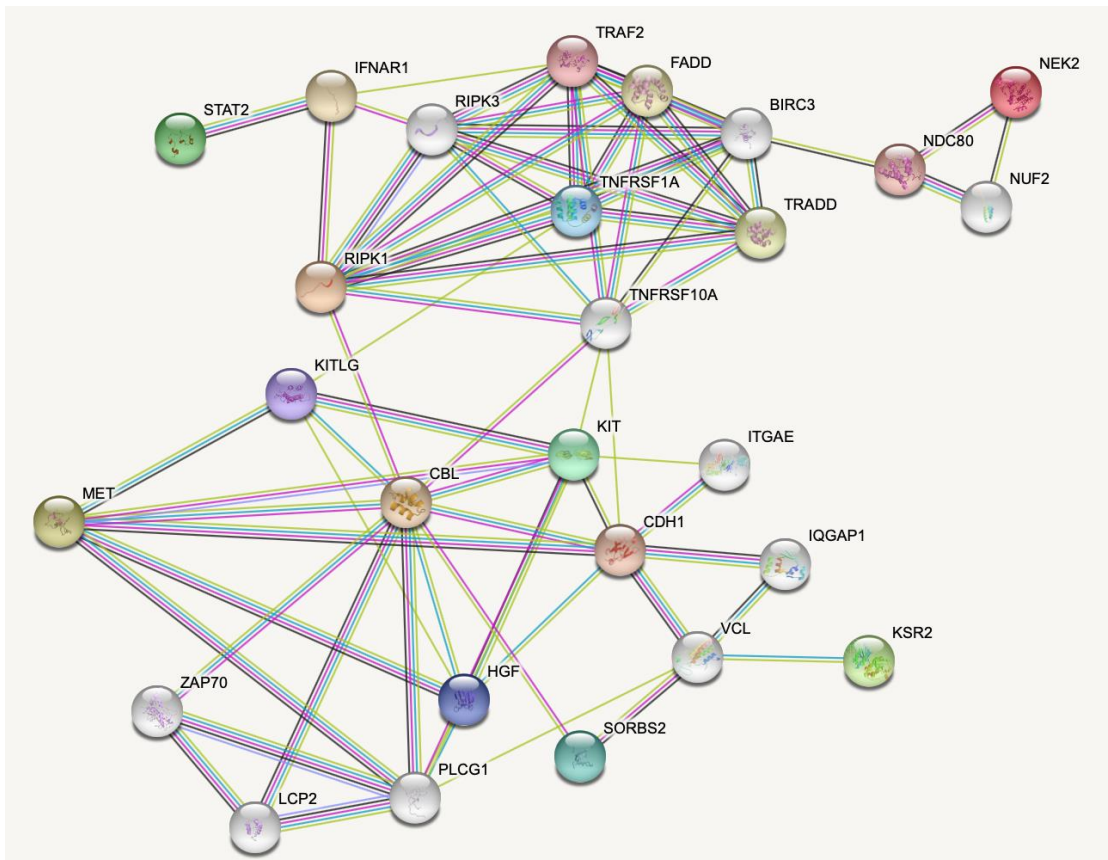


Figure 5.5 Proteins inhibited in MDA-MB-231 but activated in MCF-7 cells following knocking down ALCAM (<https://string-db.org>).

Table 5.3 Protein/kinase pattern contrasted in MDA-MB-231 and MCF-7 cells following ALCAM knockdown.

Protein Target Name	Phospho Site (Human)	Full Target Protein Name	Average Normalized (MDA-MB-231 control) *	Average Normalized (MDA-MB-231 ALCAM-KD) *	%CFC [‡]	Z-Score Ratio [#]	Average Normalized (MCF7 control) *	Average Normalized (MCF7 ALCAM-KD) *	%CFC [‡]	Z-Score Ratio [#]
PKCh (PRKCH)	T656	Protein-serine kinase C eta	1117	511	-54	-1.57	933	1729	85	1.64
PKCb (PRKCB1)	Pan-specific	Protein-serine kinase C beta 1	469	271	-42	-1.21	544	1614	197	2.56
TrkB (NTRK2)	Y702	BDNF/NT3/4/5 receptor- tyrosine kinase	107	51	-52	-1.75	70	164	133	2.47
VEGFR3 (Flt4)	Pan-specific	Vascular endothelial growth factor receptor-protein-tyrosine kinase 3 (VEGFR3)	221	76	-65	-2.29	111	341	206	2.87
Abl (Abl1)	Pan-specific	Abelson proto-oncogene-encoded protein-tyrosine kinase	185	968	422	2.92	782	305	-61	-1.10
Ksr2	S490	Kinase suppressor of Ras 2	37	104	179	1.54	207	48	-77	-1.80
Kit	Pan-specific	'Mast/stem cell growth factor receptor Kit	70	211	202	1.76	278	88	-68	-1.29
MEK1 (MKK1, MAP2K1)	T292	MAPK/ERK protein-serine kinase 1 (MKK1)	48	144	200	1.7	292	55	-81	-2.22
MEK1 (MKK1, MAP2K1)	T292	MAPK/ERK protein-serine kinase 1 (MKK1)	2179	3789	74	1.07	4754	1835	-61	-1.41

MEK2 (MKK2, MAP2K2)	T394	MAPK/ERK protein- serine kinase 2 (MKK2) (mouse)	293	1306	345	2.66	1316	405	-69	-1.60
Met	Y1234	Hepatocyte growth factor (HGF) receptor-tyrosine kinase	31	234	658	3.44	761	31	-96	-5.10
MKK4 (MEK4, MAP2K4)	Pan-specific	MAPK/ERK protein- serine kinase 4 (MKK4)	49	384	680	3.54	542	79	-85	-2.78
Nek2	Pan-specific	NIMA (never-in- mitosis)-related protein-serine kinase 2	284	584	106	1.17	830	284	-66	-1.34
p38a MAPK (MAPK14)	T180+Y182	Mitogen-activated protein-serine kinase p38 alpha	60	180	201	1.73	311	101	-67	-1.27
p38g MAPK (MAPK12, ERK6)	Pan-specific	Mitogen-activated protein-serine kinase p38 gamma (MAPK12)	1804	3159	75	1.06	3512	1523	-57	-1.16
p38g MAPK (MAPK12, ERK6)	Pan-specific	Mitogen-activated protein-serine kinase p38 gamma (MAPK12)	908	1699	87	1.12	1627	712	-56	-1.01
PAK1 (PAKa)	S144	p21-activated kinase 1 (alpha) (serine/threonine- protein kinase PAK 1)	890	1641	84	1.08	2435	726	-70	-1.76
Plk1 (PLK)	Y217	Polo-like protein- serine kinase 1	10	81	700	3.42	94	22	-77	-1.69

RIPK1	Y384	Receptor-interacting protein-serine kinase 1	30	91	201	1.66	229	83	-64	-1.02
ROCK1 (ROKb)	Y913	Rho-associated protein kinase 1	79	188	137	1.3	560	71	-87	-3.04
STAT1a/b	Pan-specific	Signal transducer and activator of transcription 1 alpha	50	125	148	1.34	288	97	-66	-1.19
STAT2	Y690	Signal transducer and activator of transcription 2	446	2311	418	3	2511	94	-96	-5.44

Note: * Fluorescence signal reading for the particular protein kinase normalised to housekeeping protein control; %CFC: The percent change of ALCAM knockdown cells in Normalized Intensity from the control cells. # Z ratio: a parameter showing the difference between the two comparing samples. It was obtained by dividing the Z score difference between the two samples by the standard deviation (SD).

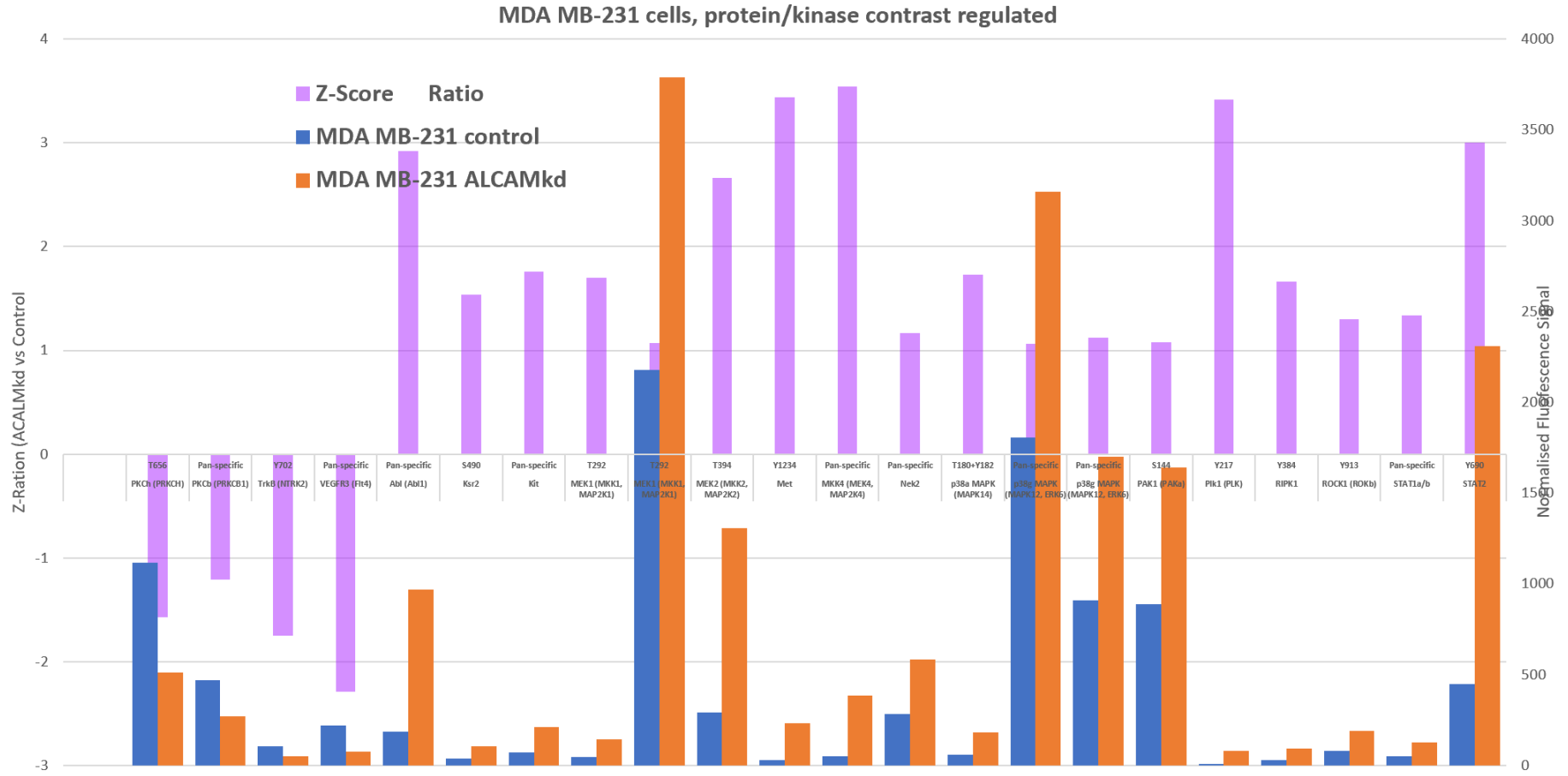


Figure 5.6 Contrast regulated protein kinases in MDA-MB-231 cells following ALCAM knockdown.

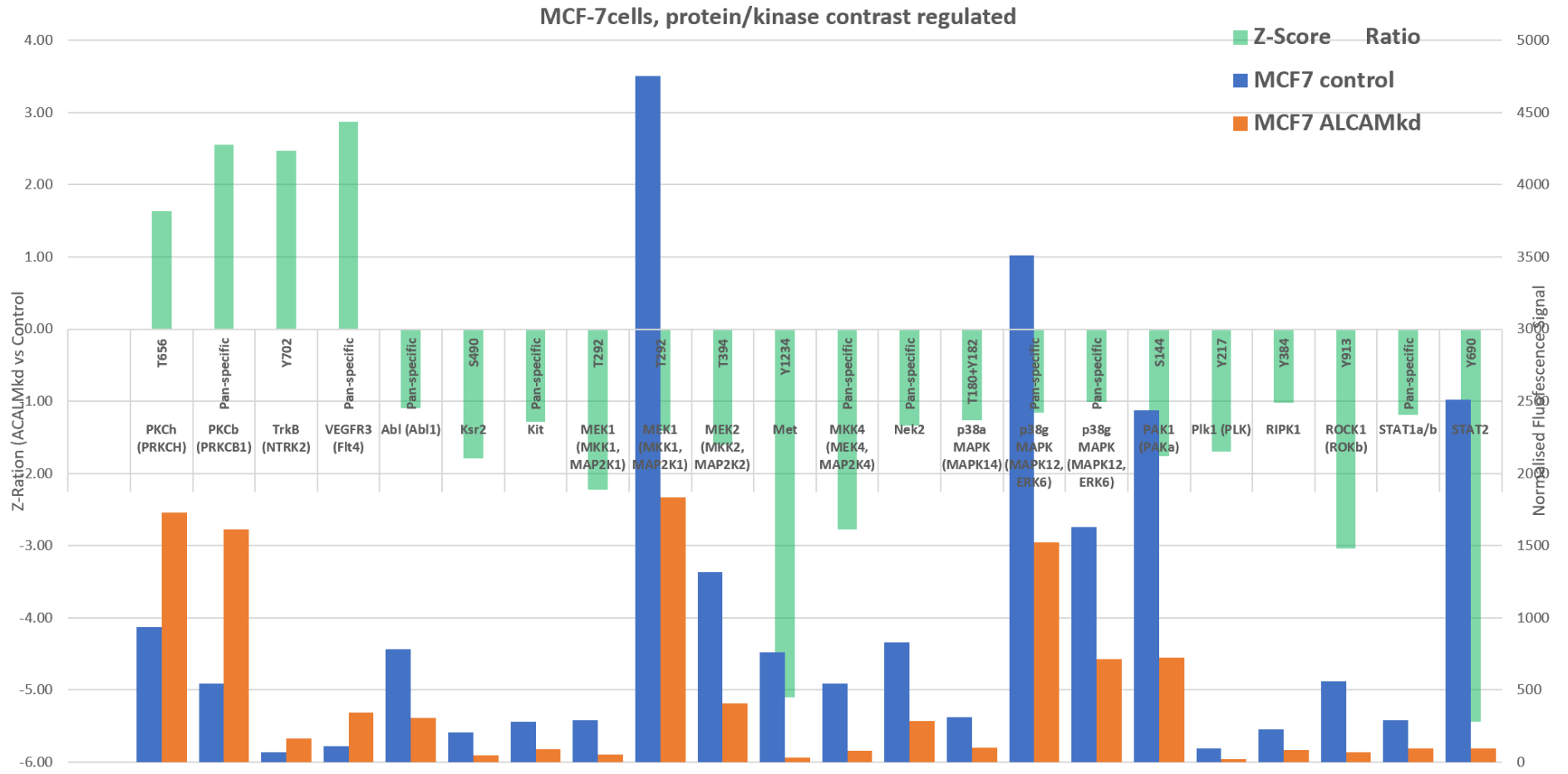


Figure 5.7 Contrast regulated protein kinases in MCF-7 cells following ALCAM knockdown.

The critical pathway analysis was completed using the online database Reactome (www.reactome.org). The top twenty-five signalling pathways based on contrast-regulated protein kinases in MDA-MB-231 and MCF-7 cells after ALCAM knockdown are shown in Table 5.4. Additionally, the genome-wide overview schematic diagram of the contrast regulated signalling pathways were created (Figure 5.8) to present a general picture of the major area of these pathways.

Table 5.4 Top twenty-five signalling pathways based on contrast regulated protein kinases in MDA-MB-231 and MCF-7 cells after ALCAM knockdown(www.reactome.org).

Pathway name	Entities				Reactions	
	found	ratio	p-value	FDR*	found	ratio
Signaling by high-kinase activity BRAF mutants	4 / 44	0.002	5.53e-06	0.002	4 / 6	4.42e-04
MAP2K and MAPK activation	4 / 49	0.002	8.42e-06	0.002	12 / 12	8.84e-04
Signaling by RAF1 mutants	4 / 49	0.002	8.42e-06	0.002	5 / 7	5.16e-04
Paradoxical activation of RAF signaling by kinase inactive BRAF	4 / 72	0.003	3.76e-05	0.004	5 / 7	5.16e-04
Signaling downstream of RAS mutants	4 / 72	0.003	3.76e-05	0.004	5 / 7	5.16e-04
Signaling by moderate kinase activity BRAF mutants	4 / 72	0.003	3.76e-05	0.004	5 / 7	5.16e-04
Signaling by RAS mutants	4 / 72	0.003	3.76e-05	0.004	5 / 9	6.63e-04
Signaling by BRAF and RAF1 fusions	4 / 73	0.003	3.97e-05	0.004	5 / 5	3.68e-04
Signalling to ERKs	5 / 74	0.003	4.18e-05	0.004	8 / 32	0.002
DSCAM interactions	3 / 35	0.002	1.07e-04	0.008	3 / 6	4.42e-04
Signaling by MAP2K mutants	2 / 6	2.79e-04	1.15e-04	0.008	1 / 1	7.37e-05
Oncogenic MAPK signaling	4 / 111	0.005	1.97e-04	0.013	30 / 46	0.003
RAF/MAP kinase cascade	8 / 478	0.022	2.15e-04	0.013	22 / 75	0.006
RHOH GTPase cycle	3 / 54	0.003	3.78e-04	0.02	1 / 3	2.21e-04
Myogenesis	5 / 132	0.006	3.79e-04	0.02	8 / 14	0.001
MAPK1/MAPK3 signaling	10 / 576	0.027	6.56e-04	0.033	29 / 82	0.006
Activation of RAC1	2 / 15	6.99e-04	7.07e-04	0.033	1 / 4	2.95e-04
p38MAPK events	2 / 20	9.31e-04	0.001	0.051	2 / 5	3.68e-04
Activation of PPARGC1A (PGC-1alpha) by phosphorylation	2 / 23	0.001	0.002	0.051	1 / 2	1.47e-04
activated TAK1 mediates p38 MAPK activation	2 / 27	0.001	0.002	0.051	5 / 5	3.68e-04
Signalling to RAS	2 / 27	0.001	0.002	0.051	2 / 10	7.37e-04
Drug resistance of KIT mutants	1 / 1	4.66e-05	0.003	0.051	7 / 7	5.16e-04
KIT mutants bind TKIs	1 / 1	4.66e-05	0.003	0.051	2 / 2	1.47e-04
Regorafenib-resistant KIT mutants	1 / 1	4.66e-05	0.003	0.051	1 / 1	7.37e-05
Nilotinib-resistant KIT mutants	1 / 1	4.66e-05	0.003	0.051	1 / 1	7.37e-05

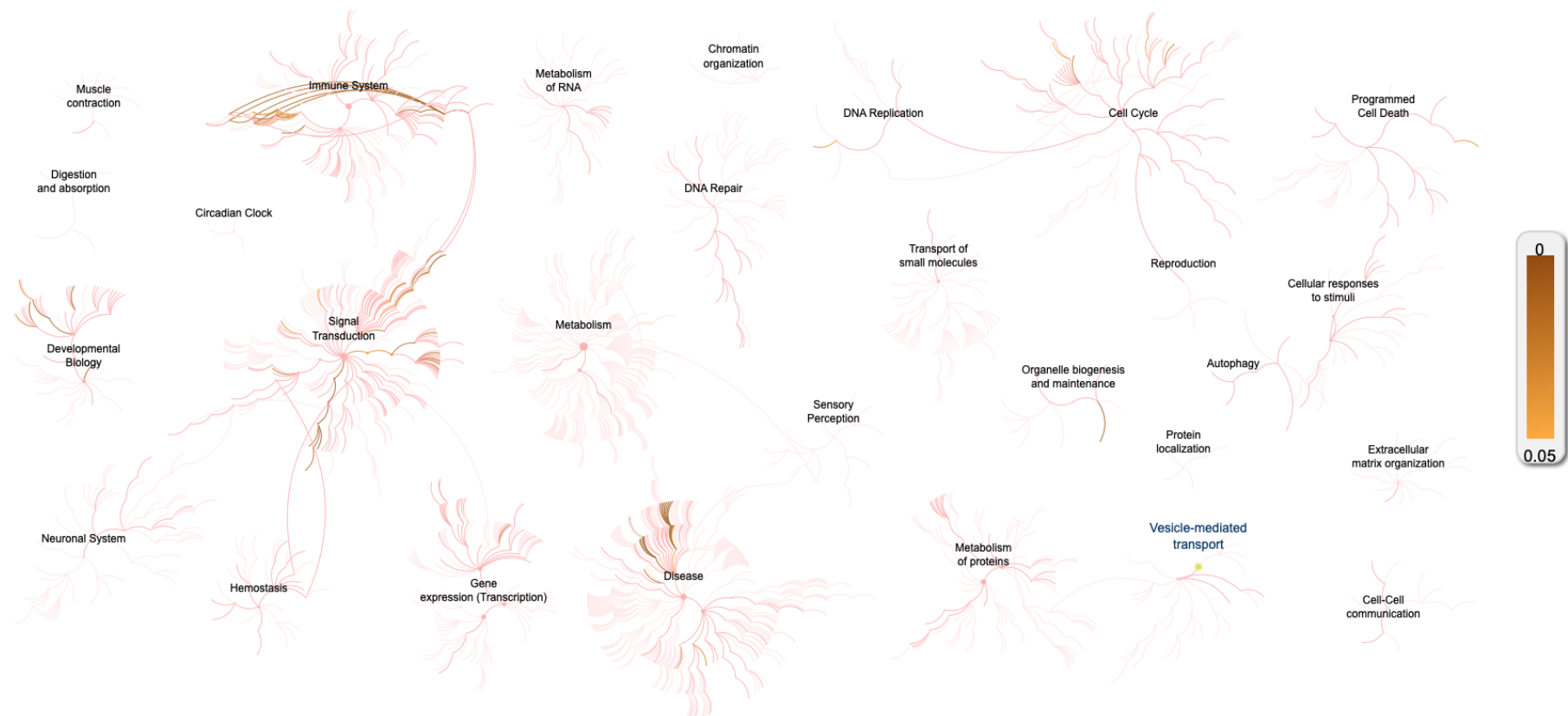


Figure 5.8 Events of contrast regulated kinases in cellular events. Pathways were rank ordered based on their relationships of cellular interaction. Each circular symbolises the top-level pathway's root in its centre. The lower level of the pathway rank is represented by each step taken away from the centre. Source: www.reactome.org.

Of the number of protein kinase changes following ALCAM knockdown, the HGF receptor MET was amongst the most striking. Given the importance of HGF/MET in cancer, the link between HGF/MET with metastasis (including bone metastasis) and the extensive experience and expertise in the host laboratory, we chose MET as a candidate from the kinases which was contrast regulated in ER positive and ER negative cells, and was the subject of further studies. As shown in Figure 5.9, most of the phosphorylated sites tested were significantly altered (Z-score ratio >1 or < -1) following ALCAM knockdown in MDA-MB-231 cells and MCF-7 cells.

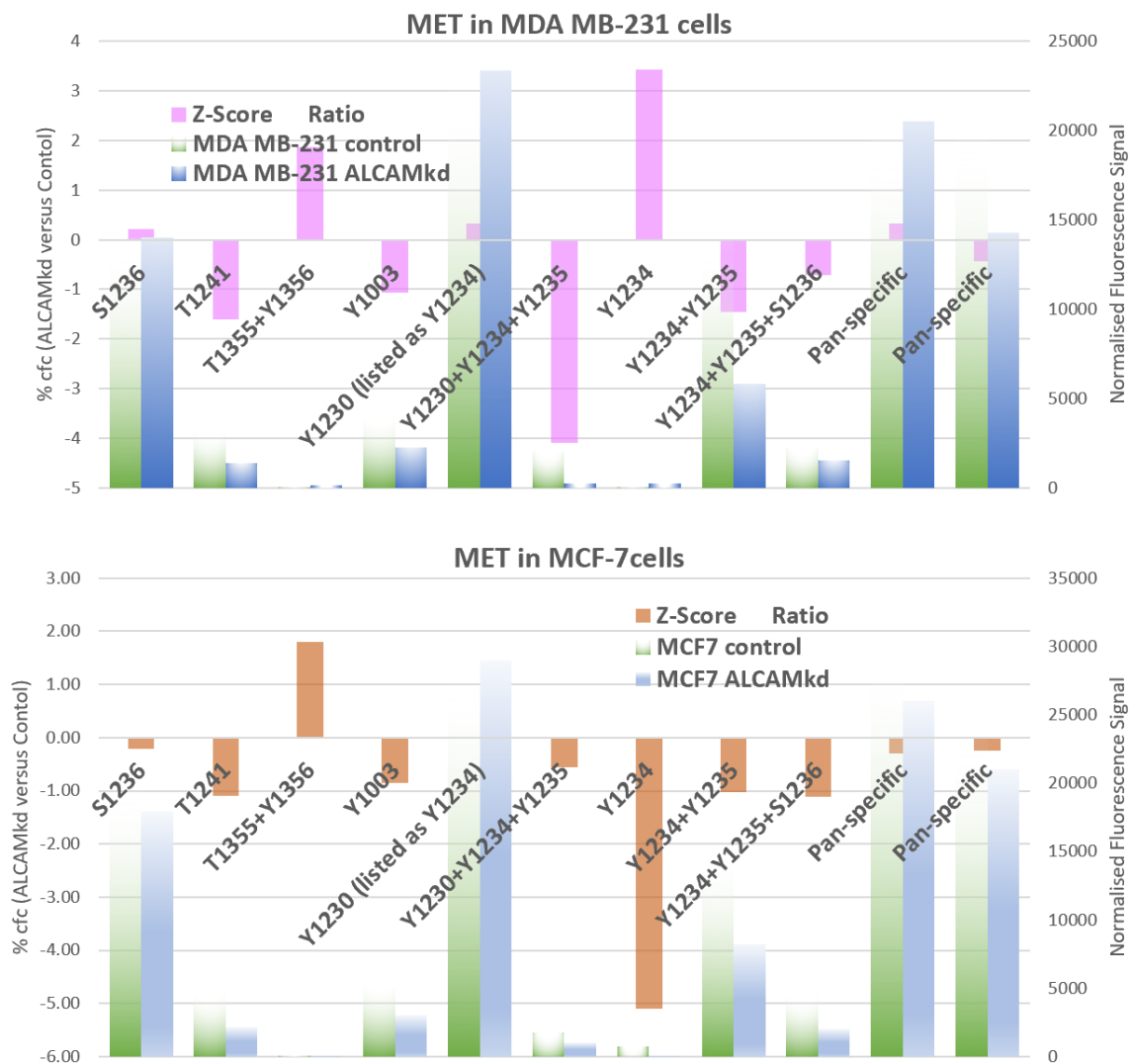


Figure 5.9 MET as an example of those changes after ALCAM knockdown in MDA-MB-231 (top) and MCF7 (bottom) cells.

5.3.2 Immunoprecipitation of ALCAM interacting protein

To verify the interaction between ALCAM and MET in breast cancer cell lines with different ER status, immunoprecipitation was conducted in MCF-7, MDA-MB-361 and MDA-MB-231 cells. Both ALCAM and MET primary antibody were used to generate ALCAM-MET immunoprecipitants, respectively. As shown in Figure 5.10, MDA-MB-361 and MDA-MB-231 were weakly positive in Western blotting when precipitated with ALCAM antibody and probed with MET antibody. However, no band could be seen in either ALCAM precipitated or control groups of MCF-7 cells. There was also no ALCAM band observed in the MET precipitated group of MCF-7, MDA-MB-361 and MDA-MB-231 cells (Figure 5.11). These results indicated the presence of a potential protein interaction between ALCAM and MET in MDA-MB-361 cells and MDA-MB-231 cells, but not in MCF-7 cells.

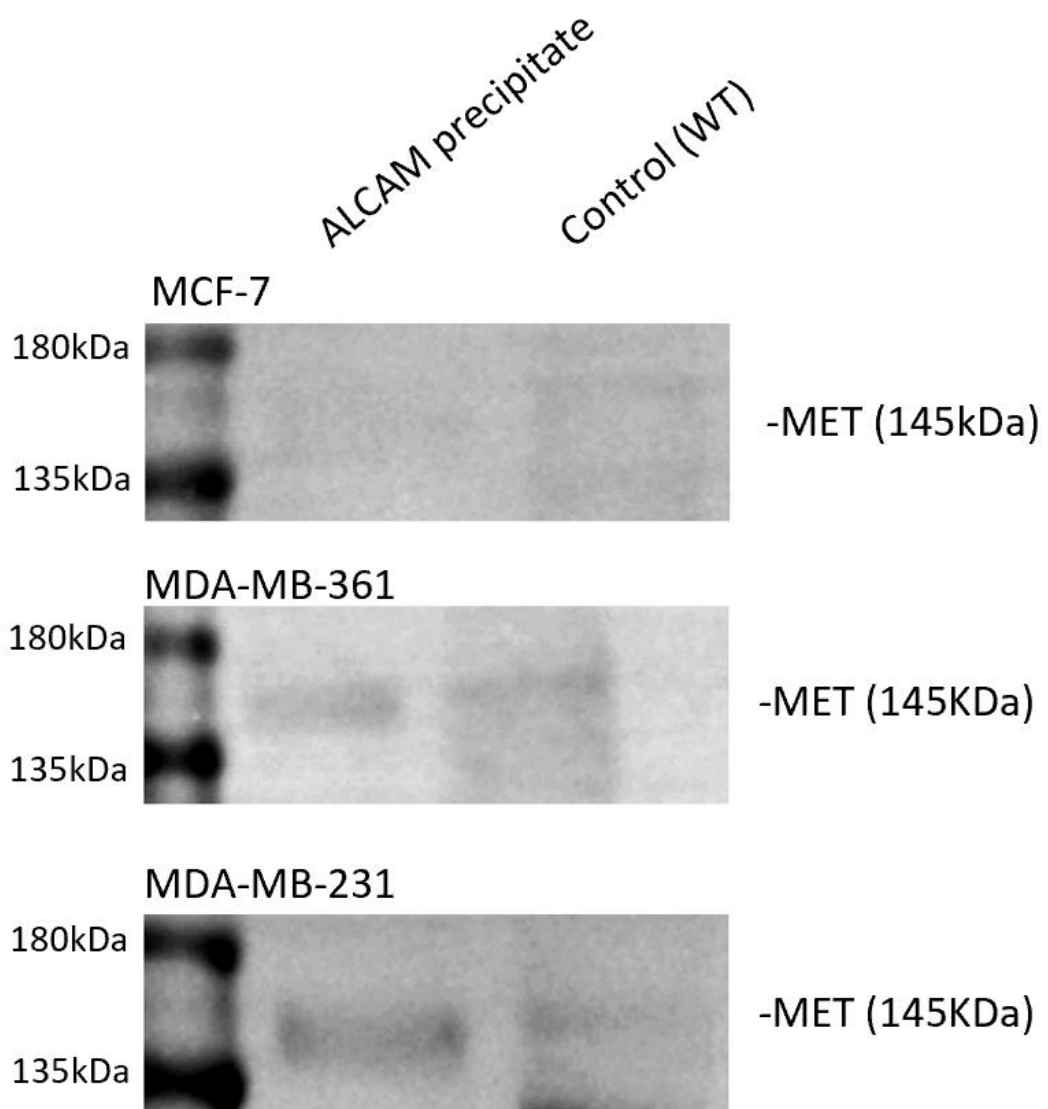


Figure 5.10 Western blotting results of ALCAM immunoprecipitation in MCF-7 (top), MDA-MB-361 (middle) and MDA-MB-231 (bottom) cell lines.

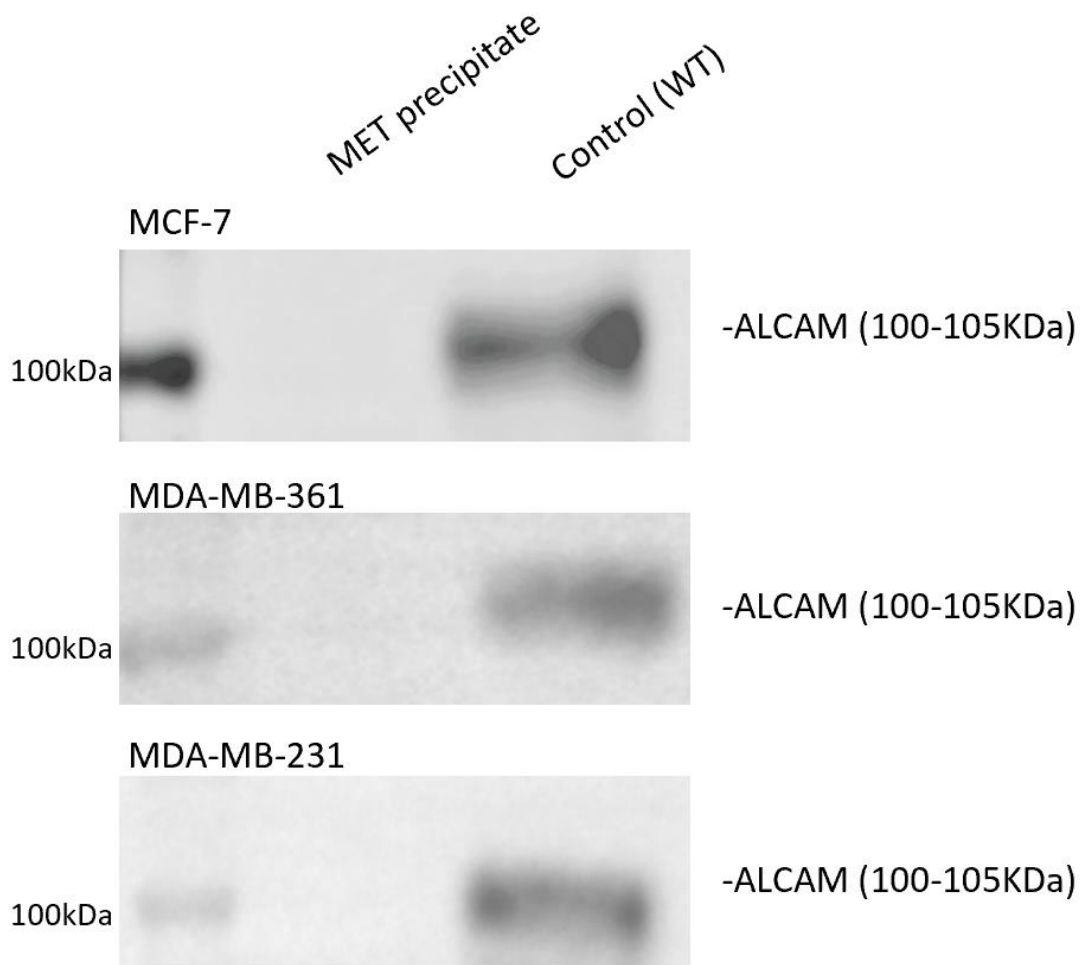


Figure 5.11 Western blotting results of MET immunoprecipitation in MCF-7 (top), MDA-MB-361 (middle) and MDA-MB-231 (bottom) cell lines.

5.3.3 The interaction of ALCAM and MET in different ER status and in bone microenvironment, an ECIS based analysis

To further explore the relationship between MET and ALCAM in ER positive and ER negative breast cancer cell lines, we conducted a series of ECIS assays by using the ALCAM knockdown models mentioned previously. HGF and MET inhibitor were used to either activate or inhibit MET in both control and ALCAM knockdown cells to observe the differences in cell adhesion among groups. BME (bone matrix extract) was introduced to the assays to stimulate tumour microenvironment of bone metastasis. We also made use of a HER2 targeted chemotherapy drug, Neratinib, to explore the change of cell adhesion in HER2 positive and negative cell lines following

ALCAM knockdown. In addition, ROCK1 (Rho-associated, coiled-coil-containing protein kinase 1) was another contrast-regulated kinase in ER positive and ER negative cells after knocking down ALCAM, similar to MET as mentioned in section 5.3.1. We utilized ROCK inhibitor to investigate its role in ALCAM signalling as a complement to the study. The concentrations of the reagents used in the ECIS assay were based on relevant literature and the previous studies in our laboratory (Table 5.5).

Table 5.5 Concentrations of the reagents used in ECIS.

	Concentration
BME	50µg/ml
MET inhibitor	200nM
HGF	50ng/ml
Neratinib	200nM
ROCK inhibitor	5µM

5.3.3.1 Alterations in cell adhesion ability following ALCAM knockdown in normal and bone microenvironment.

Figure 5.12 shows the 3D images of electrical impedance changes of the control and ALCAM knockdown groups under different frequencies. The electrical impedance for each group would be higher as the cell adhesion increased. To compare the differences between groups, we performed statistical analysis for the impedance of each group after the experiment began 3 hours (Table 5.6). In comparisons between groups, the alteration of impedance appeared under a particular frequency indicating the significant difference of cell adhesion ability under the respective condition.

In MCF-7 cells, no difference was seen between control and ALCAM knockdown groups in all frequencies ($p>0.05$). There was also no statistical difference ($p>0.05$) when BME was added into each group.

In MDA-MB-361 cells, the impedance of the control group without BME was higher compared to that with BME under 4000Hz ($p=0.022$) and 16000Hz ($p=0.036$). The rest of the differences between groups, however, did not reach statistical significance.

In MDA-MB-231 cells, the impedance of the control group was significantly higher than in the ALCAM knockdown group ($p=0.034$) at the 64000Hz condition. This difference could still be seen after BME was added ($p=0.016$) in the same conditions, which indicated that knocking down ALCAM resulted in the reduction of cell adhesion in both normal and bone microenvironment. The results also showed that the cell adhesion of the control group without BME was stronger than that with BME ($p=0.002$) under 4000Hz, 16000Hz and 64000Hz. The impedance of the ALCAM knockdown group without BME was also higher than the ALCAM knockdown group with BME under 64000Hz ($p=0.028$).

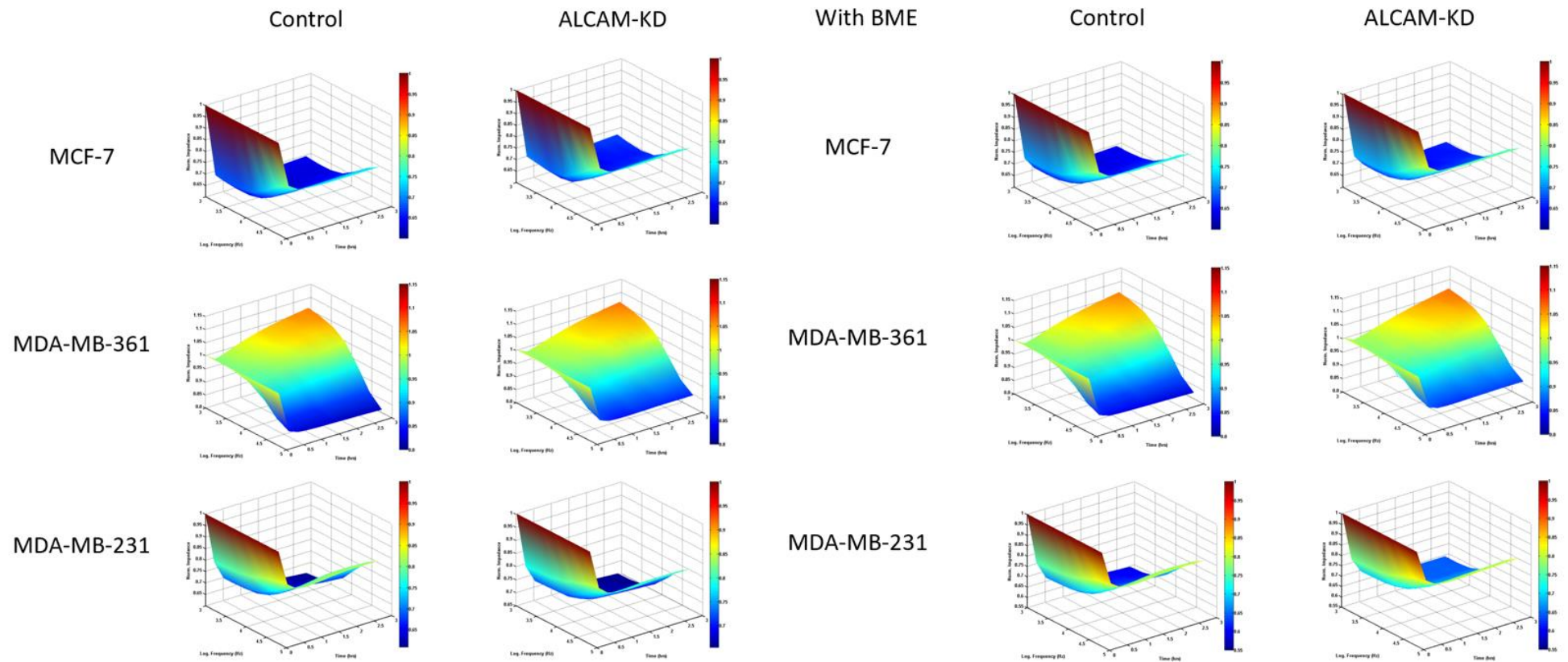


Figure 5.12 The cell adhesion of control and ALCAM-KD groups as detected by ECIS (Left: without BME; Right: with BME). Shown are cells responses (Z-axis, normalised impedance in ohms) in 3D model, over time (X-axis, in hours) and cross multiple frequencies (Y-axis, in Hz).

Table 5.6 Comparison of electrical impedance between Control and ALCAM-KD groups in ECIS assays (with and without BME).

		4000Hz			16000Hz			64000Hz		
		Mean	p* (Control/ALC AM-KD)	p# (With/without BME)	Mean	P* (Control/ALCA M-KD)	p# (With/without BME)	Mean	p* (Control/ALCA M-KD)	p# (With/withou t BME)
MCF-7	Control	5972.902± 95.086	0.209		2115±95.086	0.272		1399.088±1 0.405	0.930	
	ALCAM-KD	5883.761± 83.879			2096.959±83 .879			1399.638±6 .141		
	Control (with BME)	6546.506± 563.101	0.541	0.091	2235.949±12 6.831	0.684	0.110	1411.262±2 2.289	0.560	0.360
	ALCAM-KD (with BME)	6298.442± 518.724		0.166	2198.608±12 0.189		0.145	1421.373±2 3.982		0.560
MDA- MB- 361	Control	6668.437± 222.921	0.077		2259.54±37. 961	0.337		1431.108±6 .697	0.319	
	ALCAM-KD	6219.128± 288.794			2201.466±87 .138			1466.754±5 4.177		
	Control (with BME)	6255.863± 111.605	0.065	0.022	2187.132±30 .024	0.192	0.036	1432.638±1 9.117	0.997	0.902
	ALCAM-KD (with BME)	6110.635± 63.745		0.491	2161.24±18. 345		0.401	1432.683±1 5.132		0.271
MDA- MB- 231	Control	767.977±1 6.775	0.922		884.579±11. 164	0.617		2078.847±2 3.426	0.034	
	ALCAM-KD	770.055±3 0.287			875.556±26. 613			2020.941±2 1.548		
	Control (with BME)	727.806±1 1.489	0.992	0.013	847.711±10. 358	0.479	0.006	2006.069±5 .794	0.016	0.002
	ALCAM-KD (with BME)	727.935±2 1.821		0.083	839.692±18. 542		0.087	1977.03±16 .573		0.028

Note: * Comparasion between control and ALCAM-KD groups; # Comparasion between groups with and without BME.

5.3.3.2 The effect of HGF and MET inhibitor on cell adhesion following ALCAM knockdown

Figure 5.13 shows the 3D images of electrical impedance changes of the control and ALCAM knockdown groups treated with HGF, under different frequencies. The statistical comparison between control/ALCAM knockdown and with/without BME is shown in Table 5.7. In MCF-7 cells, the impedance was higher in the ALCAM knockdown group without BME compared with the control group when treated with HGF ($p=0.003$) under 64000Hz. The impedance of the control group without BME was lower compared to that with BME under 64000Hz ($p=0.006$). In MDA-MB-361 cells, the impedance was higher in the ALCAM knockdown group with BME compared with the control group with BME, when treated with HGF under 4000Hz ($p=0.011$) and 16000Hz ($p=0.001$). The impedance was higher in the control group without BME compared with the control group with BME, when treated with HGF under 16000Hz ($p=0.046$). In MDA-MB-231 cells, no changes could be seen among each group.

The 3D images of electrical impedance changes of control and ALCAM knockdown group when treated with MET inhibitor under different frequencies are shown in Figure 5.14 and the statistical comparison is shown in Table 5.8. In MCF-7 cells, no change was seen between groups after treatment with MET. In MDA-MB-361 cells, the impedance was higher in the control group without BME compared to that with BME under 16000Hz ($p=0.016$). In MDA-MB-231 cells, the impedance was lower in the control group with BME compared with the ALCAM knockdown group with BME under 4000Hz ($p=0.014$), and the same result could be found between control/ALCAM knockdown groups without BME under 64000Hz ($p=0.045$)

Figure 5.15 shows the 3D images of electrical impedance changes of control and ALCAM knockdown groups treated with both HGF and MET under different frequencies. The statistical comparison between control/ALCAM knock-down and with/without BME groups is shown in Table 5.9. In MCF-7 cells, the impedance of control cells without BME was lower compared to control cells with BME under 64000Hz ($p=0.029$). The significant difference was also found in control and ALCAM knockdown cells without BME under 4000Hz ($p=0.006$) and 16000Hz ($p=0.048$).

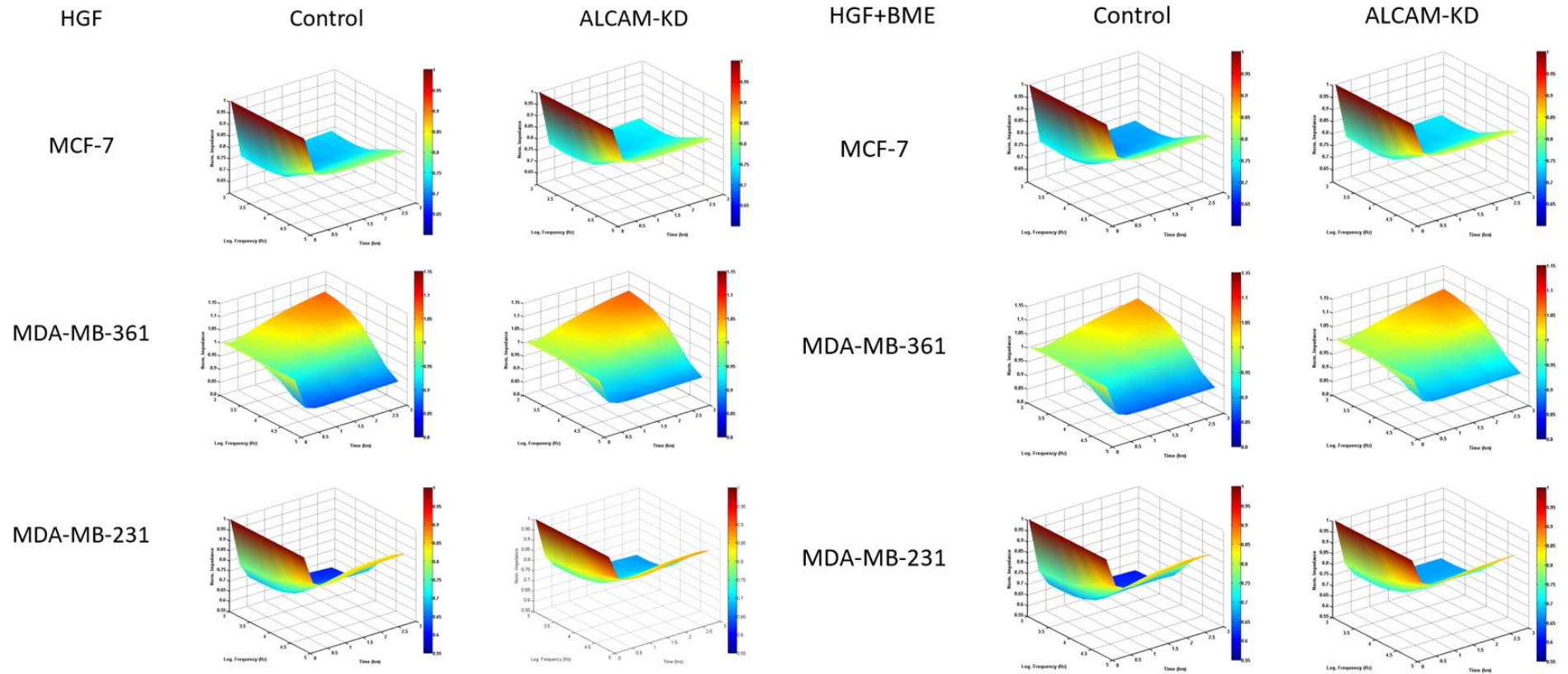


Figure 5.13 The cell adhesion of control and ALCAM-KD group with HGF as detected by ECIS (Left: without BME; Right: with BME). Shown are cells responses (Z-axis, normalised impedance in ohms) in 3D model, over time (X-axis, in hours) and cross multiple frequencies (Y-axis, in Hz).

Table 5.7 Comparison of electrical impedance between Control and ALCAM-KD groups with HGF in ECIS assays (with and without BME)

		4000Hz			16000Hz			64000Hz		
		Mean	p* (Control/ALCAM-KD)	p# (With/without BME)	Mean	p* (Control/ALCAM-KD)	p# (With/without BME)	Mean	p* (Control/ALCAM-KD)	p# (With/without BME)
MCF-7	Control	5745.799±109.955	0.400		2076.659±109.955	0.074		1408.567±3.77	0.003	
	ALCAM-KD	5805.205±71.565			2101.165±71.565			1426.121±6.449		
	Control (with BME)	6121.108±349.186	0.974	0.086	2176.566±81.589	0.819	0.055	1442.104±15.639	0.222	0.006
	ALCAM-KD (with BME)	6113.461±293.519		0.087	2163.1±78.074		0.167	1425.166±19.322		0.928
MDA-MB-361	Control	6127.517±146.741	0.163		2176.025±22.167	0.100		1449.51±20.938	0.880	
	ALCAM-KD	6369.418±266.379			2220.971±40.602			1447.655±10.674		
	Control (with BME)	6020.141±86.124	0.011	0.254	2143.715±13.119	0.001	0.046	1429.871±12.221	0.118	0.156
	ALCAM-KD (with BME)	6268.827±106.165		0.509	2198.989±15.081		0.349	1444.723±10.766		0.712
MDA-MB-231	Control	716.059±34.314	0.126		849.834±29.695	0.232		2058.328±99.651	0.420	
	ALCAM-KD	803.058±91.889			929.531±116.162			2183.68±271.814		
	Control (with BME)	699.455±36.627	0.570	0.533	844.492±68.502	0.743	0.891	2068.232±195.228	0.572	0.931
	ALCAM-KD (with BME)	712.247±21.702		0.103	831.949±25.254		0.152	2006.792±64.182		0.252

Note: * Comparasion between control and ALCAM-KD groups; # Comparasion between groups with and without BME.

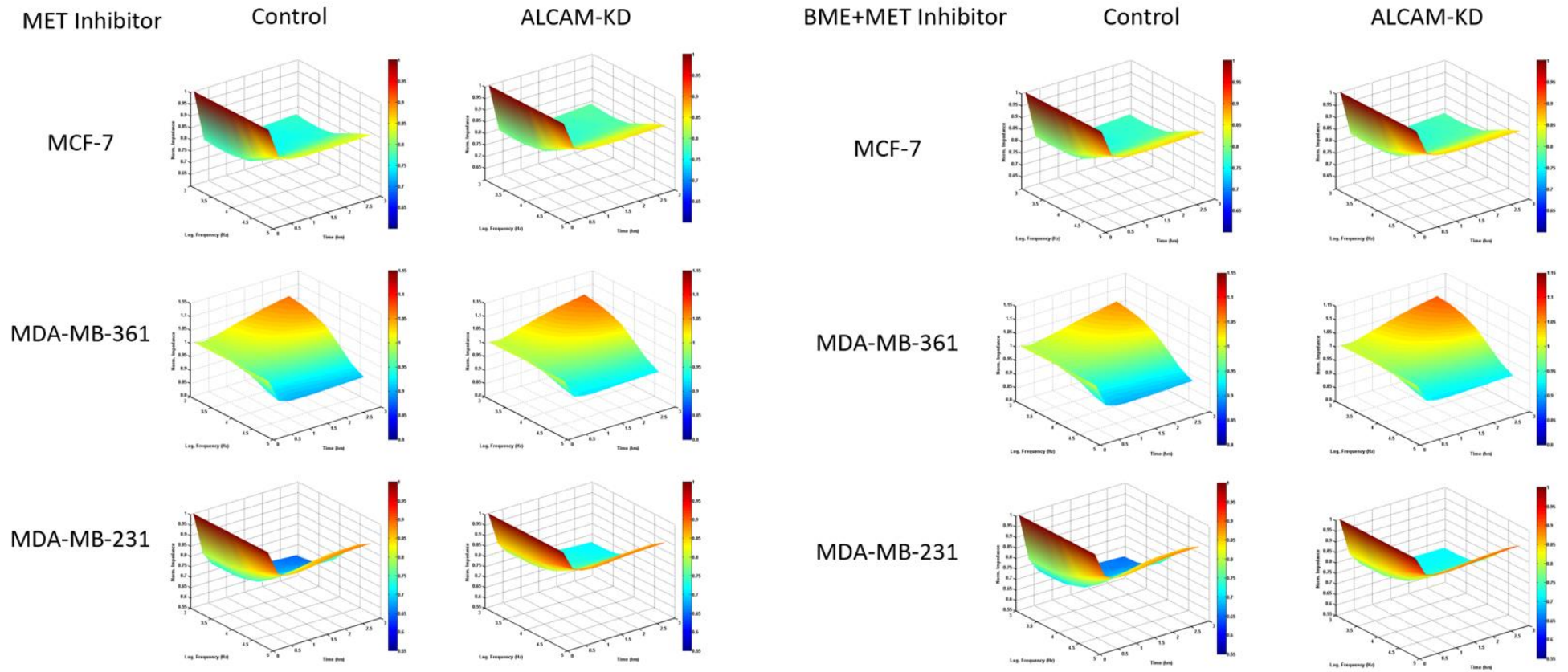


Figure 5.14 The cell adhesion of control and ALCAM-KD group with MET inhibitor as detected by ECIS (Left: without BME; Right: with BME). Shown are cells responses (Z-axis, normalised impedance in ohms) in 3D model, over time (X-axis, in hours) and cross multiple frequencies (Y-axis, in Hz).

Table 5.8 Comparison of electrical impedance between Control and ALCAM-KD groups with MET inhibitor in ECIS assays (with and without BME)

		4000Hz			16000Hz			64000Hz		
		Mean	p* (Control/ALC AM-KD)	p# (With/with out BME)	Mean	p* (Control/ALC AM-KD)	p# (With/with out BME)	Mean	p* (Control/ALC AM-KD)	p# (With/with out BME)
MCF-7	Control	5901.291±111.322	0.839		2118.497±111.322	0.887		1428.572±6.22	0.907	
	ALCAM-KD	5914.899±63.861			2120.572±63.861			1428.979±2.449		
	Control (with BME)	6147.212±343.991	0.646	0.223	2179.355±85.102	0.747	0.220	1440.02±25.045	0.576	0.409
	ALCAM-KD (with BME)	6287.349±466.062		0.164	2203.33±113.26		0.196	1430.281±21.36		0.908
MDA-MB-361	Control	6188.963±126.826	0.931		2180.612±14.163	0.499		1442.464±15.243	0.420	
	ALCAM-KD	6197.736±145.787			2188.453±16.565			1452.178±16.497		
	Control (with BME)	6011.284±29.725	0.886	0.068	2149.523±4.471	0.855	0.016	1439.667±13.009	0.854	0.809
	ALCAM-KD (with BME)	6021.095±107.616		0.099	2153.163±31.843		0.097	1442.204±19.384		0.463
MDA-MB-231	Control	714.902±52.414	0.208		833.865±44.145	0.234		1992.268±27.043	0.045	
	ALCAM-KD	770.193±58.32			875.624±45.07			2040.052±26.334		
	Control (with BME)	673.482±17.244	0.014	0.184	800.45±16.097	0.060	0.205	1961.27±12.262	0.156	0.082
	ALCAM-KD (with BME)	720.59±21.267		0.161	842.798±32.91		0.284	2031.971±86.266		0.864

Note: * Comparasion between control and ALCAM-KD groups; # Comparasion between groups with and without BME.

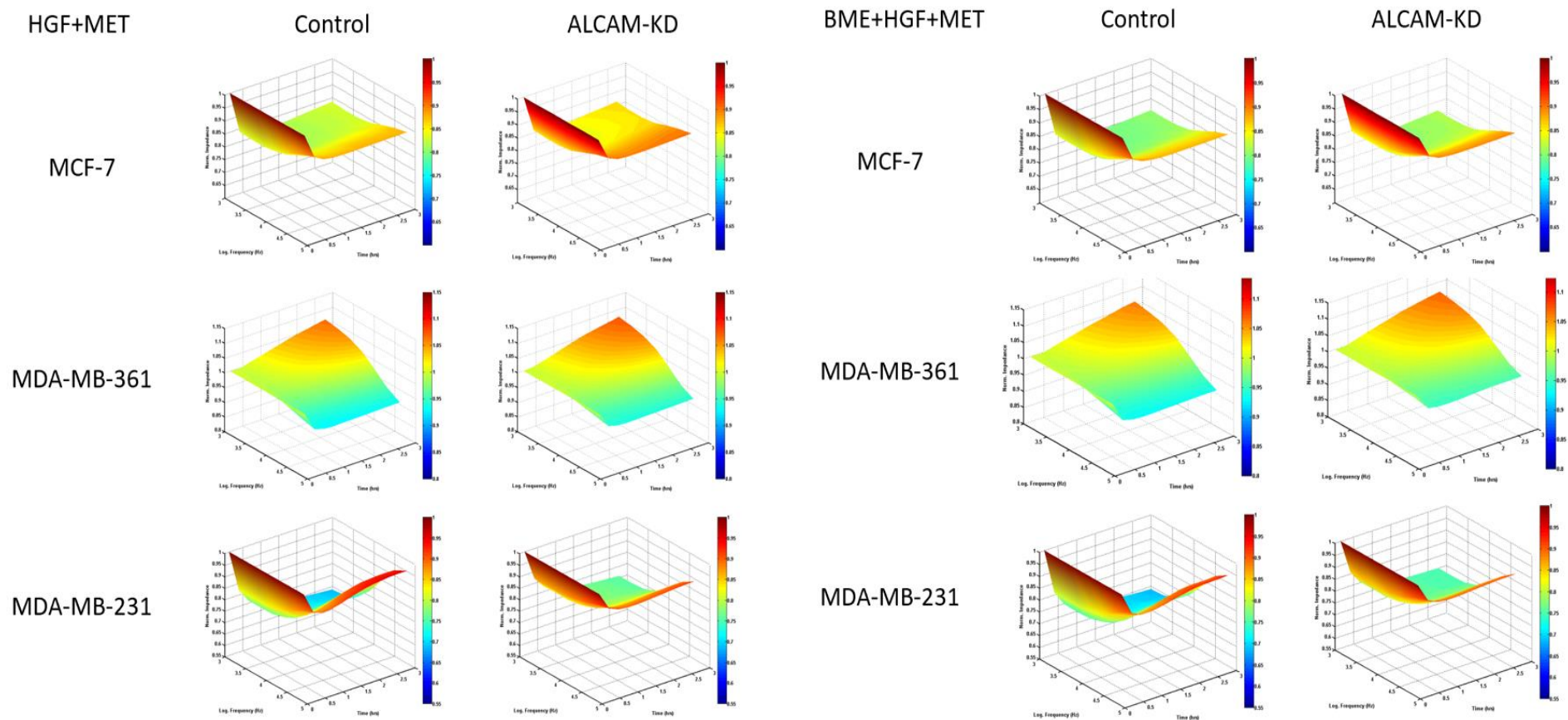


Figure 5.15 The cell adhesion of control and ALCAM-KD group with HGF and MET inhibitor as detected by ECIS (Left: without BME; Right: with BME). Shown are cells responses (Z-axis, normalised impedance in ohms) in 3D model, over time (X-axis, in hours) and cross multiple frequencies (Y-axis, in Hz).

Table 5.9 Comparison of electrical impedance between Control and ALCAM-KD groups with HGF and MET inhibitor in ECIS assays (with and without BME)

		4000Hz			16000Hz			64000Hz		
		Mean	p* (Control/ALC AM-KD)	p# (With/with out BME)	Mean	p* (Control/ALC AM-KD)	p# (With/with out BME)	Mean	p* (Control/ALC AM-KD)	p# (With/with out BME)
MCF-7	Control	5905.663±45.2 72	0.917		2100.125±45.2 72	0.166		1399.567±5.3 53	0.038	
	ALCAM-KD	5909.373±50.6 54			2114.997±50.6 54			1421.945±15. 998		
	Control (with BME)	6257.018±428. 003	0.941	0.154	2193.776±103. 794	0.907	0.124	1429.585±20. 366	0.738	0.029
	ALCAM-KD (with BME)	6281.436±462. 644		0.161	2203.139±112. 519		0.170	1435.064±23. 773		0.395
MDA- MB- 361	Control	6229.482±202. 747	0.965		2191.105±37.7 19	0.990		1444.746±10. 588	0.931	
	ALCAM-KD	6224.03±128.7 58			2191.383±15.7 21			1445.421±10. 578		
	Control (with BME)	6197.458±173. 142	0.130	0.818	2187.794±32.9 61	0.145	0.899	1444.985±8.0 58	0.333	0.973
	ALCAM-KD (with BME)	6372.996±99.9 91		0.117	2238.32±50.46 9		0.126	1475.248±56. 918		0.343
MDA- MB- 231	Control	690.58±26.33	0.006		820.786±24.35 5	0.048		2006.079±47. 88	0.864	
	ALCAM-KD	750.836±12.91 7			855.828±14.55 1			2000.747±35. 775		
	Control (with BME)	764.833±103.1 09	0.802	0.212	874.018±79.08 2	0.778	0.246	2023.428±46. 237	0.940	0.621
	ALCAM-KD (with BME)	779.946±51.81 3		0.317	887.95±51.732		0.277	2020.793±48. 346		0.530

Note: * Comparasion between control and ALCAM-KD groups; # Comparasion between groups with and without BME.

5.3.3.3 The effect of Neratinib on cell adhesion following ALCAM knockdown

Figure 5.16 shows the 3D images of electrical impedance changes of control and ALCAM knockdown groups treated with Neratinib, under different frequencies. The statistical comparison between the control/ALCAM knockdown and with/without BME groups is shown in Table 5.10. In MCF-7 cells, no significant change could be seen between control/ALCAM knockdown and with/without BME groups after treatment with Neratinib. In MDA-MB-361 cells, the impedance of control cells without BME was lower compared with control groups with BME under 4000Hz ($p < 0.001$) and 16000Hz ($p < 0.001$) conditions. The impedance of ALCAM knockdown cells without BME was also lower than that with BME in 4000Hz ($p = 0.001$) and 16000Hz ($p < 0.001$). In MDA-MB-231 cells, the impedance of control cells with BME was significantly lower than in the ALCAM knockdown group with BME under 4000Hz ($p < 0.001$), 16000Hz ($p < 0.001$) and 64000Hz ($p = 0.032$). In the comparison between ALCAM knockdown cells, the cells without BME had significantly higher impedance compared with those with BME under 64000Hz ($p = 0.023$).

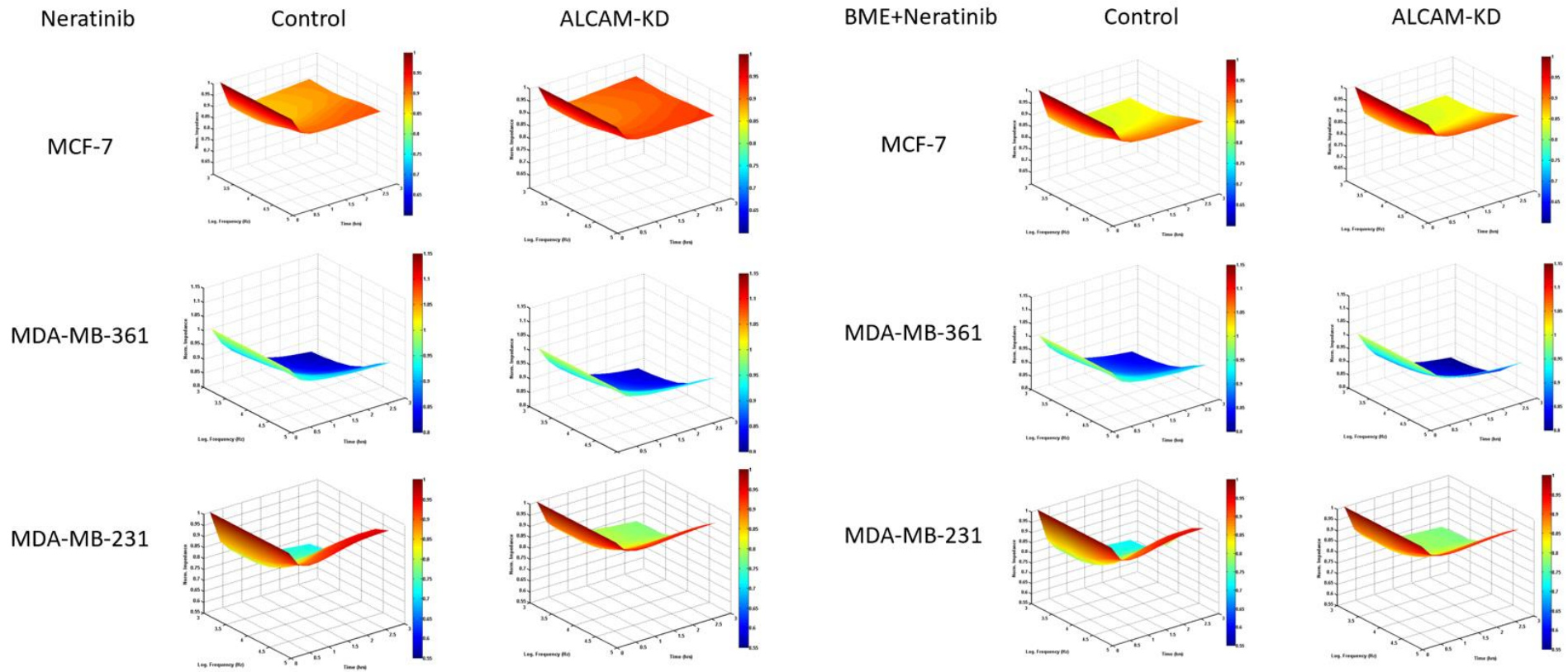


Figure 5.16 The cell adhesion of control and ALCAM-KD group with Neratinib as detected by ECIS (Left: without BME; Right: with BME). Shown are cells responses (Z-axis, normalised impedance in ohms) in 3D model, over time (X-axis, in hours) and cross multiple frequencies (Y-axis, in Hz).

Table 5.10 Comparison of electrical impedance between Control and ALCAM-KD group with Neratinib in ECIS assays (with and without BME)

		4000Hz			16000Hz			64000Hz		
		Mean	p* (Control/ALC AM-KD)	p# (With/with out BME)	Mean	p* (Control/ALC AM-KD)	p# (With/with out BME)	Mean	p* (Control/ALC AM-KD)	p# (With/with out BME)
MCF-7	Control	5960.04±72.74 2	0.312		2142.205±72.7 42	0.225		1447.575±34. 775	0.220	
	ALCAM-KD	5919.182±13.5 39			2117.549±13.5 39			1422.902±9.3 24		
	Control (with BME)	6339.12±502.8 97	0.941	0.186	2207.963±119. 714	0.880	0.333	1426.538±22. 402	0.509	0.348
	ALCAM-KD (with BME)	6365.682±463. 026		0.102	2221.05±115.5 06		0.124	1438.817±26. 818		0.305
MDA- MB- 361	Control	10549.217±49. 378	1.000		3161.777±13.9 29	0.840		1600.018±21. 626	0.540	
	ALCAM-KD	10549.21±279. 747			3167.252±49.9 03			1610.459±23. 806		
	Control (with BME)	11343.161±118 .822	0.107	0.000	3349.554±31.9 17	0.053	0.000	1620.75±9.66 5	0.321	0.131
	ALCAM-KD (with BME)	11468.741±58. 562		0.001	3399.098±25.9 35		0.000	1647.785±49. 095		0.220
MDA- MB- 231	Control	758.209±70.52 4	0.125		876.081±62.72 5	0.180		2029.719±40. 107	0.083	
	ALCAM-KD	843.882±65.54 1			938.079±52.37 6			2081.539±29. 704		
	Control (with BME)	708.87±12.704	0.000	0.218	831.614±13.90 8	0.000	0.216	1989.525±21. 263	0.032	0.127
	ALCAM-KD (with BME)	796.436±10.81 9		0.203	893.952±7.435		0.146	2028.709±18. 427		0.023

Note: * Comparasion between control and ALCAM-KD groups; # Comparasion between groups with and without BME.

5.3.3.4 The effect of ROCK inhibitor on cell adhesion following ALCAM knockdown

Figure 5.17 shows the 3D images of electrical impedance changes of control and ALCAM knockdown groups treated with ROCK inhibitor, under different frequencies. The statistical comparison between control/ALCAM knockdown and with/without BME groups is shown in Table 5.11. In MCF-7 cells, no significant change could be seen between control/ALCAM knockdown groups as well as with/without BME groups after treatment with ROCK inhibitor. In MDA-MB-361 cells, the impedance of control cells without BME were significantly lower than those with BME under 4000Hz ($p=0.002$) and 16000Hz ($p=0.029$). Similarly, the impedance of ALCAM knockdown cells without BME were significantly lower than those with BME under 4000Hz ($p=0.002$), 16000Hz ($p=0.002$) and 64000Hz ($p=0.030$). In MDA-MB-231 cells, the impedance of the control group with BME was lower than the ALCAM knockdown group with BME in 4000Hz ($p=0.002$) and 16000Hz ($p=0.003$). In the comparison between ALCAM knockdown cells, the cells without BME had significantly higher impedance compared with those with BME under 4000Hz ($p=0.028$) and 16000Hz ($p=0.038$).

ROCK Inhibitor

Control

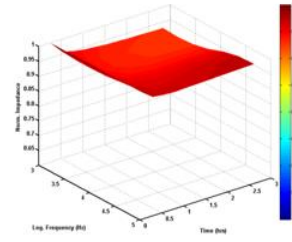
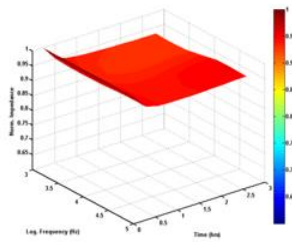
ALCAM-KD

BME+ROCK Inhibitor

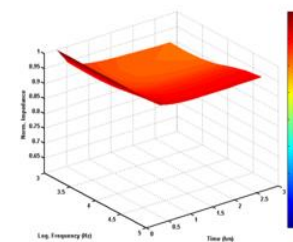
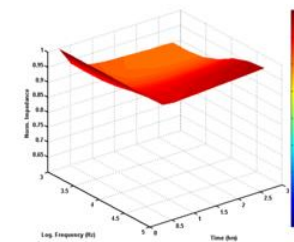
Control

ALCAM-KD

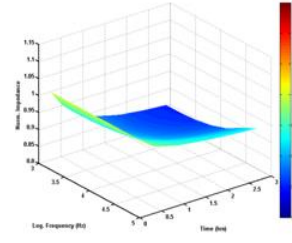
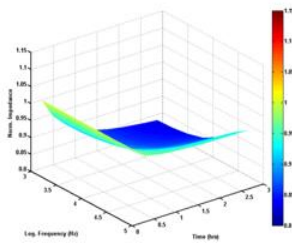
MCF-7



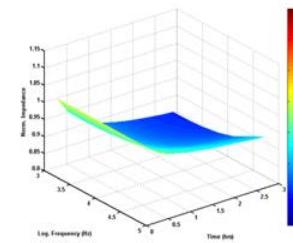
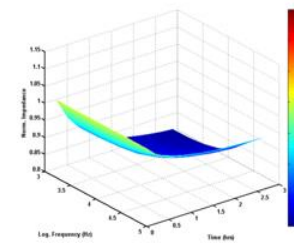
MCF-7



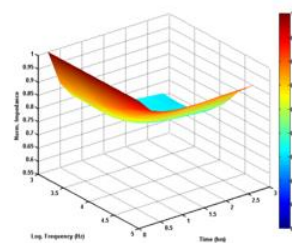
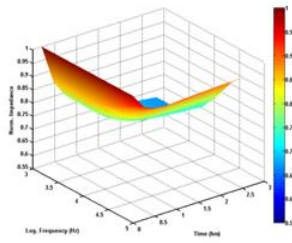
MDA-MB-361



MDA-MB-361



MDA-MB-231



MDA-MB-231

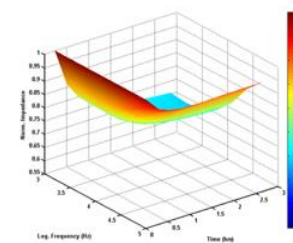
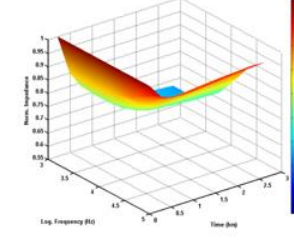


Figure 5.17 The cell adhesion of control and ALCAM-KD group with ROCK inhibitor as detected by ECIS (Left: without BME; Right: with BME). Shown are cells responses (Z-axis, normalised impedance in ohms) in 3D model, over time (X-axis, in hours) and cross multiple frequencies (Y-axis, in Hz).

Table 5.11 Comparison of electrical impedance between Control and ALCAM-KD group with ROCK inhibitor in ECIS assays (with and without BME)

		4000Hz			16000Hz			64000Hz		
		Mean	p* (Control/ALC AM-KD)	p# (With/with out BME)	Mean	p* (Control/ALC AM-KD)	p# (With/with out BME)	Mean	p* (Control/ALC AM-KD)	p# (With/with out BME)
MCF-7	Control	5697.43±11.818	0.889		2084.547±11.818	0.396		1419.050±31.588	0.268	
	ALCAM-KD	5701.717±57.879			2061.558±57.879			1383.217±49.428		
	Control (with BME)	5755.225±119.864	0.898	0.374	2117.529±94.931	0.204	0.530	1412.195±77.562	0.145	0.875
	ALCAM-KD (with BME)	5744.468±106.421		0.507	2047.818±24.093		0.589	1347.069±4.332		0.195
MDA-MB-361	Control	10118.168±266.86	0.770		3095.75±111.853	0.441		1597.113±94.534	0.239	
	ALCAM-KD	10068.695±182.903			3047.034±38.199			1535.350±3.490		
	Control (with BME)	10859.586±42.848	0.691	0.002	3256.563±13.589	0.948	0.029	1576.198±18.987	0.435	0.680
	ALCAM-KD (with BME)	10912.867±251.889		0.002	3254.19±68.642		0.002	1564.549±20.375		0.030
MDA-MB-231	Control	712.514±50.541	0.153		799.286±14.169	0.140		1930.393±8.939	0.080	
	ALCAM-KD	764.623±38.768			842.49±14.678			1966.056±40.460		
	Control (with BME)	655.035±17.812	0.002	0.076	843.204±64.618	0.003	0.097	1959.132±17.872	0.342	0.387
	ALCAM-KD (with BME)	707.321±8.321		0.028	825.344±1.087		0.038	1946.409±12.036		0.828

Note: * Comparasion between control and ALCAM-KD groups; # Comparasion between groups with and without BME.

5.4 Discussion

In the previous Chapters we found out that the effect of ALCAM on the survival of breast cancer patients was roughly opposite in ER positive and negative breast cancer. The clinical results also showed that ALCAM expression levels in breast cancer patients with bone metastasis were significantly lower than those without bone metastasis. To explain the contrasting effect of ALCAM on different hormonal receptor status of breast cancer patients, and to explain the effect of ALCAM on bone metastasis, we created both ER positive and negative ALCAM knockdown cell models and performed protein/kinase microarray analysis.

The protein kinase platform returned some very interesting patterns of changes in protein kinases, in that a significant number of kinases were found to be upregulated in both ER positive and ER negative breast cancers, whereas the other large group of kinases were seen to be down regulated in both cells. These protein kinases are involved in a large number of signalling pathways which have diverse roles in cancer and cells. This information forms an important and interesting theme to pursue in future understanding of the overall role of ALCAM in breast cancer.

However, and of particular interest to the current study, a group of protein kinases were identified that were regulated in contrasting directions in ER positive and ER negative breast cancers. First, PRKCH, PRKCB1, TrkB and VEGFR3 were upregulated in ER positive cells but down regulated in ER negative cells.

There is little information on the role of PRKCH, TrkB and VEGFR3 in breast cancer, in particular in connection to ER and hormone status. PRKCH has been shown to be a responsive gene in ER positive cells to certain stimuli including progesterone related stimuli (McFall et al. 2015). It has been reported that TrkB is a responsive gene to oestradiol in triple negative breast cancer cells (Contreras-Zarate et al. 2019). Yehia *et al.* (Yehia et al. 2015) has reported that in triple negative breast cancer, VEGFR3 is seen to rise in connection with HIF1A (Hypoxia-inducible factor 1-alpha).

Among the proteins/kinases altered following ALCAM knockdown, we chose MET as a typical kinase to explore its relationship with ALCAM signalling pathway in ER positive/negative cells, as well as in normal/bone microenvironment.

MET and its ligand HGF are known to participate in the progression of varying cancer types, especially breast cancer (Moosavi et al. 2019). A meta-analysis (Zhao et al. 2017) which consisted of 32 studies with 8281 breast cancer patients showed that the overexpression of MET was associated with shorter overall survival and relapse-free survival, as well as high histological grade, large tumour size and the occurrence of metastasis. Work by Knudsen *et al.*, (Knudsen et al. 2002) showed that the bone metastatic lesions of prostate cancer had significantly higher levels of MET expression. In a phase II trial, patients with metastatic hormone receptor-positive breast cancer responded with 38% improvement on bone scans after a minimum duration of 12 weeks on Cabozantinib, a tyrosine kinase inhibitor targeting MET (Xu et al. 2020).

The observed results in this Chapter, including the Kinexus antibody microarray analysis, immunoprecipitation and ECIS indicated that MET has direct or indirect cellular interaction with ALCAM and this interaction could affect the cell adhesion of breast cancer. However, different cell lines react differently towards ALCAM knockdown and HGF/MET inhibitor treatment. In the immunoprecipitation assay, no ALCAM-MET precipitate could be detected by Western blotting in MCF-7 (ER+/HER2-) cells, while positive results were shown in MDA-MB-361 (ER+/HER2+) and MDA-MB-231 (ER-/HER2-) cells. We believe a possible reason for this is that the MET expression in MCF-7 cell line was too low to be detected by Western blotting, since the wildtype MCF-7 cells also showed no band when probed with MET antibody. Another possibility is that the interaction between ALCAM and MET is different in the ER+/HER2- subgroup compared with other subgroups of breast cancer.

The ECIS assay in this Chapter did not show a consistent result with obvious regularity as we expected. It seems that MDA-MB-231 cells (ER-/HER2-) were the most sensitive to ALCAM knockdown. The MDA-MB-231 cell model showed a reduced cell adhesion following knocking down ALCAM, while MCF-7 and MDA-MB-361 (ER+/HER2+) cells showed no

changes of cell adhesion as detected by ECIS. This finding may prove that breast cancer cells react differently, in terms of cell adhesion, towards ALCAM knockdown based on their ER status. When the cells were treated with HGF and MET inhibitor, clear changes of cell adhesion appeared in all three cell lines. It is interesting to mention that when MET was activated or inhibited, the cell adhesion ability of ALCAM knockdown cells usually turned out to be higher than control cells, which is in contrast with the results in the groups without any treatment.

We also explored the effect of HER-2 inhibitor (Neratinib) and ROCK inhibitor on cell adhesion following ALCAM knock-down. The results were similar to HGF and MET inhibitor, namely the cell adhesion ability of ALCAM knockdown cells become higher than control cells after respective treatment. In the groups with BME, although some difference between groups did reach statistical significance, we were unable to come to a conclusion with sufficient consistency. However, it is clear that the effect of ALCAM on cell adhesion was affected by the presence of bone microenvironment.

In conclusion, MET is found to be a vital kinase in ALCAM signalling pathway, and the effect of ALCAM and MET on cell adhesion is affected by hormonal receptors of breast cancer cells and the presence of bone microenvironment.

Chapter-6

ALCAM and drug response to chemotherapies

6.1 Introduction

ALCAM, as a vital member of cell adhesion molecules, is involved in cancer progression and metastasis in various cancer types, especially breast cancer. As outlined in previous Chapters, the effect of ALCAM levels on survival of breast cancer patients is associated with ER and HER2 status, and the alteration of ALCAM signalling pathways was observed in breast cancer cell lines with varying receptor status *in vitro*. Critically to breast cancer, there has been gentle indication that the expression of ALCAM in breast cancer cells may be an indicator to cell and indeed patients' response to therapeutic drug and chemotherapies. Wang *et al.*, (Wang et al. 2011) and Chen *et al.*, (Chen *et al.* 2017) have shown that levels of ALCAM in breast cancer cells are connected to cell's response to endocrine therapy including Tamoxifen. These early studies have tentatively suggested a possible link between the resistance and hormone receptor status, including ER status of the cells. Similar observations on ALCAM and drug resistance were made with a small number of other cancer types including pancreatic cancer (Hong et al. 2010), Colorectal cancer (El Khoury et al. 2016), bladder cancer (Amantini et al. 2016), and lung cancer (Su et al. 2016).

To explore if expression of ALCAM in breast cancer with differing hormone receptors has an impact on cells response to drugs, I performed drug toxicity assays using ALCAM knockdown cell models generated from breast cancer cells with different hormone receptor status. In addition, I have also interrogated clinical profiles of ALCAM and drug response in patients within a public database (www.rocplot.org) in order to establish the link between the *in vitro* findings and clinical observations, again emphasizing the link with the hormone receptor status and the molecular subtypes of breast tumours.

6.2 Methods

6.2.1 Genetic preparation of breast cancer cells

The transcription level of ALCAM in different breast cancer cell lines was tested by PCR as mentioned previously in Chapter 3. Among them, three cell lines MCF-7 (ER+/HER2-), MDA-MB-361(ER+/HER2+), and MDA-MB-231 (ER-/HER2-) were selected to create ALCAM knockdown models. Plasmids which contained both scramble control and shRNA targeting ALCAM were used in gene transfection. The transfection was performed using Fugene HD (Promega, Southampton, UK) transfection reagent in accordance with manufacturer's instructions.

6.2.2 Cell cytotoxicity assay

The cell cytotoxicity assay was performed by a highly effective and well-established method, crystal violet colourimetric assay, which was able to detect viable cell numbers of adherent cancer cells in drug sensitivity tests. To be more specific, the control and transfected cell lines were seeded into 96-well plates and treated with serial-diluted chemotherapy drugs, then incubated in suitable conditions. The concentration of the chemotherapy drug was respectively chosen based on their IC50 and previous research. After 72 hours, the cells were fixed with 4% formalin, stained with 0.5% crystal violet and extracted with 10% acetic acid after washing. The absorbance was measured at 595 nm using a spectrophotometer to detect their respective cell density. The percentage toxicity was calculated as follows:

Percentage drug toxicity = (Absorbance in untreated well - Absorbance in drug treated well) / Absorbance in untreated well.

The scatter plots of percentage toxicity and drug concentration were plotted, and fitting curves were used to calculate IC50 value. Each group of the experiment was repeated three to five times.

6.2.3 Online datasets analysis

To explore the potential clinical implications, I have explored online datasets through ROC plotter (www.rocplot.org) in this study. The dataset included patients' data from 36 publicly available datasets, and Relapse-free survival (RFS) status at 5 years was used to determine the response to certain therapy. The breast cancer cohort being used contained 2108 cases of chemotherapy, 971 cases of endocrine therapy and 267 cases of anti-HER2 therapy (Fekete and Gyorffy 2019). The ROC model was used to determine the significance of ALCAM in distinguishing the drug resistance and drug sensitive patients and Mann-Whitney U test was used to compare the levels of ALCAM in the respective drug response group.

6.2.4 Statistical methods

Two sample T-Test, ROC analysis and Mann-Whitney U test were used in the Chapter. All the analyses were carried out using SPSS version 26. The statistical significance was defined as $p < 0.05$.

6.3 Results

6.3.1 The effect of knocking down ALCAM in breast cancer cell lines on chemotherapy drug sensitivity

We used four representative chemotherapy drugs, namely Paclitaxel, Docetaxel, Cisplatin and Gemcitabine to test the drug toxicity with ALCAM knockdown breast cancer cells. As shown in Figure 6.1 and Table 6.1, the respective mean IC50 of the

four drugs showed no difference ($p>0.05$) between control and ALCAM knockdown groups in MCF-7 cells. There was also no statistical significance between the IC₅₀ of control and ALCAM knockdown groups ($p>0.05$) when BME (50 μ g/ml) was added (Figure 6.2 and Table 6.2)

Similar results were also observed in MDA-MB-361 cells. The IC₅₀ of Paclitaxel, Docetaxel, Cisplatin and Gemcitabine showed no statistical difference between control and ALCAM knockdown groups (Figure 6.3 and Table 6.1), as well as when treated with BME (Figure 6.4 and Table 6.2).

In MDA-MB-231 cells, the IC₅₀ of Docetaxel was higher in the control group compared with the ALCAM knockdown group (0.017 ± 0.003 versus 0.011 ± 0.001 , $p=0.031$). The difference could also be observed when the cells were treated with BME (0.017 ± 0.002 versus 0.010 ± 0.002 , $p= 0.002$). The rest of the chemotherapy drugs showed no statistical difference between groups (Figure 6.5, Figure 6.6, Table 6.1 and Table 6.2).

Table 6.1 IC50 of chemotherapy drugs in control and ALCAM knockdown groups of different breast cancer cell lines, without BME.

		Mean \pm SD (μ M)		p
		Control	ALCAM-KD	
MCF-7	Paclitaxel	0.024 \pm 0.007	0.02 \pm 0.001	0.407
	Docetaxel	0.057 \pm 0.003	0.063 \pm 0.007	0.233
	Cisplatin	0.24 \pm 0.14	0.162 \pm 0.012	0.388
	Gemcitabine	6.033 \pm 0.931	6.333 \pm 0.775	0.691
MDA-MB-361	Paclitaxel	0.027 \pm 0.005	0.031 \pm 0.006	0.451
	Docetaxel	0.034 \pm 0.003	0.027 \pm 0.003	0.087
	Cisplatin	4.708 \pm 0.245	4.669 \pm 0.108	0.818
	Gemcitabine	5.827 \pm 0.1	5.962 \pm 0.968	0.822
MDA-MB-231	Paclitaxel	0.015 \pm 0.002	0.016 \pm 0.001	0.338
	Docetaxel	0.017 \pm 0.003	0.011 \pm 0.001	0.031
	Cisplatin	6.935 \pm 0.043	6.663 \pm 0.225	0.110
	Gemcitabine	3.839 \pm 0.894	4.69 \pm 0.445	0.214

Table 6.2 IC50 of chemotherapy drugs in control and ALCAM knockdown group of different breast cancer cell lines, with 50 μ g/ml BME

		Mean \pm SD (μ M)		p
		Control	ALCAM KD	
MCF-7	Paclitaxel	0.057 \pm 0.005	0.066 \pm 0.004	0.060
	Docetaxel	0.063 \pm 0.009	0.053 \pm 0.003	0.167
	Cisplatin	5.815 \pm 0.176	4.579 \pm 2.087	0.365
	Gemcitabine	5.473 \pm 1.941	5.963 \pm 0.48	0.693
MDA-MB-361	Paclitaxel	0.043 \pm 0.004	0.039 \pm 0.003	0.256
	Docetaxel	0.05 \pm 0.029	0.029 \pm 0.009	0.304
	Cisplatin	5.335 \pm 0.088	5.52 \pm 0.104	0.079
	Gemcitabine	2.834 \pm 0.306	2.818 \pm 0.021	0.932
MDA-MB-231	Paclitaxel	0.026 \pm 0.012	0.017 \pm 0.003	0.302
	Docetaxel	0.017 \pm 0.001	0.010 \pm 0.001	0.002
	Cisplatin	5.81 \pm 0.729	6.427 \pm 0.343	0.256
	Gemcitabine	3.423 \pm 1.795	2.826 \pm 0.122	0.596

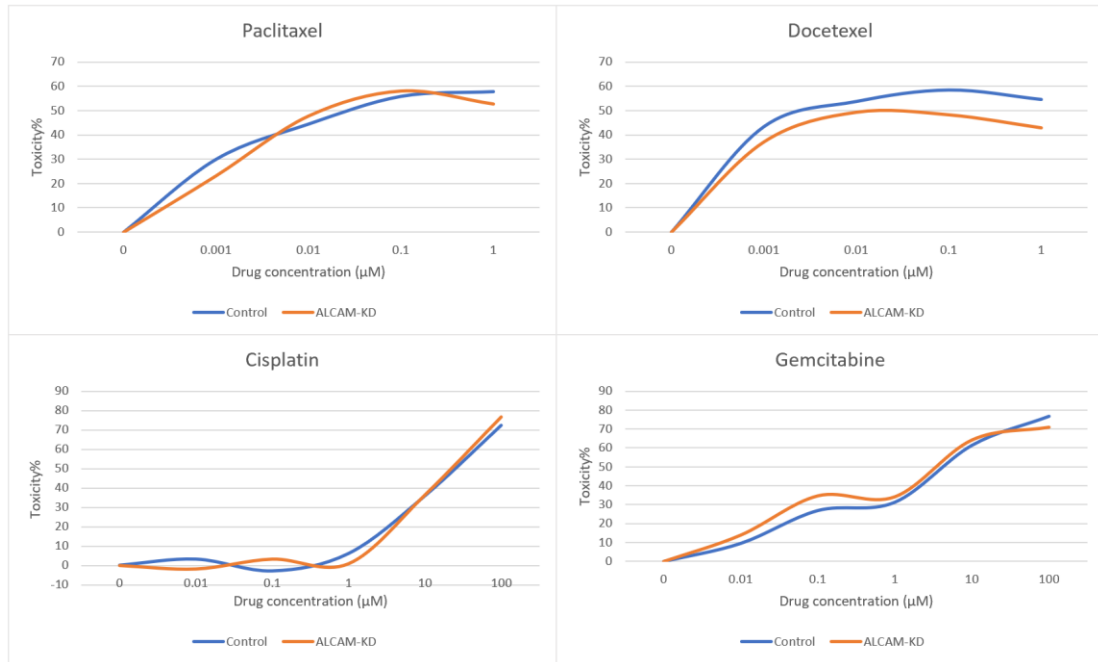


Figure 6.1 Effect of ALCAM knockdown on chemotherapy drug toxicity in MCF-7 cells without BME, using ALCAM knockdown cell model. Representative curves shown.

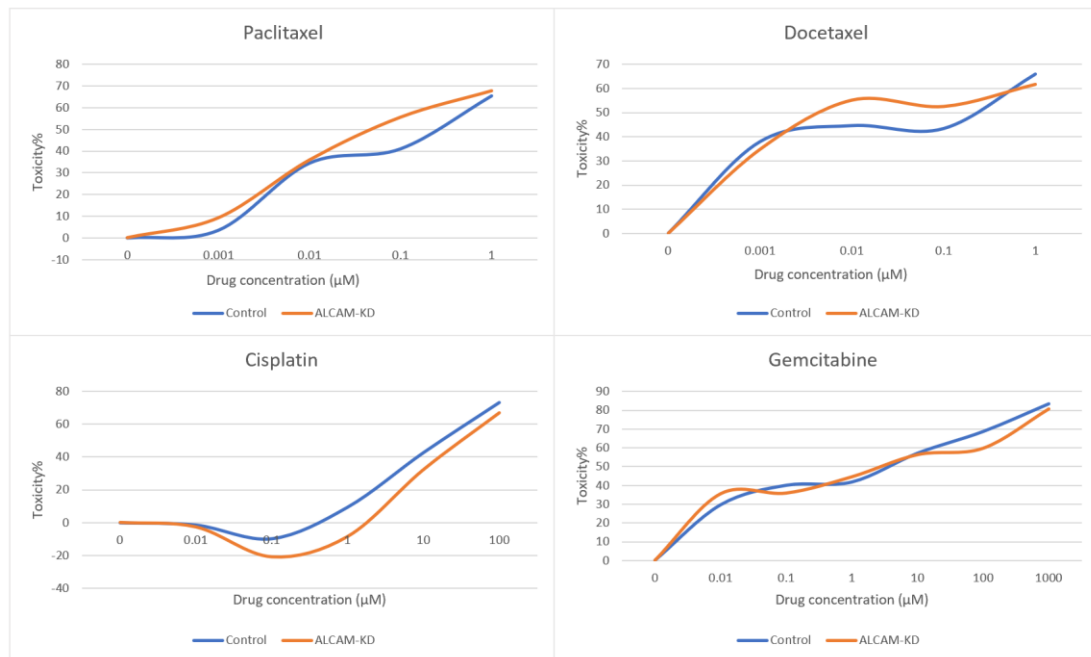


Figure 6.2 Effect of ALCAM knockdown on chemotherapy drug toxicity in MCF-7 cells with BME (50 μg/ml), using ALCAM knockdown cell model. Representative curves shown.

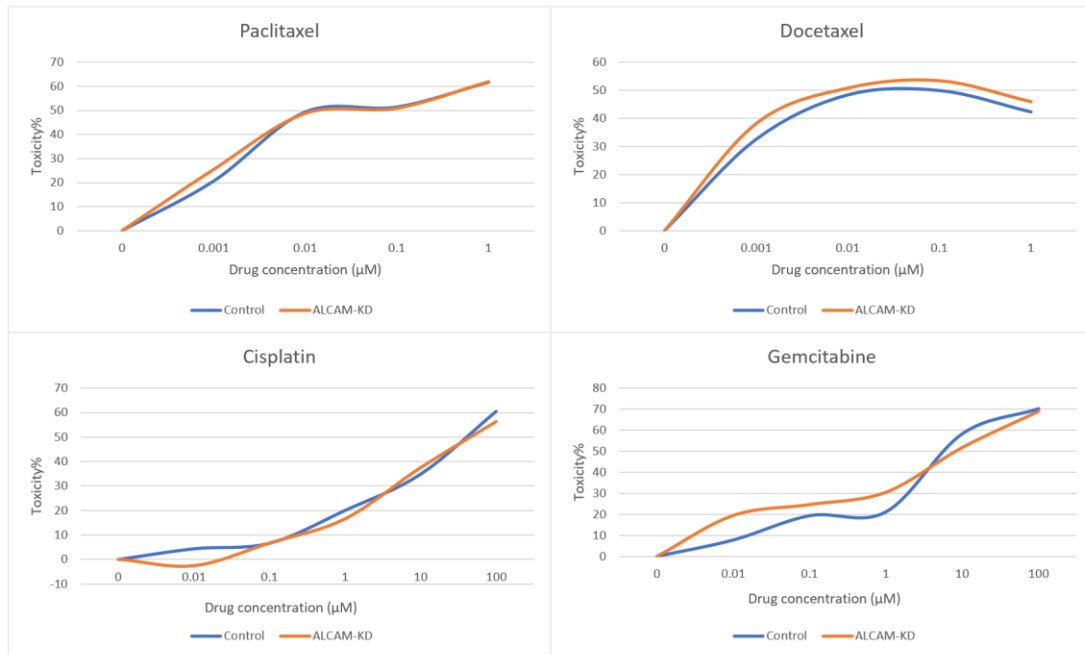


Figure 6.3 Effect of ALCAM knockdown on chemotherapy drug toxicity in MDA-MB-361 cells without BME, using ALCAM knockdown cell model. Representative curves shown.

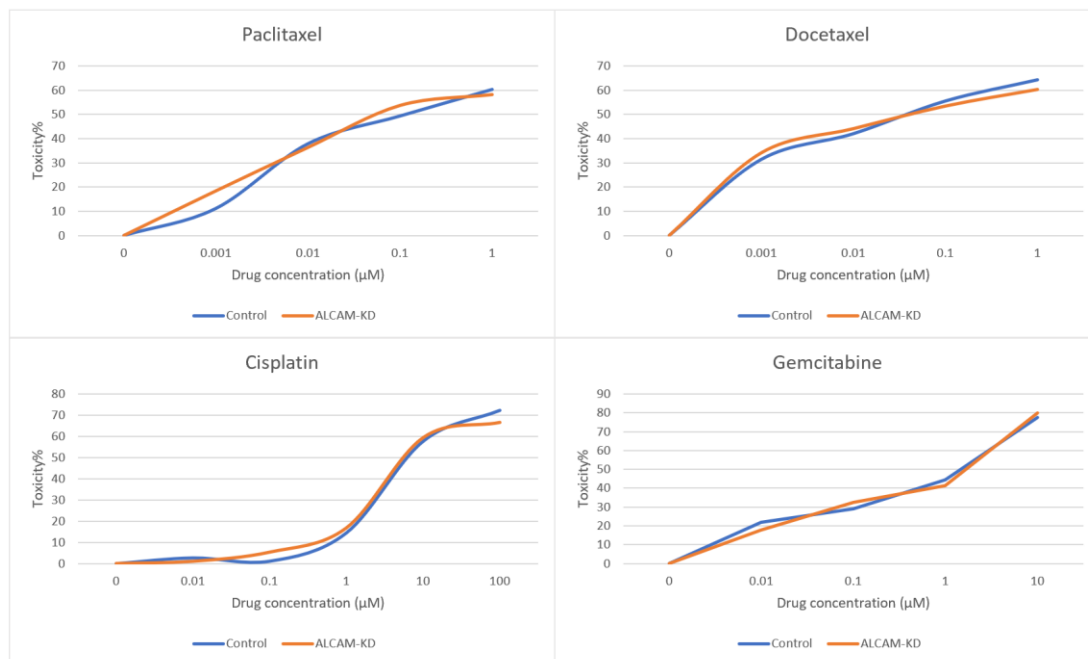


Figure 6.4 Effect of ALCAM knockdown on chemotherapy drug toxicity in MDA-MB-361 cells with BME (50 μ g/ml), using ALCAM knockdown cell model. Representative curves shown.

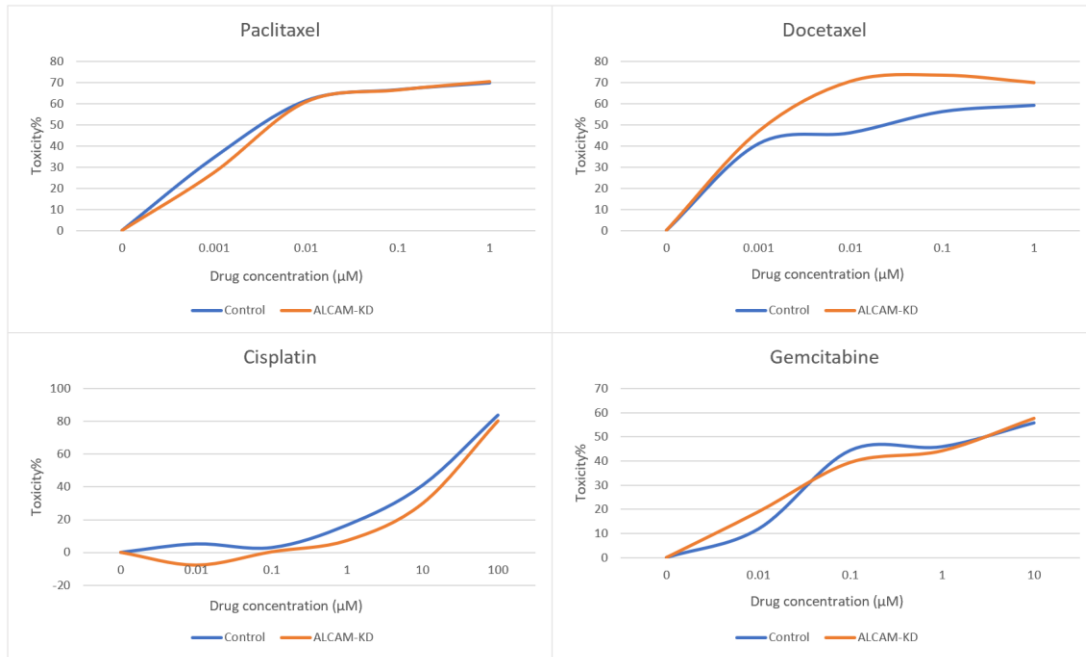


Figure 6.5 Effect of ALCAM knockdown on chemotherapy drug toxicity in MDA-MB-231 cells without BME, using ALCAM knockdown cell model. Representative curves shown.

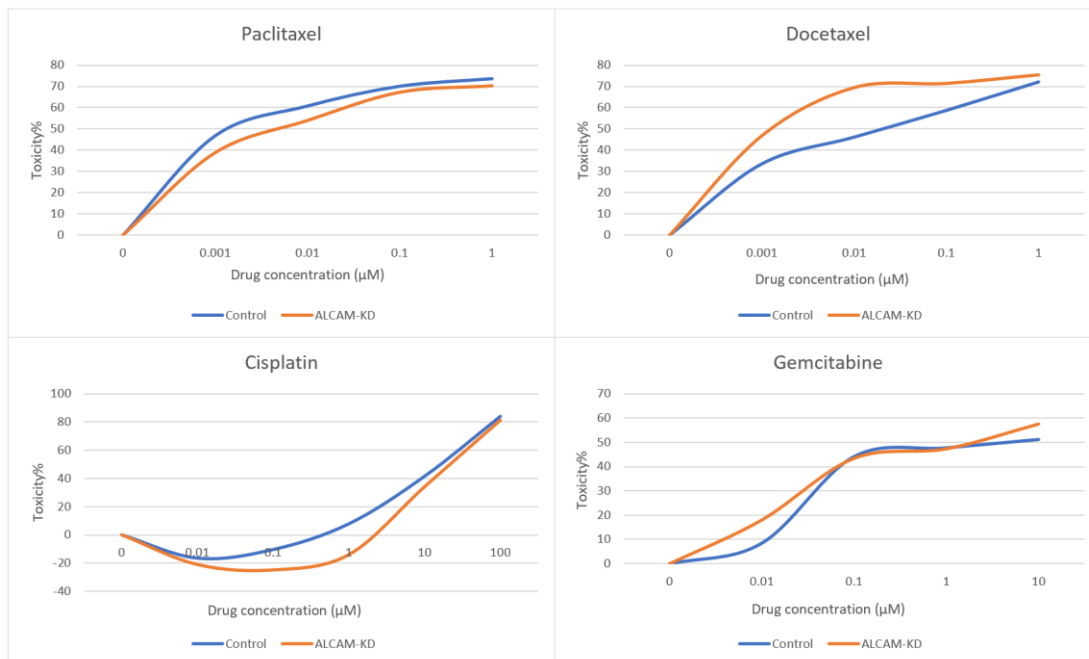


Figure 6.6 Effect of ALCAM knockdown on chemotherapy drug toxicity in MDA-MB-231 cells with BME (50 μg/ml), using ALCAM knockdown cell model. Representative curves shown.

6.3.2 The relation of ALCAM expression levels and drug responsiveness in different breast cancer subgroups

The effect of ALCAM expression levels on chemotherapy curative effect has been demonstrated by previous studies (Chen et al. 2017; Darvishi et al. 2020). We also found that knocking down ALCAM could affect the drug sensitivity in certain breast cancer cell lines in the last section. To further validate our findings, online dataset ROC Plotter (<https://rocplot.org>) was used (Fekete and Gyorffy 2019) to explore the correlation between ALCAM gene expression level and drug responsiveness in breast cancer. Treatment data of the breast cancer cohort contained 2108 cases of chemotherapy, 971 cases of endocrine therapy and 267 cases of anti-HER2 therapy. The ALCAM expression level was examined in both responder (patients who responded to certain treatment) and non-responder (patients who did not respond to certain treatment) groups. Mann-Whitney test was used to perform comparisons between groups and ROC analysis was used to analyze the predictive value of ALCAM for treatment effectiveness. Relapse-free survival was assessed after five-year clinical follow-up and recorded in the datasets.

6.3.2.1 ALCAM expression and endocrine therapy

Figure 6.7 shows the ALCAM expression in responder and non-responder groups when patients were treated with any endocrine therapy (Tamoxifen or Aromatase inhibitor). In patients with ER positive breast cancer, no difference was seen between the groups (Figure 6.7A, $p=0.21$). There was also no expressional difference in HER2 positive (Figure 6.7B, $p=0.78$) and HER2 negative (Figure 6.7C, $p=0.27$) subgroups.

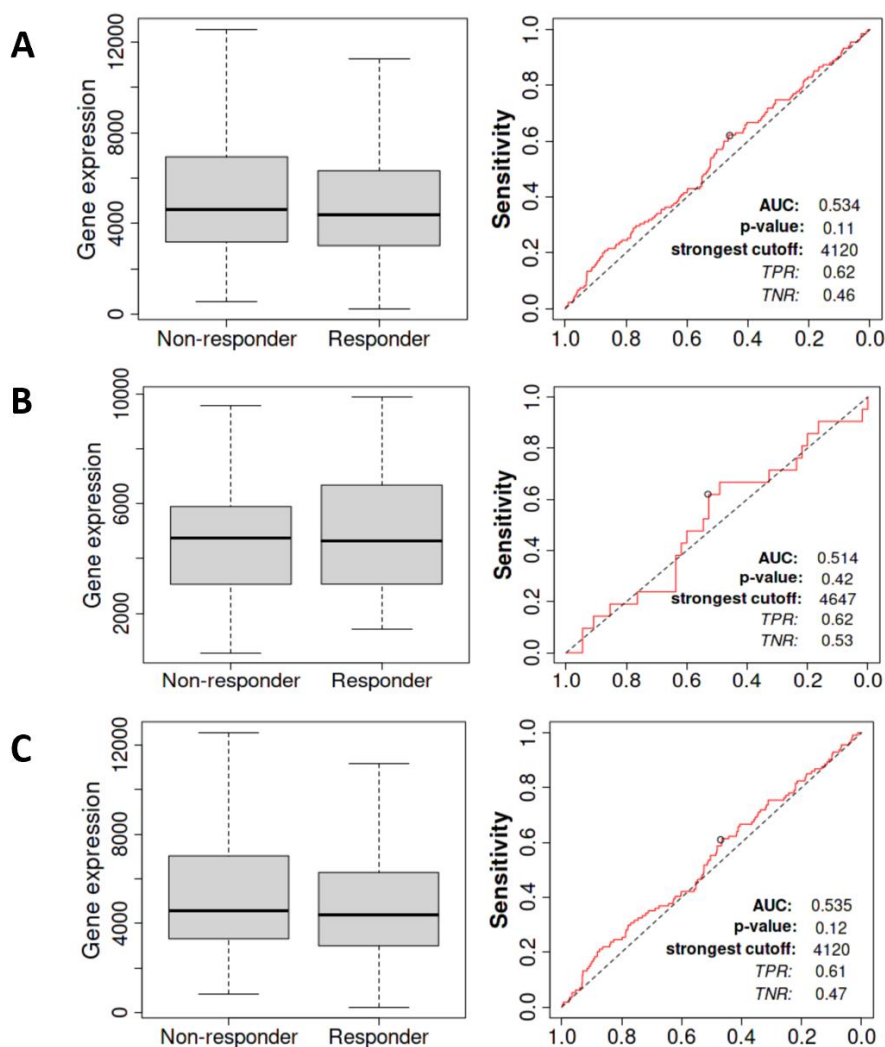


Figure 6.7 Expression of ALCAM in different subgroups of breast cancer patients who received endocrine therapies (Tamoxifen or Aromatase inhibitor). A: ER positive group; B: HER2 positive group; C: HER-2 negative group.

6.3.2.2 ALCAM expression and anti-HER2 therapy

The expression level of ALCAM was higher in the non-responder group compared with the responder group in ER negative (Figure 6.8B, $p=0.025$) and HER2 negative groups (Figure 6.8C, $p=0.012$), while the difference did not reach statistical significance in the ER positive group (Figure 6.8A, $p=0.32$). ROC analysis showed that ALCAM had a relatively good predictive value for the efficacy of anti-HER2 treatment in ER negative (AUC=0.753, $p=0.004$) and HER2 positive (AUC=0.722, $p=0.004$) patients.

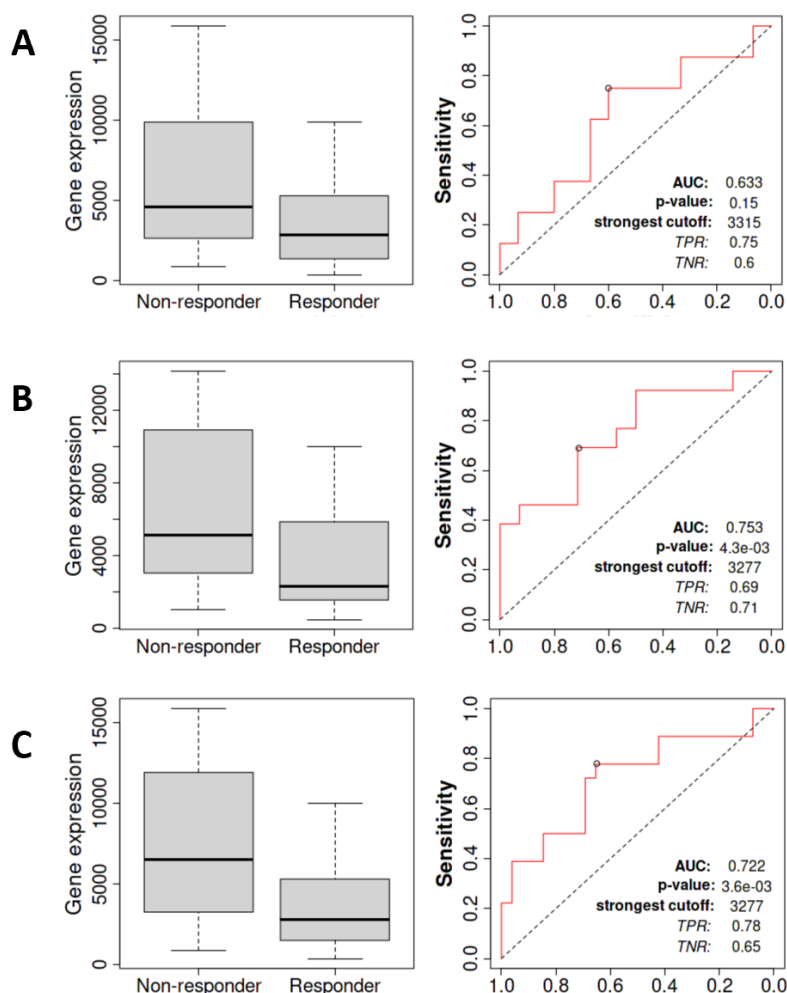


Figure 6.8 Expression of ALCAM in different subgroups of breast cancer patients who received anti-HER2 therapy (Trastuzumab or Lapatinib). A: ER positive group; B: ER negative group; C: HER-2 positive group.

6.3.2.3 ALCAM expression and chemotherapy

Figure 6.9 shows the ALCAM expression level in breast cancer patients treated with any kind of chemotherapy, including Taxane, Anthracycline, CMF (Cyclophosphamide, Methotrexate and Fluorouracil), FAC (Fluorouracil, Adriamycin and Cytoxan) and FEC (Fluorouracil, Epirubicin Hydrochloride, Cyclophosphamide).

Of all the patients of the breast cancer cohort who were treated with chemotherapy, there was no significant difference in ALCAM expression between responder and non-responder groups (Figure 6.9A, $p=0.110$). The same results could also be found in ER positive (Figure 6.9B, $p=0.052$), ER negative (Figure 6.9C, $p=0.940$) and HER2 positive groups (Figure 6.9D, $p=0.120$). While in patients with HER2 negative breast cancer, the ALCAM expression in the chemotherapy non-responder group was significantly lower than in the responder group (Figure 6.9E, $p=0.029$). The ROC curve of the HER2 negative group suggested that ALCAM expression could predict the responsiveness of this subgroup of breast cancer to chemotherapy ($AUC=0.567$, $p=0.014$).

We also analyzed the expression level of ALCAM and different kinds of chemotherapy separately. As shown in Figure 6.10, The expression of ALCAM was higher in the responder group of all patients (Figure 6.10A, $p=0.002$), ER positive group (Figure 6.10B, $p=0.007$) and the HER2 negative group (Figure 6.10E, $p<0.001$) compared with the non-responder groups, when treated with Taxane only. In the ER negative group, although this showed the same trend as the total group, it did not reach statistical significance (Figure 6.10C, $p=0.220$). In contrast with the rest of the group, ALCAM level was significantly lower in cases who responded to Taxane (Figure 6.10D, $p=0.023$) in the HER2 positive group. ALCAM had significant predictive effect on drug responsiveness in all patients ($AUC=0.616$, $p<0.001$), ER positive group

(AUC=0.630, $p=0.002$), HER2 positive group (AUC=0.707, $p<0.001$) and HER2 negative group (AUC=0.663, $p<0.001$) according to the results of ROC analysis.

The ALCAM expression, with respect to response to Anthracycline treatment, is shown in Figure 6.11. Compared with the non-responder group, ALCAM expression was significantly higher in the Anthracycline responder group in the total cohort (Figure 6.11A, $p<0.001$), ER positive group (Figure 6.11B, $p<0.001$) and HER2 negative group (Figure 6.11E, $p<0.001$). However, in patients with ER negative (Figure 6.11C, $p=0.210$) and HER2 positive (Figure 6.11D, $p=0.190$) breast cancer, the ALCAM expression between the responder and non-responder groups did not appear to be significantly different. The ROC analysis showed that ALCAM had a predictive effect on the drug efficacy of Anthracycline in all patients (AUC=0.605, $p<0.001$), in particular ER positive (AUC=0.666, $p<0.001$) and HER2 negative subgroups (AUC=0.637, $p<0.001$).

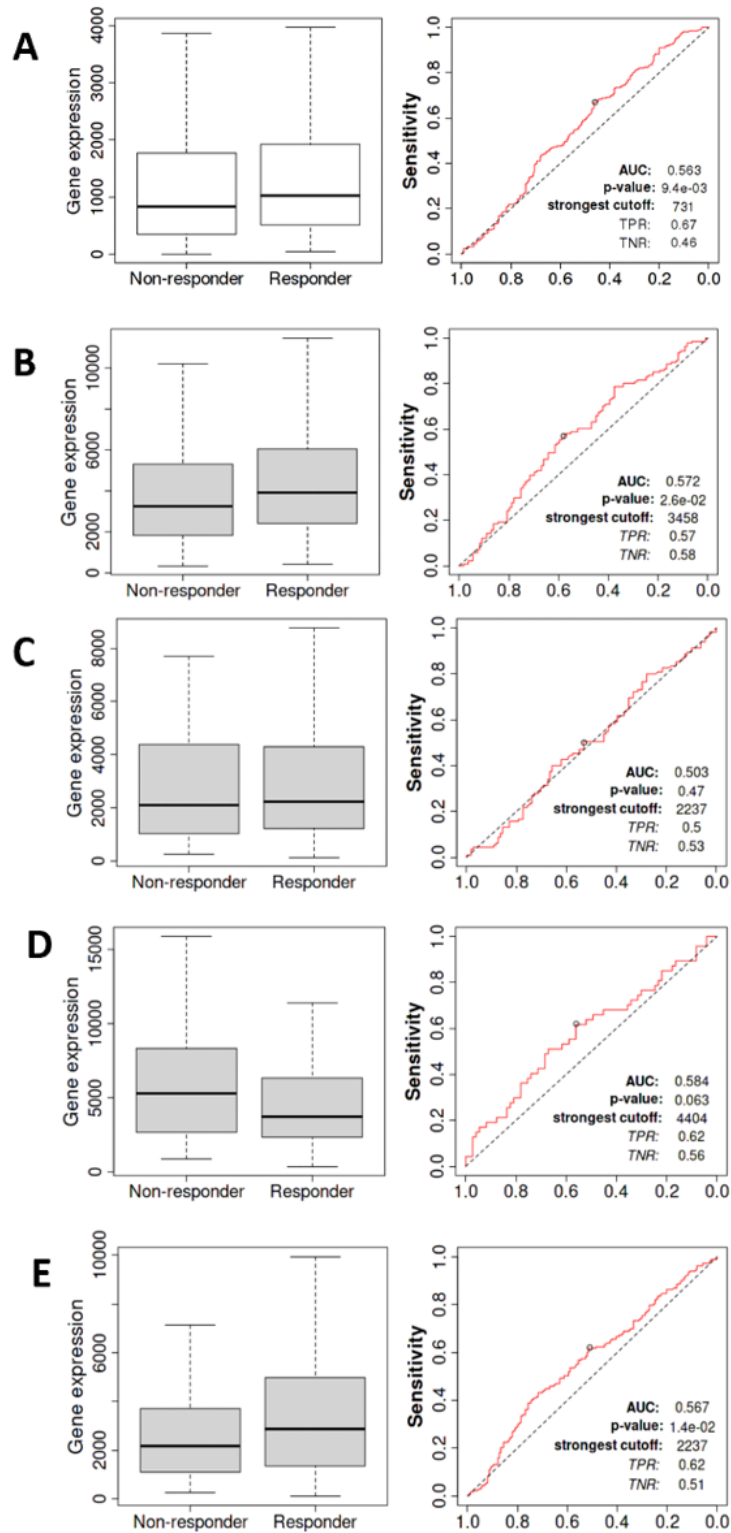


Figure 6.9 Expression of ALCAM in different subgroups of breast cancer patients who received any chemotherapy (Taxane, Anthracycline, CMF, FAC or FEC). A: All patients; B: ER positive group; C: ER negative group; D: HER2 positive group; E: HER2 negative group.

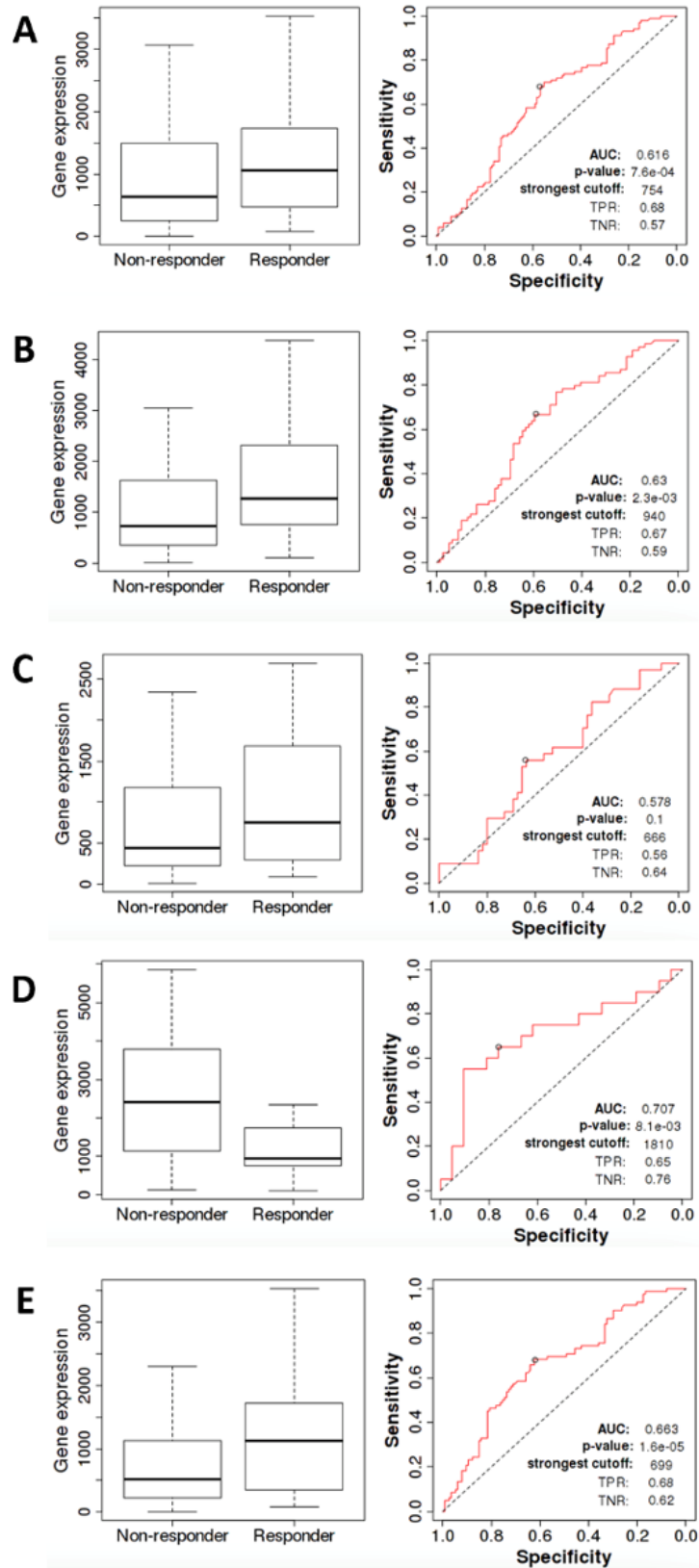


Figure 6.10 Expression of ALCAM in different subgroups of breast cancer patients who received Taxane treatment. A: All patients; B: ER positive group; C: ER negative group; D: HER2 positive group; E: HER2 negative group.

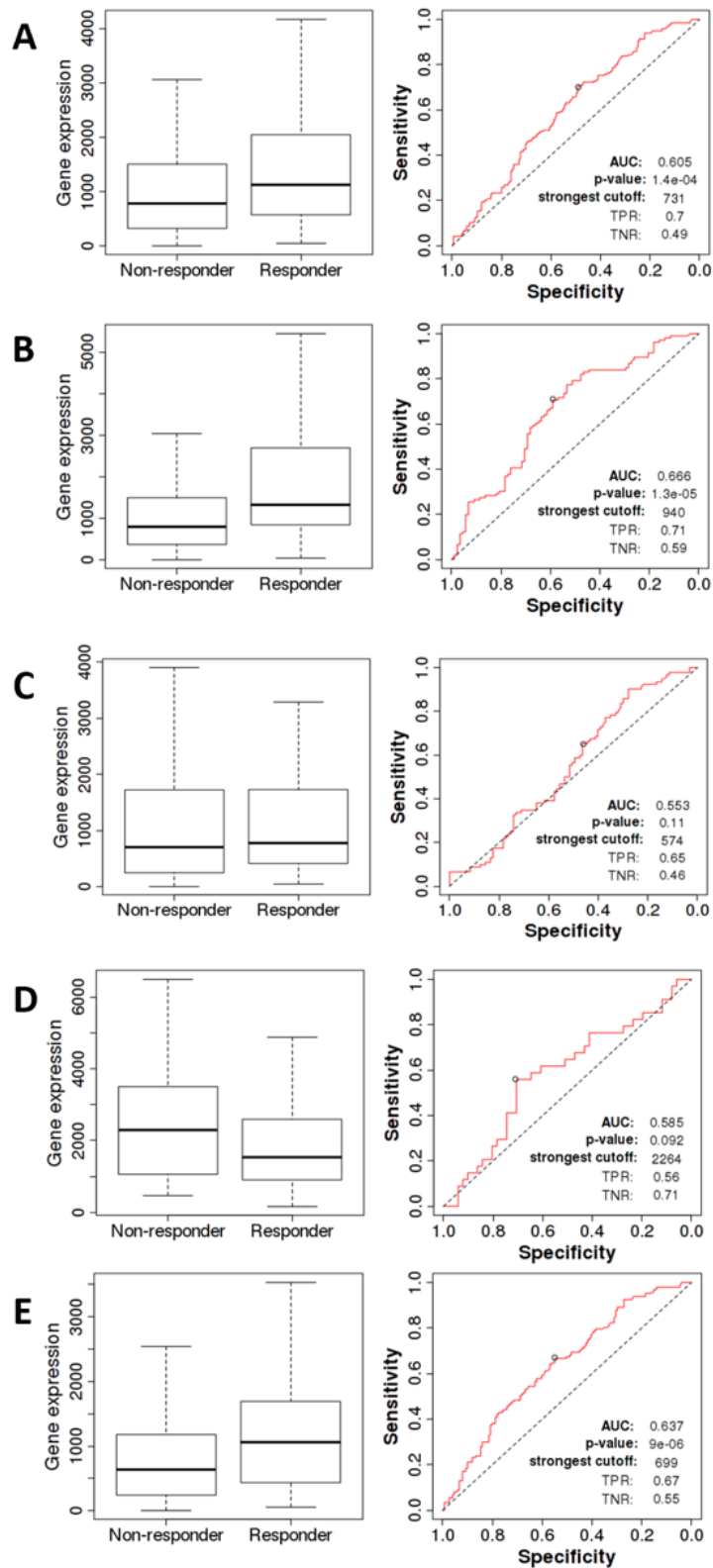


Figure 6.11 Expression of ALCAM in different subgroups of breast cancer patients who received Anthracycline treatment. A: All patients; B: ER positive group; C: ER negative group; D: HER2 positive group; E: HER2 negative group.

6.3.2.4 ALCAM and chemo-response in molecular subtypes of breast cancer

Breast cancer is classified based on the molecular subtypes of ER, HER2 and PR into four major types, namely Luminal-A, Luminal-B, HER2 enriched and triple negative breast cancer. Figure 6.12 compares directly these four molecular types. It is clear that in Luminal-A type, tumours with high levels of ALCAM are most sensitive to all the major chemotherapies listed and, interestingly, HER2 enriched tumours showed the opposite.

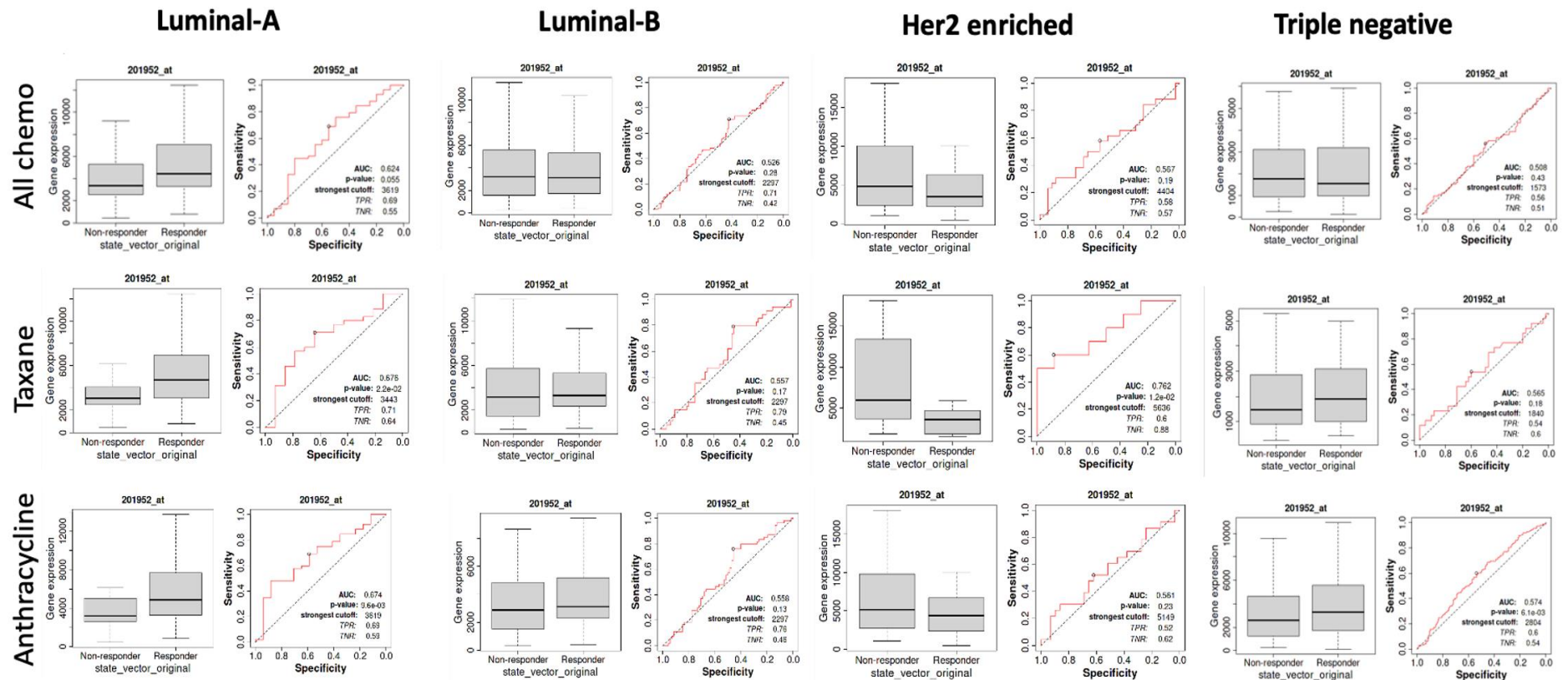


Figure 6.12 ALCAM expression and patient's response to chemotherapeutics in different molecular subtypes of breast cancer.

6.4 Discussion

In this Chapter, I explored the effect of differential ALCAM expression on the cytotoxicity of four representative chemotherapy drugs, which were available in the host laboratory, on different subgroups of breast cancer cells. In addition, I interrogated the link between ALCAM expression of breast cancers and patient's clinical response to drug treatment, mainly chemotherapeutics from the available public database.

The influence of ALCAM on the sensitivity to chemotherapeutic drugs has been demonstrated in various tumour types. For instance, in colorectal cancer, increased ALCAM/CD166 expression was found in chemotherapy drug-resistant cells (El Khoury et al. 2016). In giant cell bone tumours, ALCAM positive tumour cells were more resistant to chemotherapeutic agents including cisplatin, and also more resistant to radiotherapy (Zhou et al. 2018). Su *et al.*, (Su et al. 2016) also reported that non-small cell lung cancer cells with high ALCAM expression had higher resistance to the chemotherapy drug cisplatin. Furthermore, it has been demonstrated that patients with overexpressed ALCAM protein levels responded well to chemotherapy in cervical cancers (Ihnen et al. 2012).

In terms of breast cancer, a study by Chen and colleagues (Chen et al. 2017) showed a clear link between ALCAM/CD166 and resistance to endocrine related therapies, namely tamoxifen in ER positive breast cancer. The IHC staining of ALCAM was stronger in the tamoxifen non-responder group compared with the responder group and upregulation of ALCAM was also found in tamoxifen resistant MCF-7 cells. Darvishi *et al.*, (Darvishi et al. 2020) successfully enhanced the anti-proliferative effects of tamoxifen against drug resistant MCF-7 cell lines, using an anti-ALCAM scFv (single chain antibody fragment).

In my *in vitro* based testing, I chose three cell lines, each representing a subtype of breast cancer, by way of their hormone receptor status. The cell toxicity assay results are interesting in that the responses appear to be cell type dependent and drug dependent. The cells showing a more marked difference in response was the ER(-)/HER2(-) breast cancer MDA-MB-231 cells, in that it was shown that the drug sensitivity of Docetaxel significantly increased following ALCAM knockdown in MDA-MB-231 cells. It is interesting to note that in ER positive breast cancer cell lines, namely MCF-7 and MDA-MB-361 cell lines, no significant difference could be observed between control and ALCAM knockdown groups. These results indicated that ALCAM expression could have different effects on drug sensitivity in ER positive and ER negative cells.

The data from online datasets also provided a lot of suggestive information. The effect of ALCAM on drug treatment was mainly in chemotherapy and anti-HER2 treatment, but not in endocrine therapy. This result did not agree with the findings in the previous studies (Chen et al. 2017; Darvishi et al. 2020), which showed that high levels of ALCAM could increase tamoxifen drug resistance in breast cancer. In terms of the drug responsiveness to chemotherapy and anti-HER2 treatment, ALCAM expression indeed showed different trends in certain subgroups of breast cancer. For example, in ER positive breast cancer, higher levels of ALCAM expression were found in Taxane responder groups, but such results did not appear in ER negative breast cancer, even in contrast with the results in HER2 positive cases. These results were broadly in line with our hypothesis, namely that ALCAM had different biological effects in cells with different ER statuses, which resulted in an opposite role of ALCAM towards the survival and prognosis of ER positive and ER negative breast cancer patients.

Apart from ER, the association between the effect of ALCAM on chemotherapy and HER2 status is also of interest to discuss. In Chapter 5, we used an anti-HER2 drug

Neratinib in the cell adhesion assays, which showed a possible impact of HER2 on ALCAM mediated cell adhesion. As shown in Section 6.3.2, the ALCAM expression level was significantly higher in patients who did not respond to anti-HER2 treatment. In terms of chemotherapy, the drug responder group had higher ALCAM expression in HER2 negative breast cancer but lower ALCAM expression in HER2 positive breast cancer. These above results have shown that ALCAM and HER2 have a potential link to some extent and their correlation with regard to anti-HER2 treatment/chemotherapy warrants further investigation.

CHAPTER-7

ALCAM in pancreatic cancer, a pivotal link to clinical outcome and tumour vascular embolism

7.1 Introduction

In previous chapters, we have discussed the impact of ALCAM on the progression of endocrine related cancer, namely breast cancer. The study has also presented (Chapter 3) that in another endocrine related cancer, namely pituitary tumours, where ALCAM also acted as an inhibitory factor to bone metastasis. Together with other reports indicating the possibility that ALCAM acts as tumour suppressive role in other endocrine related cancers, namely thyroid cancer (Chaker et al. 2013), prostate cancer (Minner et al. 2011), and the neuroendocrine tumours of pancreas (Hong et al. 2010; Tachezy et al. 2011), it collectively suggests that ALCAM has a different, and more likely a contrasting role, in endocrine tumours from non-endocrine tumours. To further validate this possibility, the present study explored an exocrine tumour, namely pancreatic ductal carcinoma to explore whether ALCAM plays a different role in non-endocrine related cancers compared to endocrine related cancer types. In a tissue microarray study, we were also able to compare the ductal carcinoma with a small set of endocrine related tumours, pancreatic islet tumours, rare type of hormone producing endocrine tumours of the pancreas gland. Due to a surprising finding that ALCAM was related to the presence of tumour vascular embolism, we investigated the role of ALCAM in pancreatic cancer-endothelial interactions.

7.2 Methods

7.2.1 Cohorts

Pancreatic cancer cohort: Pancreatic cancer tissues, together with normal unaffected normal tissues, were collected immediately after surgery at Peking University Cancer Hospital and Institute. Tissues obtained from surgery theatre were immediately stored in liquid nitrogen until use. Ethical approval was granted by the

Ethics Research Committee of Peking University Cancer Hospital (Ethics approval number 2006021) and is fully in accordance with the Helsinki declarations. Consents were obtained from the patients. In total, 223 patients were recruited to the study. Patients were followed in the clinics and the current study had a median follow-up period of 12 months. Clinical, pathological information and follow-up information were collected retrospectively.

The TCGA public datasets: The present study has taken advantage of the available TCGA database of pancreatic cancer, in order to gather additional support to our cohort-based studies. I have analysed the relationship between ALCAM and clinical outcome (overall survival and relapse free survival). In these analyses, we have chosen the ROC predicted best cut-off point to divide patients whose pancreatic tumour had either high levels or low levels of ALCAM expression. Here, the web resource kmplot.com was used.

7.2.2 Cell lines and culture conditions

Human pancreatic cancer cell lines, PANC-1 and Mia PaCa-2 were obtained from the ATCC (American Type Culture Collection), provided by the LGC Standards (LGCstandards.com), ATCC's European supplier (Teddington, Middlesex, UK). An immortalised human vascular endothelial cell line HECV, was purchased from Interlab, Naples, Italy. All of the cell lines were cultured in Dubecco's Modified Eagle Medium (DMEM)/Ham's F12 with L-glutamine (Sigma-Aldrich, Dorset, UK). All the mediums were supplemented with 10% foetal calf serum (FCS) (Sigma-Aldrich, Dorset, UK) and antimicrobial solutions (Sigma-Aldrich, Dorset, UK). Cells were cultured at 95% humidity, 5% CO₂ and 37° C.

7.2.3 Key materials

Recombinant human ALCAM-Fc chimera (soluble ALCAM), containing ALCAM Trp28 – Ala526 and the human IgG Fc region, was purchased from R&D systems (Abingdon, UK). A monoclonal antibody to human ALCAM was purchased from Novacastra, Milton Keynes, UK.

7.2.4 Anti-ALCAM shRNA and ALCAM expression constructs

To modify the expression of ALCAM in target cell lines multiple plasmid systems were designed and purchased from VectorBuilder (Chicago, USA). A number of shRNAs targeting ALCAM and control scramble sequences were designed in order to affect ALCAM expression. Additionally, the ALCAM expression sequence or stuffer control sequence was used for ALCAM over-expression models. Plasmids were transfected into cell lines using Fugene HD (Promega, Southampton, UK).

7.2.5 Establishing pancreatic cancer and endothelial cell models with differential expression of ALCAM

The anti-ALCAM shRNA plasmids were used to transfect PANC-1 and HECV cells, by way of chemical transfections FuGene HD (Promega, Southampton, UK) as described in Chapter 2. The cells which had successfully survived the selection were tested for the expression profile of ALCAM, to establish the success of genetic manipulation by way of PCR. We established ALCAM knockdown PANC-1 (designated as PANC1^{ALCAMkd}) and HECV (designated HECV^{ALCAMkd}) cell models together with the respective scramble controls. Mia PaCa-2, which expressed low levels of ALCAM, was transfected with ALCAM expression construct, using a similar procedure as the knockdown, except that a plasmid with full coding region of human ALCAM was used in the transfection. This resulted in the establishment of the ALCAM over-expression sub model, MiaPaCa2^{ALCAMexp}. These models were then used for the *in vitro* investigations.

7.2.6 Tumour-endothelial interaction assay

Tumour-endothelial interaction was assessed using a method previously described (Hiscox and Jiang 1997). Briefly, pancreatic cancer cells, control and transfected were cultured to sub confluence. On collection of the cell suspension, they were stained with 5 μ M Dil (1,1'-Diocadecyl-3,3,3',3'Tetramethylindocarbocyanine Perchlorate) for 30 minutes. After extensive washing to remove the free dyes, a fixed number of cells was added to an endothelial cell monolayer (control (HECV^{control}) or ALCAM knockdown (HECV^{ALCAMkd})), previously established on the 96-well plates. After 20 minutes, the culture wells were carefully washed with PBS to remove the non-adherent cancer cells. The remaining cells, that adhered to the endothelial cell monolayer, were fixed with 4% formalin. Representative bright field and fluorescence images were captured on a EVOS automated cell analyser. The merged images were generated and attached cancer cells were quantified using the cell counting function provided by the EVOS system.

7.2.7 Cell adhesion and migration assay by ECIS (Electric Cell-Substrate Impedance Sensing)

ECIS assay, an automated and human interface free method, was applied to investigate cellular behaviour, based on the impedance parameter detected from gold electrodes coated on the bottom of a 96-well array (Applied Biophysics Inc., NJ, USA). The assay was modified from the previously described method (Keese et al. 2002; Jiang et al. 2009).

In brief, prior to cell seeding, ECIS arrays containing growth medium were stabilised using the stabilisation function within the system and washed in order to prepare the gold surface for cell adhesion. Cells at equal numbers were seeded at an appropriate

density in the 96-well electrode arrays (96W1E) and immediately placed on the ECIS station (ECIS model theta). The instrument was programmed to automatically trace the rate of cell adhesion at multiple frequencies (from 1,000Hz-64,000Hz). Changes in resistance/impedance were measured over the course of the experiment. The first 4 hours of data was analysed for initial attachment and spreading. Once the resistance curve reached a plateau, electric wounding method was applied to the cells allowing automated generation of a fixed-sized wound over the gold electrode, by way of electric generated killing of any cells located on the electrode. In the present study, the electric wounding condition was 2000 μ A at 60,000 Hz for 20 seconds for each well. Following wounding, the resistance was immediately recorded over a four-hour period when the migration of cells took place.

The second ECIS assay used was the automated tracking of cancer-endothelial interactions. Here, HECV cells, control or HECV^{ALCAM^{kd}}, were plated in the ECIS array and allowed to reach confluence. Pancreatic cancer cells were added to the endothelium and the interaction was monitored immediately at a fixed frequency of 4,000Hz.

7.2.8 Pancreatic cancer tissue arrays (TMA) and staining of ALCAM by immunohistochemical assay

A pancreatic tissue array (No. PA2081c) (Supplement-2) was obtained from (Biomax Inc. Rockville, MD, USA). Following antigen retrieval, the TMA was blocked for 2 hours with 10% horse serum before being incubated with ALCAM primary antibody (2 μ g/ml). We used a universal secondary antibody and biotin tertiary reagents to bind to the ALCAM antibody and to conjugate peroxidase (Vectastain Elite Universal ABC kit, Vector Laboratories Ltd., Peterborough, UK). DAB (diaminobenzidine, 5mg/ml; Sigma-Aldrich, Dorset, UK) was used to develop colour and the TMA was counterstained with Gill's hematoxylin (Vector Laboratories Ltd., Peterborough, UK).

The staining was assessed by three independent assessors and scored as no staining (0), weak (1), moderate (2), or strong (3), based on a method previously reported (Sanders et al. 2019; Xin et al. 2021).

7.2.9 Extraction of RNA from tissues and quantitative analysis of ALCAM gene transcript

Tumour and normal tissues were retrieved from liquid nitrogen storage vessels and subsequently homogenised in an RNA isolation buffer. Total RNA was extracted using an ether-based method. After extensive washing, total RNA was purified and quantified by a UV spectrophotometer and standardised to the same concentration. Reverse transcription was carried out using a reverse transcription kit (Promega). Quantitative analysis of ALCAM gene transcript was performed on a StepOne Plus thermocycler (Fisher Scientific UK). The primers used in the study are listed in Table-2.3. The chemistry employed here was the FAM tagged Uniprimer™ which worked with the reverse primer via a unique sequence (z-sequence, underlined in Table 2.3). GAPDH was used as a house keeping control.

7.2.10 Statistical methods

Pairwise comparisons were made by Mann-Whitney U test and Kruskal Wallis test. ROC model was used to categorise patients into groups with differential expression in accordance with clinical outcome and presence of tumour embolism. Survival analysis was carried out with the Kaplan-Meier method and Cox regression model. Multiple variate analysis and logistic regression were used for multiple factor comparison with survival. All the analyses were carried out using SPSS version 26. The statistical significance was defined as $p < 0.05$.

7.3 Results

7.3.1 Levels of ALCAM expression in pancreatic tissues and pancreatic cancer tissues determined by immunohistochemistry (IHC)

Pancreatic tissues, normal and tumour, all stained positive for ALCAM (Figure 7.1 and Table 7.1). The staining is of membranous and cytoplasmic nature. Most of the tissues had both cytoplasmic and membrane ALCAM staining except for several cases in which only cytoplasmic staining could be observed. The intensity of ALCAM staining was different among different pathological types of tissues ($p < 0.001$). Therein, adjacent normal pancreas tissue ($p = 0.028$) had significantly lower levels of ALCAM staining compared to ductal adenocarcinoma, whilst metastatic tumours ($p = 0.732$) and chronic pancreatitis ($p = 0.126$) showed no statistical difference with ductal adenocarcinoma. There was no difference in ALCAM staining among different differentiation grade ($p = 0.408$), TNM staging ($p = 0.241$), tumour staging ($p = 0.074$) nor node metastasis ($p = 0.662$). In general, despite the small sample size, tumour tissues stained stronger than normal tissues and benign tumour tissues.

It was noteworthy that the small cohort of islet tumours ($n = 20$, Figure 7.1d), a hormone producing endocrine tumour of pancreas, showed significantly lower levels of ALCAM staining compared with pancreatic ductal carcinoma ($p = 0.017$).

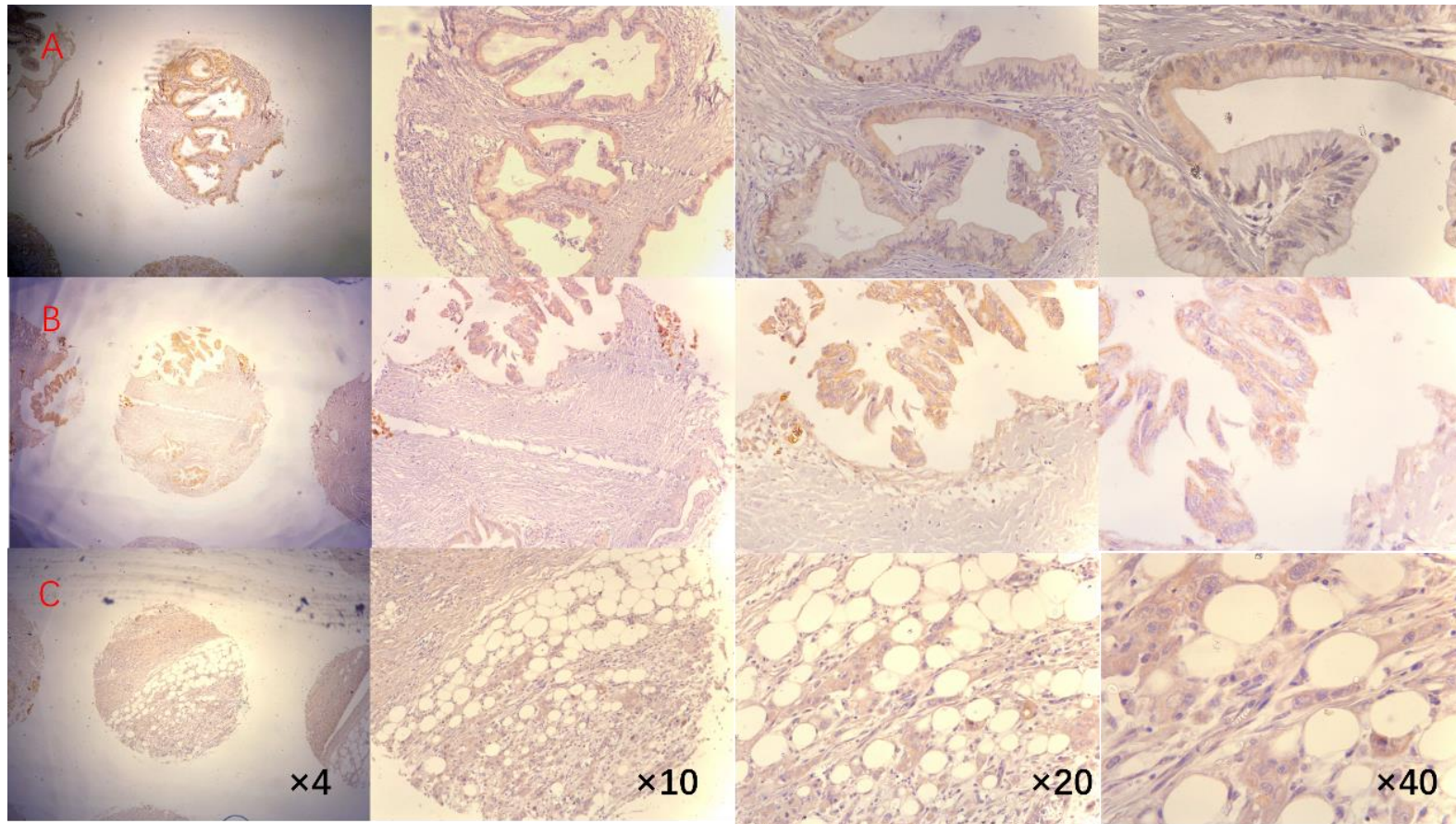


Figure 7.1a ALCAM staining in pancreatic duct adenocarcinoma tissues. Shown are representative staining from TMN stage T2N0M0 (line A), T3N0M0 (line B), T4N0M0 (line C). The magnification was from $\times 4$ to $\times 40$.

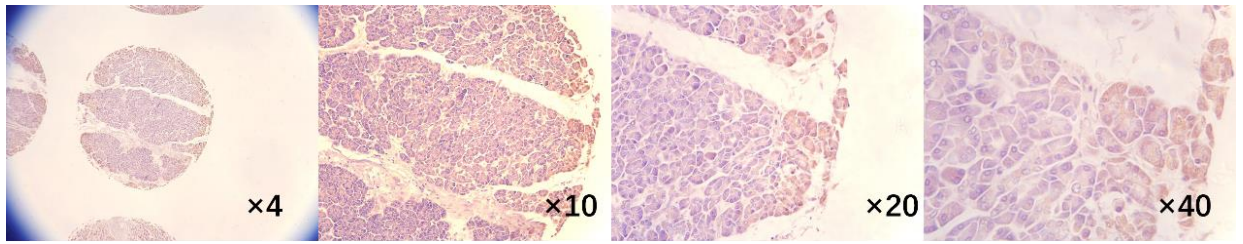


Figure 7.1b ALCAM staining in normal pancreatic tissues

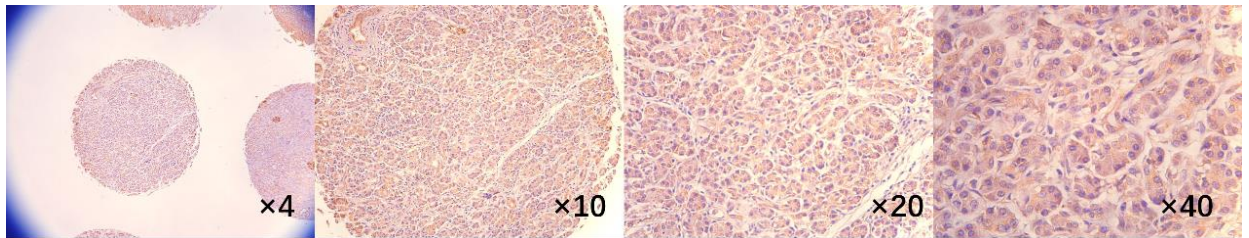


Figure 7.1c ALCAM staining in chronic pancreatitis.

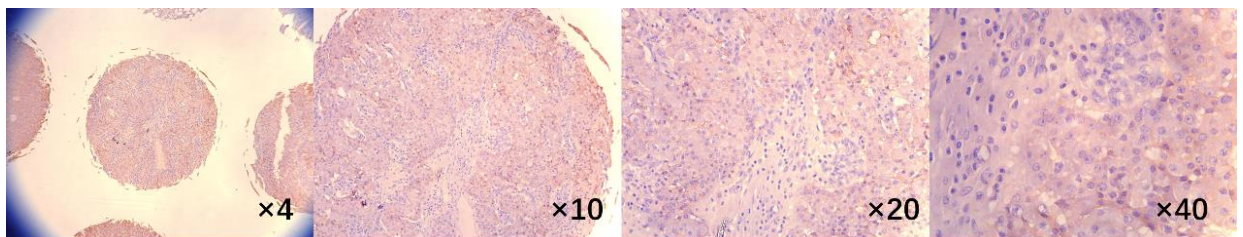


Figure 7.1d ALCAM staining in islet cell tumours.

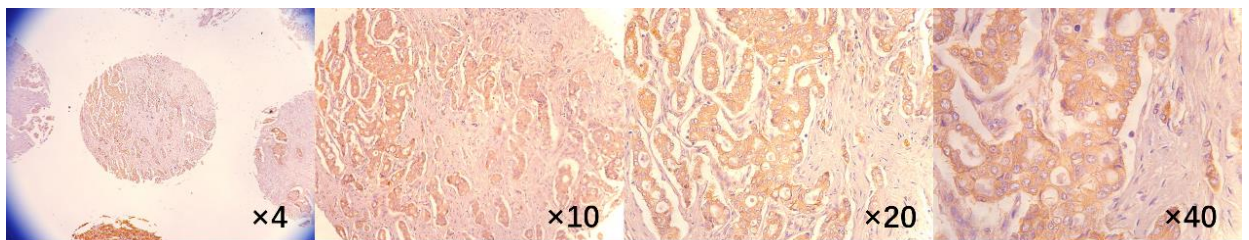


Figure 7.1e ALCAM staining in metastatic adenocarcinoma (liver originate).

Table 7.1 ALCAM staining score in pancreatic tissues

Group	N	Distribution			Intensity			Statistical significance	
		Both	Cytoplasm	Membrane	1	2	3	Chi value	p
Pathology									
Duct adenocarcinoma	54	53	1	0	6	37	11	42.492	<0.001 ^a
Adjacent normal pancreas tissue	48	37	11	0	13	32	3	7.185	0.028 ^b
Metastatic	10	10	0	0	2	6	2	0.625	0.732 ^b
Islet cell tumour	20	20	0	0	8	10	2	8.120	0.017 ^b
Chronic pancreatitis	12	10	2	0	4	7	1	4.135	0.126 ^b
Differentiation									
Grade									
1	11	11	0	0	1	7	3		
2	19	19	0	0	0	13	6	1.794	0.408 ^c
3	2	2	0	0	2	0	0	NA	NA
TNM stage									
I	22	22	0	0	1	14	7		
II	30	29	1	0	3	23	4	2.844	0.241 ^d
III	2	2	0	0	2	0	0	NA	NA
Tumour stage									
T2	28	28	0	0	1	18	9		
T3	24	23	1	0	3	19	2	5.205	0.074 ^e
T4	2	2	0	0	2	0	0	NA	NA
Node metastasis									
N0	42	42	0	0	4	30	8	0.825	0.662
N1	12	11	1	0	2	7	3		

^a Overall chi-square test among all pathology types; ^b Compared with Duct adenocarcinoma; ^c Compared with differentiation Grade 1; ^d Compared with TNM stage I; ^e Compared with Tumour stage T2.

7.3.2 Expression of ALCAM gene transcript in pancreatic cancer

Pancreatic cancer tissues had markedly high levels of ALCAM transcript compared with normal tissues ($p < 0.000001$) (Figure 7.2A and Table 7.2). Whilst the difference between different groups of histological types, differentiation, tumour staging, TNM staging, and nodal metastasis did not reach significant difference (Table 7.2).

Tumours from patients who died of pancreatic cancer during the follow-up period had significantly higher levels of ALCAM than tumours from those who remained alive ($p = 0.018$) (Figure 7.2B).

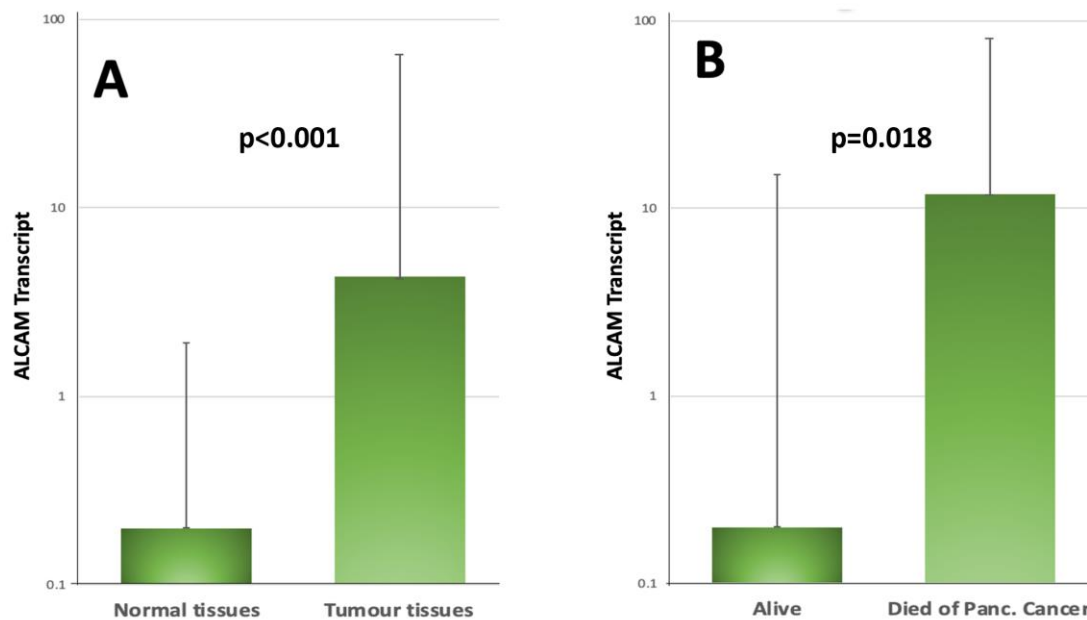


Figure 7.2 A: Levels of expression of ALCAM transcript in normal and pancreatic cancer tissues. B: Expression of ALCAM in those who died and remain alive. Statistical method was Mann-Whitney U test. Shown are median and IQR.

Table 7.2 Expression of ALCAM transcript and the clinical and pathological groupings

Group	Median	Q1	Q3	P^a
Tissue types				<0.001
Tumour	68.2	0.1	60.2	
Normal	15.5	0	1.7	
Sex				0.452
Male	2.43	0.09	76.3	
Female	7.8	0	56	
Differentiation				0.312
High	0	0	162.9	
High-Medium	16.5	0.1	165	
Medium	0.76	0.07	53.64	
Medium-Low	6	0.09	52.373	
Low	11	2	34	
Anatomical site				0.427
Head	3.3	0.1	50.97	
Body	24.4	0	76.4	
Body/Tail	13.2	0	87.57	
Tail	19.3	11.4	113.3	
Other locations	108.3	21.2	176.3	
Tumour staging				0.315
T1	18.1	8.3	89.2	
T2	7.6	0	108.1	
T3	0.3	0	28.6	
T4	14.3	0.1	84.1	
Lymph nodes				0.73
Negative	15.85	0.08	85.5	
Positive	18.1	8.3	89.2	
Metastatic at diagnosis				0.996
No	3.5	0.1	61.51	
Yes	6	0.12	16.62	
TNM stage				0.924
1	13	0	135	
2	0.4	0.1	50.33	
3	11.6	0.1	84.1	
4	10.9	0.1	33.5	
Combined				0.473
TNM1-2	0.4	0.1	52.7	
TNM3-4	11.6	0.1	68.8	
Clinical Outcome				0.018
Alive	0.2	0	14.9	
Died	11.9	0.1	67.9	

^a by Mann-Whitney U test and Kruskal–Wallis H test

7.3.3 Levels of ALCAM transcript and clinical outcomes

Using the ROC model, it was demonstrated that levels of ALCAM have significant power in predicting the mortality of the patients (AUC=0.614, $p=0.016$), and that high levels of ALCAM indicate high probability of pancreatic cancer related death. Based on the cut-off value from the ROC model, we divided patients into two groups, with high levels of expression and low levels of expression, respectively. Using the Kaplan-Meier model, it was found that patients with high levels of ALCAM had a significantly shorter survival, compared with those of low ALCAM levels with median survival time being 19.7 vs 24.7 months, respectively ($p=0.041$) (Figure 7.3). Although in univariate analysis, ALCAM expression level and nodal status are significant factors for the clinical outcome, only ALCAM was found to be an independent prognostic factor for the mortality of the patients by using univariate analysis ($p=0.005$, HR =3.0) and multivariate analysis ($p=0.023$, HR=5.485) (Table 7.3).

We have also explored the TCGA dataset (RNAseq) which has a smaller number of patients than the present study (Uhlen et al. 2017; Nagy et al. 2021). As shown in Figure 7.4 and Figure 7.5, the links between ALCAM gene transcript and patients' survival, OS (overall survival) and RFS (relapse free survival), are not significant. However, it is noteworthy that high levels of ALCAM were seen to be associated with a shorter RFS survival but longer OS survival, although neither was statistically significant.

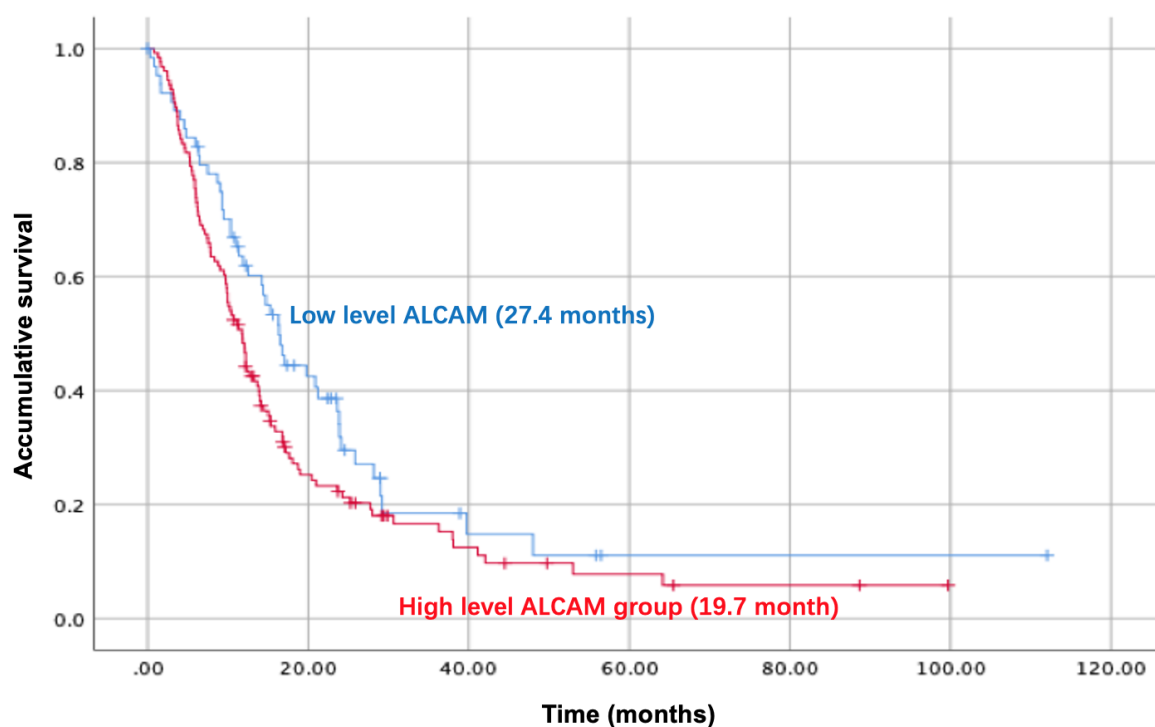


Figure 7.3 ALCAM levels and overall survival of the patients by Kaplan-Meier survival analysis. Patients with high levels of ALCAM transcript had significantly shorter survival (P=0.041).

Table 7.3 ALCAM expression, clinical and pathological factors in relationship with the survival of the patients

Factor	Univariate analysis		Multivariate analysis ^a	
	P value	HR	P value	HR ^b
ALCAM expression	0.005	3.000	0.023	5.485
Gender	0.268	1.456	0.915	1.075
Age	0.264	1.016	0.397	1.025
Tumour differentiation	0.138	1.293	0.930	1.029
Location of tumours	0.906	1.024	0.875	0.940
Local invasion	0.855	0.946	0.713	0.666
Nodal involvement	0.005	2.750	0.187	2.578
TNM staging	0.147	1.509	0.441	3.020

^a Cox Regression model against pancreatic related death; ^b Hazard Ratio.

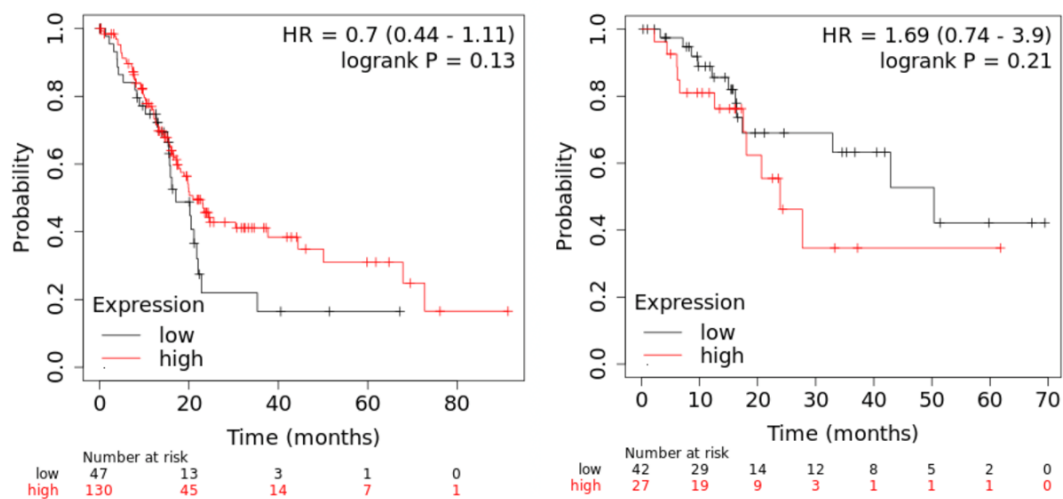


Figure 7.4 TCGA dataset of ALCAM transcription expression in human pancreatic cancer detected by RNAseq (www.kmplot.org) for overall survival (OS) (n=207) (Left) and relapse free survival (RFS) (n=69) (right). Patients with high levels of ALCAM had a median overall survival of 20.9 months compared with 17.03 months for those with low levels (p=0.21). In contrast and statistically non-significant fashion, patients with high levels of ALCAM had a median relapse free survival of 23.9 months compared with 50.4 months for those with low levels (p=0.21) (Nagy et al. 2021).

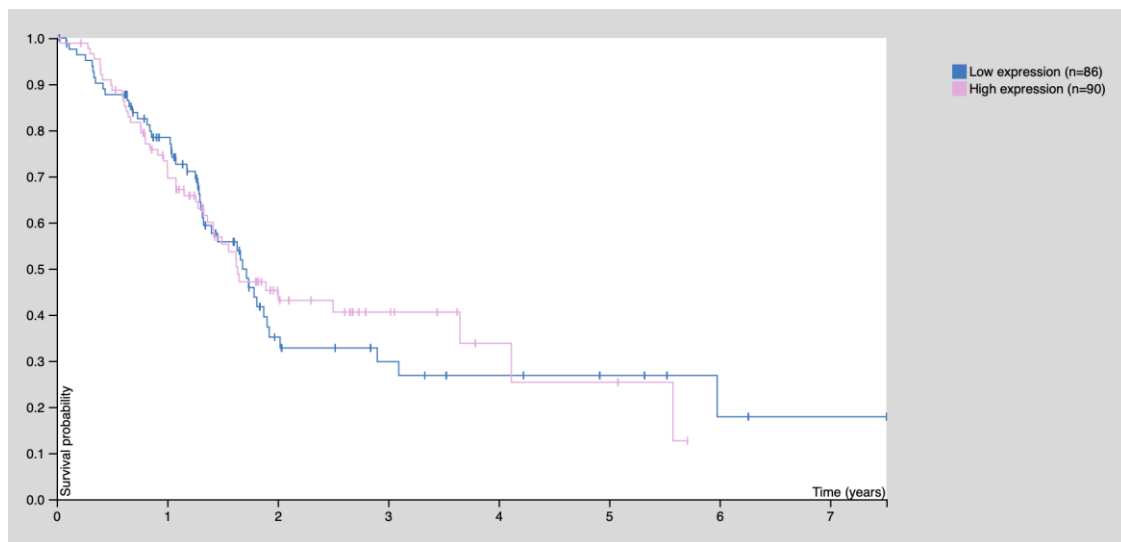


Figure 7.5 ALCAM protein expression in pancreatic adenocarcinoma from the protein atlas dataset (n=176) (Uhlen et al. 2017) (www.proteinatlas.org). Cut-off point was median level. p=0.88.

7.3.4 ALCAM expression and link to tumour vascular embolism

Our data has further revealed that tumours with cancer emboli in microvessels had significantly higher levels of ALCAM compared to those without ($p=0.021$) (Figure 7.6A). It was further revealed that the presence of microvessel emboli had a significant impact on the overall survival of the patients (Figure 7.6B). ROC analysis (Figure 7.6C) showed that the levels of ALCAM had a significant value in predicting the presence of embolism (AUC=0.613, $p=0.013$).

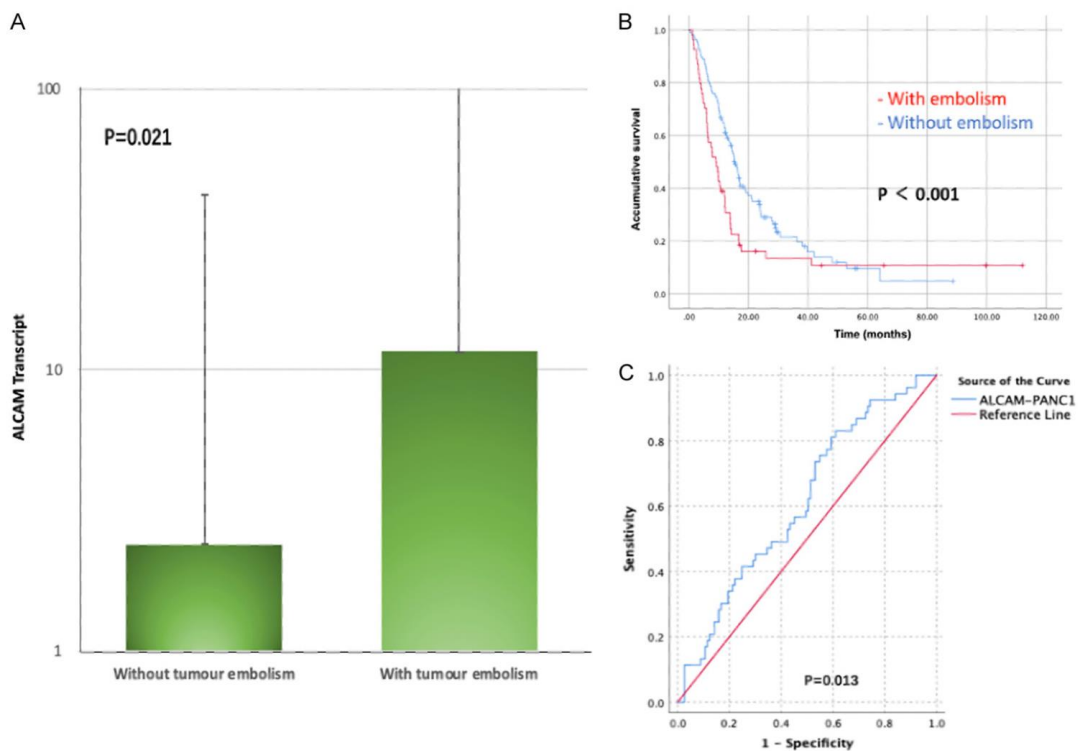


Figure 7.6 A: Levels of ALCAM in tumour without and with microvessel emboli. $p=0.021$ by Mann-Whitney U test. B: relationship between the presence of microvessel embolism and survival of the patients. C: Levels of ALCAM had a significant value in predicting tumour microvessel embolism (AUC=0.613, $p=0.013$).

7.3.5 Creation of cell models from pancreatic cancer cells and vascular endothelial cells that differentially express ALCAM and the impact on pancreatic cancer cells

With the findings that both ALCAM and tumour embolism were significantly linked to clinical outcome, and that levels of ALCAM had significant connection with the presence of embolism, we sought to explore if levels of ALCAM in pancreatic cancer cells and in vascular endothelial cells may contribute to the tumour-endothelial interactions, a significant factor leading to formation of tumour embolism. PANC-1 cancer cells had positive expression of ALCAM, in contrast to Mia PaCa-2 which was weakly positive for ALCAM. Using anti-ALCAM shRNA, we created PANC-1 knockdown sub model, designated here as PANC1^{ALCAMkd}, together with a transfection control (designated as PANC1^{control}) (Figure 7.7). Similarly, we created an ALCAM over-expression subline from Mia PaCa-2 cell line with a respective control that are designated as MiaPaCa-2^{ALCAMexp} and MiaPaCa-2^{control}.

Using an automated cell analyser, it was clearly demonstrated that loss of ALCAM in PANC1^{ALCAMkd}, resulted in significant reduction in both cell adhesion (left) and migration (right) (Figure 7.8 top). In a less striking contrast to PANC-1 cells, over expression of ALCAM in Mia PaCa-2 cells resulted in cells being more adhesive (left) and less mobile (right), although the difference is not highly significant (Figure 7.8 bottom).

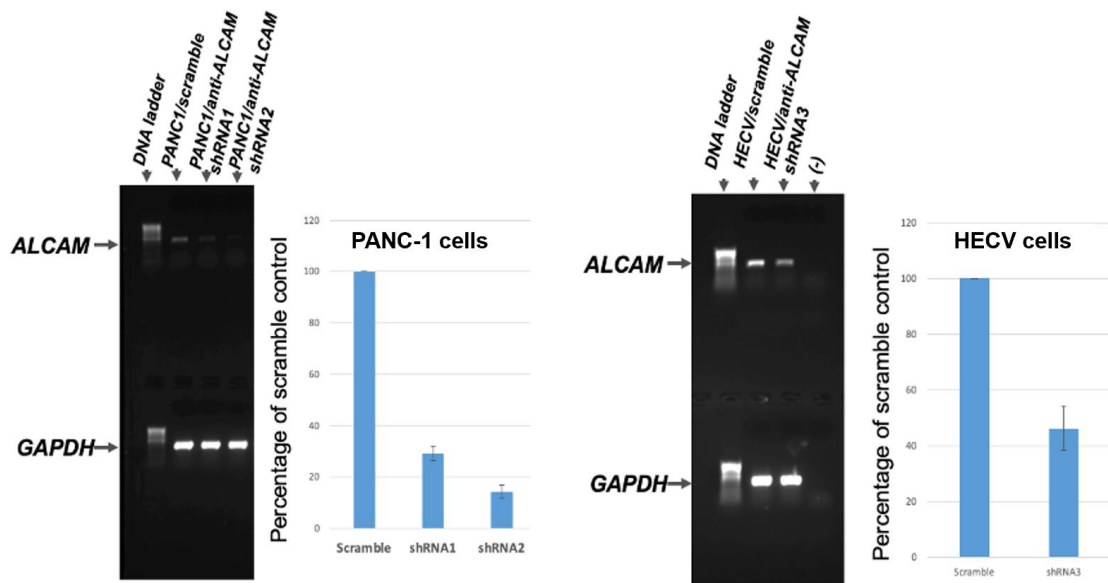


Figure 7.7 Creation of pancreatic and endothelial cell models. Expression of ALCAM in the cells were verified by PCR.

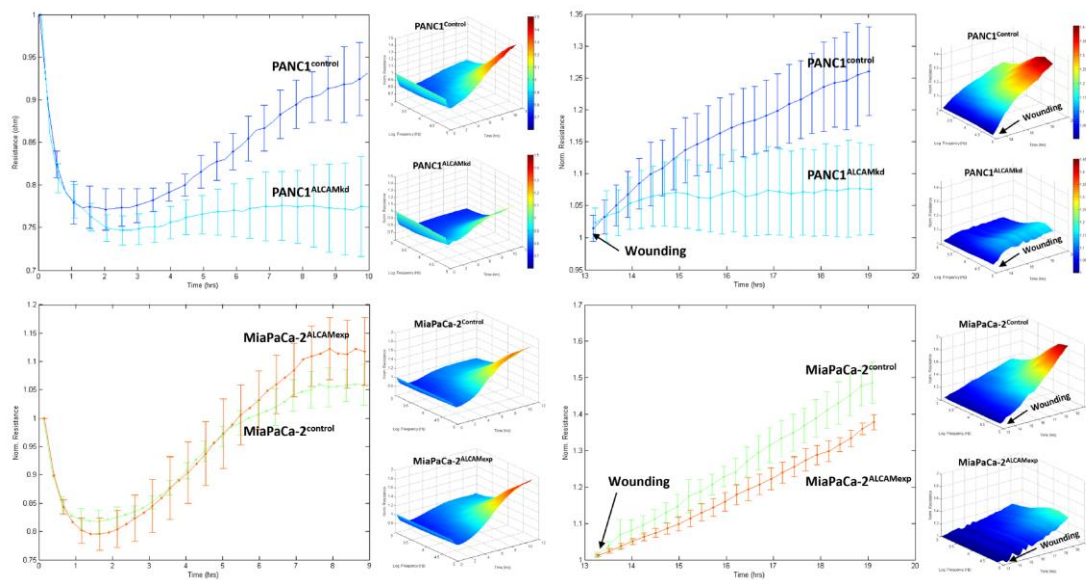


Figure 7.8 ALCAM differential expression, cell adhesiveness and migration as detected by ECIS. Top panel: PANC1 cells; Bottom Panel: Mia PaCa-2 cells. Left: cell adhesiveness; Right: Wounding assay for cellular migration.

7.3.6 ALCAM expression in endothelial cells and in pancreatic cancer cells, the impact on tumour-endothelial interactions

We conducted a direct tumour-endothelial interaction assay to determine how expression of ALCAM in vascular endothelial cells influences the interaction and adhesiveness between the two cell populations. As shown in Figure 7.9, knockdown of ALCAM from PANC-1 cells significantly reduced the adhesion of cancer cells to endothelial cells. In contrast, over-expression of ALCAM in Mia PaCa-2 cells significantly increased the adhesiveness between the two cell types. It was also demonstrated that soluble ALCAM (sALCAM) at a higher concentration blocked this interaction to a significant degree.

The tumour-endothelial interactions affected by ALCAM expression were similarly reproduced in the ECIS based cell-cell interaction assay, in that loss of ALCAM in endothelial cells resulted in a rapid rise of capacitance when the PANC-1 cancer cells were added. It is noteworthy that when both PANC1 and HECV cells were knocked down for ALCAM, the capacitance reached the maximum (Figure 7.10). To confirm the reproducibility of the knockdown, we tested two separate shRNAs, which showed a reproducible outcome.

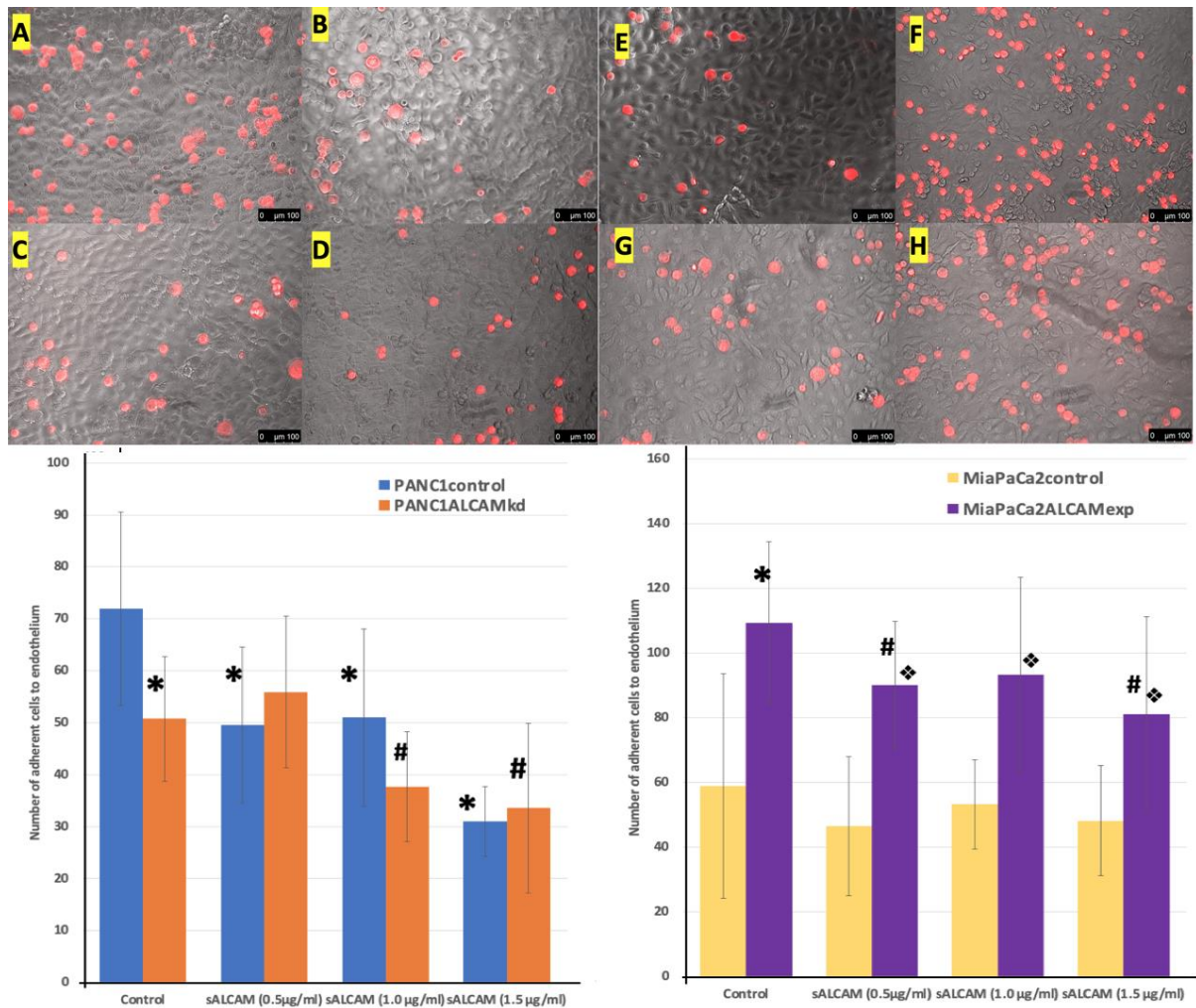


Figure 7.9 Top panel: images showing adherence of PANC1 (A-D) and Mia PaCa-2 (E-H) cells to endothelial cells. A/C and E/G are the respective control cells. B/D and F/G are ALCAM knockdown cells. Top row (A/B/E/F) are control treatment; Bottom row (C/D/G/H) are cells treated with 1.0 μg/ml sALCAM. Red coloured cells are the respective cancer cells labelled with DiI. The background cells are endothelial cells. Bottom: Graphical representation of pancreatic cancer cells adherence to endothelial cells. Left: * vs PANC1^{control} without treatment; # vs PANC1^{ALCAMkd} without treatment. Right: * vs Mia PaCa-2^{control} without treatment; # vs Mia PaCa-2^{ALCAMexp} without treatment; ✦ vs Mia PaCa-2^{control} with similar sALCAM concentration.

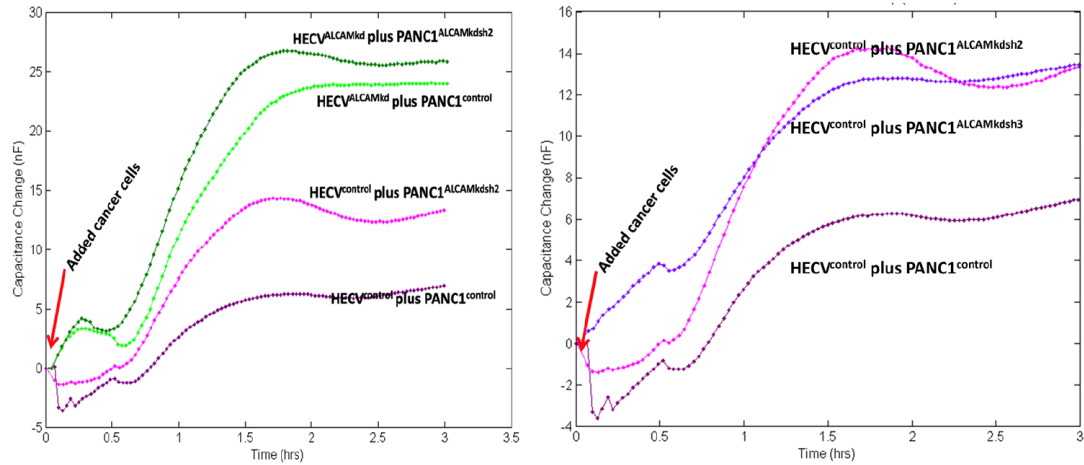


Figure 7.10 ECIS based analyses of tumour-endothelial cell interaction. Shown are two ALCAM knockdown cell models over endothelial cells which also had ALCAM expression modified.

7.4 Discussion

In this Chapter, we have explored the expression pattern of ALCAM in pancreatic adenocarcinoma and the link with the clinical outcome. The above results demonstrated that ALCAM acted as a tumour promoter in pancreatic cancer tissue in multiple terms:

1. ALCAM transcript levels in the pancreatic cancer cohort were increased in pancreatic tumour tissues compared with normal tissues, and this increase in tumour tissues was particularly high in tumours from patients who died from pancreatic cancer. Collectively, raised levels of ALCAM transcript presented an independent prognostic factor for overall survival of the patients.
2. Hormone producing endocrine tumours of pancreas, pancreatic islet tumours, had less ALCAM protein compared with non-endocrine pancreatic ductal carcinoma.
3. The levels of ALCAM in pancreatic cancer are linked with the presence of vessel embolism, and that vessel embolism and ALCAM are clearly linked with the survival of the patients.

4. The immunohistochemical staining of ALCAM in the pancreas TMA was higher in pancreatic tissues compared to normal tissue.
5. ALCAM in both pancreatic cancer cells and endothelial cells is a key determining factor for cancer-endothelial cell adhesion in the cell adhesion assays, using ALCAM manipulated cell models.

The oncogenic effect of ALCAM in pancreatic cancer we found seems in contrast with our previous results in breast cancer and pituitary tumours, namely patients with higher levels of ALCAM tend to have longer survival. Amantini *et al.*, (Amantini et al. 2019) reported that in a pancreatic ductal adenocarcinoma cohort, circulating cancer cells had higher levels of ALCAM message, along with a few other markers, than tumour cells at the primary site and, that when circulating cancer cells had high levels of ALCAM, patients tended to have significantly shorter survival. In a sharp contrast to that in pancreatic adenocarcinoma, ALCAM in endocrine tumours from the pancreas, namely pancreatic neuroendocrine tumours (PNET), was found to be a favourable prognostic factor for both recurrence free survival and disease specific survival (n=38) (Hong et al. 2010; Tachezy et al. 2011). The same was seen in the present study in that the endocrine islet tumour of the pancreas had significantly lower levels of ALCAM protein staining than the non-endocrine ductal carcinoma of the pancreas. In fact, a number of studies have indicated that high levels of ALCAM in endocrine-related cancers, including breast (Ihnen et al. 2010b; Burandt et al. 2014), prostate (Minner et al. 2011) and thyroid (Chaker et al. 2013) are linked to favourable outcome of the patients, and less bony metastasis. However, high levels of ALCAM in cancer cells and tissues often leads to poor clinical outcome for the patients in non-endocrine related cancers, including cancers derived from squamous cell lineages (namely squamous cell carcinoma) in skin and oesophagus (Verma et al. 2005; Tachezy et al. 2012a) as well as in malignant melanoma (Donizy et al. 2015), gastrointestinal cancers (Tachezy et al. 2012b; Hansen et al. 2013; Ye et al. 2015) and neurological malignancies (Kijima et al. 2012). The present study, together with

those demonstrated in the literature has shown indeed those endocrine tumours, including that of pancreas, have a differing and contrasting ALCAM expression from non-endocrine tumours. From previous studies and our results, we may preliminarily conclude that in most endocrine-related cancers, especially breast cancer, ALCAM is a positive prognostic factor for cancer patients' survival and the relationships between ALCAM and the clinical course of the patients are in contrast to non-endocrine related cancers. This strongly suggests that the endocrine system plays an important role in ALCAM mediated tumour progression. However, the reason behind the difference between endocrine-related cancers and other solid cancers remains unknown and makes it a very fertile area of research in the future.

CHAPTER-8

General discussion

8.1 Aims of the study

Activated leukocyte cell adhesion molecule (ALCAM) is a member of cell adhesion molecules which belongs to the immunoglobulin superfamily. Numerous studies have demonstrated that ALCAM regulates cell adhesion and migration in multiple cancer types and is strongly correlated with cancer patients' survival and prognosis, especially in breast cancer. The previous study from the host laboratory (King et al. 2004) has shown that patients with higher levels of ALCAM had longer survival compared with those who had lower ALCAM expression. Another previous study from the host laboratory (Davies et al. 2008) demonstrated that reduced ALCAM expression in breast cancer was associated with bone metastasis.

Hence, we hypothesised that ALCAM had an important regulatory role with respect to bone metastasis in endocrine-related cancers. This endocrine regulation is of particular importance in breast cancer, in which ALCAM has correlated with hormone receptor status and can influence the patient's survival and prognosis. We further speculated that the intracellular signalling interplay between ALCAM complex and hormonal receptors is key to this interplay. Thus, the aim of the study, firstly, was to fully explore the molecular correlation between ALCAM and its hormone receptors (ER), along with other partners, in the context of survival benefits and bone metastasis. The study also aimed to recruit additional cohorts (pituitary and pancreatic cancer cohort) beyond breast cancer, to validate our findings in both endocrine and non-endocrine related cancer types, and further establish a role between ALCAM and bone metastasis and clinical outcomes. Another vital part of the study was to establish cellular mechanisms of ER interaction with ALCAM and how this influences the establishment of breast cancer cells in the bone microenvironment. Finally, we aimed to explore the influence of ALCAM on effectiveness of chemotherapy treatments and the effect of this on breast cancer metastasis.

8.2 Clinical implication of ALCAM in endocrine related cancer (breast and pituitary tumour)

It has been reported by studies from the host laboratory that ALCAM has a clear relationship with breast cancer patients' survival and bone metastasis of breast cancer. In Chapter 3, to further explore such a relationship, we performed ROC analysis using the same breast cancer cohort, which showed that ALCAM had a reasonable predictive value towards the development of bone metastasis. The comparison of ALCAM expression levels between different receptor statuses subgroups of breast cancer showed that no clear expression difference of ALCAM was seen between ER positive and negative, as well as HER2 positive and negative breast cancer patients.

To investigate the prognostic impact of ALCAM on breast cancer patients in relation to hormone receptors, we separated the cohort into different subgroups based on their receptor status (ER and HER2) and conducted survival analysis respectively using both the Cardiff breast cancer cohort and a cohort from TCGA online database. The results suggested that the effects of ALCAM on survival were seemingly opposite in patients with different ER statuses. HER2 status was also found to be of importance to the correlation of ALCAM and breast cancer patients' prognosis.

When considering the importance of ALCAM in clinical cancer and as reported in the literature, one must consider the role of the circulating soluble ALCAM. As discussed in the introduction, soluble ALCAM (sALCAM) is an ectodomain cleavage product by proteinases. sALCAM frequently acted as an antagonist to ALCAM mediated functions, by interacting with ALCAM and blocking the homotypic ALCAM-ALCAM interactions. Here, I also conducted ELISA assays to explore the effect of circulating ALCAM in patients with breast cancer, by using the breast cancer serum cohort. The comparison of the serum level of ALCAM found differences among tumour stages, but no significant difference was observed between the ER positive and ER negative

group, as well as HER2 positive and negative group. This is possibly owing to the relatively small size of the patient samples and there is a possibility that, with a much larger cohort, certain significance may be established. However, the other possibility also holds true that sALCAM may not be a highly aberrant feature in patients with breast cancer and that it is the mature intact membrane ALCAM may hold a stronger impact on the progression and metastasis of breast cancer.

In addition to breast cancer, I also analysed another endocrine tumour, available to my study from the host laboratory, namely a pituitary cohort as a supplementary part of the study. This was to establish if the ALCAM and endocrine related cancer connection may hold true in an independent endocrine cancer type. The effect of ALCAM in pituitary tumour appeared to be similar to that in breast cancer. High levels of ALCAM were associated with adjacent bone invasion, indicating that ALCAM related bone metastasis did not confine to a specific tumour type, but existed in a wider endocrine context.

8.3 Signalling events underlying ALCAM and their involvement in hormonal receptor related bone metastasis of breast cancer

From the previous study and analysis of clinical cohorts, as presented in Chapter 3, it was clear that ALCAM indeed has an important connection to bone metastasis and this connection has an endocrine and hormone receptor dimension. In Chapters 4 and 5, I further advanced the scientific exploration by creating cell models with differential expression of ALCAM from cell lines with varying hormonal receptor status. These cell models have shown to be highly valuable in exploring mechanisms underlying the action of ALCAM in these cells, with different hormone receptor status. Using an ALCAM manipulated cell model has been particularly fruitful in exploring the potential protein interacting partners of ALCAM, as well as the

molecular pathways underlying ALCAM, and their involvement in hormonal receptor related bone metastasis of breast cancer.

The PCR results showed that ALCAM expression was positive in all nine breast cancer cell lines available in the laboratory. MCF-7 was selected as an ER positive/HER2 negative cell line, MDA-MB-361 was selected as an ER positive/HER2 positive cell line and MDA-MB-231 was selected as an ER negative/HER2 negative cell line to create ALCAM knockdown models. The transfection efficiency was verified at both gene and protein level.

Cell growth assays were conducted based on the ALCAM knockdown model mentioned above. Bone matrix extract was used to mimic the skeletal microenvironment *in vitro*. The results showed that the cell growth rates of ALCAM knockdown breast cancer cells, including both ER positive and negative ones, were higher than cells in the control group. The skeletal microenvironment did not influence the growth-promoting effect of ALCAM on breast cancer cells. This is an intriguing finding because ALCAM tended to be a tumour suppressor in endocrine related cancer, especially in breast cancer, according to previous research and our analysis of clinical cohort data in Chapter 3. This indicated the complexity of the regulatory role of ALCAM in cancer progression.

Protein samples from both ER positive and ER negative ALCAM knockdown cell models were collected and Kinexus™ protein microarray analysis was performed. This antibody-based analysis could present a comprehensive view of protein/kinase interaction change following ALCAM knockdown. There are a rather large number of protein kinases, showing a vigorous response, following ALCAM knockdown. One of the protein kinases stood out as being highly responsive, namely the MET proto-oncogene which is the receptor for hepatocyte growth factor (HGF). Here, MET showed opposite changes following ALCAM knockdown between ER positive and negative cell models. Next, we performed immunoprecipitation assays to validate

the protein interaction between ALCAM and MET. The immunoprecipitant of ALCAM and MET could be observed in MDA-MB-361 and MDA-MB-231 cell lines, indicating a clear cellular interaction between ALCAM and MET.

Finally, I selected an ECIS assay, a highly versatile, automated and human interface free method, to further analyse the effect of ALCAM, together with its protein partners, on the adhesion of breast cancer in both normal and bone microenvironments. In this section, MET inhibitor and HGF were used to either inhibit or activate the HGF/MET pathway. ROCK inhibitor was used to inhibit a Rho-associated serine/threonine kinase, ROCK, which proved to be a vital member of the HGF/MET pathway and also showed contrasting changes, following ALCAM knockdown, in Kinexus protein microarray analysis. A widely used anti-HER2 therapy drug, Neratinib, was also introduced in the assay to assess the correlation between HER2 and ALCAM-mediated cell adhesion. The ECIS results showed that the cell adhesion in MDA-MB-231 cells was clearly reduced in the ALCAM knockdown group, while in ER positive breast cancer cell lines, such as MCF-7 and MDA-MB-231, no cell adhesion change was observed as detected by ECIS. This finding indicated that ALCAM could have different effects on cell adhesion between ER positive and ER negative breast cancer. In addition, when the cells were treated with MET inhibitor and HGF, the cell adhesion ability of the ALCAM knockdown group was increased compared with control group instead. The same phenomenon could also be found in the group treated with ROCK inhibitor and Neratinib. In the groups with BME, although some differences between groups did reach statistical significance, we were unable to come to a conclusion with sufficient consistency. Thus, in the context of bone microenvironment and development of bone metastasis, it is likely that other bone microenvironment factors such as stromal cells (including osteocyte, osteoblast and osteoclast, fibroblast, etc.) and minerals should be considered alongside the protein BME as used in the present study. This would be a highly intriguing research direction in the future.

From the above results, we can draw a conclusion that ALCAM has a clear intracellular link with MET and its ligand HGF, while further study is required in terms of the specific mechanism behind this. Our preliminary conjecture focuses on the ERM protein family, a group of actin cytoskeleton linker molecules which plays a key role in the regulation of cell signalling and cytoskeleton in cancer progression.

The ERM (Ezrin-Moesin-Radixin) protein family is a small protein family that are also distantly linked to Merlin, EHM2. This protein family is also frequently referred to as the membrane subcoat proteins or membrane ruffling proteins. They play a vital role to link certain essential transmembrane proteins to the cytoskeleton, for example linking CD44 and ICAM to actin filaments. The other key function is the ability of the family members to translocate to the membrane of regions where cell membrane ruffles and cell migration take place. It has been shown that the ERM protein family are involved in both ALCAM and HGF/MET signalling pathways. As discussed in Chapter 1, ALCAM lacks a direct actin-binding site, and its cytoplasmic tail could be connected to the cytoskeleton via the ERM family member Ezrin (Tudor et al. 2014). In terms of the relationship between HGF/MET and ERM, Hasenauer and colleagues (Hasenauer et al. 2013) found out that the binding between Ezrin and CD44v6 mediated the internalization of MET. Work by Sperka *et al.*, (Sperka et al. 2011) showed that the activation of Ras, which is a major downstream signalling molecule of MET, requires the essential participation of ERM proteins. Similarly, Orian-Rousseau *et al.*, (Orian-Rousseau et al. 2002) demonstrated that the presence of binding between CD44 cytoplasmic domain and ERM proteins, was required in signal transduction from activated MET to MEK and ERK. Another aspect that deserves attention is the correlation between the ERM family and ER/HER2. Work by Yu and colleagues (Yu et al. 2019) showed that Moesin, another ERM family member, was an independent prognostic marker for ER positive breast cancer. Asp *et al.*, (Asp et al. 2016) demonstrated that ERM family members Ezrin and Radixin interacted with ErbB2 receptors/ HER2 at the plasma membrane, and the inhibition or depletion of

ERM proteins resulted in the reduced cellular levels of HER2 in breast cancer cell lines.

In conclusion, ALCAM can mediate cell adhesion in both normal and the mimicked bone metastasis microenvironment in breast cancer cells with different receptor statuses, and this biological function is associated with the link between ALCAM and MET. Our speculation about ALCAM and MET interaction is summarized in Figure 8.1.

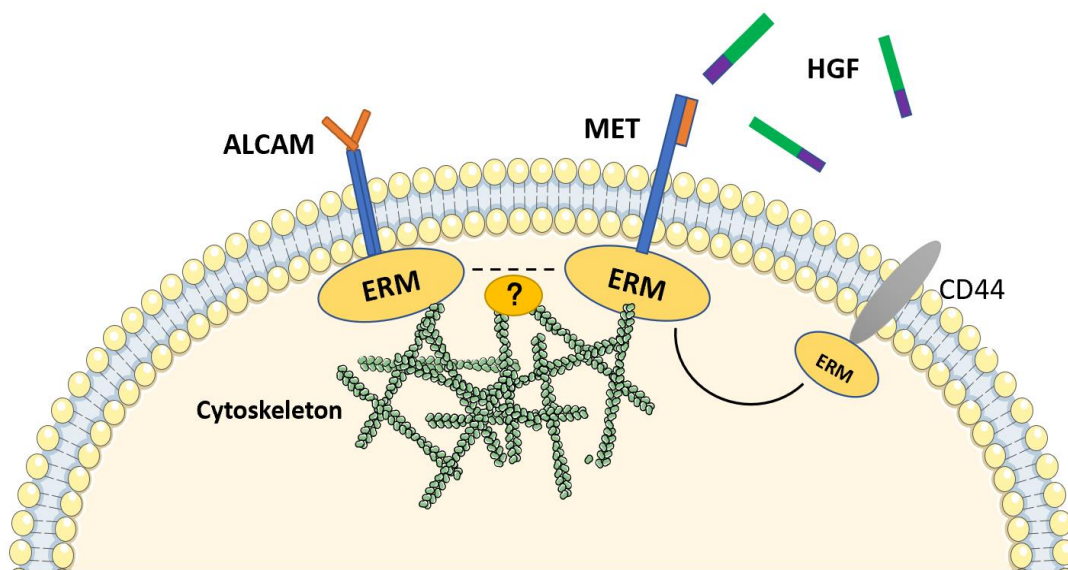


Figure 8.1 Possible molecular mechanism between ALCAM and MET interaction. Both ALCAM and MET have been shown to interact with scaffold protein ERM and anchor with actin cytoskeleton. The molecular mechanism of ALCAM-MET interaction could derive from the membrane relocation mediated by ERM and cytoskeleton.

8.4 Effect of ALCAM on chemotherapy drugs of breast cancer

The study results from Chapter 4 and 5 elucidated the effect of ALCAM in breast cancer cells with different receptor statuses, together with its potential signalling molecules. Moving forward, I explored the effect of ALCAM on chemotherapy drug resistance in breast cancer cells with different hormonal receptor statuses. The effect of ALCAM expression level on chemotherapy curative effect has been

demonstrated by previous studies (Chen et al. 2017; Darvishi et al. 2020). To validate such association, four representative chemotherapy drugs, namely Paclitaxel, Docetaxel, Cisplatin and Gemcitabine were used in drug toxicity assays. Bone matrix extract was used to mimic the microenvironment of bone metastasis. The drug toxicity assay showed that the drug sensitivity of Docetaxel increased following ALCAM knockdown in MDA-MD-231 cells (ER negative) with and without BME, while in ER positive breast cancer cell lines, no significant difference could be observed between control and ALCAM knockdown groups. The difference could also be observed when the cells were treated with BME. These results indicated that ALCAM expression could have different effects on drug sensitivity between ER positive and ER negative cells.

The breast cancer cohort with associated treatment data, from online datasets ROC plotter, was also analysed in the Chapter. The results showed that ALCAM had a significant effect on drug responsiveness in both chemotherapy and anti-HER2 therapy. In ER positive breast cancer, higher levels of ALCAM expression were found in the Taxane responder groups, but such results did not appear in ER negative breast cancer. Similarly, the Taxane responder group had higher ALCAM expression in HER2 negative breast cancer but lower ALCAM expression in HER2 positive breast cancer. These results not only further validated our findings in the *in vitro* assays we performed in section 6.3.1, but also revealed a potential correlation between ALCAM and HER2 in terms of drug responsiveness.

8.5 ALCAM in non-endocrine related cancer (pancreatic cancer)

In Chapter 3, we have demonstrated that breast cancer patients with higher levels of ALCAM had significantly longer survival, and the reduced ALCAM expression led to the development of bone metastasis. The study has also presented that, in another endocrine related cancer, namely pituitary tumours, ALCAM also acted as an

inhibitory factor to bone metastasis from pituitary tumours. Together with reports indicating the possibility that ALCAM acts as a good prognosis factor in other endocrine related cancers, namely thyroid cancer (Chaker et al. 2013), prostate cancer (Minner et al. 2011), and the neuroendocrine tumours of pancreas (Hong et al. 2010; Tachezy et al. 2011). Hence, the final part of the study was to explore whether ALCAM played a different role in non-endocrine related cancers, namely pancreatic ductal carcinoma, compared to endocrine related cancer types.

The IHC staining in pancreatic TMA showed that adjacent normal pancreas tissue had significantly lower levels of ALCAM staining compared to ductal adenocarcinoma. The staining of islet tumours, hormone producing endocrine tumours of pancreas, showed significantly lower levels of ALCAM staining compared with pancreatic ductal carcinoma.

In the pancreatic cohort analysis, the ALCAM expression in tumour tissue was significantly higher than normal tissue, and the ALCAM expression was also higher in patients who died of pancreatic cancer compared to those who lived. Survival analysis showed that patients with higher levels of ALCAM had significantly shorter overall survival. The data further revealed that tumours with cancer emboli in microvessel had significantly higher levels of ALCAM compared to those without.

Next, we created ALCAM manipulated cell models in both pancreatic cancer cells (PANC-1 and Mia PaCa-2) and human vascular endothelial cells (HECV) to explore the effect of ALCAM on the adhesion between cancer cells and endothelial cells. The ECIS results showed that reduced expression of ALCAM led to the decrease of cancer cell adhesion to vascular endothelial cells. The Dil staining assays showed that the number of adhered cancer cells significantly decreased following ALCAM knockdown.

From the above results we can see that ALCAM clearly acts as a tumour promoter in pancreatic cancer tissues. In fact, many previous studies have demonstrated that high levels of ALCAM in cancer cells and tissues often leads to poor clinical outcome for the patients in non-endocrine related cancers, including cancers derived from squamous cell lineages (namely squamous cell carcinoma) in skin and oesophagus (Verma et al. 2005; Tachezy et al. 2012a) as well as in malignant melanoma (Donizy et al. 2015), gastrointestinal cancers (Tachezy et al. 2012b; Hansen et al. 2013; Ye et al. 2015) and neurological malignancies (Kijima et al. 2012). These findings in non-endocrine related cancers are in contrast with the results in breast cancer (a typical member of endocrine related cancer) as outlined in the previous chapter, which strongly suggests that the endocrine system plays an important role in ALCAM-mediated tumour progression.

The reason why ALCAM has different expression pattern between breast cancer and pancreatic cancer is still unclear. Although the key aims of the study was to establish the impact of differing levels of ALCAM on cells and disease progress, it is interesting to consider the possible mechanisms by which ALCAM is expressed in contrast pattern in different cancer type, a task unable to be addressed in the present study. However, given the established knowledge on gene expression and gene transcription, to look at the DNA methylation pattern of the *ALCAM* gene promoter would be interesting. DNA methylation is an epigenetic mechanism widely exist in mammals' cells. It regulates gene expression by inhibiting the binding of transcription factors to DNA or by recruiting proteins involved in gene repression (Moore et al. 2013). Although DNA methylation is out of the scope of this study, I made use of online database TCGA to explore the correlation between DNA methylation of ALCAM and ALCAM mRNA in breast and pancreatic cancer. As shown in Figure 8.2, no statistical correlation was shown in both two cancer types, indicating that the different expression and biological function of ALCAM in breast and pancreatic cancer might not appear to be relevant to DNA methylation of the *ALCAM* gene promoter, although more research here is necessary.

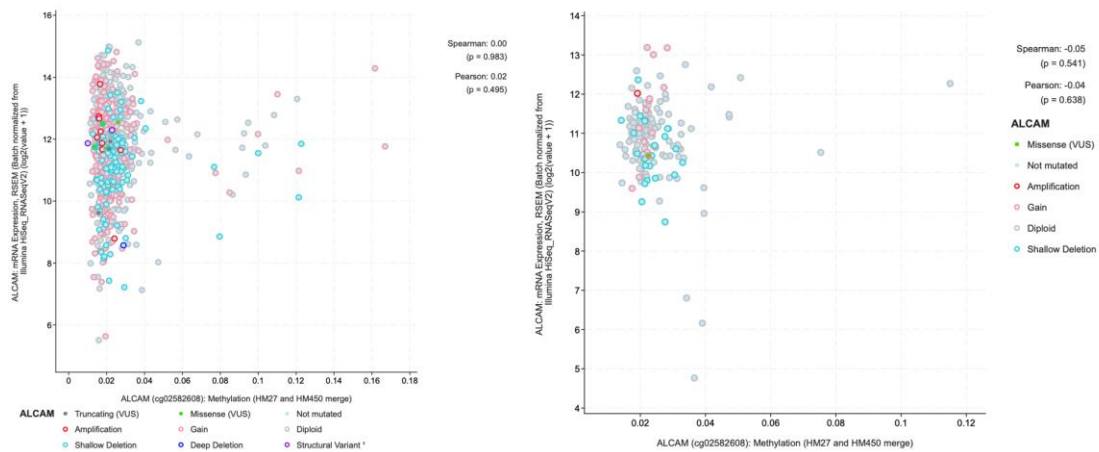


Figure 8.2 The correlation between DNA methylation and mRNA of ALCAM in breast cancer (left, $p=0.495$) and pancreatic cancer (right, $p=0.638$) from the TCGA pan-cancer cohort (www.cBioportal.org).

From previous studies and our results, we may preliminarily conclude that in most endocrine-related cancers, especially breast cancer, ALCAM is a positive prognostic factor of cancer patients' survival and the relationships between ALCAM and the clinical course of the patients are in contrast to non-endocrine related cancers.

8.6 Conclusion and future work

From the data presented in this thesis, it can be concluded that:

1. In most endocrine-related cancers, especially breast cancer, ALCAM acts as an inhibitory factor to bone metastasis and is a positive prognostic factor of cancer patients' survival, and the relationships between ALCAM and the clinical course of the patients are in contrast to non-endocrine related cancers.
2. ALCAM has different biological effects in breast cancer cell lines with different ER statuses, in both normal and mimicked bone microenvironments, and MET is found to be a vital signalling molecule of ALCAM.

3. ALCAM can influence the drug sensitivity of chemotherapy drugs in certain subgroups of breast cancer and that this influence is hormone receptor dependent.

As stated in the preface, my study began in the midst of the COVID19 pandemic and national lockdown. My early part of the study could only be carried out under restrictions which severely reduced laboratory time. Although the University and host laboratory had given its highest possible support to enable me carry out as much experimental work as the system and guidelines permitted, for which I am sincerely grateful, there are a few key experiments that were no longer able to be conducted due to time limitations. This includes planned *in vivo* tumour models for metastasis and *in vivo* evaluation of drug sensitivity. A number of interesting leads from the study are now beyond my tenure of the project. I have summarised these interesting leads in the following sections for future studies.

First, the molecular mechanism of the interaction between HGF/MET pathway and ALCAM.

In Chapter 5 MET was shown to have either direct or indirect molecular interaction with ALCAM, but the specific mechanism behind this remains unclear. Our preliminary speculation focussed on the ERM protein family, a group of actin cytoskeleton linker molecules, which is proved to be strongly correlated with both the HGF/MET pathway and ALCAM, as well as ER and HER2. The scientific questions are therefore: could the ERM proteins shuttle response proteins between the HGF/MET complex and ALCAM? Are there intermediate signalling proteins participating? What are the specific sites of MET and ALCAM responsible for these links? This speculation needs further work to demonstrate.

Second, the relationship between ALCAM and HER2.

In Chapter 3, the survival analysis showed that, similarly with ER, the survival implication of ALCAM is different between patients with different HER2 status. In Chapter 5, I found out that anti-HER2 drugs could have an effect on ALCAM-mediated cell adhesion. In Chapter 6 the analysis of breast cancer drug treatment cohort from online datasets also showed intriguing implications, in terms of HER2 and ALCAM. While the present study mainly focussed on the involvement of ALCAM in the endocrine pathway. The link between ALCAM and HER2 in breast cancer would be a fertile and fruitful area to explore, in the laboratory and in clinical research.

Third, the correlation between ALCAM and CD6.

As discussed in Chapter 1, ALCAM regulates cell to cell adhesion in two ways: Homotypic and Heterotypic interaction, and CD6 is a major heterotypic interacting partner. Whilst the significance of the impact of ALCAM-CD6 interaction, and disruption of this interaction in the context of cancer, has existed for two decades, recent findings show that disruption of this important interaction may well favour an anti-cancer related consequence (Simoes et al. 2020; Allison 2022; Chalmers et al. 2022). This interaction has not been the topic of my study. However, the findings from my study, together with these recent discoveries, have significant value in devising new studies to explore if disruption of the ALCAM-CD6 interaction indeed present a new opportunity for cancer therapies.

Chapter-9

References

Achiha, T. et al. 2020. Activated leukocyte cell adhesion molecule expression correlates with the WNT subgroup in medulloblastoma and is involved in regulating tumor cell proliferation and invasion. *PLoS One* 15(12), p. e0243272. doi: 10.1371/journal.pone.0243272

Al-Shehri, F. S. and Abd El Azeem, E. M. 2015. Activated Leukocyte Cell Adhesion Molecule (ALCAM) in Saudi Breast Cancer Patients as Prognostic and Predictive Indicator. *Breast Cancer (Auckl)* 9, pp. 81-86. doi: 10.4137/BCBCR.S25563

Allison, S. 2022. ALCAM-CD6 in lupus nephritis. *Nat Rev Nephrol* 18(3), p. 137. doi: 10.1038/s41581-022-00548-1

Amantini, C. et al. 2016. Capsaicin triggers autophagic cell survival which drives epithelial mesenchymal transition and chemoresistance in bladder cancer cells in an Hedgehog-dependent manner. *Oncotarget* 7(31), pp. 50180-50194. doi: 10.18632/oncotarget.10326

Amantini, C. et al. 2019. Expression Profiling of Circulating Tumor Cells in Pancreatic Ductal Adenocarcinoma Patients: Biomarkers Predicting Overall Survival. *Front Oncol* 9, p. 874. doi: 10.3389/fonc.2019.00874

Andisheh-Tadbir, A. et al. 2015. Clinical implication of CD166 expression in salivary gland tumor. *Tumour Biol* 36(4), pp. 2793-2799. doi: 10.1007/s13277-014-2905-x

Arnold Egloff, S. A. et al. 2017. Shed urinary ALCAM is an independent prognostic biomarker of three-year overall survival after cystectomy in patients with bladder cancer. *Oncotarget* 8(1), pp. 722-741. doi: 10.18632/oncotarget.13546

Asp, N. et al. 2016. Regulation of ErbB2 localization and function in breast cancer cells by ERM proteins. *Oncotarget* 7(18), pp. 25443-25460. doi: 10.18632/oncotarget.8327

Atukeren, P. et al. 2017. Evaluation of ALCAM, PECAM-1 and selectin levels in intracranial meningiomas. *Clin Neurol Neurosurg* 160, pp. 21-26. doi: 10.1016/j.clineuro.2017.06.002

Badic, B. et al. 2019. Radiogenomics-based cancer prognosis in colorectal cancer. *Sci Rep* 9(1), p. 9743. doi: 10.1038/s41598-019-46286-6

Bartolome, R. A. et al. 2020. SOSTDC1 promotes invasion and liver metastasis in colorectal cancer via interaction with ALCAM/CD166. *Oncogene* 39(38), pp. 6085-6098. doi: 10.1038/s41388-020-01419-4

Blake, M. L. et al. 2014. RANK expression on breast cancer cells promotes skeletal metastasis. *Clin Exp Metastasis* 31(2), pp. 233-245. doi: 10.1007/s10585-013-9624-3

Bologna, S. B. et al. 2013. Adhesion molecules in primary oral mucosal melanoma: study of claudins, integrins and immunoglobulins in a series of 35 cases. *Am J Dermatopathol* 35(5), pp. 541-554. doi: 10.1097/DAD.0b013e318276cab3

Bowen, M. A. et al. 1997. Characterization of mouse ALCAM (CD166): the CD6-binding domain is conserved in different homologs and mediates cross-species binding. *Eur J Immunol* 27(6), pp. 1469-1478. doi: 10.1002/eji.1830270625

Bowen, M. A. et al. 1996. The amino-terminal immunoglobulin-like domain of activated leukocyte cell adhesion molecule binds specifically to the membrane-proximal scavenger receptor cysteine-rich domain of CD6 with a 1:1 stoichiometry. *J Biol Chem* 271(29), pp. 17390-17396. doi: 10.1074/jbc.271.29.17390

Bowen, M. A. et al. 1995. Cloning, mapping, and characterization of activated leukocyte-cell adhesion molecule (ALCAM), a CD6 ligand. *J Exp Med* 181(6), pp. 2213-2220. doi: 10.1084/jem.181.6.2213

Bozovic-Spasojevic, I. et al. 2017. The Prognostic Role of Androgen Receptor in Patients with Early-Stage Breast Cancer: A Meta-analysis of Clinical and Gene Expression Data. *Clin Cancer Res* 23(11), pp. 2702-2712. doi: 10.1158/1078-0432.CCR-16-0979

Burandt, E. et al. 2014. Loss of ALCAM expression is linked to adverse phenotype and poor prognosis in breast cancer: a TMA-based immunohistochemical study on 2,197 breast cancer patients. *Oncol Rep* 32(6), pp. 2628-2634. doi: 10.3892/or.2014.3523

Burkhardt, M. et al. 2006. Cytoplasmic overexpression of ALCAM is prognostic of disease progression in breast cancer. *J Clin Pathol* 59(4), pp. 403-409. doi: 10.1136/jcp.2005.028209

Carbotti, G. et al. 2013. Activated leukocyte cell adhesion molecule soluble form: a potential biomarker of epithelial ovarian cancer is increased in type II tumors. *Int J Cancer* 132(11), pp. 2597-2605. doi: 10.1002/ijc.27948

Cenciarini, M. E. and Proietti, C. J. 2019. Molecular mechanisms underlying progesterone receptor action in breast cancer: Insights into cell proliferation and stem cell regulation. *Steroids* 152, p. 108503. doi: 10.1016/j.steroids.2019.108503

Chaker, S. et al. 2013. Activated leukocyte cell adhesion molecule is a marker for thyroid carcinoma aggressiveness and disease-free survival. *Thyroid* 23(2), pp. 201-208. doi: 10.1089/thy.2012.0405

Chalmers, S. A. et al. 2022. The CD6/ALCAM pathway promotes lupus nephritis via T cell-mediated responses. *J Clin Invest* 132(1), doi: 10.1172/JCI147334

Chappell, P. E. et al. 2015. Structures of CD6 and Its Ligand CD166 Give Insight into Their Interaction. *Structure* 23(8), pp. 1426-1436. doi: 10.1016/j.str.2015.05.019

Chen, G. et al. 2018. Sonic Hedgehog Signalling Activation Contributes to ALCAM Over-Expression and Poor Clinical Outcome in Patients with Oral Squamous Cell Carcinoma. *Chin J Dent Res* 21(1), pp. 31-40. doi: 10.3290/j.cjdr.a39916

Chen, M. J. et al. 2017. MiR-148a and miR-152 reduce tamoxifen resistance in ER+ breast cancer via downregulating ALCAM. *Biochem Biophys Res Commun* 483(2), pp. 840-846. doi: 10.1016/j.bbrc.2017.01.012

Clauditz, T. S. et al. 2014. Activated leukocyte cell adhesion molecule (ALCAM/CD166) expression in head and neck squamous cell carcinoma (HNSCC). *Pathol Res Pract* 210(10), pp. 649-655. doi: 10.1016/j.prp.2014.06.012

Clezardin, P. et al. 2021. Bone metastasis: mechanisms, therapies, and biomarkers. *Physiol Rev* 101(3), pp. 797-855. doi: 10.1152/physrev.00012.2019

Coleman, R. E. 2006. Clinical features of metastatic bone disease and risk of skeletal morbidity. *Clin Cancer Res* 12(20 Pt 2), pp. 6243s-6249s. doi: 10.1158/1078-0432.CCR-06-0931

Contreras-Zarate, M. J. et al. 2019. Estradiol induces BDNF/TrkB signaling in triple-negative breast cancer to promote brain metastases. *Oncogene* 38(24), pp. 4685-4699. doi: 10.1038/s41388-019-0756-z

Darvishi, B. et al. 2020. Dual in vitro invasion/migration suppressing and tamoxifen response modulating effects of a recombinant anti-ALCAM scFv on breast cancer cells. *Cell Biochem Funct* 38(5), pp. 651-659. doi: 10.1002/cbf.3525

Davies, S. and Jiang, W. 2010. ALCAM, activated leukocyte cell adhesion molecule, influences the aggressive nature of breast cancer cells, a potential connection to bone metastasis. *Anticancer research* 30(4), pp. 1163-1168.

Davies, S. R. et al. 2008. Expression of the cell to cell adhesion molecule, ALCAM, in breast cancer patients and the potential link with skeletal metastasis. *Oncol Rep* 19(2), pp. 555-561.

Debois, J. M. 2002. Metastases to the Skin, Soft-Tissues and Bone. *TxNxM1: The Anatomy and Clinics of Metastatic Cancer*. Dordrecht: Springer Netherlands, pp. 209-266.

Devis, L. et al. 2018. ALCAM shedding at the invasive front of the tumor is a marker of myometrial infiltration and promotes invasion in endometrioid endometrial cancer. *Oncotarget* 9(24), pp. 16648-16664. doi: 10.18632/oncotarget.24625

Devis, L. et al. 2017. Activated leukocyte cell adhesion molecule (ALCAM) is a marker of recurrence and promotes cell migration, invasion, and metastasis in early-stage endometrioid endometrial cancer. *J Pathol* 241(4), pp. 475-487. doi: 10.1002/path.4851

Dippel, V. et al. 2013. Influence of L1-CAM expression of breast cancer cells on adhesion to endothelial cells. *J Cancer Res Clin Oncol* 139(1), pp. 107-121. doi: 10.1007/s00432-012-1306-z

Donizy, P. et al. 2015. Prognostic significance of ALCAM (CD166/MEMD) expression in cutaneous melanoma patients. *Diagn Pathol* 10, p. 86. doi: 10.1186/s13000-015-0331-z

Duplaquet, L. et al. 2018. The multiple paths towards MET receptor addiction in cancer. *Oncogene* 37(24), pp. 3200-3215. doi: 10.1038/s41388-018-0185-4

El Khoury, F. et al. 2016. Acquisition of anticancer drug resistance is partially associated with cancer stemness in human colon cancer cells. *Int J Oncol* 49(6), pp. 2558-2568. doi: 10.3892/ijo.2016.3725

Elizalde, P. V. and Proietti, C. J. 2012. The molecular basis of progesterone receptor action in breast carcinogenesis. *Horm Mol Biol Clin Investig* 9(2), pp. 105-117. doi: 10.1515/hmbci-2011-0129

Enyindah-Asonye, G. et al. 2017. CD318 is a ligand for CD6. *Proc Natl Acad Sci U S A* 114(33), pp. E6912-E6921. doi: 10.1073/pnas.1704008114

Eom, D. W. et al. 2015. Prognostic Significance of CD44v6, CD133, CD166, and ALDH1 Expression in Small Intestinal Adenocarcinoma. *Appl Immunohistochem Mol Morphol* 23(10), pp. 682-688. doi: 10.1097/PAI.000000000000140

Esposito, M. et al. 2018. The Biology of Bone Metastasis. *Cold Spring Harb Perspect Med* 8(6), doi: 10.1101/cshperspect.a031252

Federman, N. et al. 2012. Enhanced growth inhibition of osteosarcoma by cytotoxic polymerized liposomal nanoparticles targeting the alcam cell surface receptor. *Sarcoma* 2012, p. 126906. doi: 10.1155/2012/126906

Fekete, J. T. and Gyorffy, B. 2019. ROCplot.org: Validating predictive biomarkers of chemotherapy/hormonal therapy/anti-HER2 therapy using transcriptomic data of 3,104 breast cancer patients. *Int J Cancer* 145(11), pp. 3140-3151. doi: 10.1002/ijc.32369

Ferlay, J. et al. 2021. Cancer statistics for the year 2020: An overview. *Int J Cancer*, doi: 10.1002/ijc.33588

Florencio-Silva, R. et al. 2015. Biology of Bone Tissue: Structure, Function, and Factors That Influence Bone Cells. *Biomed Res Int* 2015, p. 421746. doi: 10.1155/2015/421746

Fornetti, J. et al. 2018. Understanding the Bone in Cancer Metastasis. *J Bone Miner Res* 33(12), pp. 2099-2113. doi: 10.1002/jbmr.3618

Frasor, J. et al. 2003. Profiling of estrogen up- and down-regulated gene expression in human breast cancer cells: insights into gene networks and pathways underlying estrogenic control of proliferation and cell phenotype. *Endocrinology* 144(10), pp. 4562-4574. doi: 10.1210/en.2003-0567

Fujiwara, K. et al. 2014. CD166/ALCAM expression is characteristic of tumorigenicity and invasive and migratory activities of pancreatic cancer cells. *PLoS One* 9(9), p. e107247. doi: 10.1371/journal.pone.0107247

Gerger, A. et al. 2011. Common cancer stem cell gene variants predict colon cancer recurrence. *Clin Cancer Res* 17(21), pp. 6934-6943. doi: 10.1158/1078-0432.CCR-11-1180

Giordano, S. et al. 1989. Tyrosine kinase receptor indistinguishable from the c-met protein. *Nature* 339(6220), pp. 155-156. doi: 10.1038/339155a0

Gradishar, W. J. et al. 2020. Breast Cancer, Version 3.2020, NCCN Clinical Practice Guidelines in Oncology. *J Natl Compr Canc Netw* 18(4), pp. 452-478. doi: 10.6004/jnccn.2020.0016

- Greene, G. L. et al. 1986. Sequence and expression of human estrogen receptor complementary DNA. *Science* 231(4742), pp. 1150-1154. doi: 10.1126/science.3753802
- Grober, O. M. et al. 2011. Global analysis of estrogen receptor beta binding to breast cancer cell genome reveals an extensive interplay with estrogen receptor alpha for target gene regulation. *BMC Genomics* 12, p. 36. doi: 10.1186/1471-2164-12-36
- Gyorffy, B. 2021. Survival analysis across the entire transcriptome identifies biomarkers with the highest prognostic power in breast cancer. *Comput Struct Biotechnol J* 19, pp. 4101-4109. doi: 10.1016/j.csbj.2021.07.014
- Hamester, F. et al. 2019. Prognostic relevance of the Golgi mannosidase MAN1A1 in ovarian cancer: impact of N-glycosylation on tumour cell aggregation. *Br J Cancer* 121(11), pp. 944-953. doi: 10.1038/s41416-019-0607-2
- Hansen, A. G. et al. 2014. ALCAM/CD166 is a TGF-beta-responsive marker and functional regulator of prostate cancer metastasis to bone. *Cancer Res* 74(5), pp. 1404-1415. doi: 10.1158/0008-5472.CAN-13-1296
- Hansen, A. G. et al. 2013. Elevated ALCAM shedding in colorectal cancer correlates with poor patient outcome. *Cancer Res* 73(10), pp. 2955-2964. doi: 10.1158/0008-5472.CAN-12-2052
- Harbeck, N. et al. 2019. Breast cancer. *Nat Rev Dis Primers* 5(1), p. 66. doi: 10.1038/s41572-019-0111-2
- Hasenauer, S. et al. 2013. Internalization of Met requires the co-receptor CD44v6 and its link to ERM proteins. *PLoS One* 8(4), p. e62357. doi: 10.1371/journal.pone.0062357
- Hassan, N. J. et al. 2004. Frontline: Optimal T cell activation requires the engagement of CD6 and CD166. *Eur J Immunol* 34(4), pp. 930-940. doi: 10.1002/eji.200424856
- Hebron, K. E. et al. 2018. Alternative splicing of ALCAM enables tunable regulation of cell-cell adhesion through differential proteolysis. *Sci Rep* 8(1), p. 3208. doi: 10.1038/s41598-018-21467-x
- Hein, S. et al. 2011. Biologic role of activated leukocyte cell adhesion molecule overexpression in breast cancer cell lines and clinical tumor tissue. *Breast Cancer Res Treat* 129(2), pp. 347-360. doi: 10.1007/s10549-010-1219-y

Henderson, M. A. et al. 2006. Parathyroid hormone-related protein localization in breast cancers predict improved prognosis. *Cancer Res* 66(4), pp. 2250-2256. doi: 10.1158/0008-5472.CAN-05-2814

Hiscox, S. and Jiang, W. G. 1997. Quantification of tumour cell-endothelial cell attachment by 1,1'-dioctadecyl-3,3,3',3'-tetramethylindocarbocyanine (DiI). *Cancer Lett* 112(2), pp. 209-217. doi: 10.1016/s0304-3835(96)04573-9

Hong, X. et al. 2010. ALCAM is associated with chemoresistance and tumor cell adhesion in pancreatic cancer. *J Surg Oncol* 101(7), pp. 564-569. doi: 10.1002/jso.21538

Huang, B. et al. 2014. Differential expression of estrogen receptor alpha, beta1, and beta2 in lobular and ductal breast cancer. *Proc Natl Acad Sci U S A* 111(5), pp. 1933-1938. doi: 10.1073/pnas.1323719111

Ihnen, M. et al. 2010a. Expression levels of Activated Leukocyte Cell Adhesion Molecule (ALCAM/CD166) in primary breast carcinoma and distant breast cancer metastases. *Dis Markers* 28(2), pp. 71-78. doi: 10.3233/DMA-2010-0685

Ihnen, M. et al. 2012. Relevance of activated leukocyte cell adhesion molecule (ALCAM) in tumor tissue and sera of cervical cancer patients. *BMC Cancer* 12, p. 140. doi: 10.1186/1471-2407-12-140

Ihnen, M. et al. 2008. Predictive impact of activated leukocyte cell adhesion molecule (ALCAM/CD166) in breast cancer. *Breast Cancer Res Treat* 112(3), pp. 419-427. doi: 10.1007/s10549-007-9879-y

Ihnen, M. et al. 2010b. Combination of osteopontin and activated leukocyte cell adhesion molecule as potent prognostic discriminators in HER2- and ER-negative breast cancer. *Br J Cancer* 103(7), pp. 1048-1056. doi: 10.1038/sj.bjc.6605840

Inaguma, S. et al. 2018. Expression of ALCAM (CD166) and PD-L1 (CD274) independently predicts shorter survival in malignant pleural mesothelioma. *Hum Pathol* 71, pp. 1-7. doi: 10.1016/j.humpath.2017.04.032

Ishigami, S. et al. 2011. Clinical implication of CD166 expression in gastric cancer. *J Surg Oncol* 103(1), pp. 57-61. doi: 10.1002/jso.21756

Ishiguro, F. et al. 2013. Membranous expression of activated leukocyte cell adhesion molecule contributes to poor prognosis and malignant phenotypes of non-small-cell lung cancer. *J Surg Res* 179(1), pp. 24-32. doi: 10.1016/j.jss.2012.08.044

Ishiguro, F. et al. 2012. Activated leukocyte cell-adhesion molecule (ALCAM) promotes malignant phenotypes of malignant mesothelioma. *J Thorac Oncol* 7(5), pp. 890-899. doi: 10.1097/JTO.0b013e31824af2db

Jeong, Y. J. et al. 2018. Prognostic Significance of Activated Leukocyte Cell Adhesion Molecule (ALCAM) in Association with Promoter Methylation of the ALCAM Gene in Breast Cancer. *Molecules* 23(1), doi: 10.3390/molecules23010131

Jia, W. et al. 2013. Vascular endothelial growth inhibitor (VEGI) is an independent indicator for invasion in human pituitary adenomas. *Anticancer Res* 33(9), pp. 3815-3822.

Jiang, W. et al. 2020. Incidence, prevalence, and outcomes of systemic malignancy with bone metastases. *J Orthop Surg (Hong Kong)* 28(2), p. 2309499020915989. doi: 10.1177/2309499020915989

Jiang, W. G. et al. 2009. The prostate transglutaminase (TGase-4, TGaseP) regulates the interaction of prostate cancer and vascular endothelial cells, a potential role for the ROCK pathway. *Microvasc Res* 77(2), pp. 150-157. doi: 10.1016/j.mvr.2008.09.010

Jiang, W. G. et al. 2005. Hepatocyte growth factor, its receptor, and their potential value in cancer therapies. *Crit Rev Oncol Hematol* 53(1), pp. 35-69. doi: 10.1016/j.critrevonc.2004.09.004

Jin, Z. et al. 2011. MicroRNA-192 and -215 are upregulated in human gastric cancer in vivo and suppress ALCAM expression in vitro. *Oncogene* 30(13), pp. 1577-1585. doi: 10.1038/onc.2010.534

Kahlert, C. et al. 2009. Increased expression of ALCAM/CD166 in pancreatic cancer is an independent prognostic marker for poor survival and early tumour relapse. *Br J Cancer* 101(3), pp. 457-464. doi: 10.1038/sj.bjc.6605136

Kalantari, E. et al. 2022. Significant co-expression of putative cancer stem cell markers, EpCAM and CD166, correlates with tumor stage and invasive behavior in colorectal cancer. *World J Surg Oncol* 20(1), p. 15. doi: 10.1186/s12957-021-02469-y

- Kaur, J. et al. 2013. Clinical significance of altered expression of beta-catenin and E-cadherin in oral dysplasia and cancer: potential link with ALCAM expression. *PLoS One* 8(6), p. e67361. doi: 10.1371/journal.pone.0067361
- Keese, C. R. et al. 2002. Real-time impedance assay to follow the invasive activities of metastatic cells in culture. *Biotechniques* 33(4), pp. 842-844, 846, 848-850. doi: 10.2144/02334rr01
- Kijima, N. et al. 2012. CD166/activated leukocyte cell adhesion molecule is expressed on glioblastoma progenitor cells and involved in the regulation of tumor cell invasion. *Neuro Oncol* 14(10), pp. 1254-1264. doi: 10.1093/neuonc/nor202
- King, J. A. et al. 2004. Activated leukocyte cell adhesion molecule in breast cancer: prognostic indicator. *Breast Cancer Res* 6(5), pp. R478-487. doi: 10.1186/bcr815
- King, J. A. et al. 2010. Mechanisms of transcriptional regulation and prognostic significance of activated leukocyte cell adhesion molecule in cancer. *Mol Cancer* 9, p. 266. doi: 10.1186/1476-4598-9-266
- Klein, W. M. et al. 2007. Increased expression of stem cell markers in malignant melanoma. *Mod Pathol* 20(1), pp. 102-107. doi: 10.1038/modpathol.3800720
- Knudsen, B. S. et al. 2002. High expression of the Met receptor in prostate cancer metastasis to bone. *Urology* 60(6), pp. 1113-1117. doi: 10.1016/s0090-4295(02)01954-4
- Kobayashi, Y. et al. 2018. Wnt5a-induced cell migration is associated with the aggressiveness of estrogen receptor-positive breast cancer. *Oncotarget* 9(30), pp. 20979-20992. doi: 10.18632/oncotarget.24761
- Krishnamurti, U. and Silverman, J. F. 2014. HER2 in breast cancer: a review and update. *Adv Anat Pathol* 21(2), pp. 100-107. doi: 10.1097/PAP.000000000000015
- Kristiansen, G. et al. 2005. Expression profiling of microdissected matched prostate cancer samples reveals CD166/MEMD and CD24 as new prognostic markers for patient survival. *J Pathol* 205(3), pp. 359-376. doi: 10.1002/path.1676
- Kristiansen, G. et al. 2003. ALCAM/CD166 is up-regulated in low-grade prostate cancer and progressively lost in high-grade lesions. *Prostate* 54(1), pp. 34-43. doi: 10.1002/pros.10161

Kuiper, G. G. et al. 1996. Cloning of a novel receptor expressed in rat prostate and ovary. *Proc Natl Acad Sci U S A* 93(12), pp. 5925-5930. doi: 10.1073/pnas.93.12.5925

Kulasingam, V. et al. 2009. Activated leukocyte cell adhesion molecule: a novel biomarker for breast cancer. *Int J Cancer* 125(1), pp. 9-14. doi: 10.1002/ijc.24292

Legler, K. et al. 2018. Reduced mannosidase MAN1A1 expression leads to aberrant N-glycosylation and impaired survival in breast cancer. *Br J Cancer* 118(6), pp. 847-856. doi: 10.1038/bjc.2017.472

Li, L. et al. 2020. MicroRNA expression profiling and the role of ALCAM modulating tumor growth and metastasis in benzo[a]pyrene-transformed 16HBE cells. *Toxicology* 442, p. 152539. doi: 10.1016/j.tox.2020.152539

Lin, H. et al. 2017. Serum CD166: A novel biomarker for predicting nasopharyngeal carcinoma response to radiotherapy. *Oncotarget* 8(38), pp. 62858-62867. doi: 10.18632/oncotarget.16399

Loibl, S. and Gianni, L. 2017. HER2-positive breast cancer. *The Lancet* 389(10087), pp. 2415-2429. doi: 10.1016/s0140-6736(16)32417-5

Low, S. K. et al. 2019. Identification of two novel breast cancer loci through large-scale genome-wide association study in the Japanese population. *Sci Rep* 9(1), p. 17332. doi: 10.1038/s41598-019-53654-9

Lu, X. Y. et al. 2017. Predicting Value of ALCAM as a Target Gene of microRNA-483-5p in Patients with Early Recurrence in Hepatocellular Carcinoma. *Front Pharmacol* 8, p. 973. doi: 10.3389/fphar.2017.00973

Ma, L. et al. 2015. Serum CD166: a novel hepatocellular carcinoma tumor marker. *Clin Chim Acta* 441, pp. 156-162. doi: 10.1016/j.cca.2014.12.034

Macedo, F. et al. 2017. Bone Metastases: An Overview. *Oncol Rev* 11(1), p. 321. doi: 10.4081/oncol.2017.321

Matthews, J. and Gustafsson, J. A. 2003. Estrogen signaling: a subtle balance between ER alpha and ER beta. *Mol Interv* 3(5), pp. 281-292. doi: 10.1124/mi.3.5.281

McFall, T. et al. 2015. Role of the short isoform of the progesterone receptor in breast cancer cell invasiveness at estrogen and progesterone levels in the pre- and post-menopausal ranges. *Oncotarget* 6(32), pp. 33146-33164. doi: 10.18632/oncotarget.5082

McGuigan, A. et al. 2018. Pancreatic cancer: A review of clinical diagnosis, epidemiology, treatment and outcomes. *World J Gastroenterol* 24(43), pp. 4846-4861. doi: 10.3748/wjg.v24.i43.4846

Mezzanzanica, D. et al. 2008. Subcellular localization of activated leukocyte cell adhesion molecule is a molecular predictor of survival in ovarian carcinoma patients. *Clin Cancer Res* 14(6), pp. 1726-1733. doi: 10.1158/1078-0432.CCR-07-0428

Micciche, F. et al. 2011. Activated leukocyte cell adhesion molecule expression and shedding in thyroid tumors. *PLoS One* 6(2), p. e17141. doi: 10.1371/journal.pone.0017141

Migliorini, F. et al. 2020. Bone metastases: a comprehensive review of the literature. *Mol Biol Rep* 47(8), pp. 6337-6345. doi: 10.1007/s11033-020-05684-0

Minner, S. et al. 2011. Low activated leukocyte cell adhesion molecule expression is associated with advanced tumor stage and early prostate-specific antigen relapse in prostate cancer. *Hum Pathol* 42(12), pp. 1946-1952. doi: 10.1016/j.humpath.2011.02.017

Moore, L. D. et al. 2013. DNA methylation and its basic function. *Neuropsychopharmacology* 38(1), pp. 23-38. doi: 10.1038/npp.2012.112

Moosavi, F. et al. 2019. HGF/MET pathway aberrations as diagnostic, prognostic, and predictive biomarkers in human cancers. *Crit Rev Clin Lab Sci* 56(8), pp. 533-566. doi: 10.1080/10408363.2019.1653821

Munsterberg, J. et al. 2020. ALCAM contributes to brain metastasis formation in non-small-cell lung cancer through interaction with the vascular endothelium. *Neuro Oncol* 22(7), pp. 955-966. doi: 10.1093/neuonc/noaa028

Nagy, A. et al. 2021. Pancancer survival analysis of cancer hallmark genes. *Sci Rep* 11(1), p. 6047. doi: 10.1038/s41598-021-84787-5

Nakamura, T. et al. 1989. Molecular cloning and expression of human hepatocyte growth factor. *Nature* 342(6248), pp. 440-443. doi: 10.1038/342440a0

Nakashima, T. et al. 2011. Evidence for osteocyte regulation of bone homeostasis through RANKL expression. *Nat Med* 17(10), pp. 1231-1234. doi: 10.1038/nm.2452

- Need, E. F. et al. 2012. Research resource: interplay between the genomic and transcriptional networks of androgen receptor and estrogen receptor alpha in luminal breast cancer cells. *Mol Endocrinol* 26(11), pp. 1941-1952. doi: 10.1210/me.2011-1314
- Nelissen, J. M. et al. 2000. Dynamic regulation of activated leukocyte cell adhesion molecule-mediated homotypic cell adhesion through the actin cytoskeleton. *Mol Biol Cell* 11(6), pp. 2057-2068. doi: 10.1091/mbc.11.6.2057
- Nicolau-Neto, P. et al. 2020. Transcriptome Analysis Identifies ALCAM Overexpression as a Prognosis Biomarker in Laryngeal Squamous Cell Carcinoma. *Cancers (Basel)* 12(2), doi: 10.3390/cancers12020470
- O'Carrigan, B. et al. 2017. Bisphosphonates and other bone agents for breast cancer. *Cochrane Database Syst Rev* 10, p. CD003474. doi: 10.1002/14651858.CD003474.pub4
- Okamoto, K. 2021. Role of RANKL in cancer development and metastasis. *J Bone Miner Metab* 39(1), pp. 71-81. doi: 10.1007/s00774-020-01182-2
- Orian-Rousseau, V. et al. 2002. CD44 is required for two consecutive steps in HGF/c-Met signaling. *Genes Dev* 16(23), pp. 3074-3086. doi: 10.1101/gad.242602
- Owen, S. et al. 2016. Importance of osteoprotegerin and receptor activator of nuclear factor kappaB in breast cancer response to hepatocyte growth factor and the bone microenvironment in vitro. *Int J Oncol* 48(3), pp. 919-928. doi: 10.3892/ijo.2016.3339
- Paget, S. 1889. The distribution of secondary growths in cancer of the breast *The Lancet* 133(3421), pp. 571-573. doi: 10.1016/S0140-6736(00)49915-0.
- Pareek, A. et al. 2019. Bone metastases incidence and its correlation with hormonal and human epidermal growth factor receptor 2 neu receptors in breast cancer. *J Cancer Res Ther* 15(5), pp. 971-975. doi: 10.4103/jcrt.JCRT_235_18
- Park, W. et al. 2021. Pancreatic Cancer: A Review. *JAMA* 326(9), pp. 851-862. doi: 10.1001/jama.2021.13027
- Paschke, K. A. et al. 1992. Neurolin, a cell surface glycoprotein on growing retinal axons in the goldfish visual system, is reexpressed during retinal axonal regeneration. *J Cell Biol* 117(4), pp. 863-875. doi: 10.1083/jcb.117.4.863

Patel, D. D. et al. 1995. Identification and characterization of a 100-kD ligand for CD6 on human thymic epithelial cells. *J Exp Med* 181(4), pp. 1563-1568. doi: 10.1084/jem.181.4.1563

Pellegrini, P. et al. 2013. Constitutive activation of RANK disrupts mammary cell fate leading to tumorigenesis. *Stem Cells* 31(9), pp. 1954-1965. doi: 10.1002/stem.1454

Piao, D. et al. 2012. Clinical implications of activated leukocyte cell adhesion molecule expression in breast cancer. *Mol Biol Rep* 39(1), pp. 661-668. doi: 10.1007/s11033-011-0783-5

Pinto, M. and Carmo, A. M. 2013. CD6 as a therapeutic target in autoimmune diseases: successes and challenges. *BioDrugs* 27(3), pp. 191-202. doi: 10.1007/s40259-013-0027-4

Piscuoglio, S. et al. 2012. Effect of EpCAM, CD44, CD133 and CD166 expression on patient survival in tumours of the ampulla of Vater. *J Clin Pathol* 65(2), pp. 140-145. doi: 10.1136/jclinpath-2011-200043

Renard, H. F. et al. 2020. Endophilin-A3 and Galectin-8 control the clathrin-independent endocytosis of CD166. *Nat Commun* 11(1), p. 1457. doi: 10.1038/s41467-020-15303-y

Ribeiro, K. B. et al. 2016. KRAS mutation associated with CD44/CD166 immunoexpression as predictors of worse outcome in metastatic colon cancer. *Cancer Biomark* 16(4), pp. 513-521. doi: 10.3233/CBM-160592

Rosso, O. et al. 2007. The ALCAM shedding by the metalloprotease ADAM17/TACE is involved in motility of ovarian carcinoma cells. *Mol Cancer Res* 5(12), pp. 1246-1253. doi: 10.1158/1541-7786.MCR-07-0060

Ruma, I. M. et al. 2016. MCAM, as a novel receptor for S100A8/A9, mediates progression of malignant melanoma through prominent activation of NF-kappaB and ROS formation upon ligand binding. *Clin Exp Metastasis* 33(6), pp. 609-627. doi: 10.1007/s10585-016-9801-2

Ryan, C. et al. 2022. Epidemiology of bone metastases. *Bone* 158, p. 115783. doi: 10.1016/j.bone.2020.115783

Sanders, A. J. et al. 2019. Importance of activated leukocyte cell adhesion molecule (ALCAM) in prostate cancer progression and metastatic dissemination. *Oncotarget* 10(59), pp. 6362-6377. doi: 10.18632/oncotarget.27279

Sawhney, M. et al. 2009. Cytoplasmic accumulation of activated leukocyte cell adhesion molecule is a predictor of disease progression and reduced survival in oral cancer patients. *Int J Cancer* 124(9), pp. 2098-2105. doi: 10.1002/ijc.24192

Selvaggi, G. and Scagliotti, G. V. 2005. Management of bone metastases in cancer: a review. *Crit Rev Oncol Hematol* 56(3), pp. 365-378. doi: 10.1016/j.critrevonc.2005.03.011

Shanesmith, R. P. et al. 2011. Tissue microarray analysis of ezrin, KBA.62, CD166, nestin, and p-Akt in melanoma versus banal and atypical nevi, and nonmelanocytic lesions. *Am J Dermatopathol* 33(7), pp. 663-668. doi: 10.1097/DAD.0b013e318214ae8a

Sim, S. H. et al. 2014. P21 and CD166 as predictive markers of poor response and outcome after fluorouracil-based chemoradiotherapy for the patients with rectal cancer. *BMC Cancer* 14, p. 241. doi: 10.1186/1471-2407-14-241

Simatou, A. et al. 2020. The Role of the RANKL/RANK Axis in the Prevention and Treatment of Breast Cancer with Immune Checkpoint Inhibitors and Anti-RANKL. *Int J Mol Sci* 21(20), doi: 10.3390/ijms21207570

Simoes, I. T. et al. 2020. Multifaceted effects of soluble human CD6 in experimental cancer models. *J Immunother Cancer* 8(1), doi: 10.1136/jitc-2019-000172

Simpson, E. and Brown, H. L. 2018. Understanding osteosarcomas. *JAAPA* 31(8), pp. 15-19. doi: 10.1097/01.JAA.0000541477.24116.8d

Smeland, S. et al. 2019. Survival and prognosis with osteosarcoma: outcomes in more than 2000 patients in the EURAMOS-1 (European and American Osteosarcoma Study) cohort. *Eur J Cancer* 109, pp. 36-50. doi: 10.1016/j.ejca.2018.11.027

Sperka, T. et al. 2011. Activation of Ras requires the ERM-dependent link of actin to the plasma membrane. *PLoS One* 6(11), p. e27511. doi: 10.1371/journal.pone.0027511

Starling, G. C. et al. 1996. Characterization of mouse CD6 with novel monoclonal antibodies which enhance the allogeneic mixed leukocyte reaction. *Eur J Immunol* 26(4), pp. 738-746. doi: 10.1002/eji.1830260403

Stashi, E. et al. 2014. Steroid receptor coactivators: servants and masters for control of systems metabolism. *Trends Endocrinol Metab* 25(7), pp. 337-347. doi: 10.1016/j.tem.2014.05.004

Stoker, M. et al. 1987. Scatter factor is a fibroblast-derived modulator of epithelial cell mobility. *Nature* 327(6119), pp. 239-242. doi: 10.1038/327239a0

Su, J. et al. 2016. Reduced SLC27A2 induces cisplatin resistance in lung cancer stem cells by negatively regulating Bmi1-ABCG2 signaling. *Mol Carcinog* 55(11), pp. 1822-1832. doi: 10.1002/mc.22430

Swart, G. W. et al. 2005. Activated leukocyte cell adhesion molecule (ALCAM/CD166): signaling at the divide of melanoma cell clustering and cell migration? *Cancer Metastasis Rev* 24(2), pp. 223-236. doi: 10.1007/s10555-005-1573-0

Tachezy, M. et al. 2012a. ALCAM (CD166) expression and serum levels are markers for poor survival of esophageal cancer patients. *Int J Cancer* 131(2), pp. 396-405. doi: 10.1002/ijc.26377

Tachezy, M. et al. 2012b. Activated leukocyte cell adhesion molecule (CD166)--its prognostic power for colorectal cancer patients. *J Surg Res* 177(1), pp. e15-20. doi: 10.1016/j.jss.2012.02.013

Tachezy, M. et al. 2011. ALCAM (CD166) expression as novel prognostic biomarker for pancreatic neuroendocrine tumor patients. *J Surg Res* 170(2), pp. 226-232. doi: 10.1016/j.jss.2011.06.002

Tachezy, M. et al. 2012c. ALCAM (CD166) expression and serum levels in pancreatic cancer. *PLoS One* 7(6), p. e39018. doi: 10.1371/journal.pone.0039018

Tahara, R. K. et al. 2019. Bone Metastasis of Breast Cancer. *Adv Exp Med Biol* 1152, pp. 105-129. doi: 10.1007/978-3-030-20301-6_7

Tan, F. et al. 2014. Enhanced down-regulation of ALCAM/CD166 in African-American Breast Cancer. *BMC Cancer* 14, p. 715. doi: 10.1186/1471-2407-14-715

Tanaka, H. et al. 1991. Molecular cloning and expression of a novel adhesion molecule, SC1. *Neuron* 7(4), pp. 535-545. doi: 10.1016/0896-6273(91)90366-8

- Tanimoto, K. et al. 1999. Regulation of estrogen receptor alpha gene mediated by promoter B responsible for its enhanced expression in human breast cancer. *Nucleic Acids Res* 27(3), pp. 903-909. doi: 10.1093/nar/27.3.903
- Te Riet, J. et al. 2007. Distinct kinetic and mechanical properties govern ALCAM-mediated interactions as shown by single-molecule force spectroscopy. *J Cell Sci* 120(Pt 22), pp. 3965-3976. doi: 10.1242/jcs.004010
- Thaler, F. J. and Michalopoulos, G. K. 1985. Hepatopoietin A: partial characterization and trypsin activation of a hepatocyte growth factor. *Cancer Res* 45(6), pp. 2545-2549.
- Trent, J. M. and Witkowski, C. M. 1987. Clarification of the chromosomal assignment of the human P-glycoprotein/mdr1 gene: possible coincidence with the cystic fibrosis and c-met oncogene. *Cancer Genet Cytogenet* 26(1), pp. 187-190. doi: 10.1016/0165-4608(87)90150-6
- Tresguerres, F. G. F. et al. 2020. The osteocyte: A multifunctional cell within the bone. *Ann Anat* 227, p. 151422. doi: 10.1016/j.aanat.2019.151422
- Tudor, C. et al. 2014. Syntenin-1 and ezrin proteins link activated leukocyte cell adhesion molecule to the actin cytoskeleton. *J Biol Chem* 289(19), pp. 13445-13460. doi: 10.1074/jbc.M113.546754
- Uchida, N. et al. 1997. The characterization, molecular cloning, and expression of a novel hematopoietic cell antigen from CD34+ human bone marrow cells. *Blood* 89(8), pp. 2706-2716.
- Uhlen, M. et al. 2017. A pathology atlas of the human cancer transcriptome. *Science* 357(6352), doi: 10.1126/science.aan2507
- van den Brand, M. et al. 2010. Activated leukocyte cell adhesion molecule expression predicts lymph node metastasis in oral squamous cell carcinoma. *Oral Oncol* 46(5), pp. 393-398. doi: 10.1016/j.oraloncology.2010.03.001
- van Kempen, L. C. et al. 2001. Molecular basis for the homophilic activated leukocyte cell adhesion molecule (ALCAM)-ALCAM interaction. *J Biol Chem* 276(28), pp. 25783-25790. doi: 10.1074/jbc.M011272200
- Verma, A. et al. 2005. MEMD/ALCAM: a potential marker for tumor invasion and nodal metastasis in esophageal squamous cell carcinoma. *Oncology* 68(4-6), pp. 462-470. doi: 10.1159/000086989

von Lersner, A. et al. 2019. Modulation of cell adhesion and migration through regulation of the immunoglobulin superfamily member ALCAM/CD166. *Clin Exp Metastasis* 36(2), pp. 87-95. doi: 10.1007/s10585-019-09957-2

Wachowiak, R. et al. 2016. Prognostic Impact of Activated Leucocyte Cell Adhesion Molecule (ALCAM/CD166) in Infantile Neuroblastoma. *Anticancer Res* 36(8), pp. 3991-3995.

Wang, J. et al. 2011. NF-kappaB P50/P65 hetero-dimer mediates differential regulation of CD166/ALCAM expression via interaction with miRNA-9 after serum deprivation, providing evidence for a novel negative auto-regulatory loop. *Nucleic Acids Res* 39(15), pp. 6440-6455. doi: 10.1093/nar/gkr302

Wang, Y. et al. 2018. The oncologic impact of hormone replacement therapy in premenopausal breast cancer survivors: A systematic review. *Breast* 40, pp. 123-130. doi: 10.1016/j.breast.2018.05.002

Wang, Z. 2017. ErbB Receptors and Cancer. *Methods Mol Biol* 1652, pp. 3-35. doi: 10.1007/978-1-4939-7219-7_1

Weichert, W. et al. 2004. ALCAM/CD166 is overexpressed in colorectal carcinoma and correlates with shortened patient survival. *J Clin Pathol* 57(11), pp. 1160-1164. doi: 10.1136/jcp.2004.016238

Weigelt, B. et al. 2005. Breast cancer metastasis: markers and models. *Nat Rev Cancer* 5(8), pp. 591-602. doi: 10.1038/nrc1670

Winters, S. et al. 2017. Breast Cancer Epidemiology, Prevention, and Screening. *Prog Mol Biol Transl Sci* 151, pp. 1-32. doi: 10.1016/bs.pmbts.2017.07.002

Witzel, I. et al. 2012. Detection of activated leukocyte cell adhesion molecule in the serum of breast cancer patients and implications for prognosis. *Oncology* 82(6), pp. 305-312. doi: 10.1159/000337222

Xin, L. et al. 2021. SIKs suppress tumor function and regulate drug resistance in breast cancer. *Am J Cancer Res* 11(7), pp. 3537-3557.

Xu, J. et al. 2020. A Phase II Trial of Cabozantinib in Hormone Receptor-Positive Breast Cancer with Bone Metastases. *Oncologist* 25(8), pp. 652-660. doi: 10.1634/theoncologist.2020-0127

- Xu, Z. et al. 2018. ILT3.Fc-CD166 Interaction Induces Inactivation of p70 S6 Kinase and Inhibits Tumor Cell Growth. *J Immunol* 200(3), pp. 1207-1219. doi: 10.4049/jimmunol.1700553
- Yan, M. et al. 2013. Plasma membrane proteomics of tumor spheres identify CD166 as a novel marker for cancer stem-like cells in head and neck squamous cell carcinoma. *Mol Cell Proteomics* 12(11), pp. 3271-3284. doi: 10.1074/mcp.M112.025460
- Yang, Y. et al. 2021a. A novel HDGF-ALCAM axis promotes the metastasis of Ewing sarcoma via regulating the GTPases signaling pathway. *Oncogene* 40(4), pp. 731-745. doi: 10.1038/s41388-020-01485-8
- Yang, Y. et al. 2021b. The Clinical and Theranostic Values of Activated Leukocyte Cell Adhesion Molecule (ALCAM)/CD166 in Human Solid Cancers. *Cancers (Basel)* 13(20), doi: 10.3390/cancers13205187
- Ye, L. et al. 2011. Bone morphogenetic protein and bone metastasis, implication and therapeutic potential. *Front Biosci (Landmark Ed)* 16(3), pp. 865-897. doi: 10.2741/3725
- Ye, M. et al. 2015. Overexpression of activated leukocyte cell adhesion molecule in gastric cancer is associated with advanced stages and poor prognosis and miR-9 deregulation. *Mol Med Rep* 11(3), pp. 2004-2012. doi: 10.3892/mmr.2014.2933
- Yehia, L. et al. 2015. Expression of HIF-1 α and Markers of Angiogenesis Are Not Significantly Different in Triple Negative Breast Cancer Compared to Other Breast Cancer Molecular Subtypes: Implications for Future Therapy. *PLoS One* 10(6), p. e0129356. doi: 10.1371/journal.pone.0129356
- Yip, C. H. and Rhodes, A. 2014. Estrogen and progesterone receptors in breast cancer. *Future Oncol* 10(14), pp. 2293-2301. doi: 10.2217/fon.14.110
- Yu, L. et al. 2019. Moesin is an independent prognostic marker for ER-positive breast cancer. *Oncol Lett* 17(2), pp. 1921-1933. doi: 10.3892/ol.2018.9799
- Zhang, X. et al. 2020. Tumoral Expression of CD166 in Human Esophageal Squamous Cell Carcinoma: Implications for Cancer Progression and Prognosis. *Cancer Biother Radiopharm* 35(3), pp. 214-222. doi: 10.1089/cbr.2019.3089

Zhang, Y. et al. 2017. Meta-analysis indicating that high ALCAM expression predicts poor prognosis in colorectal cancer. *Oncotarget* 8(29), pp. 48272-48281. doi: 10.18632/oncotarget.17707

Zhao, X. et al. 2017. Clinicopathological and prognostic significance of c-Met overexpression in breast cancer. *Oncotarget* 8(34), pp. 56758-56767. doi: 10.18632/oncotarget.18142

Zhou, P. et al. 2011. Functional polymorphisms in CD166/ALCAM gene associated with increased risk for breast cancer in a Chinese population. *Breast Cancer Res Treat* 128(2), pp. 527-534. doi: 10.1007/s10549-011-1365-x

Zhou, Z. et al. 2018. ALCAM(+) stromal cells: role in giant cell tumor of bone progression. *Cell Death Dis* 9(3), p. 299. doi: 10.1038/s41419-018-0361-z

Supplement-1. Information of the breast TMA (BR1503f)

	1	2	3	4	5	6	7	8	9	10	11	12	13	14	15	
US Biomax, Inc. BR1503f (serial)	A	●	●	●	●	●	●	●	●	●	●	●	●	●	●	●
	B	●	●	●	●	●	●	●	●	●	●	●	●	●	●	●
	C	●	●	●	●	●	●	●	●	●	●	●	●	●	●	●
	D	●	●	●	●	●	●	●	●	●	●	●	●	●	●	●
	E	●	●	●	●	●	●	●	●	●	●	●	●	●	●	●
	F	●	●	●	●	●	●	●	●	●	●	●	●	●	●	●
	G	●	●	●	●	●	●	●	●	●	●	●	●	●	●	●
	H	●	●	●	●	●	●	●	●	●	●	●	●	●	●	●
	I	●	●	●	●	●	●	●	●	●	●	●	●	●	●	●
	J	●	●	●	●	●	●	●	●	●	●	●	●	●	●	●

Legend: Bre - Breast
 ● - Benign tumor, ● - Malignant tumor, ● - NAT

Pos.	No.	Age	Sex	Organ/Anatomic Site	Pathology diagnosis	TNM	Grade	Stage	Type	ER	PR	Ki67	HER2
A1	1	46	F	Breast	Adjacent normal breast duct tissue	-	-		NAT	+	+	-	0
A2	2	46	F	Breast	Adjacent normal breast tissue	-	-		NAT	+	+	-	0
A3	3	42	F	Breast	Adjacent normal breast tissue	-	-		NAT	-	++	-	0
A4	4	42	F	Breast	Adjacent normal breast tissue (fibrous tissue)	-	-		NAT	*	*	*	*
A5	5	43	F	Breast	Adjacent normal breast tissue (fibrous tissue)	-	-		NAT	*	*	*	*
A6	6	43	F	Breast	Adjacent normal breast tissue	-	-		NAT	+	+	-	0
A7	7	48	F	Breast	Fibroadenoma	-	-		Benign	++	+	-	0
A8	8	48	F	Breast	Fibroadenoma	-	-		Benign	++	+	-	0
A9	9	19	F	Breast	Fibroadenoma	-	-		Benign	+++	+++	-	0
A10	10	19	F	Breast	Fibroadenoma	-	-		Benign	+++	+++	-	0
A11	11	54	F	Breast	Fibroadenoma	-	-		Benign	-	-	-	0
A12	12	54	F	Breast	Fibroadenoma	-	-		Benign	-	-	-	0
A13	13	49	F	Breast	Lowly malignant cystosarcoma phyllodes	-	-		Malignant	+	+++	10%+	0
A14	14	49	F	Breast	Lowly malignant cystosarcoma phyllodes	-	-		Malignant	+	+++	10%+	0

A15	15	69	F	Breast	Lowly malignant cystosarcoma phyllodes	-	-	Malignant	++	+++	15%+	0
B1	16	69	F	Breast	Lowly malignant cystosarcoma phyllodes	-	-	Malignant	-	-	15%+	0
B2	17	49	F	Breast	Intraductal carcinoma (breast tissue)	TisNOM0	-	Malignant	+	+	-	0
B3	18	49	F	Breast	Intraductal carcinoma (breast tissue)	TisNOM0	-	Malignant	+	+	-	0
B4	19	50	F	Breast	Intraductal carcinoma(sparse)	TisNOM0	-	Malignant	-	-	25%+	2+
B5	20	50	F	Breast	Intraductal carcinoma	TisNOM0	-	Malignant	-	-	55%+++	3+
B6	21	36	F	Breast	Intraductal carcinoma(blank)	TisNOM0	-	Malignant	*	*	*	*
B7	22	36	F	Breast	Intraductal carcinoma	TisNOM0	-	Malignant	+++	+++	10%+	0
B8	23	67	F	Breast	Intraductal carcinoma(sparse)	TisNOM0	-	Malignant	-	-	-	3+
B9	24	67	F	Breast	Intraductal carcinoma with early infiltrate(sparse)	TisNOM0	-	Malignant	-	-	-	3+
B10	25	43	F	Breast	Intraductal carcinoma with early infiltrate	TisNOM0	-	Malignant	+++	++	40%++	3+

B11	26	43	F	Breast	Intraductal carcinoma	TisNOM0	-	Malignant	+++	++	30%++	3+
B12	27	54	F	Breast	Intraductal carcinoma	TisNOM0	-	Malignant	+++	+++	15%+	0
B13	28	54	F	Breast	Intraductal carcinoma	TisNOM0	-	Malignant	+++	+++	10%+	0
B14	29	45	F	Breast	Intraductal carcinoma (adipose tissue)	TisNOM0	-	Malignant	*	*	*	*
B15	30	45	F	Breast	Intraductal carcinoma	TisNOM0	-	Malignant	+++	+++	10%+	0
C1	31	54	F	Breast	Invasive ductal carcinoma	T3N1M0	1	Malignant	-	-	-	3+
C2	32	54	F	Breast	Invasive ductal carcinoma	T3N1M0	1	Malignant	-	-	-	3+
C3	33	60	F	Breast	Invasive ductal carcinoma	T2N0M0	1	Malignant	-	-	55%+++	3+
C4	34	60	F	Breast	Invasive ductal carcinoma	T2N0M0	1	Malignant	-	-	60%+++	3+
C5	35	38	F	Breast	Invasive ductal carcinoma	T3N0M0	1--2	Malignant	+++	+++	45%++	3+
C6	36	38	F	Breast	Invasive ductal carcinoma	T3N0M0	1--2	Malignant	+++	+++	85%+++	3+
C7	37	41	F	Breast	Invasive ductal carcinoma	T2N0M0	1--2	Malignant	+	+	10%+	0
C8	38	41	F	Breast	Invasive ductal carcinoma	T2N0M0	1--2	Malignant	++	++	20%+	0
C9	39	71	F	Breast	Invasive ductal carcinoma	T4N2M0	2	Malignant	++	+++	15%+	0

C10	40	71	F	Breast	Invasive ductal carcinoma	T4N2M0	2	Malignant	++	+++	10%+	0
C11	41	70	F	Breast	Invasive ductal carcinoma	T2N0M0	2	Malignant	-	-	35%++	3+
C12	42	70	F	Breast	Invasive ductal carcinoma	T2N0M0	2	Malignant	-	-	45%++	3+
C13	43	64	F	Breast	Invasive ductal carcinoma	T2N0M0	2	Malignant	-	++	-	0
C14	44	64	F	Breast	Invasive ductal carcinoma(blank)	T2N0M0	2	Malignant	*	*	*	*
C15	45	47	F	Breast	Invasive ductal carcinoma	T3N0M0	2	Malignant	+++	++	-	0
D1	46	47	F	Breast	Invasive ductal carcinoma	T3N0M0	2	Malignant	+++	++	-	0
D2	47	69	F	Breast	Invasive ductal carcinoma	T4N0M0	2	Malignant	-	++	-	0
D3	48	69	F	Breast	Invasive ductal carcinoma	T4N0M0	2	Malignant	-	++	-	0
D4	49	51	F	Breast	Invasive ductal carcinoma	T2N2M0	2	Malignant	-	-	45%++	0
D5	50	51	F	Breast	Invasive ductal carcinoma	T2N2M0	2	Malignant	-	-	45%++	0
D6	51	58	F	Breast	Invasive ductal carcinoma	T2N0M0	2	Malignant	-	-	20%+	3+
D7	52	58	F	Breast	Invasive ductal carcinoma	T2N0M0	2	Malignant	-	-	20%+	3+
D8	53	31	F	Breast	Invasive ductal carcinoma	T2N0M0	2	Malignant	++	+++	20%+	0
D9	54	31	F	Breast	Invasive ductal carcinoma	T2N0M0	2	Malignant	++	+++	20%+	0

D10	55	64	F	Breast	Invasive ductal carcinoma	T2N0M0	2	Malignant	-	-	30%++	3+
D11	56	64	F	Breast	Invasive ductal carcinoma	T2N0M0	2	Malignant	-	-	30%++	3+
D12	57	55	F	Breast	Invasive ductal carcinoma	T3N2M0	2	Malignant	+++	+++	40%++	0
D13	58	55	F	Breast	Invasive ductal carcinoma	T3N2M0	2	Malignant	+++	+++	40%++	0
D14	59	52	F	Breast	Invasive ductal carcinoma	T2N2M0	2	Malignant	+	+++	10%+	2+
D15	60	52	F	Breast	Invasive ductal carcinoma	T2N2M0	2	Malignant	+	+++	45%++	2+
E1	61	42	F	Breast	Invasive ductal carcinoma	T2N2M0	2	Malignant	+++	+++	30%++	0
E2	62	42	F	Breast	Invasive ductal carcinoma	T2N2M0	2	Malignant	+++	+++	30%++	0
E3	63	47	F	Breast	Invasive ductal carcinoma	T4N1M0	2	Malignant	++	+++	15%+	0
E4	64	47	F	Breast	Invasive ductal carcinoma	T4N1M0	2	Malignant	++	+++	15%+	0
E5	65	50	F	Breast	Invasive ductal carcinoma	T2N1M0	2	Malignant	+	+++	10%+	0
E6	66	50	F	Breast	Invasive ductal carcinoma	T2N1M0	2	Malignant	++	+++	10%+	0
E7	67	74	F	Breast	Invasive ductal carcinoma(blank)	T2N1M0	-	Malignant	*	*	*	*
E8	68	74	F	Breast	Invasive ductal carcinoma	T2N1M0	2	Malignant	+++	+++	15%+	0
E9	69	41	F	Breast	Invasive ductal carcinoma	T2N2M0	2	Malignant	+++	+++	40%++	0

E10	70	41	F	Breast	Invasive ductal carcinoma	T2N2M0	2	Malignant	+++	+++	45%+++	0
E11	71	34	F	Breast	Invasive ductal carcinoma	T3N0M0	2	Malignant	-	+++	60%+++	0
E12	72	34	F	Breast	Invasive ductal carcinoma	T3N0M0	2	Malignant	-	+++	50%+++	0
E13	73	60	F	Breast	Invasive ductal carcinoma	T2N2M0	2	Malignant	-	-	55%+++	3+
E14	74	60	F	Breast	Invasive ductal carcinoma	T2N2M0	2	Malignant	-	-	75%+++	3+
E15	75	50	F	Breast	Invasive ductal carcinoma	T4N0M0	2	Malignant	-	-	80%+++	1+
F1	76	50	F	Breast	Invasive ductal carcinoma	T4N0M0	2	Malignant	-	-	65%+++	1+
F2	77	55	F	Breast	Invasive ductal carcinoma	T2N0M0	2	Malignant	+	+++	60%+++	2+
F3	78	55	F	Breast	Invasive ductal carcinoma	T2N0M0	2	Malignant	+	+++	75%+++	2+
F4	79	65	F	Breast	Invasive ductal carcinoma	T2N1M0	2	Malignant	-	-	30%+	3+
F5	80	65	F	Breast	Invasive ductal carcinoma	T2N1M0	2	Malignant	-	-	50%+++	3+
F6	81	48	F	Breast	Invasive ductal carcinoma	T2N2M0	2	Malignant	+++	+++	85%+++	0
F7	82	48	F	Breast	Invasive ductal carcinoma	T2N2M0	2	Malignant	+++	+++	85%+++	0
F8	83	38	F	Breast	Invasive ductal carcinoma	T2N1M0	2	Malignant	-	-	-	3+
F9	84	38	F	Breast	Invasive ductal carcinoma	T2N1M0	2	Malignant	-	-	-	3+

F10	85	45	F	Breast	Invasive ductal carcinoma	T4N2M0	2	Malignant	+++	+++	20%+	0
F11	86	45	F	Breast	Invasive ductal carcinoma	T4N2M0	2	Malignant	+++	+++	20%+	0
F12	87	43	F	Breast	Invasive ductal carcinoma	T2N0M0	2	Malignant	+++	++	-	0
F13	88	43	F	Breast	Invasive ductal carcinoma (adipose tissue)	T2N0M0	2	Malignant	*	*	*	*
F14	89	48	F	Breast	Invasive ductal carcinoma	T2N0M0	2	Malignant	+	+++	60%+++	0
F15	90	48	F	Breast	Invasive ductal carcinoma	T2N0M0	2	Malignant	++	+++	60%+++	0
G1	91	52	F	Breast	Invasive ductal carcinoma (fibrous tissue)	T2N0M0	-	Malignant	*	*	*	*
G2	92	52	F	Breast	Invasive ductal carcinoma	T2N0M0	2	Malignant	++	+++	40%++	3+
G3	93	51	F	Breast	Invasive ductal carcinoma	T3N1M0	2	Malignant	-	-	75%+++	3+
G4	94	51	F	Breast	Invasive ductal carcinoma	T3N1M0	2	Malignant	-	-	80%+++	3+
G5	95	52	F	Breast	Invasive ductal carcinoma	T3N0M0	2	Malignant	-	++	30%++	0
G6	96	52	F	Breast	Invasive ductal carcinoma	T3N0M0	2	Malignant	-	+++	35%++	0
G7	97	45	F	Breast	Invasive ductal carcinoma	T1N0M0	2	Malignant	-	-	27%++	0
G8	98	45	F	Breast	Invasive ductal carcinoma	T1N0M0	2	Malignant	-	-	28%++	0

G9	99	40	F	Breast	Invasive ductal carcinoma	T2N0M0	2	Malignant	++	++	15%+	0
G10	100	40	F	Breast	Invasive ductal carcinoma	T2N0M0	2	Malignant	++	++	10%+	0
G11	101	30	F	Breast	Invasive ductal carcinoma	T4N0M0	2--3	Malignant	+++	+++	45%++	0
G12	102	30	F	Breast	Invasive ductal carcinoma	T4N0M0	2--3	Malignant	+++	+++	48%++	0
G13	103	33	F	Breast	Invasive ductal carcinoma	T1N0M0	2--3	Malignant	+	+	30%++	0
G14	104	33	F	Breast	Invasive ductal carcinoma	T1N0M0	2--3	Malignant	+	+	30%++	0
G15	105	35	F	Breast	Invasive ductal carcinoma	T2N0M0	2--3	Malignant	-	-	45%++	0
H1	106	35	F	Breast	Invasive ductal carcinoma	T2N0M0	2--3	Malignant	-	-	30%++	0
H2	107	44	F	Breast	Invasive ductal carcinoma	T2N0M0	2--3	Malignant	-	++	55%+++	0
H3	108	44	F	Breast	Invasive ductal carcinoma	T2N0M0	2--3	Malignant	-	++	55%+++	0
H4	109	43	F	Breast	Invasive ductal carcinoma	T2N1M0	2--3	Malignant	+	+++	70%+++	2+
H5	110	43	F	Breast	Invasive ductal carcinoma	T2N1M0	2--3	Malignant	+	+++	80%+++	2+
H6	111	41	F	Breast	Invasive ductal carcinoma	T3N1M0	2--3	Malignant	-	-	65%+++	0
H7	112	41	F	Breast	Invasive ductal carcinoma	T3N1M0	2--3	Malignant	-	-	60%+++	0
H8	113	59	F	Breast	Invasive ductal carcinoma	T2N0M0	2--3	Malignant	++	+++	40%++	0

H9	114	59	F	Breast	Invasive ductal carcinoma	T2N0M0	2--3	Malignant	++	+++	50%++	0
H10	115	34	F	Breast	Invasive ductal carcinoma	T4N0M0	2--3	Malignant	+	+++	10%+	0
H11	116	34	F	Breast	Invasive ductal carcinoma	T4N0M0	2--3	Malignant	+	+++	15%+	0
H12	117	47	F	Breast	Invasive ductal carcinoma	T2N0M0	2--3	Malignant	++	+	15%+	0
H13	118	47	F	Breast	Invasive ductal carcinoma	T2N0M0	2--3	Malignant	++	+	20%++	0
H14	119	45	F	Breast	Invasive ductal carcinoma	T3N0M0	3	Malignant	-	-	60%+++	2+
H15	120	45	F	Breast	Invasive ductal carcinoma with necrosis	T3N0M0	3	Malignant	-	-	70%+++	2+
I1	121	34	F	Breast	Invasive ductal carcinoma	T2N0M0	3	Malignant	-	-	-	0
I2	122	34	F	Breast	Invasive ductal carcinoma	T2N0M0	3	Malignant	-	-	-	0
I3	123	56	F	Breast	Invasive ductal carcinoma	T3N0M0	3	Malignant	+	+++	45%++	0
I4	124	56	F	Breast	Invasive ductal carcinoma	T3N0M0	3	Malignant	+	+++	30%++	0
I5	125	44	F	Breast	Invasive ductal carcinoma	T2N2M0	3	Malignant	-	-	-	3+
I6	126	44	F	Breast	Invasive ductal carcinoma	T2N2M0	3	Malignant	-	-	-	3+
I7	127	62	F	Breast	Invasive ductal carcinoma (fibrous tissue)	T2N1M0	-	Malignant	*	*	*	*

I8	128	62	F	Breast	Invasive ductal carcinoma	T2N1M0	3	Malignant	-	-	-	1+
I9	129	49	F	Breast	Invasive ductal carcinoma	T3N1M0	3	Malignant	-	-	70%+++	0
I10	130	49	F	Breast	Invasive ductal carcinoma	T3N1M0	3	Malignant	-	-	60%+++	0
I11	131	50	F	Breast	Invasive ductal carcinoma	T2N0M0	3	Malignant	+++	+++	90%+++	0
I12	132	50	F	Breast	Invasive ductal carcinoma	T2N0M0	3	Malignant	++	+++	85%+++	0
I13	133	50	F	Breast	Invasive ductal carcinoma	T2N2M0	3	Malignant	-	-	45%++	0
I14	134	50	F	Breast	Invasive ductal carcinoma	T2N2M0	3	Malignant	-	-	30%++	0
I15	135	62	F	Breast	Invasive ductal carcinoma	T1N0M0	3	Malignant	-	-	25%+	0
J1	136	62	F	Breast	Invasive ductal carcinoma	T1N0M0	3	Malignant	-	-	20%+	0
J2	137	58	F	Breast	Invasive ductal carcinoma	T2N0M0	3	Malignant	-	-	10%+	0
J3	138	58	F	Breast	Invasive ductal carcinoma	T2N0M0	3	Malignant	-	-	20%+	0
J4	139	57	F	Breast	Invasive ductal carcinoma	T3N0M0	3	Malignant	-	-	20%+	0
J5	140	57	F	Breast	Invasive ductal carcinoma	T3N0M0	3	Malignant	-	-	20%+	0
J6	141	56	F	Breast	Invasive ductal carcinoma	T2N0M0	3	Malignant	+	++	10%+	0
J7	142	56	F	Breast	Invasive ductal carcinoma	T2N0M0	3	Malignant	++	++	20%+	0

J8	143	50	F	Breast	Invasive ductal carcinoma	T2N2M0	3	Malignant	++	+++	80%+++	0
J9	144	50	F	Breast	Invasive ductal carcinoma	T2N2M0	3	Malignant	++	+++	85%+++	0
J10	145	53	F	Breast	Invasive ductal carcinoma	T4N2M0	3	Malignant	-	+++	10%+	0
J11	146	53	F	Breast	Invasive ductal carcinoma	T4N2M0	3	Malignant	-	+++	10%+	0
J12	147	43	F	Breast	Invasive ductal carcinoma	T2N0M0	3	Malignant	-	-	90%+++	3+
J13	148	43	F	Breast	Invasive ductal carcinoma	T2N0M0	3	Malignant	-	-	80%+++	3+
J14	149	81	F	Breast	Invasive ductal carcinoma	T3N0M0	3	Malignant	-	-	10%+	0
J15	150	81	F	Breast	Invasive ductal carcinoma (sparse)	T3N0M0	-	Malignant	-	-	10%+	0

Supplement-2. Information of the pancreatic TMA (PA2081c).

US Biomax, Inc. PA2081c (serial)	1	2	3	4	5	6	7	8	9	10	11	12	13	14	15	16	
	A	Pan															
	B	Pan															
	C	Pan															
	D	Pan															
	E	Pan	Ome	Ome													
	F	Abd	Abd	Liv	Liv	Liv	Liv	Liv	Liv	Pan							
	G	Pan															
	H	Pan															
	I	Pan															
	J	Pan															
	K	Pan															
	L	Pan	Adr														

Legend: Abd - Abdominal cavity, Liv - Liver, Ome - Omentum, Pan - Pancreas

PA2081c A15

No.:15

Age:38

Sex:F

Organ/Anatomic Site:Pancreas

Pathology diagnosis:Duct adenocarcinoma

TNM:T2N0M0

Grade:1

Stage:IB

Type:Malignant

Pos.	No.	Age	Sex	Organ/Anatomic Site	Pathology diagnosis	TNM	Grade	Stage	Type
A1	1	56	M	Pancreas	Duct adenocarcinoma	T2N1M0	*	IIB	Malignant
A2	2	56	M	Pancreas	Duct adenocarcinoma	T2N1M0	2	IIB	Malignant
A3	3	58	F	Pancreas	Duct adenocarcinoma	T2N0M0	2	IB	Malignant
A4	4	58	F	Pancreas	Duct adenocarcinoma	T2N0M0	2	IB	Malignant
A5	5	41	M	Pancreas	Mucinous adenocarcinoma	T2N0M0	1	IB	Malignant
A6	6	41	M	Pancreas	Mucinous adenocarcinoma	T2N0M0	1	IB	Malignant
A7	7	48	F	Pancreas	Duct adenocarcinoma	T3N0M0	1	IIA	Malignant
A8	8	48	F	Pancreas	Duct adenocarcinoma	T3N0M0	1	IIA	Malignant
A9	9	40	F	Pancreas	Duct adenocarcinoma invades small intestine	T3N1M0	1	IIB	Malignant
A10	10	40	F	Pancreas	Duct adenocarcinoma invades small intestine	T3N1M0	1	IIB	Malignant
A11	11	64	F	Pancreas	Duct adenocarcinoma	T2N0M0	1	IB	Malignant
A12	12	64	F	Pancreas	Duct adenocarcinoma	T2N0M0	*	IB	Malignant
A13	13	54	F	Pancreas	Duct adenocarcinoma	T2N0M0	1	IB	Malignant
A14	14	54	F	Pancreas	Duct adenocarcinoma	T2N0M0	*	IB	Malignant
A15	15	38	F	Pancreas	Duct adenocarcinoma	T2N0M0	1	IB	Malignant
A16	16	38	F	Pancreas	Duct adenocarcinoma	T2N0M0	1	IB	Malignant
B1	17	47	M	Pancreas	Duct adenocarcinoma	T2N0M0	1	IB	Malignant
B2	18	47	M	Pancreas	Duct adenocarcinoma	T2N0M0	*	IB	Malignant
B3	19	62	F	Pancreas	Duct adenocarcinoma	T2N1M0	1	IIB	Malignant
B4	20	62	F	Pancreas	Duct adenocarcinoma	T2N1M0	1	IIB	Malignant
B5	21	64	M	Pancreas	Duct adenocarcinoma	T3N0M0	2--3	IIA	Malignant
B6	22	64	M	Pancreas	Duct adenocarcinoma	T3N0M0	2--3	IIA	Malignant
B7	23	47	M	Pancreas	Duct adenocarcinoma	T3N0M0	2	IIA	Malignant
B8	24	47	M	Pancreas	Duct adenocarcinoma	T3N0M0	2	IIA	Malignant
B9	25	58	F	Pancreas	Duct adenocarcinoma	T3N1M0	2	IIB	Malignant

B10	26	58	F	Pancreas	Duct adenocarcinoma	T3N1M0	2	IIB	Malignant
B11	27	52	M	Pancreas	Duct adenocarcinoma (sparse)	T3N1M0	2	IIB	Malignant
B12	28	52	M	Pancreas	Duct adenocarcinoma	T3N1M0	*	IIB	Malignant
B13	29	58	F	Pancreas	Duct adenocarcinoma	T4N0M0	*	III	Malignant
B14	30	58	F	Pancreas	Duct adenocarcinoma	T4N0M0	*	III	Malignant
B15	31	59	M	Pancreas	Duct adenocarcinoma	T2N0M0	3	IB	Malignant
B16	32	59	M	Pancreas	Duct adenocarcinoma	T2N0M0	3	IB	Malignant
C1	33	55	M	Pancreas	Duct adenocarcinoma	T2N0M0	*	IB	Malignant
C2	34	55	M	Pancreas	Duct adenocarcinoma	T2N0M0	*	IB	Malignant
C3	35	39	M	Pancreas	Duct adenocarcinoma	T3N0M0	2	IIA	Malignant
C4	36	39	M	Pancreas	Duct adenocarcinoma	T3N0M0	2	IIA	Malignant
C5	37	42	M	Pancreas	Duct adenocarcinoma	T3N0M0	2	IIA	Malignant
C6	38	42	M	Pancreas	Duct adenocarcinoma	T3N0M0	2	IIA	Malignant
C7	39	72	F	Pancreas	Duct adenocarcinoma	T3N0M0	2	IIA	Malignant
C8	40	72	F	Pancreas	Duct adenocarcinoma	T3N0M0	2	IIA	Malignant
C9	41	40	M	Pancreas	Duct adenocarcinoma invades small intestine	T2N1M0	*	IIB	Malignant
C10	42	40	M	Pancreas	Duct adenocarcinoma invades small intestine	T2N1M0	*	IIB	Malignant
C11	43	68	F	Pancreas	Duct adenocarcinoma	T2N0M0	2	IB	Malignant
C12	44	68	F	Pancreas	Duct adenocarcinoma	T2N0M0	2	IB	Malignant
C13	45	64	M	Pancreas	Duct adenocarcinoma	T3N0M0	2	IIA	Malignant
C14	46	64	M	Pancreas	Duct adenocarcinoma	T3N0M0	2	IIA	Malignant
C15	47	50	M	Pancreas	Duct adenocarcinoma	T2N0M0	2	IB	Malignant
C16	48	50	M	Pancreas	Duct adenocarcinoma	T2N0M0	*	IB	Malignant
D1	49	72	F	Pancreas	Adenocarcinoma	T3N0M0	2--3	IIA	Malignant
D2	50	72	F	Pancreas	Adenocarcinoma	T3N0M0	2--3	IIA	Malignant
D3	51	62	M	Pancreas	Adenocarcinoma	T2N0M0	2--3	IB	Malignant
D4	52	62	M	Pancreas	Adenocarcinoma	T2N0M0	2--3	IB	Malignant

D5	53	43	F	Pancreas	Adenocarcinoma	T4N0M0	3	III	Malignant
D6	54	43	F	Pancreas	Adenocarcinoma	T4N0M0	3	III	Malignant
D7	55	23	F	Pancreas	Adenocarcinoma	T3N0M0	3	IIA	Malignant
D8	56	23	F	Pancreas	Adenocarcinoma	T3N0M0	*	IIA	Malignant
D9	57	55	M	Pancreas	Duct adenocarcinoma	T2N0M0	3	IB	Malignant
D10	58	55	M	Pancreas	Duct adenocarcinoma	T2N0M0	3	IB	Malignant
D11	59	51	F	Pancreas	Duct adenocarcinoma	T2N0M0	3	IB	Malignant
D12	60	51	F	Pancreas	Duct adenocarcinoma	T2N0M0	3	IB	Malignant
D13	61	62	F	Pancreas	Duct adenocarcinoma	T3N0M0	3	IIA	Malignant
D14	62	62	F	Pancreas	Duct adenocarcinoma	T3N0M0	3	IIA	Malignant
D15	63	39	F	Pancreas	Duct adenocarcinoma	T3N0M0	3	IIA	Malignant
D16	64	39	F	Pancreas	Duct adenocarcinoma	T3N0M0	3	IIA	Malignant
E1	65	66	F	Pancreas	Adenocarcinoma	T2N1M0	3	IIB	Malignant
E2	66	66	F	Pancreas	Adenocarcinoma	T2N1M0	3	IIB	Malignant
E3	67	40	F	Pancreas	Adenocarcinoma	T2N0M0	3--4	IB	Malignant
E4	68	40	F	Pancreas	Adenocarcinoma	T2N0M0	3--4	IB	Malignant
E5	69	65	M	Pancreas	Undifferentiated adenocarcinoma	T3N0M0	-	IIA	Malignant
E6	70	65	M	Pancreas	Undifferentiated adenocarcinoma	T3N0M0	-	IIA	Malignant
E7	71	62	F	Pancreas	Adenosquamous carcinoma	T3N0M0	-	IIA	Malignant
E8	72	62	F	Pancreas	Adenosquamous carcinoma	T3N0M0	-	IIA	Malignant
E9	73	49	F	Pancreas	Adenosquamous carcinoma	T3N1M0	-	IIB	Malignant
E10	74	49	F	Pancreas	Adenosquamous carcinoma	T3N1M0	-	IIB	Malignant
E11	75	50	M	Pancreas	Adenosquamous carcinoma	T3N0M0	-	IIA	Malignant

E12	76	50	M	Pancreas	Adenosquamous carcinoma	T3N0M0	-	IIA	Malignant
E13	77	40	F	Pancreas	Neuroendocrine tumor	T2N0M0 G1	-	I	Malignant
E14	78	40	F	Pancreas	Neuroendocrine tumor	T2N0M0 G1	-	I	Malignant
E15	79	66	M	Omentum	Metastatic adenocarcinoma from pancreas	-	1--2	-	Metastasis
E16	80	66	M	Omentum	Metastatic adenocarcinoma from pancreas	-	1--2	-	Metastasis
F1	81	51	F	Abdominal cavity	Metastatic adenocarcinoma of fibrofatty from pancreas	-	2	-	Metastasis
F2	82	51	F	Abdominal cavity	Metastatic adenocarcinoma of fibrofatty from pancreas	-	2	-	Metastasis
F3	83	60	M	Liver	Metastatic adenocarcinoma from pancreas	-	2	-	Metastasis
F4	84	60	M	Liver	Metastatic adenocarcinoma from pancreas	-	2	-	Metastasis
F5	85	53	M	Liver	Metastatic adenocarcinoma from pancreas	-	3	-	Metastasis
F6	86	53	M	Liver	Metastatic adenocarcinoma from pancreas	-	3	-	Metastasis

F7	87	59	M	Liver	Metastatic adenocarcinoma from pancreas	-	3	-	Metastasis
F8	88	59	M	Liver	Metastatic adenocarcinoma from pancreas	-	3	-	Metastasis
F9	89	47	M	Pancreas	Islet cell tumor	-	-	-	Benign
F10	90	47	M	Pancreas	Islet cell tumor	-	-	-	Benign
F11	91	47	F	Pancreas	Islet cell tumor	-	-	-	Benign
F12	92	47	F	Pancreas	Islet cell tumor	-	-	-	Benign
F13	93	37	F	Pancreas	Islet cell tumor	-	-	-	Benign
F14	94	37	F	Pancreas	Islet cell tumor	-	-	-	Benign
F15	95	77	M	Pancreas	Islet cell tumor	-	-	-	Benign
F16	96	77	M	Pancreas	Islet cell tumor	-	-	-	Benign
G1	97	35	F	Pancreas	Islet cell tumor	-	-	-	Benign
G2	98	35	F	Pancreas	Islet cell tumor	-	-	-	Benign
G3	99	40	M	Pancreas	Islet cell tumor	-	-	-	Benign
G4	100	40	M	Pancreas	Islet cell tumor	-	-	-	Benign
G5	101	48	F	Pancreas	Islet cell tumor	-	-	-	Benign
G6	102	48	F	Pancreas	Islet cell tumor	-	-	-	Benign
G7	103	23	F	Pancreas	Islet cell tumor	-	-	-	Benign
G8	104	23	F	Pancreas	Islet cell tumor	-	-	-	Benign
G9	105	64	M	Pancreas	Islet cell tumor	-	-	-	Benign
G10	106	64	M	Pancreas	Islet cell tumor	-	-	-	Benign
G11	107	17	F	Pancreas	Islet cell tumor	-	-	-	Benign
G12	108	17	F	Pancreas	Islet cell tumor	-	-	-	Benign
G13	109	10	M	Pancreas	Chronic pancreatitis	-	-	-	Inflammation
G14	110	10	M	Pancreas	Chronic pancreatitis	-	-	-	Inflammation
G15	111	46	F	Pancreas	Chronic pancreatitis	-	-	-	Inflammation
G16	112	46	F	Pancreas	Chronic pancreatitis	-	-	-	Inflammation

H1	113	50	F	Pancreas	Chronic pancreatitis	-	-	-	Inflammation
H2	114	50	F	Pancreas	Chronic pancreatitis	-	-	-	Inflammation
H3	115	60	F	Pancreas	Chronic pancreatitis	-	-	-	Inflammation
H4	116	60	F	Pancreas	Chronic pancreatitis	-	-	-	Inflammation
H5	117	66	M	Pancreas	Chronic pancreatitis	-	-	-	Inflammation
H6	118	66	M	Pancreas	Chronic pancreatitis	-	-	-	Inflammation
H7	119	33	F	Pancreas	Chronic pancreatitis	-	-	-	Inflammation
H8	120	33	F	Pancreas	Chronic pancreatitis	-	-	-	Inflammation
H9	121	55	F	Pancreas	Adjacent normal pancreas tissue	-	-	-	NAT
H10	122	55	F	Pancreas	Adjacent normal pancreas tissue	-	-	-	NAT
H11	123	53	M	Pancreas	Adjacent normal pancreas tissue	-	-	-	NAT
H12	124	53	M	Pancreas	Adjacent normal pancreas tissue	-	-	-	NAT
H13	125	62	M	Pancreas	Acute pancreatitis	-	-	-	Inflammation
H14	126	62	M	Pancreas	Acute pancreatitis	-	-	-	Inflammation
H15	127	73	F	Pancreas	Adjacent normal pancreas tissue	-	-	-	NAT
H16	128	73	F	Pancreas	Adjacent normal pancreas tissue	-	-	-	NAT
I1	129	60	M	Pancreas	Adjacent normal pancreas tissue	-	-	-	NAT
I2	130	60	M	Pancreas	Adjacent normal pancreas tissue	-	-	-	NAT
I3	131	75	F	Pancreas	Adjacent normal pancreas tissue	-	-	-	NAT
I4	132	75	F	Pancreas	Adjacent normal pancreas tissue	-	-	-	NAT

I5	133	54	M	Pancreas	Adjacent normal pancreas tissue	-	-	-	NAT
I6	134	54	M	Pancreas	Adjacent normal pancreas tissue	-	-	-	NAT
I7	135	52	M	Pancreas	Adjacent normal pancreas tissue	-	-	-	NAT
I8	136	52	M	Pancreas	Adjacent normal pancreas tissue	-	-	-	NAT
I9	137	60	M	Pancreas	Adjacent normal pancreas tissue	-	-	-	NAT
I10	138	60	M	Pancreas	Adjacent normal pancreas tissue	-	-	-	NAT
I11	139	69	F	Pancreas	Adjacent normal pancreas tissue	-	-	-	NAT
I12	140	69	F	Pancreas	Adjacent normal pancreas tissue	-	-	-	NAT
I13	141	53	F	Pancreas	Adjacent normal pancreas tissue	-	-	-	NAT
I14	142	53	F	Pancreas	Adjacent normal pancreas tissue	-	-	-	NAT
I15	143	66	F	Pancreas	Adjacent normal pancreas tissue	-	-	-	NAT
I16	144	66	F	Pancreas	Adjacent normal pancreas tissue	-	-	-	NAT
J1	145	64	M	Pancreas	Adjacent normal pancreas tissue	-	-	-	NAT
J2	146	64	M	Pancreas	Adjacent normal pancreas tissue	-	-	-	NAT
J3	147	47	M	Pancreas	Adjacent normal pancreas tissue	-	-	-	NAT

J4	148	47	M	Pancreas	Adjacent normal pancreas tissue	-	-	-	NAT
J5	149	56	F	Pancreas	Adjacent normal pancreas tissue	-	-	-	NAT
J6	150	56	F	Pancreas	Adjacent normal pancreas tissue	-	-	-	NAT
J7	151	62	M	Pancreas	Adjacent normal pancreas tissue	-	-	-	NAT
J8	152	62	M	Pancreas	Adjacent normal pancreas tissue	-	-	-	NAT
J9	153	48	M	Pancreas	Adjacent normal pancreas tissue	-	-	-	NAT
J10	154	48	M	Pancreas	Adjacent normal pancreas tissue	-	-	-	NAT
J11	155	48	M	Pancreas	Adjacent normal pancreas tissue	-	-	-	NAT
J12	156	48	M	Pancreas	Adjacent normal pancreas tissue	-	-	-	NAT
J13	157	60	M	Pancreas	Acute necrotizing pancreatitis	-	-	-	Inflammation
J14	158	60	M	Pancreas	Acute necrotizing pancreatitis	-	-	-	Inflammation
J15	159	63	M	Pancreas	Adjacent normal pancreas tissue	-	-	-	NAT
J16	160	63	M	Pancreas	Adjacent normal pancreas tissue	-	-	-	NAT
K1	161	51	M	Pancreas	Adjacent normal pancreas tissue	-	-	-	NAT
K2	162	51	M	Pancreas	Adjacent normal pancreas tissue	-	-	-	NAT

K3	163	38	M	Pancreas	Adjacent normal pancreas tissue	-	-	-	NAT
K4	164	38	M	Pancreas	Adjacent normal pancreas tissue	-	-	-	NAT
K5	165	66	F	Pancreas	Adjacent normal pancreas tissue	-	-	-	NAT
K6	166	66	F	Pancreas	Adjacent normal pancreas tissue	-	-	-	NAT
K7	167	64	M	Pancreas	Adjacent normal pancreas tissue	-	-	-	NAT
K8	168	64	M	Pancreas	Adjacent normal pancreas tissue	-	-	-	NAT
K9	169	50	F	Pancreas	Adjacent normal pancreas tissue	-	-	-	NAT
K10	170	50	F	Pancreas	Adjacent normal pancreas tissue	-	-	-	NAT
K11	171	21	F	Pancreas	Adjacent normal pancreas tissue	-	-	-	NAT
K12	172	21	F	Pancreas	Adjacent normal pancreas tissue	-	-	-	NAT
K13	173	37	M	Pancreas	Pancreas tissue	-	*	-	Normal
K14	174	37	M	Pancreas	Pancreas tissue (sparse)	-	-	-	Normal
K15	175	38	F	Pancreas	Pancreas tissue	-	-	-	Normal
K16	176	38	F	Pancreas	Pancreas tissue	-	-	-	Normal
L1	177	40	M	Pancreas	Pancreas tissue	-	-	-	Normal
L2	178	40	M	Pancreas	Pancreas tissue	-	-	-	Normal
L3	179	35	M	Pancreas	Pancreas tissue	-	-	-	Normal
L4	180	35	M	Pancreas	Pancreas tissue	-	-	-	Normal
L5	181	25	M	Pancreas	Pancreas tissue	-	-	-	Normal
L6	182	25	M	Pancreas	Pancreas tissue	-	-	-	Normal

L7	183	40	F	Pancreas	Pancreas tissue	-	-	-	Normal
L8	184	40	F	Pancreas	Pancreas tissue	-	-	-	Normal
L9	185	47	M	Pancreas	Pancreas tissue	-	-	-	Normal
L10	186	47	M	Pancreas	Pancreas tissue	-	-	-	Normal
L11	187	50	M	Pancreas	Pancreas tissue	-	-	-	Normal
L12	188	50	M	Pancreas	Pancreas tissue	-	-	-	Normal
L13	189	21	F	Pancreas	Tail of pancreas tissue	-	-	-	Normal
L14	190	21	F	Pancreas	Tail of pancreas tissue	-	-	-	Normal
L15	191	50	M	Pancreas	Pancreas tissue	-	-	-	Normal
L16	192	50	M	Pancreas	Pancreas tissue	-	-	-	Normal